Reaktionen auf Hitzestress und funktionelle Analyse von LIM6 und LIM14 in den späten Stadien der Pollenentwicklung bei Mais

DISSERTATION

ZUR ERLANGUNG DES DOKTORGRADES DER NATURWISSENSCHAFTEN (DR. RER. NAT.) DER FAKULTÄT FÜR BIOLOGIE UND VORKLINISCHE MEDIZIN

UNIVERSITÄT REGENSBURG

vorgelegt von

Xingli Li

aus Hebei, China

Key word: Mais, Pollen, Hitzestress

im Juni. 2023

Heat stress responses and functional analysis of LIM6 and LIM14 during late stages of pollen development in maize

DISSERTATION

ZUR ERLANGUNG DES DOKTORGRADES DER NATURWISSENSCHAFTEN (DR. RER. NAT.) DER FAKULTÄT FÜR BIOLOGIE UND VORKLINISCHE MEDIZIN

UNIVERSITÄT REGENSBURG

vorgelegt von

Xingli Li

aus Hebei, China

Key word: Maize, Pollen, Heat stress

im Juni. 2023

Das Promotionsgesuch wurde eingereicht am 14.06.2023.

Die Arbeit wurde angeleitet von

Prof. Dr. Thomas Dresselhaus und Dr. Kevin Begcy

Unterschrift:_____

Unterschrift Doktorand:_____

Xingli Li

我不去想是否能够成功
既然选择了远方
便只顾风雨兼程

我不去想能否赢得爱情
既然钟情于玫瑰
就勇敢地吐露真诚

我不去想身后会不会袭来寒风冷雨
既然目标是地平线
留给世界的只能是背影

我不去想未来是平坦还是泥泞
只要热爱生命
一切，都在意料中

– 热爱生命·汪国真

I don't want to consider
If I'll be able to succeed.
Since I've decided to go to a distant place,
I'll try my best to make the trip.

I don't want to consider
If I'll be able to obtain love.
Since I'm deep in love with roses,
I'll show my sincerity boldly.

I don't want to consider
If I'll meet with the cold wind and rain.
Since my destination is the horizon,
I'll leave a deep impression on the Earth.

I don't want to consider
If my future will be smooth or bumpy.
If only I love my life,
Everything is to be expected.

- Loving Life · Guozhen Wang

CONTENTS

ABSTRACT

Die Entwicklung der männlichen Gametophyten in blühenden Pflanzen ist ein komplexer Prozess, der durch die Transkription reguliert wird und der sehr empfindlich auf abiotische und biotische Stressfaktoren reagiert. Insbesondere die Übergänge zwischen den Entwicklungsphasen der pflanzlichen Fortpflanzung spielen eine entscheidende Rolle für die normale Gametophytenbildung und die erfolgreiche doppelte Befruchtung. Aus der diploiden Pollenmutterzelle (2N) entstehen bei Mais nach der Meiose vier haploide Mikrosporen (1N). Nach zwei Mitoserunden werden die Pollenentwicklungsphasen anhand des Entwicklungszustands der Kerne definiert, zu denen das einzellige, zweizellige und dreizellige Stadium gehören. Wurden Maispflanzen im unizellulären und bizellulären Stadium einer moderaten Hitzestressbehandlung (35°C/25°C Tag/Nacht) ausgesetzt, zeigten die Pollen Stadien-spezifische Hitzestressreaktionen (HSR). Während der Behandlung im einzelligen Stadium der Entwicklung waren die Lebensfähigkeit und die Befruchtungsfähigkeit der Pollen stark beeinträchtigt, was zu einem reduzierten Samenansatz führte. Im zweizelligen Stadium hatte der Hitzestress jedoch keine starken Auswirkungen auf die Polleneigenschaften, führte aber dennoch zu fehlendem Samenansatz. Außerdem wurde festgestellt, dass die Spermazellen sowohl in ihrer Morphologie als auch in ihren biologischen Funktionen stark verändert waren. Durch Transkriptom- und Proteom-Analysen wurde festgestellt, dass die Metaphase der Mitose während des PMII-Stadiums teilweise gestoppt wurde, was zur Bildung von nicht funktionsfähigen Samenzellen führte. Darüber hinaus wurden die Spermazellen nicht zur Befruchtung in den Pollenschlauch transportiert, was wahrscheinlich auf den Hitzestress zurückzuführen ist, der die Zytoskelettstruktur des Pollenschlauchs beeinträchtigt.

Zwei LIM-Transkriptionsfaktorgene, *ZmLIM6* und *ZmLIM14*, werden während der bizellulären und trizellulären Pollenstadien stark exprimiert. CRISPR/Cas9-Knock-out-Mutanten von *ZmLIM6/14* produzierten einen Spermazell-ähnlichen Kern oder es wurden keine Spermazellen im reifen Pollen beobachtet. Darüber hinaus wuchsen die Pollenschläuche in einem verdrehten Muster. Im Inneren des Pollenkorns waren ZmLIM6/14 mit α-Tubulin kolokalisiert. Daher konnte α-Tubulin in LIM-mutierten Pollen keine normale Hülle bilden. Bei der Untersuchung der LIM-mutierten Spermazellmarkerlinie YFP-Tubulin+/*lim14* waren die Störungen in der Tubulinstruktur oder -lokalisierung und der Kernverlust jedoch unabhängig. Darüber hinaus funktionierten die ZmLIM6/14-Proteine während der Nukleolusbildung in Keimzellen, was wahrscheinlich die *lim6/14*-Phänotypen erklärt. In weitergehenden Analysen wurde *ZmRALF3*

als potenzielles Zielgen von ZmLIM14 identifiziert, das die Integrität der Pollenschläuche reguliert. Insgesamt zeigen alle Ergebnisse, dass ZmLIMs mehrere Funktionen bei der ordnungsgemäßen Mikrotubuli-Bündelung und Nukleolenbildung während des bi- bis trizellulären Übergangsstadiums in Maispollen haben.

Generell deuten die obigen Ergebnisse darauf hin, dass Hitzestress die Bildung von Spermazellen während des PMII-Übergangs in der Pollenentwicklung beeinflusst. Darüber hinaus zeigten sich neue Funktionen von ZmLIMs in der Mikrotubuli-Dynamik und der Spermazellbildung während des PMII-Übergangs. Zusammenfassend lässt sich sagen, dass diese Arbeit weitere Beweise für phasenspezifische Regulierungsmuster des männlichen Gametophyten und weitere Einblicke in die späten Stadien der Pollenentwicklung von Mais liefert.

ABSTRACT

Male gametophyte development in flowering plants undergoes a complex process that is transcriptionally regulated and that it is highly sensitive to abiotic and biotic stresses. Particularly, developmental phase transitions of plant reproduction play a crucial role in normal gametophyte generation and successful double fertilization. In maize, the diploid pollen mother cell (2N) releases haploid microspores (1N) after meiosis. Following two rounds of mitosis, pollen development phases are defined based on the developmental state of nuclei, which include the unicellular, bicellular, and tricellular stages. When a moderate (35°C/25°C day/night) heat stress treatment was imposed on maize plants at the unicellular and bicellular stages, pollen showed stage-specific heat stress responses (HSR). During unicellular development, pollen viability and fertilization ability were severely affected, resulting in reduced seed set. However, at the bicellular stage, heat stress did not have strong effects on pollen abilities, but still caused seed abortion. Furthermore, sperm cells were found strongly altered both in morphology and biological functions. Through transcriptome and proteome profile analyses, the metaphase of mitosis during PMII was found partially arrested, resulting in the generation of nonfunctional sperm cells. Meanwhile, sperm cells could not travel into the pollen tube for fertilization, probably due to heat stress impairing pollen tube cytoskeleton structure.

Two LIM transcription factors genes, ZmLIM6 and ZmLIM14, are highly expressed during the bicellular and tricellular pollen stages. CRISPR/Cas9 knock-out mutants of ZmLIM6/14 produced one sperm-like nucleus or sperm cells were not observed inside the mature pollen. In addition, pollen tubes grew in a twisted pattern. Inside the pollen grain, LIM6/14 colocalized with α-tubulin. Therefore, in LIM-mutated pollen, α-tubulin failed to form a normal envelope. However, tubulin disorder and nuclei loss were independent by investigating the LIM-mutated sperm cell marker line, YFP-tubulin+/lim14. Moreover, ZmLIM6/14 proteins functioned during nucleolus formation in germ cells, which was likely explained by the lim6/14 phenotypes. Further, ZmRALF3 was identified as the potential target of ZmLIM14 and thus regulating pollen tube integrity. Altogether, all findings reveal multiple functions of ZmLIMs in proper microtubule bundling and nucleoli formation during the bi- to tricellular transition stage in maize pollen.

In general, above findings indicate that heat stress affects sperm cell formation during the PMII transition in pollen development. Moreover, it is revealed that the novel functions of ZmLIMs

in microtubule dynamics and sperm cell formation during the PMII transition. In conclusion, this thesis provides more evidences for male gametophyte phase-specific regulation patterns and more insights into the late stages of maize pollen development.

CHAPTER 1. INTRODUCTION

- This chapter was written by myself

1.1 Angiosperm gametophyte development

Plant gametophyte development is a critical stage of the plant life cycle, culminating in the emergence of haploid male and female gametophytes that engender gametes involved in fertilization. The generation of competent gametophytes necessitates a plethora of molecular mechanisms, which are intricately involved in this process. This chapter will provide a brief introduction to the male and female gametophyte development of flowering plants.

The transition in angiosperms from vegetative to floral bud production heralds the commencement of the sexual reproduction phase. These floral buds will subsequently differentiate into specialized floral organs, such as the ovaries or anthers. At the early stages of floral bud development, bisexual primordia can be discerned in male or female spikelets (Cheng et al., 1983). It is during this process that sex determination plays a key role in ensuring the proper formation of sexual organs, ultimately giving rise to the female and male gametophytes.

1.1.1 Angiosperm female gametophyte development

The female gametophyte, or the embryo sac, that originates from a somatic hypodermal cell differentiates further into a megaspore mother cell (MMC), the initiation of the female germline lineage. The development of the female gametophyte can be subdivided into two steps: megasporogenesis and megagametogenesis.

There are more than 15 types of megasporogenesis formations across plant kingdom (Schmid et al., 2015). However, the *Polygonum*-type development pattern is the most common among flowering plants, including maize (Figure 1.1). *Polygonum*-type megasporogenesis encompasses the meiosis of the MMC, the generation of four megaspores, and the degradation of three spores, leaving a single functional megaspore. Megasporogenesis produces haploid spores that are primed for subsequent female germline development.

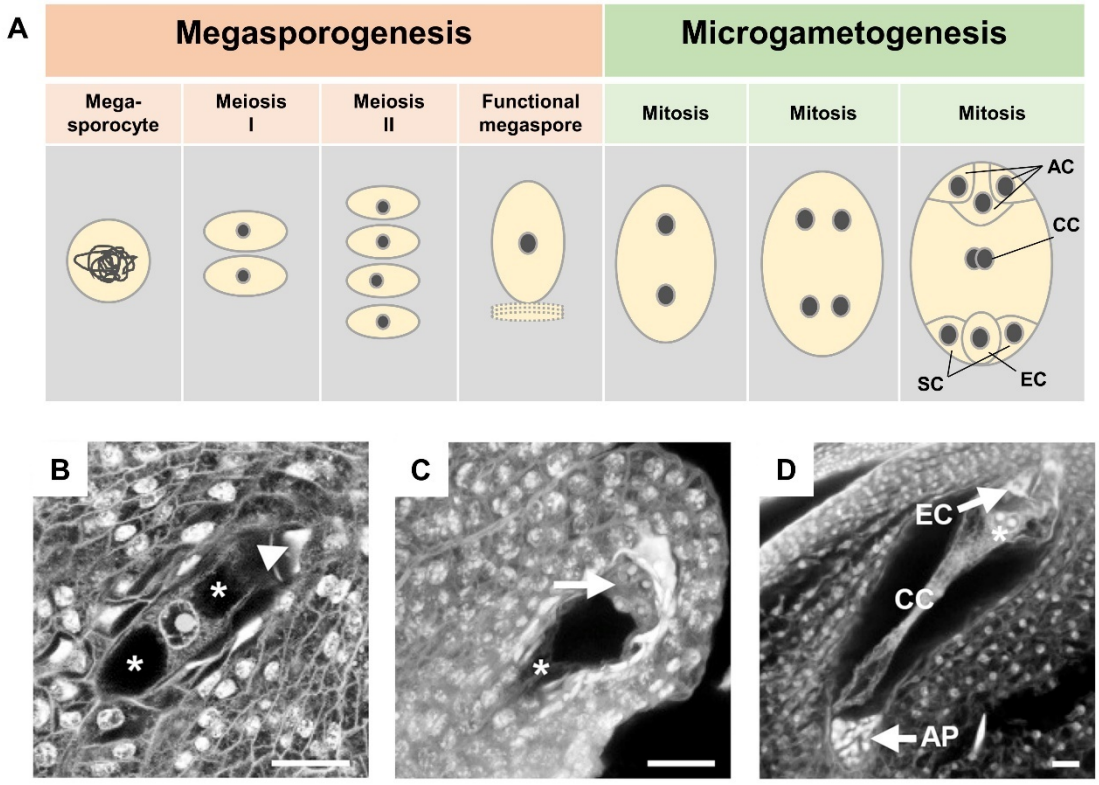

Figure 1.1 The *Polygonum* pattern of female gametophyte development. (A) Schematic representation of MMC to embryo sac development. (B)-(D) Microscopy of the different stages maize embryo sac. (B) Functional megaspore. Asterisks indicate two separate vacuoles. Arrowhead points toward degenerated megaspores. (C) Four nuclei at the micropylar pole (arrow) and the other four nuclei at the chalzal pole (asterisk, not in focus) (D) Mature embryo sac with female gametes. Asterisk indicates polar nuclei. AC, antipodal cell. SC, synergid cell. EC, egg cell. CC, central cell. Image was modified from (Zhou et al., 2017) and https://en.wikipedia.org/wiki/Double_fertilization

In megagametogenesis, the solitary megaspore undergoes three syncytial mitoses within the embryo sac, yielding eight evenly distributed nuclei within a single cell (Berger and Twell, 2011). The two nuclei produced from the first mitosis migrate in opposite directions and continue additional rounds of mitosis spontaneously. After the third division, the nuclei from both sides near the center merge to form the central cell nucleus (2N). Meanwhile, the central cell nucleus (2N) and the other six nuclei (1N) develop into diploid or haploid cells by cell wall partitioning within the embryo sac. Finally, seven cells are produced, comprising three antipodal cells, a diploid central cell, two synergid cells, and an egg cell. Among these cells, the three antipodal cells situated close to the chalazal region undergo proliferate and form a polyploid cell cluster in grasses (Krohn et al., 2012), whereas in *Arabidopsis thaliana*, they

undergo degradation (Sprunck and Groß-Hardt, 2011). The cells located near the micropyle region continue to differentiate into an egg cell and two synergid cells, with their cell fate determined by their precise positional relationship (Sun et al., 2021). The synergid cells locate on either side of the egg cell and specify the micropyle region through a filiform apparatus, which are required for pollen tube attraction (Márton et al., 2005). The pollen tube was attracted and to deliver sperm cells through one of the synergid cells (Zhou et al., 2017).

1.1.2 Angiosperm male gametophyte development

Compared to female gametophyte development, male germline formation follows a highly conserved pattern in all flowering plants (Bedinger and Fowler, 2009; van der Linde and Walbot, 2019). The development of male gametophytes can be divided into three phases: pre-meiotic, microsporogenesis, and microgametogenesis.

1.1.2.1 Pre-meiotic development

The initiation of pre-meiotic development commences with the differentiation of central archesporial cells in the four corners of male primordia. The archesporial cells give rise to the pollen mother cell (PMC), while the surrounding primary parietal cells undergo division, resulting in four somatic cell layers: epidermis (EPI), endothecium (EN), middle layer (ML), and tapetum (T) (Figure 1.2 A-B). The EPI, formed by the L1 layer, serves as a structural cell layer and takes on a butterfly shape. EN, ML and T arise from the L2 layer, which in dicots corresponds to the internal L2 and L3 layers (Walbot and Egger, 2016). The EN functions as an energy storage tissue to ensure anther development. The role of the ML is poorly understood, and as far as it is known, it does not contribute to anther formation (van der Linde and Walbot, 2019). The tapetum is a hot topic in angiosperm anther research, as it plays a vital role in subsequent pollen grain development by providing essential compounds, exine and callase necessary for microspore release, offering nutrition and energy to neighboring microspores, and undergoing programmed cell death (PCD) for proper microspore development and pollen maturation (Scott et al., 2004; Parish and Li, 2010)

During this process, the plant germline diverges from somatic tissue. Thus, defects in cell fate specification or proper multi-layered formation can strongly affect germline development. The first gene related to male germline cell fate and meristem identification is MALE STERILE CONVERTED ANTHER 1 (MSCA1). The differentiation of hypodermal to archesporial cells is blocked in *msca1*, resulting in mature anthers lacking pollen (Chaubal et al., 2003).

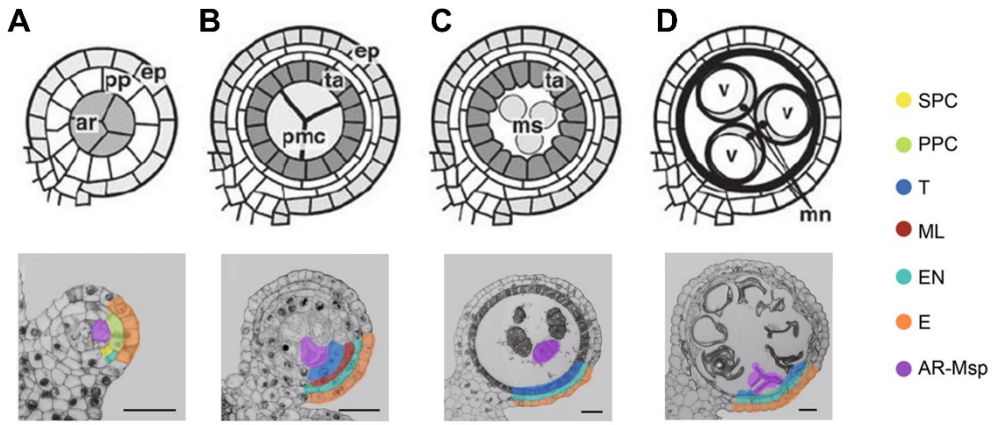

Figure 1.2 Pre-meiotic and microsporogenesis development of the male gametophyte in maize. Upper panel is schematic of male gametophyte development, bottom panel is transverse sections of different stages maize anthers. (A)-(B) Pre-meiotic development. (C)-(D) microsporogenesis development. SPC (L2), secondary parietal cell (yellow); PPC (L1), primary parietal cell (light green); T, tapetum (blue); ML, middle layer (deep red); En, endothecium (aquamarine); E, epidermis (orange); AR-Msp, germinal cells from archesporial cells to microspores (purple). Scale bar = 30μm. Image was modified from (Bedinger and Fowler, 2009) and (Han et al., 2022)

As MSCA1 encodes a glutaredoxin, the redox status is a crucial environmental factor in plant germline development (Kelliher and Walbot, 2012; Yang et al., 2021). MULTIPLE ARCHESPORIAL CELLS 1 (MAC1) is identified as regulating proper archesporial cell formation in both male and female flowers. Mutation of MAC1 causes extra archesporial cells from the hypodermal layer (Sheridan et al., 1996, 1999). MAC1 is a small protein secreted by newly specified archesporial cells, and the surrounding cell layers recognize the signal, further forming EN and following ML, T (van der Linde et al., 2018). As proper tapetum cell layer formation is essential to pollen development, extensive genetic analysis of male-sterile mutants has revealed a tapetal-specific transcription factor family - basic helix-loop-helix (bHLH). Four bHLH genes, *Ms23*, *Ms32*, *bHLH122*, and *bHLH51*, are sequentially expressed in the tapetum. They regulate each other, and their encoded proteins also form heterodimers. Through regulation of 24-nt phased secondary small interfering RNAs (phasiRNAs) transcription, these four bHLH genes ensure tapetal cell differentiation during pre-meiotic anther development (Moon et al., 2013; Nan et al., 2017; Jiang et al., 2021; Nan et al., 2022). There are still hundreds of male sterile lines waiting for analysis, which may be related to the formation of other anther cell types, indicating the numerous and complex regulation mechanisms behind this developmental stage.

1.1.2.2 Microsporogenesis

Similar to female microsporogenesis, pollen mother cells (PMC) produce a tetrad of haploid microspores through two rounds of meiosis. However, in contrast to the one functional female microspore, all four male microspores are capable of subsequent mitotic division. After the second meiotic division, callose is synthesized around each microspore and within the tetrad. The haploid microspores are released into the anther locule by the activity of callase, which is secreted from the tapetum and breaks down the callose wall (Scott et al., 2004). The single microspore contains a central nucleus and begins to acquire a specialized pollen wall consisting of an inner intine and outer exine. As an independent biological unit, the microspore continues to develop by fusing small vesicles into a large vacuole and communicating with the tapetum to obtain necessary nutrients and signals for proper development. This stage is generally referred to as the unicellular stage of pollen. During cell wall synthesis and vacuole fusion, the nucleus migrates to the cell wall and is ready for the following asymmetric mitotic division. (Chang and Neuffer, 1989; Begcy and Dresselhaus, 2017)

Meiosis is a basic biological process that occurs in all sexually-reproducing organisms, the molecular mechanism has been well-studied in animals and fungi, but with little is known in plants. The first maize meiotic mutant *divergent spindle* (*dv*) was identified over 80 years. The *dv* mutant exhibits defective microtubule spindle formation during metaphase I, resulting in errors in chromosome segregation and a decrease in pollen viability. (Clark, 1940; Staiger and Cande, 1990). The *Divergent Spindle* gene encodes a kinesin-14A motor protein involved in the pole-sharpening phase of spindle assembly (Higgins et al., 2016). Another maize mutant, *ameiotic1*, the PMC cannot enter meiosis (Staiger and Cande, 1992), as AMEIOTIC1 protein is required for multiple early meiotic processes. In loss-of-function mutants, premeiotic cells enter mitosis instead of meiosis because AMEIOTIC1 regulates leptotene–zygotene progression, a key step in early meiotic prophase (Pawlowski et al., 2009). The mechanism that triggers AMEIOTIC1 function in the PMC transition to meiosis still needs to be elucidated.

In addition to the discovery of several key genes involved in PMC meiosis, transcriptional studies have aimed to understand the reprogramming mechanism leading to the developmental transition from sporophytic to gametophytic tissues. Germinal cells from different maize inbred lines including B73, W22, Chang7-2, Zheng58 and others are harvested at the mitosis-meiosis transition and analyzed by sequencing (Dukowic-Schulze et al., 2014; Zhai et al., 2015; Yuan et al., 2018; Nelms and Walbot, 2019; Jiang et al., 2021; Han et al., 2022). As maize anther development is strongly associated with anther length, data from various collections using the

same staging approach can be compared. The expression profiles for different stages are similar across inbred lines (Han et al., 2022; Zhai et al., 2015). Cells in the mitosis-meiosis transition stage exhibited significant transcriptional changes and higher protein turnover efficiency. Through single-cell RNA-seq, it is discovered that many meiotic genes were already transcribed before meiosis, and the reorganization point was likely the leptotene–zygotene transition during prophase I of meiosis (Nelms and Walbot, 2019). Specific subsets of transcription factors (TFs) play a critical role in the transition stage. Around 30 genes encoding TF show a preferentially expressed pattern in premeiotic cells, while approximately 19 TF genes are specifically expressed during the meiosis stage, primarily belonging to the myeloblastosis (MYB), basic helix-loop-helix (bHLH), and MADS-box (MADS) families (Dukowic-Schulze et al., 2014; Yuan et al., 2018; Han et al., 2022). Many homologous genes in Arabidopsis and rice that are involved in meiosis and tapetum development have already been discovered. One of them, AtMYB80, controls callase synthesis and secretion, which is necessary for the release of microspores from tetrads (Phan et al., 2011).

1.1.2.3 Microgametogenesis

Microgametogenesis starts with the first mitotic division in unicellular pollen, referred to as pollen mitosis I (PMI). During this stage, the nucleus migrates to one side in the released microspore, creating cellular asymmetry. Subsequent to nuclear migration, the first mitotic division occurs adjacent to the cell wall, leading to the generation of a larger vegetative cell (VC) and a smaller generative cell (GC). The VC engulfs the GC after the division, resulting in early bicellular pollen. Once the GC moves to the opposite pole of the VC nucleus, the pollen is known as late bicellular pollen. The GC proceeds with the second mitotic division (pollen mitosis II, PMII), while the VC does not enter the cell cycle and instead serves as a support cell for the GC. Therefore, PMI is considered a determinative division that specifies the male germline by different cell fates (Berger and Twell, 2011; Horvitz and Herskowitz, 1992). The PMII produces two sperm cells via the GC, leading to the development of tricellular pollen. In approximately 70% of flowering plants, PMII occurs in the pollen tube after pollination (Williams and Reese, 2019). Maize belongs to the other 30% and releases fully mature tricellular pollen, making it ideal for studying male gametophyte development. Additionally, the pollen wall undergoes extra formation during these two mitotic divisions. Following PMI, the intine is formed between the plasma membrane and exine. Degeneration of tapetal cells before PMII results in the transfer of additional lipids and proteins onto the surface of exine,

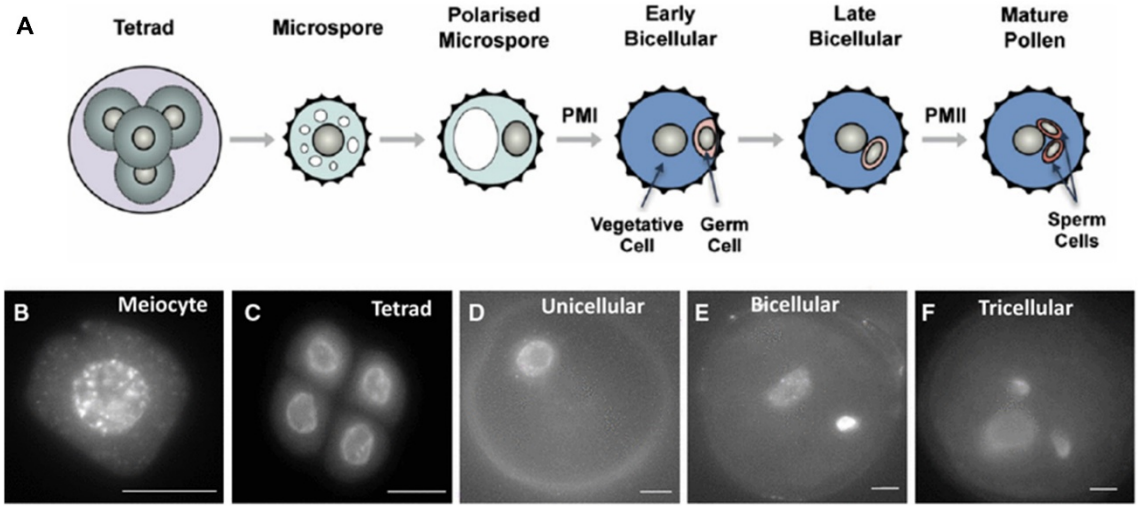

Figure 1.3 Microgametogenesis development of the male gametophyte in maize. (A) Schematic of maize male gametophyte development. (B)-(F) DAPI staining of different stages maize pollen. Scale bar = 10μm. Images were modified from (Borg et al., 2009) and (Begcy and Dresselhaus, 2017).

forming a pollen coat layer. After extensive dehydration, the tri-nuclei pollen is fully mature and ready for anther dehiscence.

During microgametogenesis, the specification and differentiation of the male germline are achieved. *MAB1* is a gene required for asymmetric PMI, and its mutation leads to the generation of two VC-like nuclei and no GCs in mature pollen. The MAB1 protein, which contains the MATH-BTB domain, interacts with the E3 ubiquitin ligase component Cullin 3a (CUL3a). It probably regulates the microtubule-severing subunit p60 of katanin to ensure proper spindle apparatus during meiosis and mitosis (Juranić et al., 2012). The *gem-1* mutant also generates two VC-like cells due to the interruption of nucleus migration before mitosis, resulting in no GCs specification and differentiation. These findings highlight the critical role of asymmetric division in germ cell fate determination (Twell et al., 2002, 1990). The first identified transcription factor involved in generative cell division is the R2R3 Myb-domain protein *DUO POLLEN 1* (*DUO1*) in Arabidopsis (Rotman et al., 2005). The GCs in *duo1* pollen are able to finish DNA replication at S-phase, but fail to enter PMII due to the reduction in expression of the mitotic cyclin gene, *CYCB1;1* (Brownfield et al., 2009). DUO1 forms a regulatory module with DUO1-ACTIVATED ZINC FINGER PROTEIN 1 (DAZ1) and DAZ2 to control generative cell mitotic division and sperm cell differentiation (Brownfield et al., 2009; Borg et al., 2011). Besides the intrinsic key fate determinant of pollen, surrounding cell layers are also important for viable pollen generation. Several male-sterile maize mutants, including *ms25* and

ms26, show premature vacuolation and death of tapetal cells (Loukides et al., 1995). Also, the tapetum-expressed *ms45* mutant fails in forming normal cell wall deposition (Cigan et al., 2001), indicating the importance of tapetal function during microgametogenesis.

Comparisons of the transcriptomic profiles between germ cells and other types of cells have been investigated due to the high specificity of male germ cells. In *Arabidopsis thaliana*, gene expression showed a decreasing trend during pollen development (11,565 genes in microspores, 11,909 in bicellular pollen, 8,788 in tricellular pollen, and 7,235 in mature pollen) due to chromatin becoming more condensed during the pollen maturation process (Honys and Twell, 2004). Similar expression patterns are found in maize, with our group identifying 19,767 genes in tetrad pollen, 21,251 in unicellular pollen, 15,227 in bicellular pollen, 15,150 in tricellular pollen, 8,008 in mature pollen, and 9,576 in isolated sperm cells (Begcy and Dresselhaus, unpublished). These findings are consistent with previous expression patterns during the four male reproductive stages of maize (tassel primordia, microspores, mature pollen, and sperm cells) (Warman et al., 2020), indicating conserved transcriptome alterations during male germline differentiation among plant species. Based on transcriptome data from the four developmental stages of pollen, stage-specific gene sets are identified. Several transcription factor families show accumulations at particular developmental stages, indicating their potential functions in these stages (described in this thesis).

Maize is an excellent plant model species to study pollen development because it generates a significant number of pollen grains that are easily accessible for harvest. As one of the most important crops, understanding how the male gametophyte develops is crucial for improving yield production.

1.2 Heat stress effects on male gametophyte development

The increasingly frequent heatwaves caused by global warming pose a threat to agricultural security by significantly reducing the yields of major crops such as rice, wheat, and maize (Resurreccion et al., 1977; Peng et al., 2004; Lobell et al., 2011). The male reproductive program, encompassing both microsporogenesis and microgametogenesis, is particularly sensitive to abiotic stresses such as high and low temperatures, salt stress, osmotic shock, and water deficit, leading to the generation of aborted pollen grains and male sterility (Begcy and Dresselhaus, 2018; De Storme and Geelen, 2014). Therefore, understanding plant heat stress

response during male gametophyte development has become an urgent and critical research topic.

During microspore development within anthers, several checkpoints ensure proper male germ unit formation, coordinating pollination and fertilization. Of these, the meiosis of PMC generating microspores and the microspore released from tetrad development towards PMI are one of the most susceptible stages to heat stress (De Storme and Geelen, 2014; Müller and Rieu, 2016; Begcy et al., 2019). Meiosis in particular, induces crossing over and homologous recombination events more frequently at high temperatures (10°C above optimal) (Boyko et al., 2005; Francis et al., 2007). Heat stress also causes cytoskeletal alterations and spindle orientation changes (De Storme and Geelen, 2013). Similar to some male-sterile mutants caused by tapetal cell defects, heat stress results in aberrant tapetal development and pollen dysfunction. This has been reported in barley (*Hordeum vulgare*) (Abiko et al., 2005), cowpea (*Vigna unguiculata*) (Ahmed et al., 1992) and wheat (*Triticum aestivum* L) (Saini et al., 1984). The tapetum is a resource for nutrition of pollen grains, and premature degeneration of tapetal cells strongly affects male gametogenesis progression, preventing microspores from completing PMI (Abiko et al., 2005; Saini et al., 1984). Accumulation of reactive oxygen species (ROS) induces cell death (Mittler, 2017). Failure or premature programmed cell death (PCD) of the tapetum is caused by ROS accumulation in anthers induced by heat stress (Zhao et al., 2018). ROS is also a signaling molecule, its accumulation in pollen can induce the expression of HEAT SHOCK TRANSCRIPTION FACTOR A1 (HsfA1), which stimulates heat stress (HS) -responsive gene expression (Yoshida et al., 2011).

Under heat stress conditions, plants undergo cellular adjustments aiming to maintain basic activities and to minimize the injuries derived from HS conditions, which are reflected at the transcriptome level. In *Arabidopsis thaliana*, heat stress results in a 15% alteration in the transcriptome of heat stressed mature pollen compared to nonstressed pollen (Rahmati Ishka et al., 2018), a finding similar in maize pollen (Begcy and Dresselhaus, unpublished). The transcriptional analysis not only shows the regulation of gene expression under heat stress but also allows us to understand how heat stress alters post-transcriptional gene regulation. In pollen, as well as in vegetative tissues, alternative splicing of genes induced by heat stress has been reported (Jiang et al., 2017; Keller et al., 2017). Among those induced genes, the heat stress transcription factors (HSFs) and heat shock proteins (HSPs), which are generally considered as the main controllers and regulators of plant development and survival under stress conditions (Fragkostefanakis et al., 2015), show an increase in alternative splicing events, indicating the

adaptation mechanism of plants under heat stress (Lee et al., 2017). Small noncoding RNAs (sncRNAs) are also found to be affected by heat stress, which may have an influence on pollen development at the transcriptional and epigenetic levels (Bokszczanin et al., 2015). Heat stress also affects the homeostasis of metabolism during pollen development. The flavonoid abundance, which is necessary for ROS detoxification, is induced under heat stress in microspores (Paupière et al., 2014). At plants hormones level, auxin has been reported to enhance heat tolerance in rice reproductive organs (Zhang et al., 2018), and jasmonic acid probably regulates water transport in the anther through the carbohydrate metabolism pathway (Ishiguro et al., 2001), indicating the vital roles of plants hormones in heat stress response.

1.3 Aims of this study

During male gametophyte development in maize, there are several key transition points: ① Differentiation of central archesporial cells into PMC, which initiates male germline formation. ② Release of microspores from tetrads, signifying individual pollen formation. ③ Asymmetric division of PMI, resulting in the generation of a true male germ cell. ④ PMII, where two sperm cells are produced, leading to the formation of the male germ unit for double fertilization. Each transition point denotes cell fate specification or the emergence of crucial nuclei. While ①&② have been extensively studied, the knowledge of ③and④, late stages of maize pollen development, is comparatively limited. **This thesis focuses on the response of pollen to heat stress and gene regulation during the uni- and bicellular stages.**

Previous studies have shown that moderate heat stress during the tetrad stage of pollen development causes male sterility, indicating a specific-stage heat stress response in pollen (De Storme and Geelen, 2014; Begcy et al., 2019). To gain a deeper understanding of heat stress during the following stages of uni- and bicellular stage pollen development, this study applies the same approach on pollen at the appropriate stages. Surprisingly, uni- and bicellular stage pollen exhibit significantly different responses to heat stress. To elucidate the underlying mechanism, transcriptome and proteome profiling are combined to provide a more realistic insight into pollen heat stress response

Unpublished RNA-seq data of the different developmental stages maize pollen reveals that two LIM transcription factor genes, *ZmLIM6* and *ZmLIM14*, are highly expressed during the bicellular to maturation transition. Additionally, based on their expression pattern in the sperm cell, these LIM genes are considered crucial genes during sperm cell formation. As a

comprehensive study of the LIM gene family in maize is lacking, this thesis reports a genome-wide analysis of LIMs and further investigates the functions of ZmLIM6/14 during PMII by generating CRISPR-Cas9 knock-out mutants and identifying their importance at the cell biology and molecular levels.

.

CHAPTER 2. HEAT STRESS EFFECTS ON UNI- AND BICELLULAR STAGE

- I performed all experiments and this chapter was written by Dr. Kevin Begcy and me

2.1 Introduction

Global warming is generating heat waves hotter, longer, and more frequent. When these high temperature episodes occur during reproductive development significant decrease in yield is commonly observed (Folsom et al., 2014; Chen et al., 2016; Begcy et al., 2018). Within reproductive development, male gametophyte formation is one of the most susceptible stages. In angiosperms, male gametophyte development undergoes two phases, microsporogenesis and microgametogenesis. During microgametogenesis, two rounds of mitotic division give rise to a tricellular pollen grain. The first division, known as pollen mitosis I (PMI), is asymmetric and produces a small generative cell and a large vegetative cell. Throughout PMI, while the small generative cell goes through symmetric division, pollen mitosis II (PMII), the large vegetative cell enters into the G0 phase of mitosis and stops its division. Thus, a mature pollen grain contains two small sperm cells engulfed by a large vegetative cell. In most gymnosperms, sperm cells are non-motile and thus are only able to move through the pollen tube to reach the ovule. After pollen germination, sperm cells travel along the pollen tube as a male germ unit separating before fertilization.

The symmetric division occurring during PMII is fundamental for the generation of the two sperm cells that will arise from the generative cell either within the pollen grain or after germination inside the pollen tube. To ensure accurate chromosome segregation and to produce two genetically identical cells during pollen mitosis II, cell clycle checkpoint mechanisms are executed along the process. During mitosis, the spindle-assembly checkpoint (SAC) is one of these mechanisms that safeguard the transition from the metaphase to the anaphase. SAC monitors the proper attachment of spindle microtubules to the surface of the kinetochores. In Arabidopsis, SAC architecture is different from the one characterized in yeast and animals. Also, plant cells are able to reset the cell cycle with duplicated chromosomes but no nuclear division. In maize, some of the major components of the SAC have been identified and showed conserved function. While the impact of heat stress on microgametogenesis have been

intensively investigated, little is known about sperm cell dynamics and behavior during heat stress and sperm cell release.

Reduction in fertilization and yield due to male gametophyte performance have been largely attributed to the lack of pollen viability or inability to germinate under high temperatures. Low starch content decreased enzymatic activity, energy and lipid formation are the main cellular process impacted by temperature. Here, this chapter showed that high temperature during bicellular stage of pollen development inhibits sperm cell formation. Spindle-assembly checkpoint hinders the transition from metaphase to anaphase due to the improper attachment of the microtubules to the kinetochore.

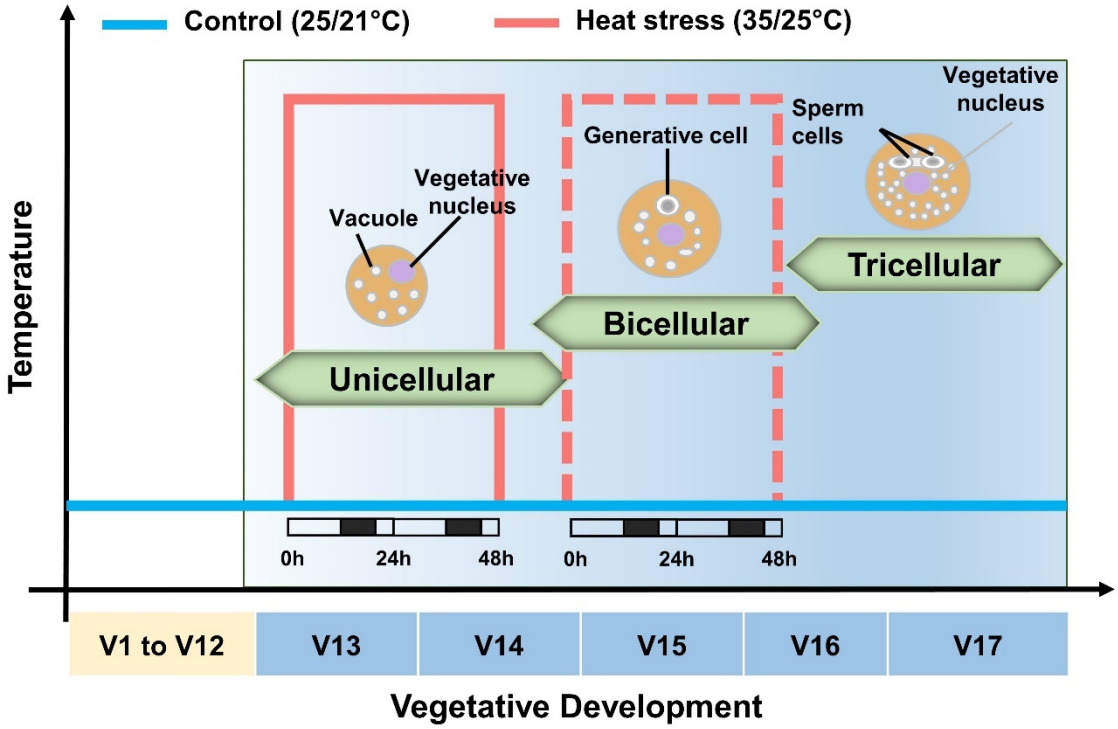

Figure 2.1 Schematic picture of Experimental setup. Maize plants were grown under control conditions, with a light/dark period of 25°C/21°C, until they reached the uni- or bicellular stage of pollen development. The specific stages were determined following the method described by (Begcy and Dresselhaus, 2017). At either stage V13-14 or V15-16, the plants were subjected to a moderate heat stress treatment, with a light/dark period of 35°C/25°C, for a duration of 48 hours. Subsequently, they were transferred back to the initial control conditions until reaching maturity. Red and blue lines represent the temperature regimes for heat stress and control, respectively

2.2 Materials and methods

2.2.1 Plant materials and growth conditions

Maize (Zea mays) B73 inbred line seeds were germinated in an incubator. After 10 days, they were transferred to a greenhouse and placed in larger pots (10 cm diameter) with 10 seedlings per pot. The pots contained a standard substrate and soil mixture (1:1, v/v). After 3 weeks, the maize seedlings were transplanted into 10L pots and grown under controlled conditions, 14 hours of light at a temperature of 25°C ± 2°C and 10 hours of darkness at 21°C ± 2°C, with a constant air humidity maintained between 60% and 65%. To adjust the duration of daylight, supplementary light with an intensity of approximately 20,000 lux was provided. An automated temperature-water-based irrigation system was used to supply water based on a preprogrammed schedule that considered plant water requirements. Twice a week, the plants were fertilized with Hakaphos at a concentration of 2% (w/v). The marker line plants followed a similar germination process, but they were genotyped before being transferred into larger pots. All plants, including both the B73 inbred line and the marker line, were monitored throughout their entire vegetative and reproductive development.

2.2.2 Heat stress treatment at the Uni- and Bicellular stage

Heat stress was applied during the bicellular stage of maize pollen development. The identification of pollen developmental stages was carried out using the Leaf Collar Method, which was previously described by (Begcy and Dresselhaus, 2017). Once the maize plants reached the bicellular stage, they were transferred to walk-in growth chambers. For the heat stress treatment, the growth chamber conditions were set at a temperature of 35°C/25°C (day/night) with a humidity of 60% and an illumination intensity of 25,000 lux, and this was maintained for a duration of 48 hours. In contrast, the nonstressed (NS) plants were kept under control conditions with a day/night temperature regime of 25°C/21°C, a humidity of 60%, and an illumination intensity of 25,000 lux. Following the 48-hour exposure to heat stress, all plants were returned to the aforementioned control conditions until pollen maturation occurred. At the bicellular stage, pollen samples were collected from both the control (NS) plants and the heat-stressed (HS) plants for morphological and physiological analyses. Samples for biochemical and RNA-Seq analysis, as well as pollen germination assays, were collected upon pollen maturation (Figure 2.1).

2.2.3 Maize pollen germination

Maize plants used for pollen germination experiments were placed close together to maintain similar conditions to ensure the good quality of the pollen harvested. For *In vitro* pollen germination, solid medium was prepared by mixing 2× Pollen germination media (PGM - 20% Sucrose; 0.005% H_3BO_3; 20mM $CaCl_2$; 0.1mM KH_2PO_4; 12% PEG4000, pH=5) liquid components and an equal volume of autoclaved 1.2% NuSieveTM GTGTM agarose (Lonza) to a final concentration of 0.6%. A total of 3mL of PGM medium mixture was pipetted into a 35mm petri dish and gently agitated horizontally to get a thin and evenly distributed medium layer after 10min solidification at room temperature (RT). Freshly collected pollen from NS and HS plants was obtained by softly shaking new released florets into petri dishes containing solid PGM. Pollen was germinated at room temperature (22-23°C) in a wet and dark chamber. The pollen germination status was monitored after 40-45 min on PGM and visualized on a Nikon Eclipse 1500 microscope with a 4x objective (Plan Fluor DL 4x/0.13, PHL) equipped with a Zeiss AxioCam MRM monochromatic camera.

In vivo pollen germination was carried out similarly as previously described (Martin, 1959) with some modifications. Maize ears before silking from NS plants were covered using small paper bags to prevent pollen contamination. Fresh pollen grains from NS and HS plants were harvested using a paper bag and used it to pollinate newly emerged silks. After one hour of *in vivo* pollen germination, a 5cm section from the top portion of the pollinated silk was cut and placed in a fixative solution (9:1 ethanol: acetic acid, v/v) at 4°C overnight. To rehydrate the fixed samples, a series of water solution were used. Next, the silks were subjected to a treatment with 8M NaOH for a period of 2-4 hours to clear and soften the tissue. Following the alkaline treatment, the softened silks were washed with water 2-4 times. For staining, the silks were immersed in an aniline blue staining solution (0.1% aniline blue; 0.1M $K_2HPO_4 \cdot 3H_2O$, pH=11) overnight at 4°C. After staining, the samples were washed and mounted on a microscope slide using fresh staining solution, and a cover slip was placed over them. Subsequently, the samples were analyzed under a fluorescence microscope (ZEISS Axio Imager 2) equipped with a 20× objective (Plan-Apochromat 20×/0.8 M27) using UV (350~400nm) excitation.

2.2.4 Maize sperm cell isolation

A discontinuous percoll density gradient centrifugation method was used as previously described (Dupuis et al., 1987)with some modifications. Fresh pollen grains from NS and HS B73 maize plants were harvested and placed into glass petri dishes, containing a moist filter

paper in the internal part of the lid. Pollen was allowed to pre-hydrate at room temperature for at least 2 hours. Then, immersed in 550mOsmol·kg^{-1} H_2O mannitol solution (100mg pollen/mL solution) and incubated on a platform shaker with slow agitation (80 rpm) for 1-2 hours. Pollen lysates were filtered in a 50mL Falcon conical tube equipped with a pluriStrainer 30 µM polyester mesh (PluriSelect) and a connector ring (PluriSelect) so that the samples could be force filtered using manual pressure using a syringe. Subsequently, a cleared lysate obtained from the filtering step was layered on top of a discontinuous 3 phase gradient percoll consisting of 30%/20%/15% (v/v) in 0.55mOsmol·kg^{-1} H_2O mannitol. Centrifugation was performed at 12,000g for 1h at 4℃. After density gradient centrifugation, the 20%/30% interphase, where sperm cells accumulated as a faint yellowish line, was collected using a pasteur pipette and transferred to a 10× volumes 0.55mOsmol·kg^{-1} H_2O mannitol, followed by centrifugation at 2,500×g to wash out pollen organelles and other cytoplasmic contaminants. The pelleted sperm cells were resuspended in 20µL of 0.55mOsmol·kg^{-1} H_2O mannitol and the number of isolated sperm cells was assessed using a cell counting chamber (Thoma). Isolated sperm cells were used immediately or shock-frozen in liquid nitrogen and stored at −80°C.

2.2.5 RNA isolation and RT-qPCR

To ensure good RNA quality, all tubes and tips used during pollen RNA extractions were RNase-free and metal beads were autoclaved. Working bench and pipettes were also cleaned with RNase Zap ® RNase Decontamination Solution (Thermo Fisher Scientific). Total RNA was isolated from NS and HS sperm cells or pollen grains using the Invitrogen™ TRIzol™ Plus RNA Purification Kit (Thermo Fisher Scientific). Approximately, 0.2g pollen were collected in a 2mL microcentrifuge tube with one metal balls inside. Samples were frozen in liquid nitrogen and ground to powder using a TissueLyser II (Qiagen). Follow by adding directly to each sample, 1mL of TRIzol™ Reagent and vortexed adequately. After 5min incubation at RT, 200mL of chloroform were added. After inverted several times and incubated for 2-3 min, samples were centrifuged 15min at 12,000g at 4°C. Around 600µL upper colorless layer supernatant containing RNA was transferred to a new tube and mixed with equal volume of 70 % ethanol by inversion. The mixture was transferred into spin cartridge provided by the kit and centrifuged at 12,000g for 15seconds. To remove DNA contamination, RNase free DNase solution (QIAGEN) were added to each column and then centrifuged. RNA on the membrane were washed by sequentially washing buffers supplied with the kit. Total RNA was eluted out from membrane by adding 50µL pre-warm 60°C RNase-free water for high RNA yield. For quantification and quality control, isolated RNA was photometrically analyzed using the

Nanodrop ND 100 (Thermo Fisher Scientific) and stored at-80°C. Complementary DNA (cDNA) synthesis was performed using 1µg of total RNA using Oligo (dT) 18 primer (Thermo Fisher Scientific) and Reverse Transcriptase (RevertAid™ reverse transcriptase, Thermo Fisher Scientific) according to the instruction as previously described (Preciado et al., 2022). For normalization, a ubiquitin gene (GRMZM2G102471) was employed as a control. PCR reactions were conducted in a 96-well reaction plate using the Master Cycler realPlex2, following the manufacturer's instructions. The primers used are listed in Supplemental Table-1. The cycling parameters consisted of an initial denaturation step at 95°C for 5 minutes, followed by 40 cycles of denaturation at 95°C for 15 seconds, annealing at 60°C for 30 seconds, and extension at 70°C for 30 seconds. Each RNA sample was subjected to triplicate reactions, and a minimum of three biological replicates were used. The specificity of the amplifications was confirmed by analyzing the melting curves. The data obtained from the Master Cycler realPlex2 detection system were further analyzed using Microsoft Excel, following the method described (Kim et al., 2021). The relative mRNA levels were determined using the $2^{-\Delta\Delta Ct}$ method, where the threshold points (Ct values) located within the log-linear range of RT-qPCR amplification plots were used for calculation.

2.2.6 Microscopy

Pollen grains at the bicellular stage of development were isolated using the method described (Begcy and Dresselhaus, 2017). The isolated pollen was then placed on glass slides containing a 1mg/mL DAPI solution in 1× phosphate-buffered saline (PBS, 0.8% (w/v) NaCl, 0.002% (w/v) KCl, 0.014% (w/v) Na_2HPO_4, and 0.0024% (w/v) KH_2PO_4). A cover slip was applied to the slides, which were sealed and observed using a Zeiss Axio Imager Z1 microscope equipped with structured illumination microscopy (Apotome) and a Zeiss AxioCam MRM monochromatic camera. DAPI fluorescence was excited using a filter set with a wavelength of 359 nm.

2.2.7 Biochemical assays

Freshly harvested mature pollen grains from both NS and HS plants were subjected to cytological analysis to assess their metabolic viability. The pollen grains were stained with FDA (fluorescein diacetate). Following staining, the pollen grains were examined using a fluorescent microscope equipped with a fluorescein isothiocyanate (FITC) filter, which allowed detection of fluorescein. The excitation filter used had a wavelength of 450 nm, and the emission filter

had a wavelength of 520 nm (both filters were from Zeiss). Pollen grains that exhibited fluorescence in the FITC channel were considered metabolically active.

2.2.8 Library preparation and RNA-Seq

Library preparation and RNA-Seq were conducted following the protocols in the Illumina TruSeq Stranded mRNA Sample Preparation Guide, the Illumina HiSeq 1000 System User Guide (Illumina), and the KAPA Library Quantification Kit-Illumina/ABI Prism User Guide (Kapa Biosystems). In brief, 250ng of total RNA from each of the three biological replicates of NS and HS sperm cells was used for purifying poly-A-containing mRNA using poly-T oligo-attached magnetic beads. After purification, the mRNA was fragmented to achieve an average insert size of 200-400 bases using elevated temperature and divalent cations. The resulting cleaved RNA fragments were reverse transcribed into first-strand cDNA using reverse transcriptase and random hexamer primers, with the addition of Actinomycin D to improve strand specificity. Subsequently, blunt-ended second-strand cDNA synthesis was performed using DNA Polymerase I, RNase H, and dUTP nucleotides. Adenylation of the resulting cDNA fragments at their 3' ends and ligation with indexing adapters were carried out, followed by PCR enrichment to create specific cDNA libraries. Libraries were quantified using the KAPA SYBR FAST ABI Prism Library Quantification Kit (Kapa Biosystems). Equimolar amounts of each library were used for cluster generation on the cBot instrument with the Illumina TruSeq PE Cluster Kit v3. Sequencing was performed on a HiSeq 1000 instrument using the indexed, 50 cycles paired-end read (PR) protocol and the TruSeq SBS v3 Reagents according to the Illumina HiSeq 1000 System User Guide. Image analysis and base calling generated bcl files, which were then converted into fastq files using the bcl2fastq v2.18 software. The library preparation and RNA-Seq procedures were conducted at the the Genomics Core Facility “KFB - Center of Excellence for Fluorescent Bioanalytics” (University of Regensburg, Regensburg, Germany).

2.2.9 Data processing, mapping, differential expression, and statistical analysis

Quality trimming and filtering of the RNA-Seq paired-end reads (PRs) were performed using Trimmomatic v.0.35 (Bolger et al., 2014). FastQC was used for data quality assessment. The processed PRs were aligned to the maize reference genome sequence AGPv3 assembly with annotation release-5b+ (corresponding to Gramene AGPv3.27) using the mapping program STAR v. 2.5.2a (Dobin et al., 2013). The alignment results were summarized per gene by identifying read pairs aligned to exonic regions with featureCounts (Liao et al., 2014). Reads

overlapping with multiple features (gene regions) were excluded from the analysis. To evaluate batch effects and outliers, raw counts were variance-stabilizing transformed and nonmerged technical replicates were analyzed using the R package DESeq2 (Love et al., 2014). Differential expression analysis was conducted using DESeq2 for pairwise comparisons based on the number of reads aligned to the genes. The thresholds for identifying differentially expressed genes (DEGs) were set at fold change >2 and adjusted $P < 0.05$ (after false discovery rate correction for multiple testing). For gene ontology analysis, the online tool agriGO(Du et al., 2010) was used.

To investigate transcriptional correlations among genes with shared expression profiles in nonstressed and heat-stressed pollen, the R package WGCNA (Langfelder and Horvath, 2008) was employed, implementing the cor function. Genes exhibiting shared expression profiles were considered seed candidates, and the STRING 10.5 database (Szklarczyk et al., 2015) was utilized to obtain direct and indirect interactions among them. Cluster correlation analysis was performed with a high confidence score threshold of 0.7, extracting only interactions with high levels of confidence from the database as valid.

2.2.10 Protein extraction and LC–MS/MS analysis

Mature pollen grains from NS and HS plants at the bicellular stage of maize pollen development were subjected to proteomic analysis. For protein extraction, 50 mg of pollen grains were ground with liquid nitrogen in a mortar and then dissolved in 250 µL of ice-cold extraction buffer (50 mM Tris/HCl, 150 mM NaCl, 0.1% sodium deoxycholate, 0.1% Triton-X100, 1 mM PMSF, pH 8.0). The proteomic analyses were performed following the methods described (Pfab et al., 2017). In brief, the total proteins from NS and HS pollen were separated on a 10% SDS-PAGE gel using the PageRuler™ Prestained Protein Ladder as a molecular weight marker (Thermo Fischer). After in-gel digestion with trypsin (Promega), the resulting peptide mixtures were loaded onto the UltiMate 3000 RSLCnano system, which was connected to an Orbitrap Elite hybrid mass spectrometer (Thermo Fisher Scientific). MS data were acquired using a data-dependent strategy that selected up to the top 10 precursors for higher-energy collisional dissociation (HCD) fragmentation. The analysis of the mass spectrometric raw data files was performed using the Proteome Discoverer software (Thermo Fisher Scientific; version 1.4), utilizing in-house Mascot (Matrix Science; version 2.6) and Sequest search engines. MS/MS ion searches were conducted against the UniProt and the Gramene protein database for maize (*Zea mays* L). Post-processing of search results was performed using Percolator. Peptides with

a q value < 0.01, rank 1, and a minimum length of 6 amino acids were considered. Protein abundance was determined using the protein area calculated by the Proteome Discoverer software (Thermo Fisher Scientific; version 1.4).

2.2.11 Statistical analysis

Statistical analyses for cellular, biochemical, and molecular data were performed using R software/environment. For all measurements, data from at least four independent experiments were used. Data represented mean and median values including standard deviations. Wilcoxon's singed-rank test was used to compare gene expression between HS and NS plants (Kim et al., 2021). Differences in means were considered significant at p-value < 0.05.

2.3 Results

Historically, pollen development studies under heat stress are performed across several developmental stages and occasionally through the entire pollen formation (Firon et al., 2006; Wang et al., 2017; Begcy et al., 2019; Wada et al., 2020). By dissecting developmentally the impact of heat stress on a single pollen stage, our group previously showed that heat stress during tetrad stage of pollen development impact starch, lipid, and energy biosynthesis transcriptionally and metabolically (Begcy et al., 2019). To elucidate whether heat stress triggers similar responses during uni- and bicellular stage of pollen development, a moderate heat stress (35°C/25°C light/dark period) for 48h was imposed on maize plants, specifically at the bicellular stage (Begcy and Dresselhaus, 2017). A parallel set of maize plants was maintained under optimal growth conditions (25°C/21°C light/dark period) in a parallel chamber and was used as a control for all experiments (see Figure. 2.1 for the experimental setup).

2.3.1 Unicellular stage pollen shows similar HSR with tetrad stage pollen.

Based on the approach, it was imperative to assess pollen viability and status using DAPI, FDA, and Alexander staining methods immediately after heat stress (Figure 2.2). The nuclei were stained with DAPI, and the numbers indicated the pollen developmental stages. Compared to nonstressed (NS) pollen, 63% of the pollen remained at the unicellular stage, whereas heat stressed (HS) pollen had progressed to the bicellular stage at 35%, and 11% had reached the tricellular stage (Figure 2.2G). This indicated that heat stress accelerated pollen development.

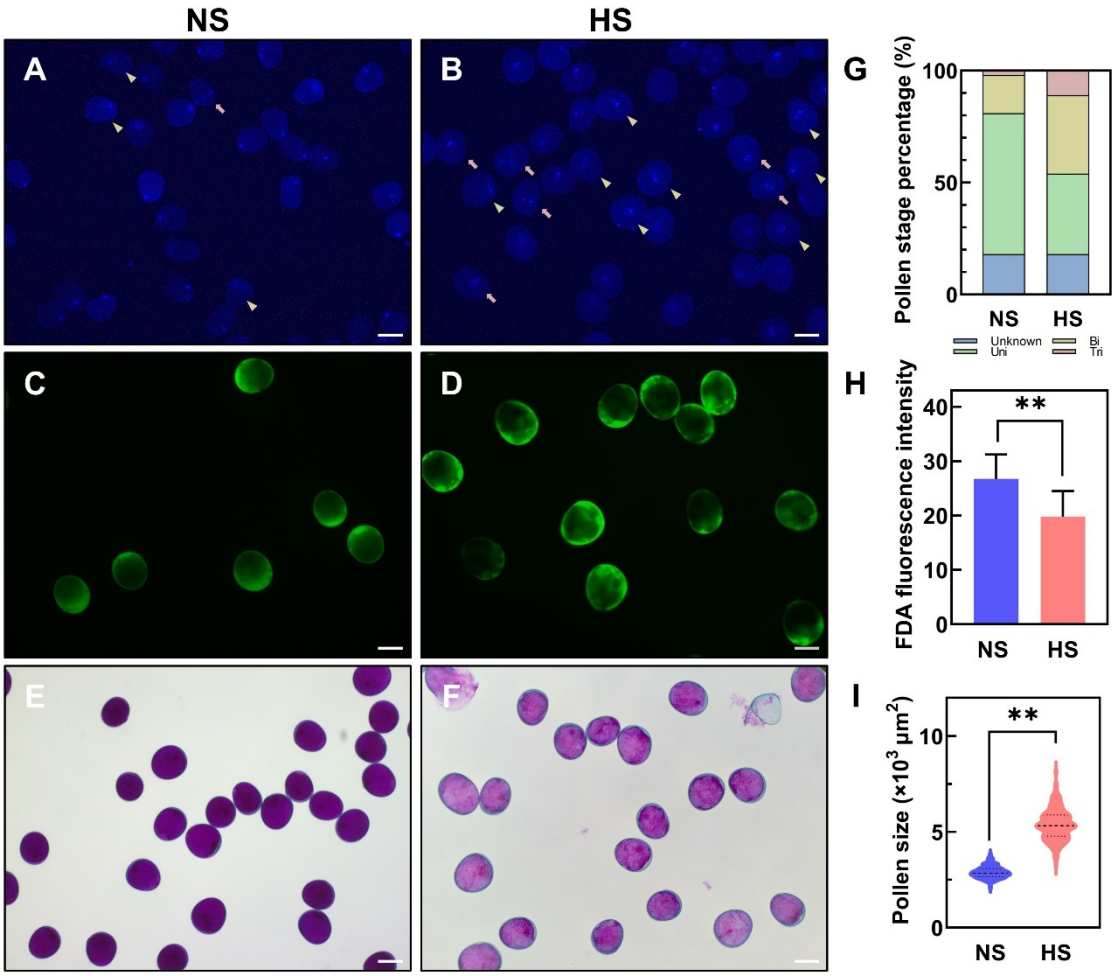

Figure 2.2 Viability test of nonstressed (NS) and right after heat stressed (HS) pollen. Pollen developmental stage was determined by DAPI staining (A&B) and quantified based on numbers, N=350 (G). Pollen cell enzymatic activity and abortion level was tested by FDA staining(C&D) and Alexander staining(E&F), correspondingly the fluorescence average intensity (H) and pollen size (I) comparisons between treatments showed. Triangle indicated bicellular stage pollen. Arrow indicated tricellular stage pollen. The asterisks indicate a significant difference at $P < 0.001$; one-tailed t test comparing heat-stressed samples to nonstressed samples. Data are presented as the mean ± SD Scale bar = 50μm.

By using Fluorescein Diacetate (FDA) as a viability probe, the staining fluorescence intensity indicated the level of pollen enzymatic activity. NS pollen displayed a strong signal on one side, while the middle part showed weak green, indicating that biological activity in unicellular pollen mainly occurred around the edge area. HS pollen showed a similar pattern, but the fluorescence accumulated in separated blocks rather than being evenly distributed. However, the average fluorescence intensity of HS pollen was significantly reduced (Figure 2.2H). To determine the pollen abortion level, Alexander staining was performed on pollen immediately

after heat stress. The color density in single pollen clearly showed that HS pollen had different levels of abortion. Due to faster development affected by heat stress, the pollen size also remarkably increased.

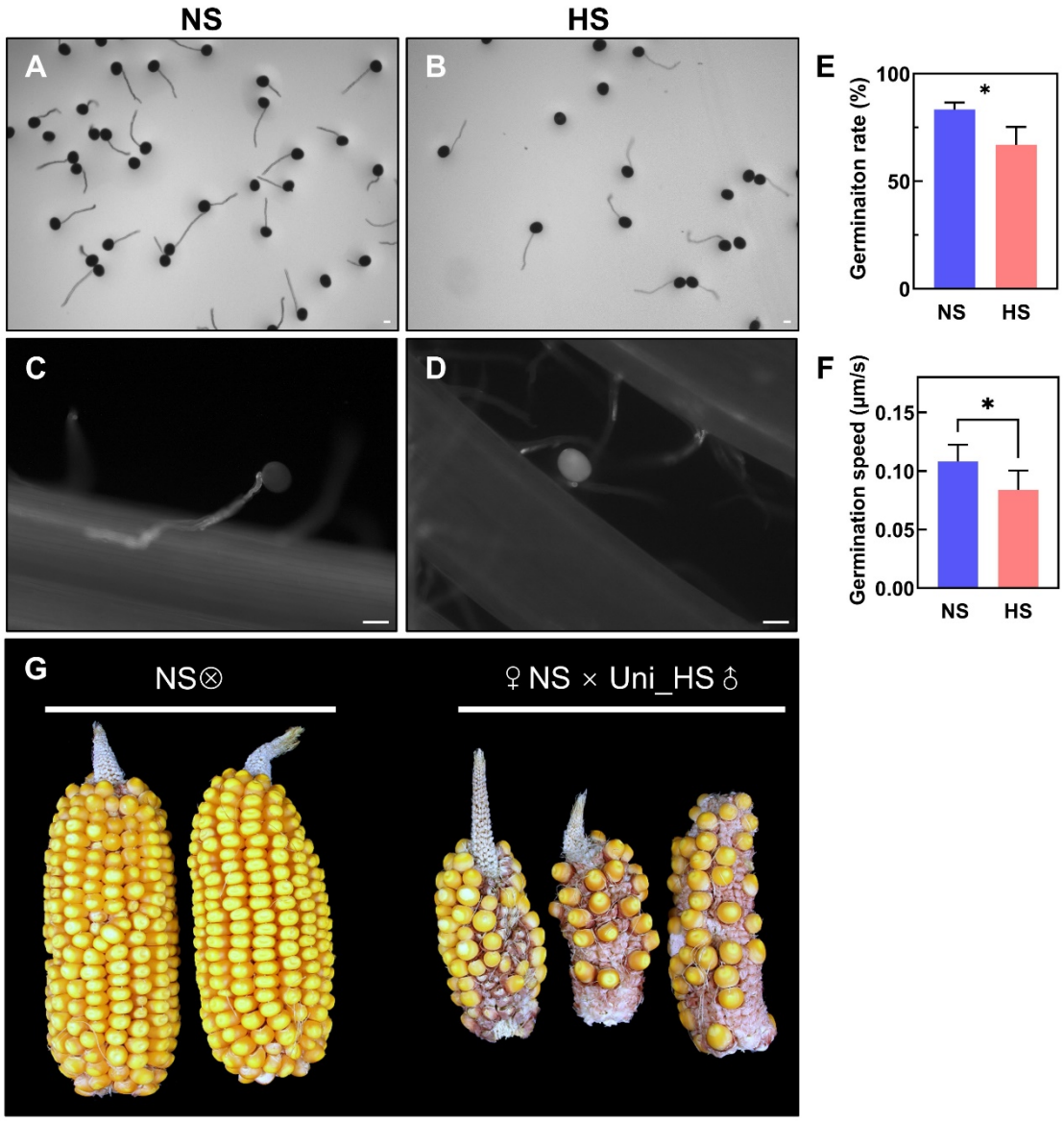

Figure 2.3 Germination and fertilization ability test of NS and HS mature pollen. pollen germination ability was investigated by *in vitro* germination (A&B) and *in vivo* germination (C&D) experiments. Germination rate (E) and germination speed (F) was quantified based on *in vitro* germination results of different treatment pollen. Pollination experiments with NS pollen and unicellular stage HS pollen harvested different level seed set cobs(G). The asterisks indicate a significant difference at $P < 0.01$; one-tailed t test comparing heat-stressed samples to nonstressed samples. Data are presented as the mean ± SD. Scale bar = 50μm.

When pollen development reached the mature stage, the germination and fertilization ability became the most important indicators to evaluate the pollen quality (Figure 2.3). *In vitro* germination was used to quantify the germination rate and germination speed between NS and HS treatments. Normally, the germination rate of NS pollen was ~83%. However, when pollen was subjected to heat stress during the unicellular stage, the germination rate was reduced to 63% (Figure 2.3 A&B). Additionally, the germination speed, which was measured by the length of the pollen tube in 45 minutes, was significantly slower after heat stress treatment. Moreover, an *in vivo* germination experiment was conducted to investigate the pollen penetration ability on silk. Unexpectedly, some HS pollen could attach to the silk, but they were unable to grow a tube into the silk to deliver sperm cells for successful double fertilization (Figure 2.3 C&D). Cobs pollinated by NS pollen produced a full set of seeds, whereas cobs pollinated by HS pollen resulted in more than half of the seeds being empty due to failed fertilization (Figure 2.3 G).

2.3.2 Starch and pollen morphology do not change after heat stress at the bicellular stage of pollen development

At the bicellular stage of pollen development, the effect of heat stress on pollen morphology was firstly explored after treatment (Figure. 2.1). Interestingly, no morphological alterations were observed. HS pollen grains resembled NS pollen (Figure. 2.4 A&B). Since a decrease in starch accumulation is one of the main effect of heat stress on pollen grains (Begcy et al., 2019; Firon et al., 2006), it was tested whether a similar reduction would be observable after high temperatures at the bicellular stage of pollen development (Figure. 2.4 C&D). Both HS and NS pollen was stained with Alexander staining (Figure. 2.4C&D). There were not any major differences observed between the pollen grains grown of both conditions. Then whether heat stress at the bicellular stage could impose differences in enzymatic activity. Therefore, fluorescein diacetate (FDA) staining was carried out and did not detect significant fluorescence differences between HS and NS pollen grains (Figure. 2.4E&F). Quantification of the fluorescence intensity corroborated the visual observations where no statistical differences were detected (Figure. 2.4L). These results suggest that heat stress at the bicellular pollen does not impact starch accumulation nor enzymatic activity. This could be due to the fact that starch accumulation starts at the unicellular stage and peak during early bicellular stage (De Storme and Geelen, 2014). Therefore, high temperatures solely after the bicellular stage might not be sufficient to impact a cellular process already preprogramed and executed. In summary, our results show that pollen morphology in maize is not altered after transient heat stress at the bicellular stage of pollen development.

2.3.3 Heat stress accelerates pollen development

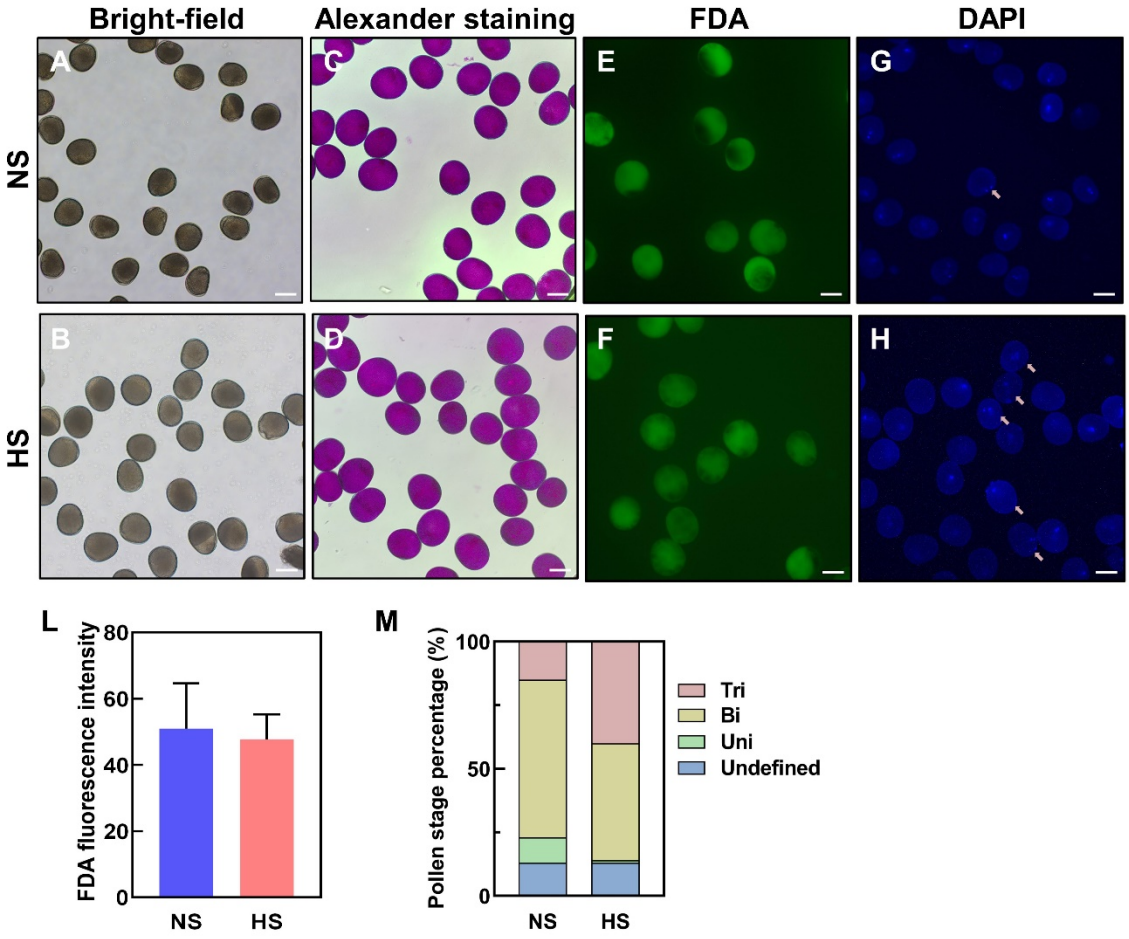

Figure 2.4 Heat stress effects on bicellular stage pollen. A and B, Bright-field images of NS and HS pollen right after treatment, respectively. C and D, Light microscopic images of NS (D) and HS pollen (E) stained with Alexander staining. E and F, Mature pollen stained with FDA in NS (E) and HS pollen (F). G and H, Microscopic images of NS (G) and HS pollen (H) stained with DAPI at bicellular stage of pollen development. Arrow indicated tricellular stage pollen. L, Quantification of enzymatic activity in NS and HS pollen at maturity. M, Characterization of pollen developmental stages after heat stress was applied at bicellular stage. Blue, undefined stage, green, unicellular stage, yellow, bicellular stage and red, tricellular stage of maize pollen development. Data are presented as the mean ± SD. Scale bars = 50μm**.**

Since the initial analysis did not show any morphological effect of heat stress applied at the bicellular stage of pollen development, a closer look at the developmental progression of pollen after heat stress was conducted. The NS and HS pollen at the bicellular stage immediately was harvested after heat exposure (Fig. 2.4 G&H) and stained pollen grains with DAPI (4′,6-diamidino-2-phenylindole). It was observed that pollen developed in NS conditions were

mostly at bicellular stage (Fig. 2.4 G&M). Pollen at the unicellular (10%) and tricellular (15%) stage were also observed (Fig. 2.4 G&M). In contrast, HS pollen showed almost no pollen at unicellular stage (1%) and most pollen at the bicellular (46%) and tricellular (39%) stage (Fig. 2.4G&M). These results indicate that heat stress speed up normal timing of pollen development.

2.3.4 Heat stress at the bicellular stage of pollen development does not impact pollen germination properties but reduce yield.

To further explore the impact of heat stress at the bicellular stage of pollen development, the heat-stressed plants were transferred to non-stressed conditions and allowed both sets of plants to continue their development until pollen maturation (Figure. 2.1). When pollen mature, *in vitro* germination with both HS and NS pollen was carried out on germination media (Figure. 2.5). No differences were observed in pollen developed in any of both conditions (Figure. 2.5A&B). Since the initial pollen germination assays were carried out in artificial conditions (Figure. 2.5A&B), *in vivo* pollen germination assays were performed by pollinating non-stressed maize silks with pollen of NS and HS plants (Figure. 2.5C&D). Similarly, as observed in the *in vitro* assays, heat stress at the bicellular stage did not alter pollen germination *in vivo*. Quantification of the germination assays showed not significant differences between both NS and HS conditions (Figure. 2.5E).

Pollen germination is a function of both speed and the length at which the pollen tube growth emerges through the pollen wall (Williams and Reese, 2019). Therefore, two important components of pollen germination are speed and pollen tube length. Thus, pollen tube length (Figure. 2.5F) and pollen tube speed (Figure. 2.5G) were quantified after heat stress at the bicellular stage. Interestingly, both processes of the pollen germination were also not impacted by heat stress.

Above cellular and biochemical data showed that heat stress at the bicellular stage did not alter pollen morphology, viability, germination, speed, or pollen tube length, indicating a potential pollen stage resilience to heat stress (Figure. 2.4&2.5). Therefore, it was expected a full seed set when crossing cobs of control plants with HS pollen. As expected, control cobs crossed with NS pollen showed full seed set (Figure. 2.5H). Surprisingly, when crossed HS pollen at the bicellular stage and control cobs, a strong reduction in the number of seeds per cob occurred (Figure. 2.5H). These unexpected results pointed out that even though no obvious alterations were observed in heat stressed pollen, heat stress at the bicellular stage negatively affects maize yield.

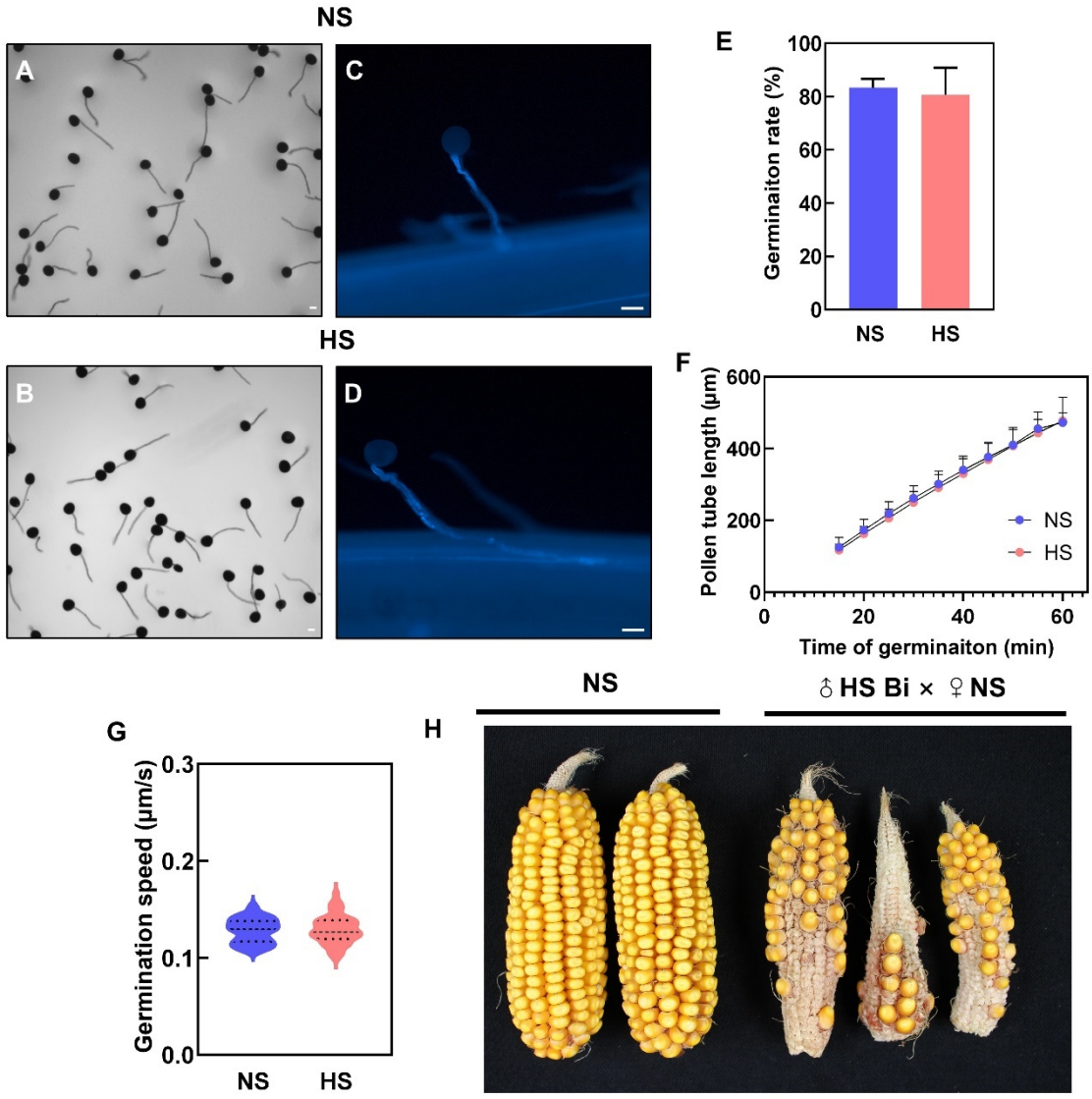

Figure 2.5. Pollen germination and fertilization ability test of HS during the bicellular stage. A and B, *in vitro* germination assays of pollen isolated from NS (A) and HS plants (B) show no germination rate differences. Scale bars = 50μm. C and D, Aniline blue staining of NS (C) and HS (D) pollen germinating on papilla hair cells. Scale bars = 100μm. E, Percentage of *in vitro* germination rate of pollen harvested from NS and HS plants. F, Pollen tube length and (G) germination speed of NS (blue) and HS (red) germinating pollen. H, NS cobs were pollinated with both NS pollen (NS × NS) and HS pollen (NS × HS). Data are presented as the mean ± SD. n = 400–500.

2.3.5 Heat stress disrupts sperm cell development and cargo delivery

To further elucidate the causes of the strong seed set reduction without noticeable changes in the cellular and biochemical properties of heat stressed pollen (Figure. 2.4-2.5), the developmental processes occurring at the transition between the bicellular to the tricellular stage of maize pollen development was explored. Bicellular stage is a transient developmental stage in which two cellular components are clearly visible, the generative and vegetative nucleus. In addition, the number of vacuoles increase due to their fragmentation. During the transition to the tricellular stage, the generative cell undergoes mitosis giving rise to two sperm cells which during fertilization will fuse with the central cell and the egg cell to form the endosperm and the embryo, respectively (Zhao et al., 2017). Therefore, since the formation of the two sperm cells is the main developmental process occurring at the bicellular stage, it was hypothesized that heat stress might impact sperm cell development. To test this hypothesis, a maize sperm cell marker line was used (Kliwer, et al., 2009). This maker line uses α-tubulin gene fused with the yellow florescence protein (YFP) with exclusive labeling of sperm cells inside mature

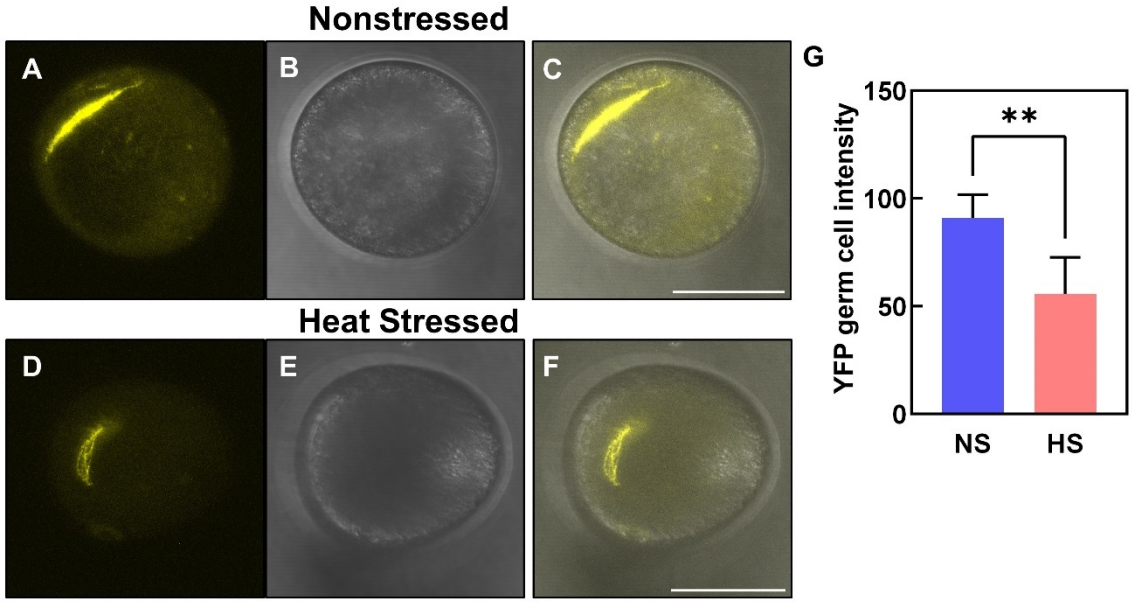

Figure 2.6 Heat stress impairs sperm cell development. A-F. Confocal images of NS (A-C) and HS pollen (D-F) at bicellular stage of pollen development. C and F, display merged images of NS (A and B) and HS pollen (D and E). Normal sperm cell spindle shape is observed in NS pollen (A-C). Impaired sperm cell development is shown in HS pollen (D-F). G, Quantification of YPF sperm cell intensity of NS and HS pollen at bicellular stage. The asterisks indicate a significant difference at $P < 0.001$; one-tailed t test comparing HS samples to NS samples. Scale bars = 50μm.

pollen grains. Thus, this maker line is an ideal tool to investigate the impact of heat stress at the bicellular stage of pollen development.

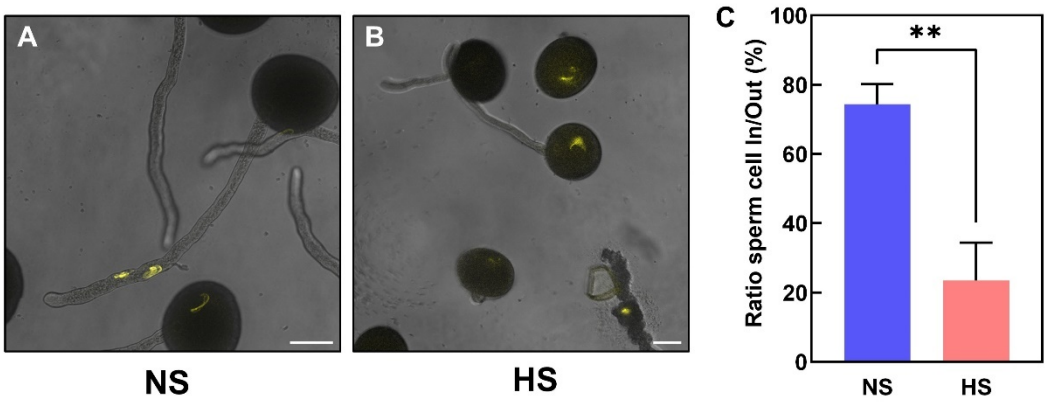

Figure 2.7 Heat stress inhibits sperm cell traveling through the pollen tube. A, Confocal images of NS pollen grains showing sperm cells travelling through the pollen tube. B, Sperm cells kept inside the pollen grain after heat stress was applied at bicellular stage of pollen development. C, Quantification of ratio of sperm travelling outside or kept inside of the pollen grain of NS and HS pollen at bicellular stage. The asterisks indicate a significant difference at $P < 0.001$; one-tailed t test comparing HS samples to NS samples. Scale bars = 50µm.

Under NS conditions, the α-Tubulin-YFP signal was identified after the first mitotic division in the generative nucleus during microsporogenesis (Figure. 2.6 A-C). The generative nucleus then divided to form two sperm cells with similar YFP signal intensity. In contrast, the α-Tubulin-YFP signal in HS pollen was reduced and the spindle shape structure was not visible clearly (Figure. 2.6 D-F). Quantification of α-Tubulin-YFP signal in HS and NS sperm cells showed significant differences between pollen in both conditions (Figure. 2.6 G). These results demonstrate even though the morphology of heat stressed pollen did not change, the sperm cell development was impaired.

To further analyze whether the sperm cells are able to travel through the pollen tube, the sperm cell journey was monitored using the α-Tubulin-YFP marker line (Figure. 2.7). Under NS conditions, it was observed a clear YFP signal in the two formed sperm cells travelling through the pollen tube (Figure. 2.7A). Remarkably, most of the sperm cell(s) of HS pollen remained inside the pollen grain and did not travel through the pollen tube (Figure. 2.7 B&C). From a fertilization perspective, sperm cells are needed for a successful process. The lack of sperm cell movement impacts the number of seeds produced since there is no genetic material contribution

from the male side (Figure. 2.5H and Figure. 2.7 B&C). These results indicate that the reduced feralization observed after crossing heat stressed pollen at the bicellular stage with control cubs are most like caused by disruption of the sperm cell development.

2.3.6 Heat stress impacts sperm cells transcription, RNA processing, and translation during bicellular pollen development

In order to elucidate the molecular mechanisms impacted by hear stress during maize sperm cell development, an RNA-Seq approach was applied to further analyze the transcriptional changes imposed by increased temperatures in sperm cells. First, the maize sperm cell isolation was conducted using a percoll gradient strategy (Chen et al., 2017). Approximately 5000 individual sperm cells were isolated in each of the three biological replicates of both NS and HS samples (Table 2.1). It was found 952 genes differentially expressed between NS and HS sperm cells samples collected at maturity (Figure. 2.8A). Within these genes, 267 were downregulated and 684 were upregulated. Gene ontology analysis showed enrichment of genes involved in chromosome and chromatin organization, DNA conformation, homeostasis, and purine-containing compound metabolic process. Previously, it showed that heat stress at the tetrad stage of maize pollen development induced the expression of several heat shock protein genes (HSPs) (Begcy et al., 2019). Thus, the sperm cells from mature pollen heat stressed at the bicellular stage was used to check whether a similar response was observed (Figure. 2.8 B). Even though, an overall low or non-expression of heat shock proteins (HSPs) and heat shock factors (HSFs) have been reported in maize sperm cells (Chen et al., 2017), a significant transcriptional increase was found in HSP11 (GRMZM2G306679), HSP70-3 (GRMZM2G145275) and HSP70-4 (GRMZM2G340251) expression after heat stress at the bicellular stage (Fig. 2.8B). HSP70-6 (GRMZM2G428391) was not induced in sperm cells after heat stress at the bicellular stage and was used as a control (Figure. 2.8B). Interestingly, two of the HSPs induced belongs to the HSP70 family. Hsp70s are molecular regulators of stress responses, as they maintain protein homeostasis by mediating protein folding and/or protein denaturation and have been shown to be active under abiotic stress conditions (Kim et al., 2021). Therefore, all the results suggest that short spikes of heat stress are able to trigger and maintain stress responses even if plants are exposed back to normal temperatures.

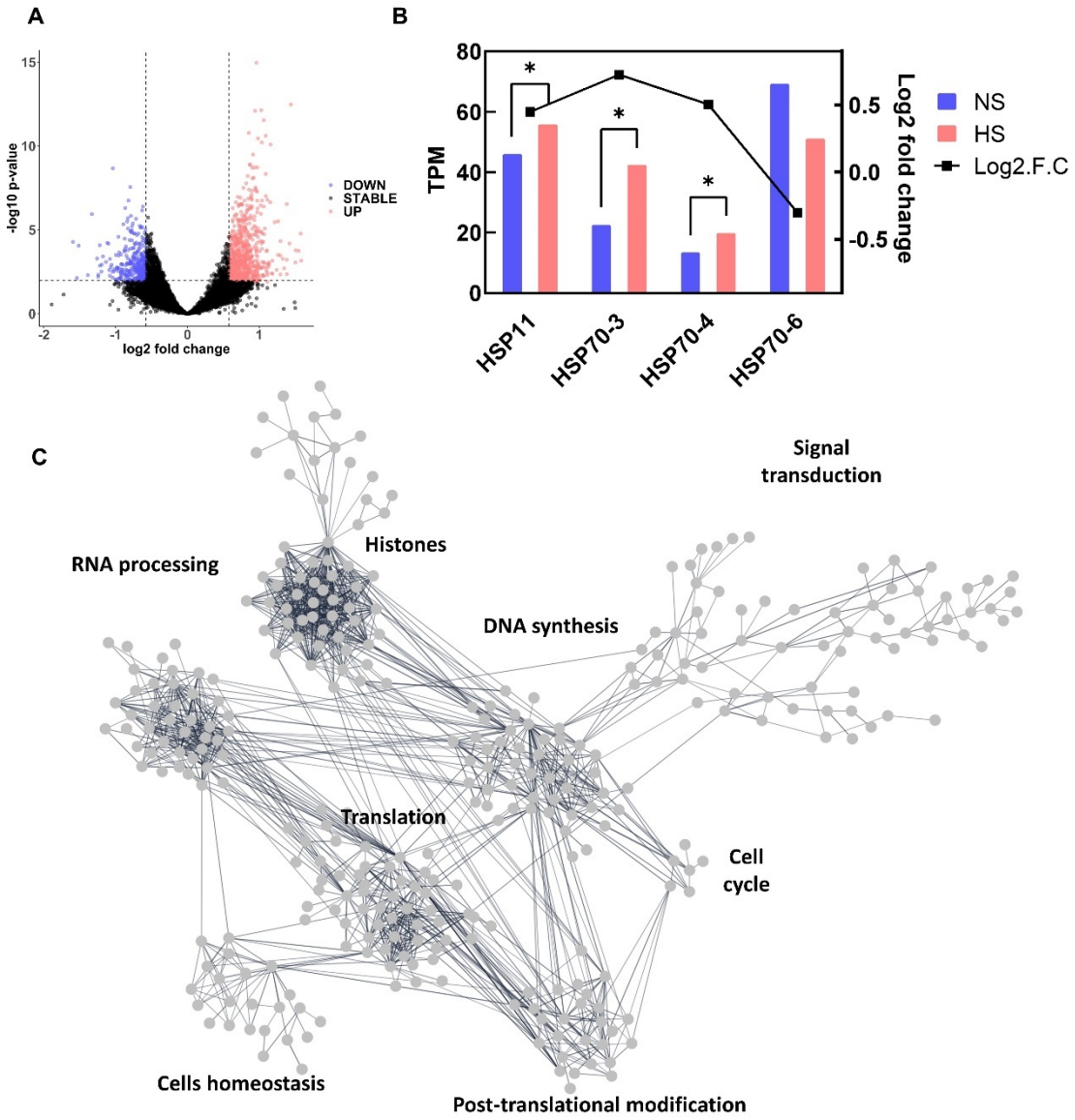

Figure 2.8 Heat stress misregulates replication associated genes in sperm cells. A, Differential gene expression (the base 2 logarithm fold change) in NS/HS sperm cells Red color indicates upregulation. Blue color indicates downregulation. Black color indicates no significant transcriptional changes. B, TPM vales and RT-qPCR analysis shows differential expression of HSP genes in sperm cells is still increased in mature pollen. The asterisk indicates significant difference at $P < 0.001$; one-tailed t test comparing HS to NS samples. n = 3 biological replicates, each with 3 technical replicates. C, Gene network analysis of interactions of differentially expressed genes in sperm cells in response to heat stress at bicellular stage. A threshold of 0.7 of edge confidence was used**.**

To further understand sperm cell development-associated genetic responses to heat stress, the list of differentially expressed genes were selected and conducted a cluster correlation analysis using the “cor” function implemented in the R package WGCNA to identify functional groups

of genes with shared expression profiles. To identify genes already described as member of any given pathway, the cluster correlation analysis was combined with the web-tool STRING (Szklarczyk et al., 2015). After removal of unrooted genes, the remaining rooted genes were queried in STRING, which identified 331 interacting genes associated with the heat stress response in sperm cells. An edge confidence of at least 0.7 was applied to selected sperm cells candidate genes. Previously using this approach, our group found five main clusters after heat stress during the tetrad stage of pollen development (Begcy et al., 2019). In this chapter, the analysis yielded 8 main hubs affected by heat stress in maize sperm cells (Figure. 2.8 C). Interestingly, these hubs are formed by genes related to histones, DNA synthesis, RNA processing, translation, post-translational modification, cell cycle and signal transduction (Figure. 2.8 C). during sperm cell formation active transcriptional and translational activity is needed to generate two viable sperm cells. Therefore, all the results suggest that heat stress at the bicellular stage impacts spermatogenesis.

2.3.7 Heat stress induces expression of highly expressed genes in maize sperm cells

To compare the transcriptional status of NS and HS sperm cells, the genome wide TPM values of both conditions were analyzed (Figure. 2.9A&B). When TPM values from the entire maize genomes are plotted, a high correlation ($R^2 = 0.9868$) in gene expression was obtained between NS and HS (Figure. 2.9B), suggesting that even though heat stress at the bicellular stage of pollen development impacts the transcriptional expression of maize sperm cells, the level of the changes is minor. However, this analysis also includes a larger portion of genes that are not expressed in any of the conditions. The sperm cell analysis of nonstressed and heat stressed yielded an average of 30% transcriptional expression of the entire maize genome in both conditions. No significant differences were observed when genes higher than 1 and lower than 100 TPM were used (Figure. 2.9B). However, when 100 TPM cutoff included to explore the transcriptional impact of heat stress on sperm cells, a lower correlation of TPM levels ($R^2 = 0.7477$) was found when only truly expressed genes were used in the analysis (Figure. 2.9C). When dissected the transcriptional response to heat stress using 150 TPM (Figure. 2.9D) and 200 TPM (Figure. 2.9E) cutoff and it was found that the impact was only significant in highly expressed genes. These results suggest that heat stress at the bicellular stage has a large effect mostly on highly expressed genes and therefore critical for sperm cell development.

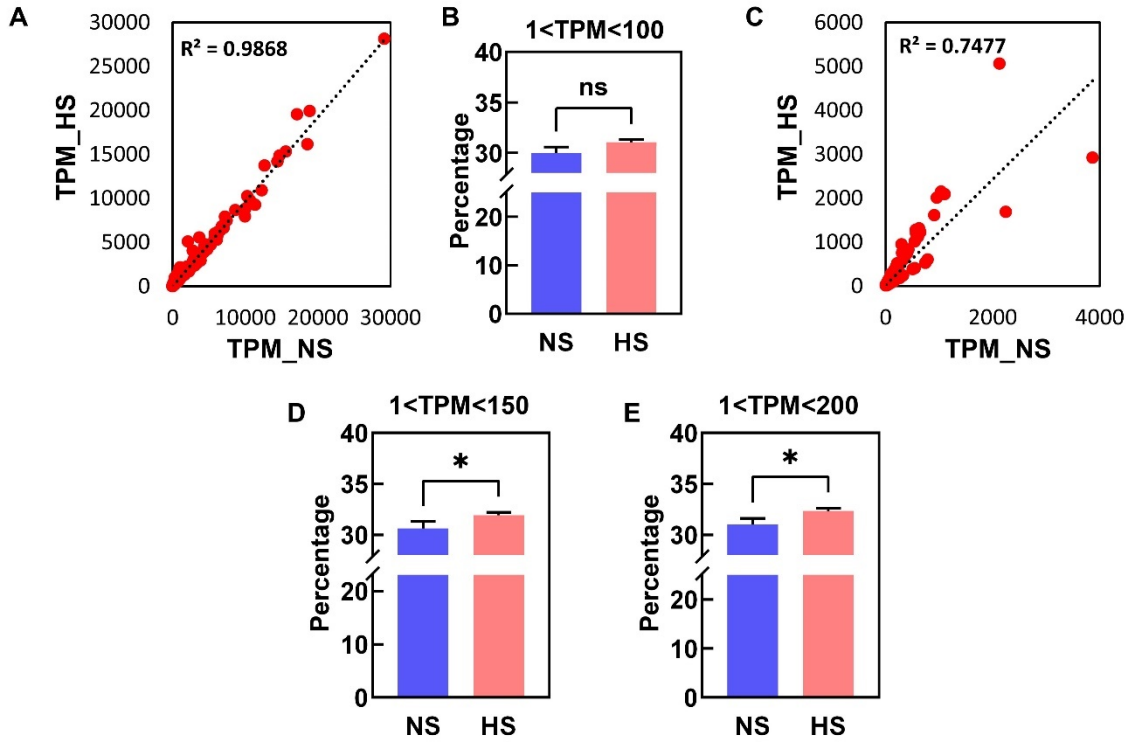

Figure 2.9 Heat stress alters transcriptional gene expression of highly expressed genes. A, Genome-wide comparison of TMP vales of HS and NS sperm cell genes. B, Percentage of genes expressed in NS and HS sperm cell samples using TPM values greater than 1 but lower than 100. C, comparison HS and NS sperm cell genes with TMP vales higher than 100. D and E, Percentage of genes expressed in NS and HS sperm cell samples using TPM values greater than 1 but lower than 150 (D) and greater than 1 but lower than 200. The asterisk indicates significant difference at $P < 0.001$; one-tailed t test comparing.

2.3.8 Heat stress alters pollen mitosis II during sperm cell development

Since our gene network analysis identified genes involved in spermatogenesis (Figure. 2.8C) as the main targets during heat stress at the bicellular stage, it was necessary to explored in more detail how heat stress affected the expression of genes involved pollen mitosis II (Figure. 2.10). it was found that heat stress induced, for instance, upregulation of the S-phase kinase-associated protein 1 (Skp), Cullin (CUL1), F-box containing (F-box) complex (SCF complex) and the anaphase promoting complex/cyclosome (APC/C) complex (Figure. 2.10A). Both, SCF and APC/C complexes are multimeric E3 ubiquitin ligase complexes that control the degradation of cell cycle regulators (Cyclin-dependent kinases - CDKs) to allow G1-to-S transition as well as S-to-G2 transition (Kim et al., 2008; Villajuana-Bonequi et al., 2019) and thus promoting

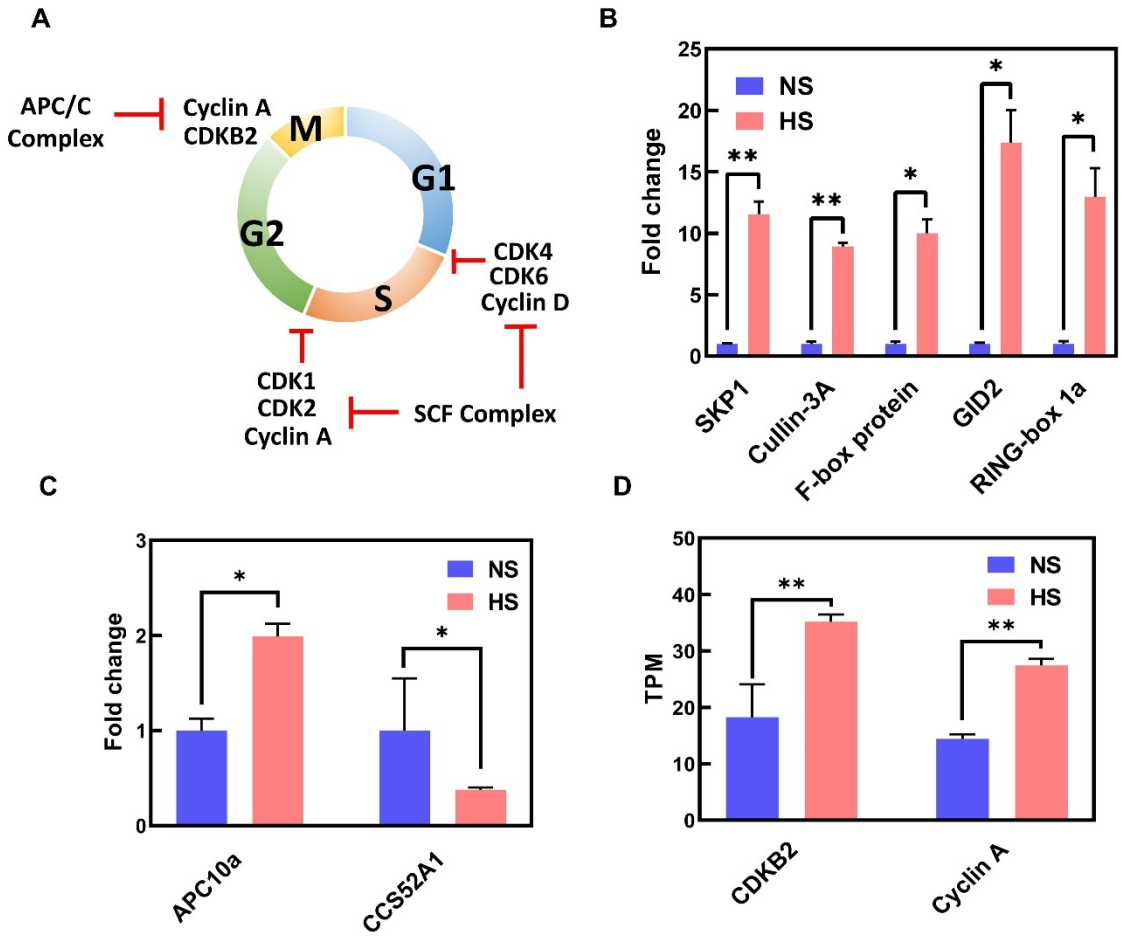

Figure 2.10 Heat stress induces upregulation of the (SCF) E3 Ubiquitin Ligase complex in sperm cells. A, Illustration of pollen mitosis II process and the regulation by cyclins and the SCF complex. B, Induction of the SCF members genes. C, misregulation of the APC/C complex. D. Upregulation of cyclins. The asterisk indicates significant difference at $P < 0.001$; one-tailed t test comparing heat-stressed (HS - red) to nonstressed (NS - blue) samples. n = 3 biological replicates, each with 3 technical replicates

cell cycle progression. In maize, the SCF complex is formed by SKP1 (Zm00001eb404320), CUL3A (Zm00001eb254590), F-box (Zm00001eb187770), F-box GID (Zm00001eb245180)

and Ring-box protein 1A (RBP1- Zm00001eb188540). Notably, all members of the SCF complex showed upregulation of more than 10-folds (Figure. 2.10B). Most members of the APC/C complex in maize had no sperm cell expression. However, APC10a (Zm00001eb342630), CCS52A1 (Zm00001eb001710) were upregulated after heat stress. Since the SCF and APC/C complexes regulate cyclins and CDKs controlling the progression of cell cycle, all maize CDKs in response to heat stress was searched. Out of the total number of cyclins and CDKs described in maize only three genes were differentially expressed in maize sperm

cells after heat stress ZmCycA1, ZmCycD4 and ZmCDKB2 (Figure. 2.10D). Noteworthy, these three genes were the only ones expressed in maize sperm cells under control conditions.

2.3.9 Heat stress activates spindle assembly check point (SAC) during sperm cell development

Since all data points towards a misregulation of genes involved pollen mitosis II, the developmental transitions involved in this process was further explored (Figure. 2.11A). Pollen mitosis undergoes the transition from prophase to prometaphase follow by metaphase, anaphase, telophase and finally cytokinesis (Figure. 2.11A). During the transition from metaphase to anaphase, where chromosomes aligned at the equator of the cell migrate to the poles, a developmental process ensures that all chromosomes are aligned at the same level. This process is control by the spindle assembly checkpoint (SAC) signaling which controls the proper partitioning of chromosomes to daughter cells during mitosis. The SAC signaling is a mechanism that it is only active when chromosomes are not properly attached to the kinetochores and thus delays the progression of the cell cycle until all kinetochores are correctly assembled (REF). It was found upregulation of Nuclear Division Cycle 80 (Ndc80), minichromosome instability 12 (Mis12) and mitotic arrest deficient 2 (Mad2), the genes part of the SAC signaling in maize, after heat stress at the bicellular stage (Figure. 2.11B). another member of the SAC signaling, budding uninhibited by benzimidazoles 3 (BUB3), did not change in response to heat stress (Figure 2.11B). These results indicate that heat stress activate SAC signaling. Therefore, microtubule related genes in the sperm cell data set were further searched. Nine microtubule related genes with TPM vales higher than 5 were identified and classified in two groups, microtube related signaling and microtubule function (Figure. 2.11C). Four of the microtube related signaling genes belong to the Phospholipase D family. Phospholipase D activation have been correlated with microtubule reorganization in living plant cells (Dhonukshe et al., 2003).All four Phospholipase D genes were downregulated in response to heat stress (Figure. 2.11C). Similarly, VILLIN3, a gene required for the generation of actin filament bundles (van der Honing et al., 2012) was downregulated after heat stress at the bicellular stage pollen development. Another microtube related signaling gene was a LIM gene (Zm00001eb268250). LIM genes encode for a cytoskeleton-associated protein that inhibit actin filament depolymerization and cross-links filaments in bundles. Downregulation of this gene was also found after heat stress (Figure. 2.11C). The last gene identified was adenylyl cyclase-associated protein (C-CAP) which similarly as all the other microtube related signaling genes was downregulated in response to heat stress (Figure. 2.11C). The only two genes

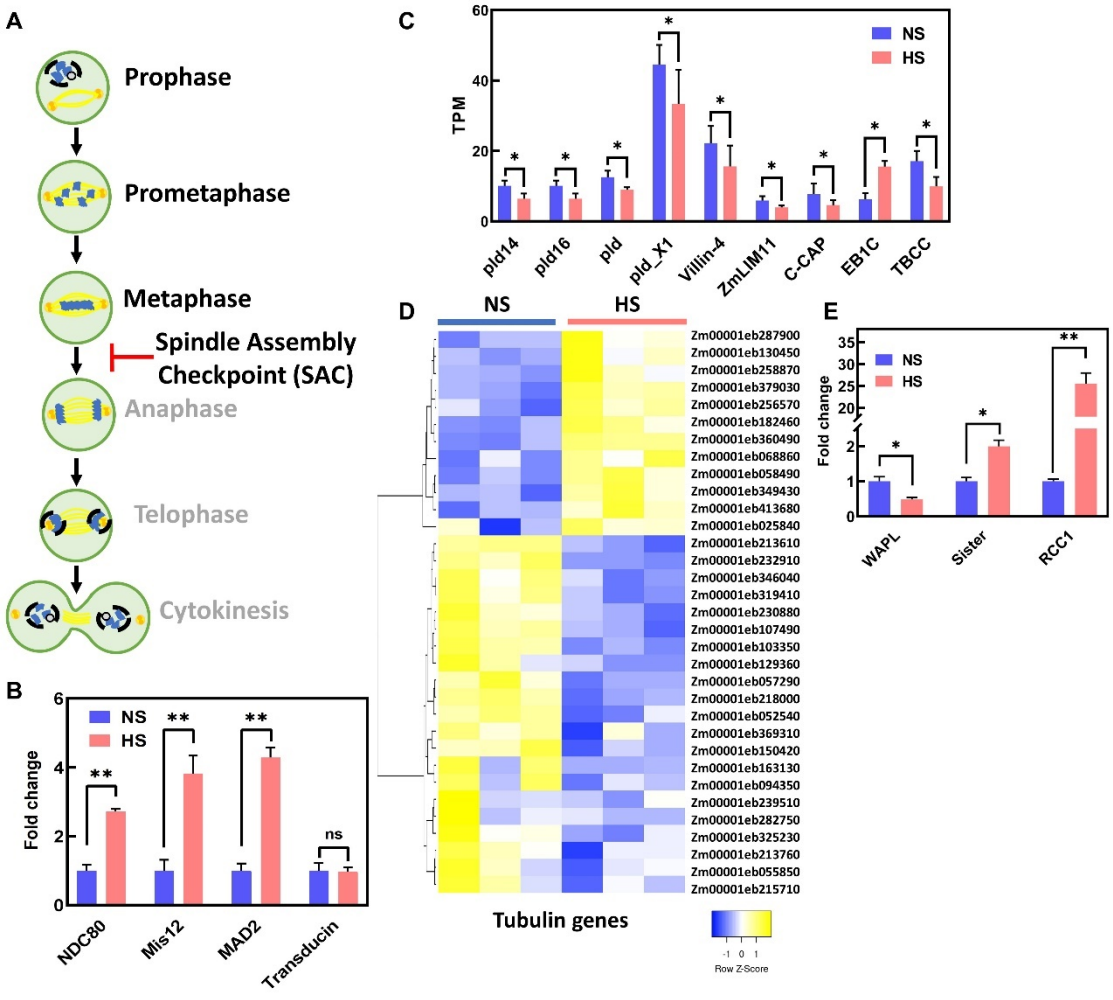

Figure 2.11 Activation of spindle assembly check point (SAC) during HS sperm cell formation. A, Illustration of SAC repressing generative cell division. B, Misregulation of genes involved in mitosis progression during the metaphase to anaphase transition. WAPL, Wings apart-like protein homolog. RCC1, regulator of chromosome condensation 1. Sister, Sister chromatid cohesion 1. C, Upregulation of SAC gene members after heat stress. NDC80, NDC80 kinetochore complex component. D. Downregulation of microtubule associated genes. The asterisk indicates significant difference at $P < 0.001$; one-tailed t test comparing heat-stressed (HS - red) to nonstressed (NS - blue) samples. n = 3 biological replicates, each with 3 technical replicates

involved in microtubule function showed opposite transcriptional expression, while microtubule-associated protein EB1C (Zm00001eb044540) was upregulated, Tubulin binding cofactor C (TBCC) (Zm00001eb236410) was downregulated as a result of the heat stress applied at the bicellular stage of pollen development (Figure. 2.11C). Correspondingly, the gene encoding tubulin chain proteins showed significantly differential expression between two conditions (Figure. 2.11D).

Another set of genes important for the transition from metaphase to anaphase are Wings apart-like protein homolog (WAPL), Sister chromatid cohesion 1 (Sister) and regulator of chromosome condensation 1 (RCC1). WALP induces cohesin dissociation from DNA allowing the progression of the mitotic cell cycle which is modulated by sister chromatid cohesion (Crawley et al., 2016). It was found that WALP was downregulated after heat stress, indicating a still high levels of cohesion attached to the chromosomes. Our transcriptional analysis also shows upregulation of sister (Figure. 2.11E) which allow the pairs of sister chromatids remain united as part of one chromosome before anaphase (REF). RCC1, another important gene that associates to chromatin dynamically controlling metaphase-to-anaphase transition was found upregulated after heat stress (Figure. 2.11E). collectively, our results show that heat stress impact sperm cell development by targeting metaphase-to-anaphase transition by activating the spindle assembly check point.

2.3.10 Heat stress alters centromere protein expression.

The histone H3 variant (CENH3) of centromeric nucleosomes is essential for kinetochore assembly and thus for chromosome segregation in eukaryotes. The knockdown of CENH3 reduces mitotic divisions and causes sterility by disturbed meiotic chromosome segregation in Arabidopsis (Lermontova et al., 2011). Given that heat stress activates the spindle assembly checkpoint (SAC) during the metaphase of PMII, which serves as a checkpoint for microtubule and kinetochore attachment, a CENH3 marker line (Gex-mRuby3-CENH3) was subjected to heat stress to investigate the impact of stress on chromosome dynamics.

Under NS conditions, the CENH3 was evenly distributed within individual sperm cell, displaying distinct signals (Figure 2.12A). But in HS pollen, the CENH3 exhibited a chiasma pattern (Figure 2.12B), similar to previous observations of "sticky" chromosomes resulting from irregular chromosome segregation under high temperatures during PMC meiosis in wheat (Draeger and Moore, 2017). Quantification of mRuby3-CENH3 signal showed significantly reduction in HS pollen compared to NS condition (Figure 2.12C). Based on the performance of the CENH3 marker line under both conditions, it could be inferred that heat stress also disrupts kinetochore activity during metaphase, leading to abnormal sperm cell formation.

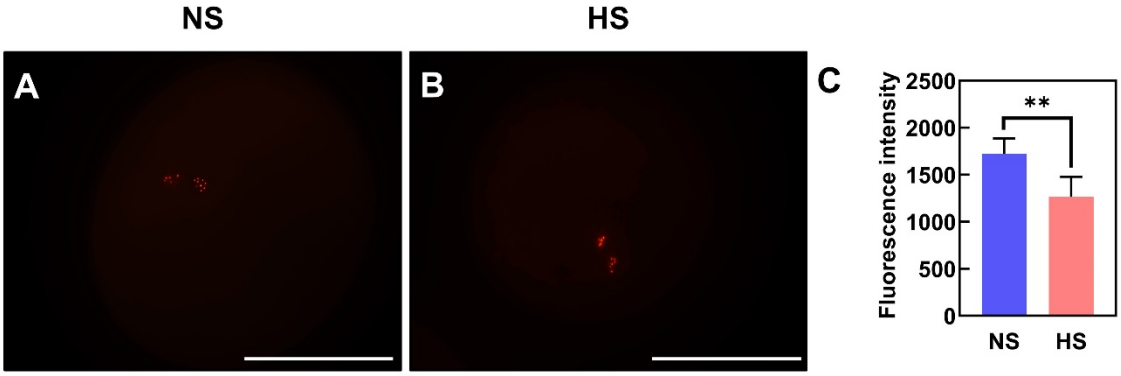

Figure 2.12 Heat stress during bicellular stage decreases centromere expressed protein. Maize centromere maker lines Gex-mRuby3-CENH3 were grown in control conditions (25°C/21°C light/dark period) until they reached the bicellular stage of pollen development and then submitted to heat stress (35°C/25°C light/dark period) for 48 h. A parallel set of marker line plants was maintained under optimal conditions and used as controls. A, Confocal images of centromere CENH3 expressed protein on mature pollen grains from NS (A) and HS plants (B). C, Quantification Gex-mRuby3-CENH3 intensity on both conditions. The asterisks indicate a significant difference at $P < 0.001$; one-tailed t test comparing HS to NS samples. Scale bars = 50μm.

2.3.11 Heat stress reduces the protein components of mature pollen

Transcriptional analysis revealed that the PMII was altered by heat stress. And the sperm cell failed to travel into pollen tube in treated pollen. To gain further insights into the effects of heat stress at proteome level, the LC–MS/MS analysis of total protein in mature pollen under non-stressed and heat-stressed conditions was conducted.

By applying a valid threshold (M. score > 10, peptides > 2), a total of 1543 proteins and 1251 proteins were identified in NS and HS mature pollen, respectively (Figure 2.13A), indicating the protein expression was strongly downregulated under heat stress. Among all the total proteins, 797 proteins were common to both samples, while 749 unique proteins were identified in NS mature pollen and 454 unique proteins were identified in HS mature pollen (Figure 2.13B). Furthermore, GO terms analysis using the unique proteins as input was performed and it was found that heat stress led to a reduction in various protein enrichments (Figure 2.13C). Notably, there was a significant decrease in the protein classes of oxidoreductase, hydrolase, and cytoskeletal proteins, including actin and microtubule proteins. These findings suggest that

heat stress alters the protein composition in mature pollen, thereby affecting PMII and the delivery of cargo in the sperm cells within the pollen tube.

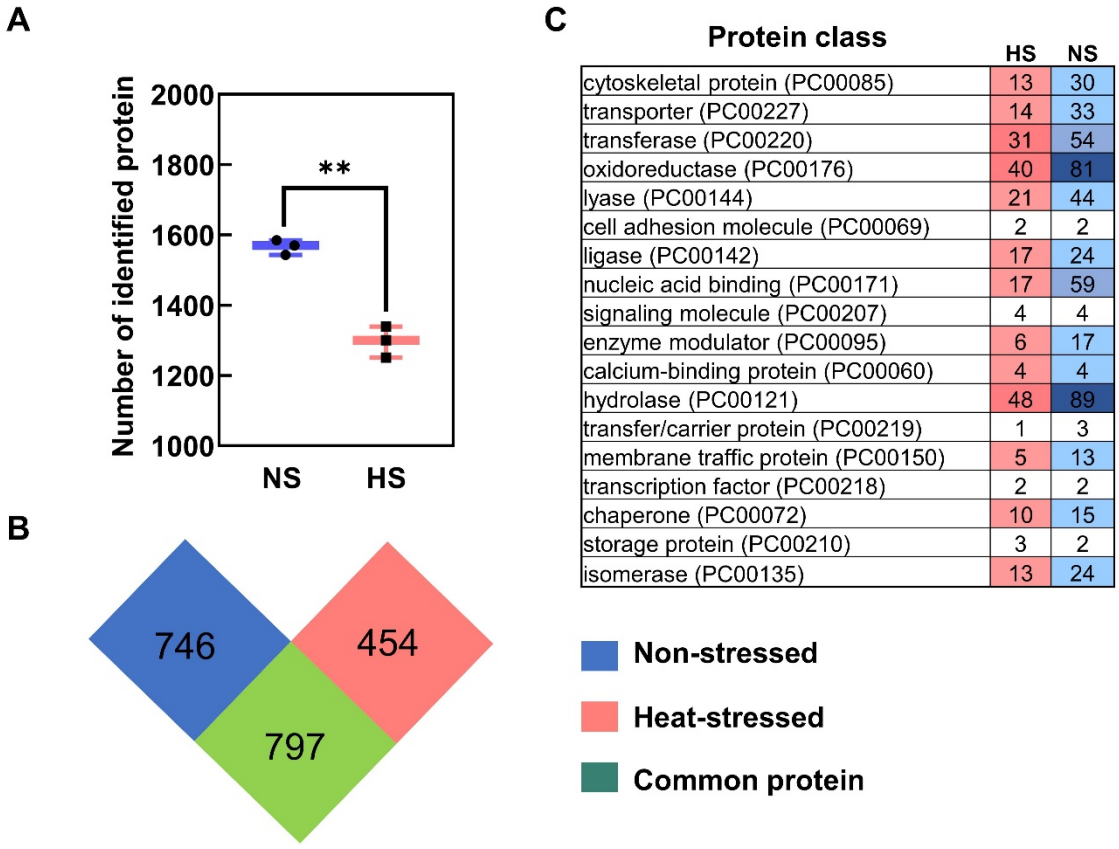

Figure 2.13 Heat stress during bicellular stage alters protein enrichment in mature pollen. Mature pollen of heat stressed during bicellular stage and control conditions were harvested and total protein of both treatments was extracted for LC-MS/MS analysis A, the number of total proteins identified of both conditions. Threshold: M.score＞10, peptides ＞ 2. B, the unique and common protein identified under two treatments. C, the unique protein from (B) GO terms analysis on protein class category. The number indicated proteins assigned at different classes. The asterisks indicate a significant difference at $P < 0.001$; one-tailed t test comparing HS to NS samples.

2.4 Discussion

Due to warming climate, heat stress directly affects the viability and fertilization processes of reproductive organs further resulting yield loss in crops, including maize (Zea mays L), rice (*Oryza sativa* L), wheat (*Triticum aestivum* L), sorghum (*Sorghum bicolor* L. Moench) and cotton (*Gossypium hirsutum* L) (Gourdji et al., 2013; Wang et al., 2020). However, the

definition of heat stress varies among different crop plants, as their optimal growth conditions differ. For instance, in rice, heat stress (above 37℃) during the middle stage of heading can cause more than 50% sterility in spikelets (Jagadish et al., 2007; Chen et al., 2020b). For wheat, the temperature threshold was found around 27℃ (Ullah et al., 2022; Liu et al., 2023). In maize, a temperature above 38℃ for nearly two weeks during the silking stage can result in a reduction of seed set by around 20%-50% in certain maize hybrids (Wang et al., 2021). In addition to heat stress during the daytime, the crop plants during the flowering time are more sensitive to high nighttime temperature. Plants attempt to escape midday heat stress by rescheduling their flowering time (Ishimaru et al., 2010; Jagadish, 2020). However, the elevated nighttime minimum temperature still induced heat stress damage (Sakai et al., 2022). By considering the optimal conditions of maize inbred line B73 and the duration of maize pollen different developmental stages, compared to control 25℃/21℃ (day/night), this thesis applied 35℃/25℃ (day/night) for 48h as a moderate heat stress treatment to allow the pollen capable to response heat stress.

Pollen development is considered as the most heat-sensitive stage during plant development. The male gametophyte development includes three phases: pre-meiotic, microsporogenesis, and microgametogenesis. Heat stress during floral organ differentiation can disrupt the differentiation and development of tapetum and pollen mother cells (PMCs), leading to male sterility due to transcriptional inhibition (Abiko et al., 2005; Draeger and Moore, 2017). When a short spike of increased temperature applied on the tetrad stage pollen, the effects showed up at starch accumulation, pollen viabilities, metabolomic alteration, lipidomic changes as well as influences in the transcriptional regulation, causing unfunctional mature pollen further leading to severe yield losses in maize (Sakata et al., 2000; Begcy et al., 2019). In this study, similar responses in unicellular stage pollen were observed as in tetrad pollen under heat stress. However, heat stress did not directly affect pollen viability, enzymatic activity, or pollen germination during the bicellular stage. Instead, it impaired the formation of sperm cells, leading to the abortion of cobs. Furthermore, under heat stress, tricellular pollen failed to undergo the normal process of anther dehiscence and exhibited reduced pollen germination ability (Egesa et al. unpublished). These observations indicate that heat stress can affect various stages of pollen development and induce male sterility. Moreover, different developmental stages of pollen exhibit phase-specific responses to heat stress.

Heat stress applied during the tetrad, unicellular, and bicellular stages of pollen development all resulted in increased male sterility. However, distinct heat stress responses were observed at

these three developmental stages. During the transition from the tetrad stage to the unicellular stage, microspores enclosed by callose in the anther locule were released, and free microspores underwent enlargement, accompanied by the formation of a single large vacuole (Bedinger and Fowler, 2009). At both heat-stressed tetrad and unicellular stage, inside the pollen, heat stress severely disrupted starch content and enzymatic activity. Meanwhile. The development of surrounding cell layer, particularly the tapetum cells, was delayed, leading to premature degeneration of the tapetal cell layer, as observed in wheat and barley (Begcy et al., 2019; Saini et al., 1984; Abiko et al., 2005), finally resulting the defective mature pollen. But for bicellular stage pollen, because of a asymmetric cell division that marks the beginning of microgametogenesis, a major change in gene expression and protein enrichment occurred (Bedinger and Edgerton, 1990), indicating the maturation step initiation. In species like tomato and tobacco, bicellular pollen is considered mature and ready for anthesis. Similarly, in maize, the genes involved in pollen development are well prepared during the bicellular stage, as evidenced by the identification of a large number of genes through RNA-seq analysis in bicellular pollen (15,227) and tricellular pollen (15,150) (Unpublished data). Additionally, the tapetal cells, which are highly sensitive to stress during male gametophyte development (De Storme and Geelen, 2014), undergo programmed cell death (PCD) and subsequently disintegrate during pollen mitosis I (PMI), marking the end of their role as a nutritive and energy source. This may explain why heat stress does not strongly affect pollen viability and germination processes. However, the mitotic processes of pollen mitosis II (PMII) during the bicellular stage were found to be susceptible to heat stress, ultimately resulting in the production of non-functional mature pollen.

Microtubules organization is sensitive to heat stress not matter in meiosis or mitosis process. In Arabidopsis, high temperature conditions interfere with the configuration of α-tubulin, affecting the construction of the spindle and phragmoplast during male meiosis I and II (Lei et al., 2020). Similarly, in tobacco cells, heat stress affects the microtubules of the mitotic spindle and phragmoplast, resulting in split spindles, altered microtubule asters, and elongation of the phragmoplast (Smertenko et al., 1997). In this study, it was observed that severe alterations in α-tubulin organization during pollen mitosis II (PMII) in the germ cells of heat-stressed pollen (Figure 2.6), indicating the conserved response of microtubules to heat stress. Furthermore, transcriptional analysis revealed upregulation of spindle assembly checkpoint (SAC) genes under heat stress, indicating the interruption of normal cell division (Caillaud et al., 2009).

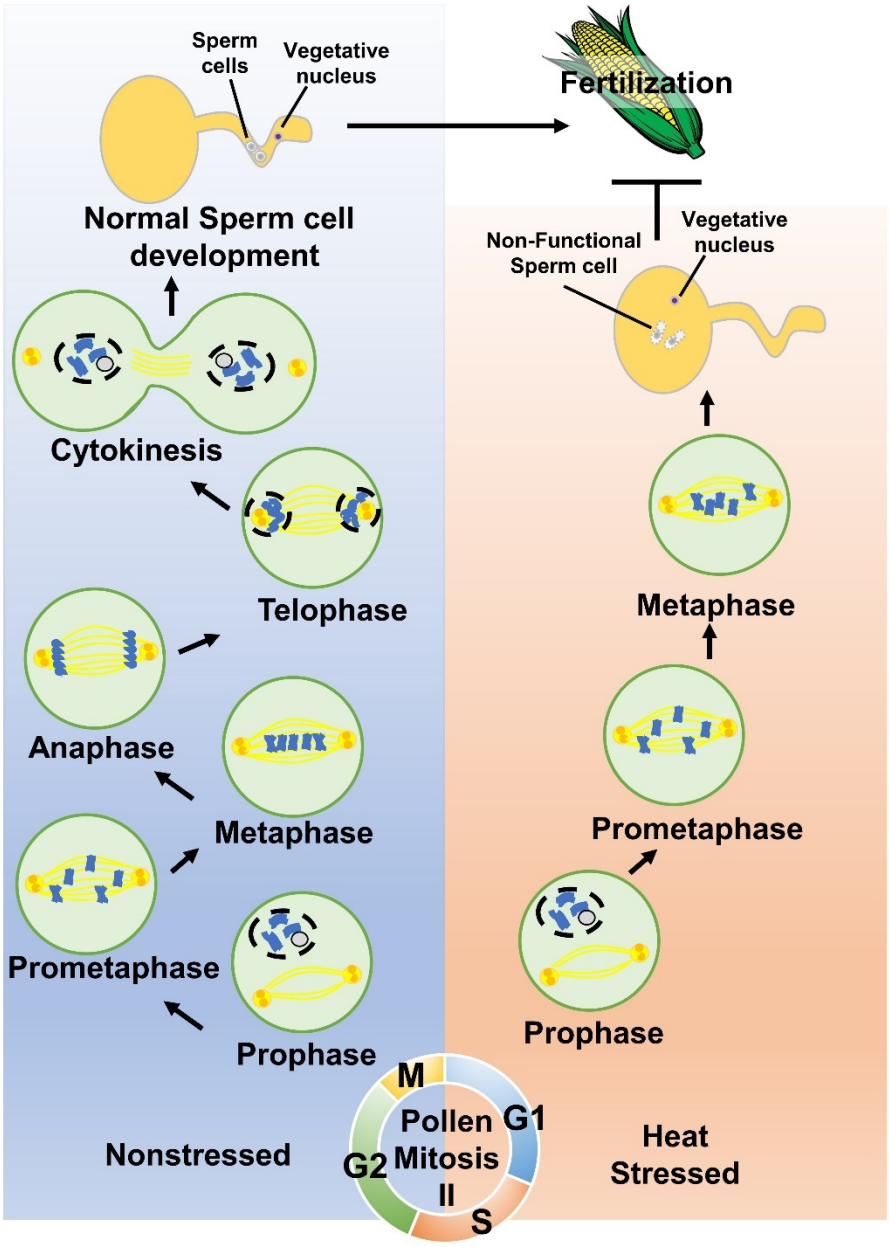

Figure 2.14 Schematic model of heat stress effects during bicellular stage of maize pollen. Under NS conditions, pollen complete PMII and produce normal sperm cells for fertilization. However, the heat stress applied at bicellular stage pollen impairs the metaphase of PMII, generating non-functional sperm cell, and results in failed fertilization, causing crop yield lose.

It was evidenced that high-temperature stress induced pollen reprogramming development to embryogenic by reorganization of microtubules and enhanced the haploid induction efficiency in CENH3 mutant (Simmonds, 1994; Ahmadli et al., 2023). This suggests that as the temperature increases, the stability of microtubules and chromosomes decreases, as evidenced by the reduced signal intensity of the CENH3 marker line under heat stress treatment.

Additionally, the proteome data indicated a decline in the number of functional proteins, particularly those involved in cytoskeletal organization and nucleic acid binding, which aligns with findings in mature tomato pollen (Keller et al., 2018). In light of these observations, a working model was proposed that hypothesizes the effects of heat stress on sperm cell formation and the process of pollen tube travel (Figure 2.14). When heat stress is applied during the bicellular stage, the metaphase of PMII is disrupted, leading to the production of non-functional sperm cells. Furthermore, the disruption of the cytoskeleton, particularly the configuration of actin proteins, in both the pollen and pollen tube, impairs proper fertility unit delivery. These combined consequences ultimately result in severe seed set reduction under heat stress.

CHAPTER 3. GENOME-WIDE ANALYSIS OF *ZMLIM* FAMILY GENES

- I performed all analyses and this chapter was written by myself

3.1 Introduction

LIM family proteins contain a cysteine-rich zinc-binding domain known as the LIM domain. The name "LIM" is derived from the acronyms of LIN11, ISL1, and MEC3, which are conserved LIM domain proteins found in animals (Freyd et al., 1990; Karlsson et al., 1990; Way and Chalfie, 1988). The LIM domain consists of two zinc fingers linked by a short two-amino acid spacer, with a consensus sequence of [C-X_2-C-X_{16}–23-H-X_2-C]-X_2-[C-X_2-C-X_{16}–21C-X_2–3-(C/D/H)] (where X represents any amino acid) (Kadrmas and Beckerle, 2004). The LIM domain is specific to eukaryotes, and the first plant protein containing a LIM domain was HaPLIM1, isolated from sunflower (*Helianthus annuus* L.) pollen (Baltz et al., 1992a). A large number of LIM genes have been identified in tobacco (*Nicotiana tabacum* L.) (Thomas et al., 2006), rice (*Oryza sativa* L.), populus (*Populus trichocarpa* L.) (Arnaud et al., 2007), lily (*Lilium longiflorum Thunb* L) (Wang et al., 2008), *Arabidopisis thaliana* (Papuga et al., 2010), Cotton (*Gossypium hirsutum* L.) (Li et al., 2013), Foxtail Millet (*Setaria italica* L.) (Yang et al., 2019), *Medicago sativa* L.(Nian et al., 2021), wheat (*Triticum aestivum* L.) (Li et al., 2022b; Yang et al., 2022), and many other plant species.

In general, LIM family in plant is divided into two sub-families based on the number of LIM domains they are composed to: DA1/DAR, single LIM domain sub-family and 2LIMs, double LIM domains sub-family. The DA1/DAR group is plant-specific LIM proteins (Zhao et al., 2014). In addition to the conserved LIM domain, the DA1/DAR group has ubiquitin interaction motifs (UIMs) in tandem, which can be further classified into two classes based on their presence. The 2LIMs only contains two LIM domains, similar to LIM sub family cysteine-rich protein (CRP) members in animals (Kadrmas and Beckerle, 2004). The first plant LIM protein identified HaPLIM1 belongs to 2LIMs group. Due to the fact that it was isolated from pollen, 2LIM gene of sunflower was named PLIM. Because of the high conservativeness of the LIM domain, LIM proteins showed uniform expression pattern across plant kingdom. Therefore, based on the expression pattern, the LIMs are name by WLIM (widely expressed in various tissues) and PLIM (specific expressed in pollen tissues).

Based on the NS pollen of different developmental stages RNA-seq data generated from last chapter and previous studies in our group, two LIM genes, ZmLIM6 and ZmLIM14, were found highly expression during bicellular and tricellular stages, which was an interesting expression pattern indicating their potential functions in maize pollen. Despite the initial identification of LIM genes in maize through a transcription factor screening (Burdo et al., 2014). a comprehensive understanding of the properties of LIM genes and their encoding proteins as a family across the maize whole genome is still necessary.

3.2 Materials and methods

3.2.1 Identification and phylogenetic analysis of LIM family genes in maize

the Hidden Markov Model (HMM) of the LIM domain (PF00412) was procured from Pfam 35.0 (pfam.xfam.org). The putative ZmLIM genes were identified and annotated using the maize genome version 4 (Jiao et al., 2017) through Tbtools (Chen et al., 2020a), employing a threshold E value of ≤ 1.0. Each potential ZmLIM gene was subsequently validated by SMART (http://smart.embl-heidelberg.de/) to confirm the presence of the LIM domain. The *Arabidopsis thaliana* (AtPLIMs and AtWLIMs) and sunflower (*Helianthus annuus*) LIM protein sequences were extracted from the protein database UniProt (Consortium, 2019). All LIM protein sequences were analyzed by MEGA11 (Tamura et al., 2021), with multiple sequence alignments conducted by ClustalW using the default parameters, and the phylogenetic tree constructed using the neighbor-joining statistical method (Jones-Taylor-Thornton model, bootstrap 1000×). To make it more understandable, phylogenetic tree was decorated by EVOLVIEW (Subramanian et al., 2019). Jalview 2.0 (Waterhouse *et al.*, 2009) was used to visualize the similarity of protein sequences, displaying the alignments in color to indicate the specific mode of sequences.

3.2.2 Chromosome locations of ZmLIM family genes

Maize chromosome lengths and ZmLIM genes position information were obtained from MaizeGDB (https://www.maizegdb.org/). Subsequently, the physical positions (bp) of all ZmLIM genes were mapped to their respective positions on the ten maize chromosomes using MapGene2Chromosome v2 (http://mg2c.iask.in/mg2c_v2.0/).

3.2.3 Gene structures and functional domains analysis of ZmLIM Family Genes

The online tool Multiple Expectation Maximization for Motif Elicitation (MEME Suite) (http://meme-suite.org/) was used to analysis the conserved motifs of maize LIM genes. The number of Motifs was set to 8 (Bailey et al., 2015). According to GFF annotation file information, all gene features visualization together with phylogenetic tree by Tbtools (Chen et al., 2020a).

3.2.4 ZmLIM genes expression pattern

Expression data of maize LIM genes were extracted from unpublished RNA-seq date from the Dresselhaus' group. Since the RNA-seq results were obtained from multiple runs, the TPM (transcriptions per kilobase million) values just offered an evidence to show the variations in expression across different tissues.

3.3 Results

3.3.1 LIM genes in maize genome.

Previous investigations have demonstrated that the LIM gene family is ubiquitously found in eukaryotes. In plants, the first LIM domain protein was discovered in sunflower (Baltz et al., 1996). In this study, the HMM of LIM domain (PF00412) was used and 13 members was identified in the maize LIM family. Notably, ZmLIM3 was not identified in genome wide analysis, contradicting the maize LIM gene family information in *Grassius* (Grasses Transcription Factors data resource - https://grassius.org/). This discrepancy can be attributed to the fact that the public dataset based its analysis using the maize genome version 3, while this chapter used version 4 as the reference genome, in which ZmLIM3 was not annotated. Therefore, it could be concluded that the maize LIM gene family consisted of 13 genes, instead of 14 as previously proposed.

A phylogenetic analysis of maize LIM genes was performed together with the first LIM gene identified in sunflower and the well-known *Arabidopsis thaliana* LIM family (Figure 3.1). The phylogenetic analysis showed that the maize LIMs clustered into two subfamilies: CRP-like and DA1&DAR. There were eight maize LIMs in the CRP-like subfamily (ZmLIM6, ZmLIM8, ZmLIM9, ZmLIM14, ZmLIM1, ZmLIM7, ZmLIM10, and ZmLIM12) clustered together with the AtPLIMs, HaPLIM2, AtWLIM1&2, and HaWLIM1 genes. On the other hand, ZmLIM2,

ZmLIM4, ZmLIM5, ZmLIM11, and ZmLIM13 were closely related to AtDA1&AtDAR genes indicating a shared evolutionary context to those in *Arabidopsis thaliana* and sunflower.

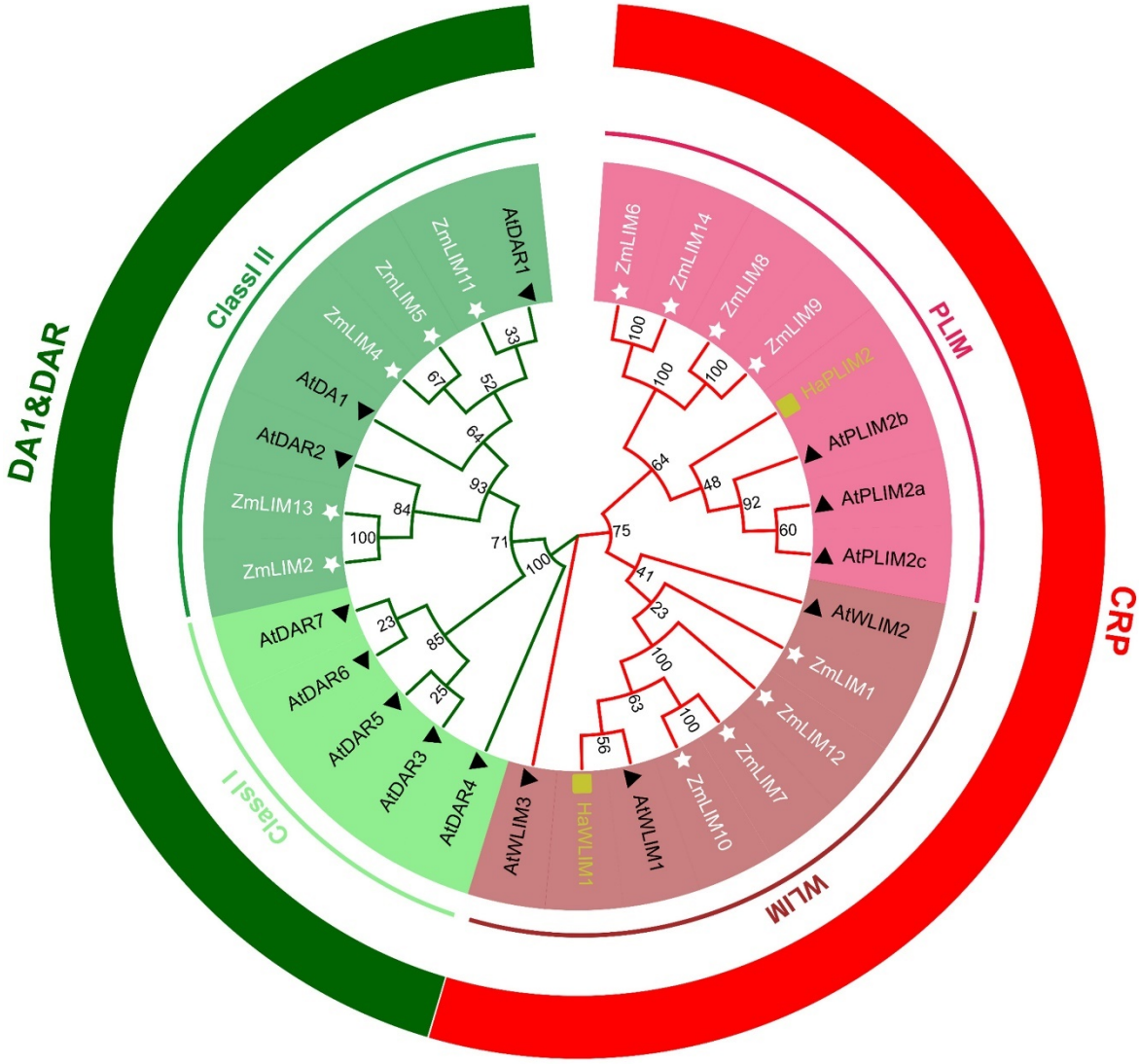

Figure 3.1 Phylogenetic analysis of Maize, Arabidopsis and Sunflower LIM protein. The phylogenetic tree was constructed based on LIM amino acid sequences (the neighbor-joining statistical method, bootstrap 1000×). Green and red represented the DA1&DAR and CRP gene clusters. In the green subgroups, two light green blocks represented subclasses of DA1&DAR. In the red subgroups, pink block represents PLIM subcluster and brown represents WLIM subcluster. A species acronym was added before each LIM protein name and a taxon maker added: Zm, *zea mays* (white star); At, *Arabidopsis thaliana* (black triangle); Ha, *Helianthus annuus* (yellow rectangle).

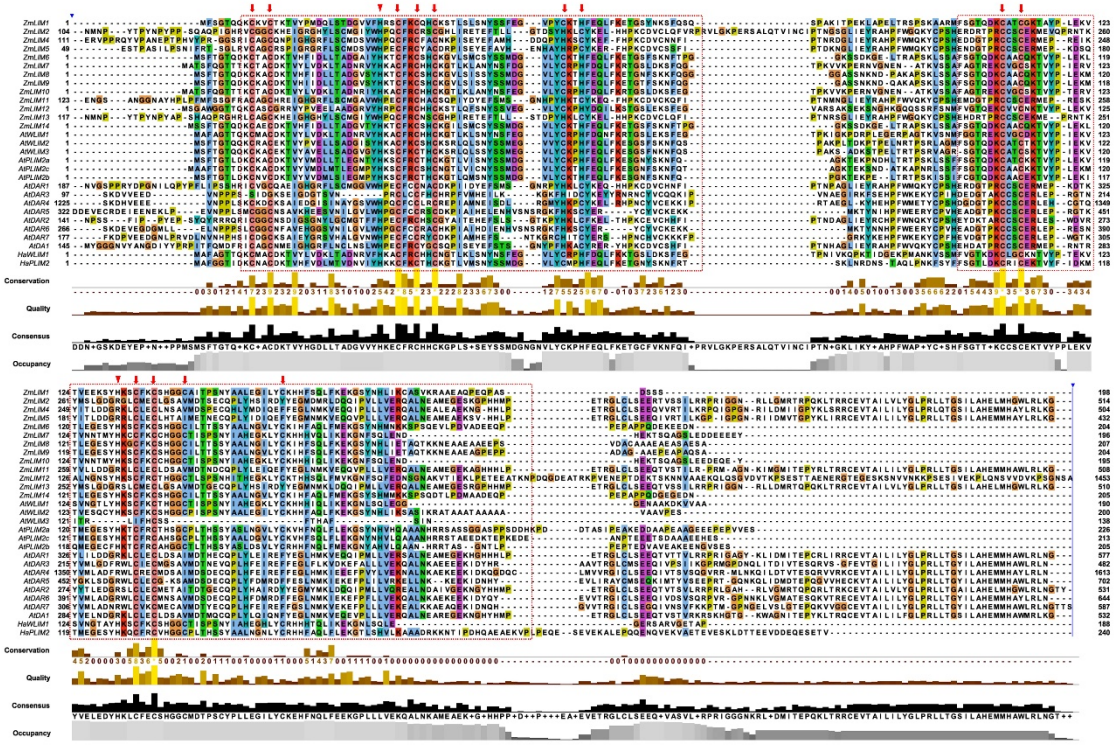

Figure 3.2 Multiple sequence alignment of Maize, Arabidopsis and Sunflower LIM proteins. Full length of LIM protein sequences was used. Only a high conserved region (conservation＞3) is shown. The conserved LIM domains are highlight in red block, Cystine marked by arrows and two hydrophobic amino acid residues marked by triangles.

A multiple sequence alignment was conducted to examine the similarity of LIM proteins (Figure 3.2). The alignment revealed that the first LIM domain, which comprises the first contiguous zinc finger, was highly conserved in all aligned LIM genes. However, the second LIM domain showed high conservation only in CRP-like LIM genes, including ZmLIM1/6/7/8/9/10/14, AtWLIM1/2/3, AtPLIM2a/b/c, HaPLIM2, and HaWLIM1. In contrast, DAR1&DAR LIM genes, including ZmLIM2/3/5/11/13, AtDA1, and AtDAR1/3/4/5/6/7, showed high conservation around 100-300 amino acids, particularly AtDAR4 after aa 1225. The sequence signature of the LIM domain [C-X_2-C-X_{16}–23-H-X_2-C]-X_2-[C-X_2-C-X_{16}–21C-X_2–3-(C/D/H)] (where X represents any amino acid). The red block in the figure indicates the conserved sequence of the LIM domain. The results of the multiple sequence alignment are consistent with the phylogenetic analysis, which divided the maize LIM genes into two subfamilies based on their sequence similarity.

3.3.2 Basic physical and chemical properties

Using the conserved LIM domain to search the maize protein database and after de-redundancy and SMART confirmation, 13 members of the maize LIM gene family were identified, and their names were kept consistent with the *Grassius* website, except for ZmLIM3 which was excluded due to its inexistence in version 4 of the maize genome (Table 3.1). The length of the gene body of ZmLIMs varied between 1023-4930 nucleotides, while their amino acid lengths ranged from 195aa to 1453aa, and the corresponding molecular weight ranged from 21.94kDa to 156.63 kDa. The theoretical PI variation range of the encoded proteins was from 4.60-8.98. The Grand Average of Hydropathicity (GRAVY) value of all ZmLIM members was below 0, indicating that these proteins were hydrophilic. Based on peptide sequence prediction, all ZmLIMs were located in the nucleus, except ZmLIM8, which was predicted to be Golgi apparatus localized.

Table 3.1 Basic information of 13 maize LIM family genes.

Gene ID	Gene	Chr	Gene length (bp)	Protein				
				Size (aa)	Molecular Weight (kDa)	Theoretical pI	Grand Average of Hydropathicity	subcellular location
Zm00001d028550	ZmLIM1	1	2030	198	21.96	8.98	-0.569	Nucleus
Zm00001d028567	ZmLIM2	1	1973	514	58.10	8.83	-0.641	Nucleus
Zm00001d030953	ZmLIM4	1	2610	504	57.17	5.63	-0.578	Nucleus
Zm00001d033297	ZmLIM5	1	2962	432	48.88	5.77	-0.434	Nucleus
Zm00001d002844	ZmLIM6	2	1086	204	22.45	6.23	-0.521	Nucleus
Zm00001d041725	ZmLIM7	3	1023	196	22.11	8.48	-0.669	Nucleus
Zm00001d051262	ZmLIM8	4	1071	207	22.22	7.5	-0.377	Golgi apparatus Nucleus
Zm00001d017382	ZmLIM9	5	1198	204	21.94	7.93	-0.428	Nucleus
Zm00001d035304	ZmLIM10	6	1439	195	22.01	8.63	-0.695	Nucleus
Zm00001d035844	ZmLIM11	6	3195	508	57.52	5.95	-0.572	Nucleus
Zm00001d037252	ZmLIM12	6	4930	1453	156.63	4.6	-0.97	Nucleus
Zm00001d047837	ZmLIM13	9	2704	510	57.98	8.27	-0.646	Nucleus
Zm00001d025926	ZmLIM14	10	1040	205	22.41	6.23	-0.486	Nucleus

3.3.3 ZmLIM genes map of maize chromosomes.

The chromosome localization map depicted the distribution of 13 ZmLIM gene members in the maize genome (Figure 3.3). The map showed that all LIM genes were distributed throughout the genome, with the exception of chromosomes 07 and 08, which lack LIM genes. Chromosomes 01 and 06 have the highest number of LIM genes, with four and three members, respectively, while the remaining chromosomes have only one LIM gene each.

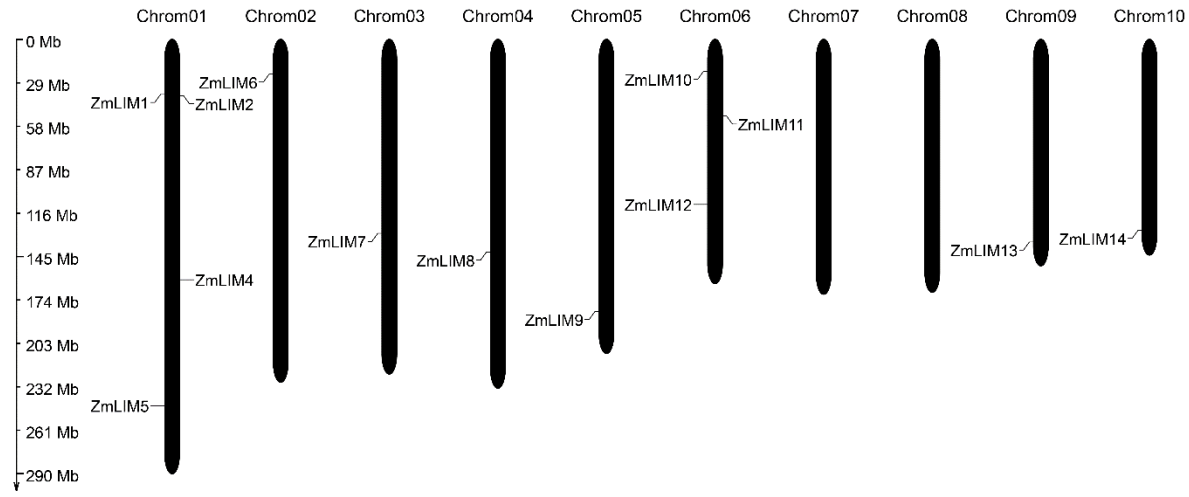

Figure 3.3 Chromosomal distribution of maize *LIM* genes. Chromosome numbers were listed on the top. Chromosomal distances are given in Mb. The names of each ZmLIM gene is based on their physical position on chromosomes.

3.3.4 ZmLIM gene structures analysis

To gain a deeper understanding of the structural characteristics and conserved motifs in the ZmLIM family, MEME, SMART and Tbtools were combined to extract gene feature structures and merged them with a phylogenetic tree (Figure 3.4). The presented phylogenetic tree clades indicated that the ZmLIMs in red belonged to the CRP subfamily, while the green ZmLIMs belonged to the DA1&DAR subfamily (Figure 3.4A). The distribution of motifs, domain arrangements, and gene structures were clearly segregated into two distinct categories (Figure 3.4 B-D). The motif searching was done by online tools MEME suite (MEME Suite) (http://meme-suite.org/). The number of identified motifs was set at 8 and all motifs signatures were showed in supplementary Figure 1. All LIM genes possessed motif1, which SMART annotated to encode a part of the LIM domain, thus verifying the reliability of the motif screening results. In addition, motif1, together with motif3, and motif8, together with motif2, were identified as LIM domains with high confidence (E-value＜0.001). The eight CRP ZmLIM genes shared four motifs and contained two LIM domains. It was observed that ZmLIM12's protein was significantly longer than the other members, consisting of 1453 amino acids. However, motif search and conserved domain detection failed to reveal any features other than the LIM domain, except for a few low-complexity regions detected by SMART (Figure 3.4B&C)

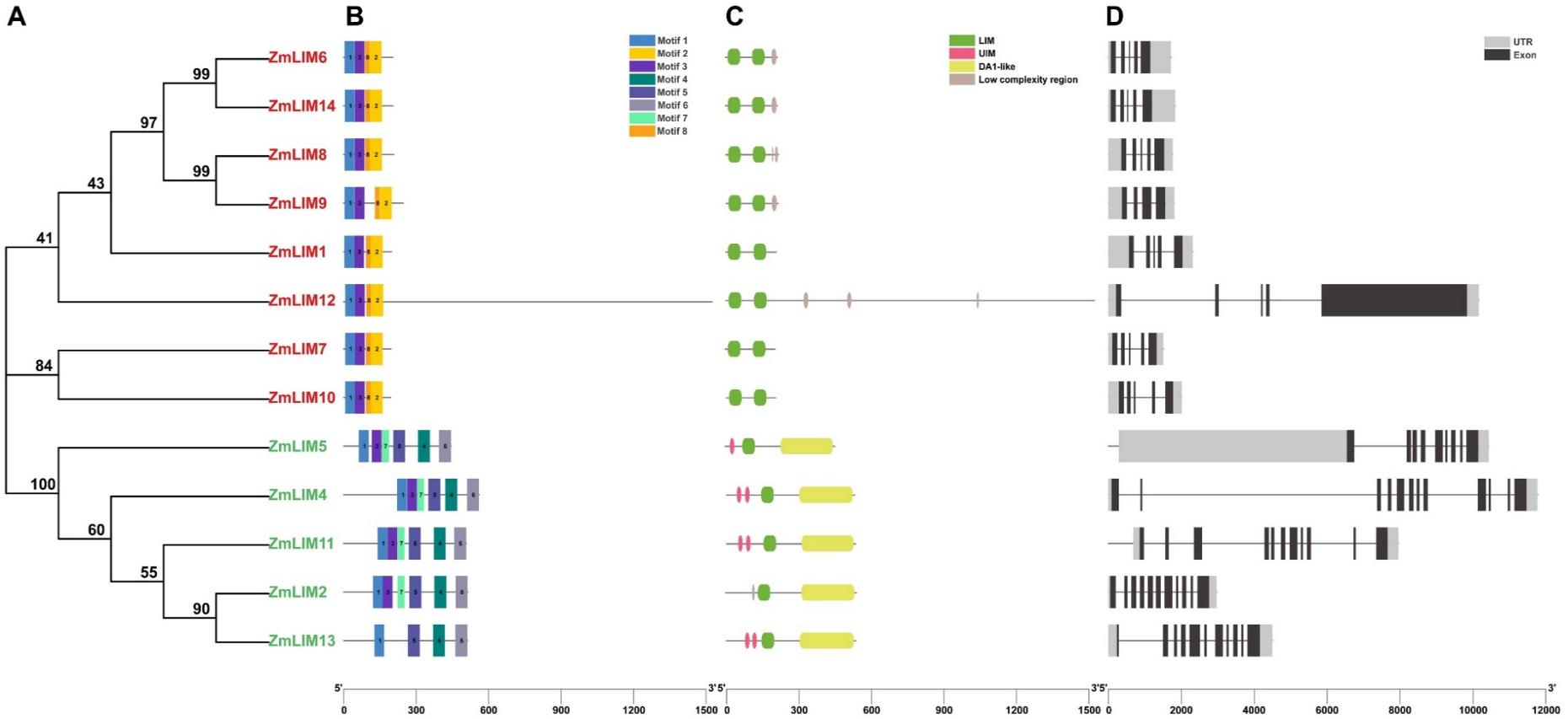

Figure 3.4 Gene structure and functional domains analysis of *ZmLIM* genes. Gene features visualization together with phylogenetic tree by Tbtools. (A) Phylogenetic tree of maize LIM genes. Red represented CRP subgroup and green represented DA1&DAR subgroup. (B)Basic motifs analysis of ZmLIM genes. Each color represented one specific motif. The x-axis below indicated the peptide length(aa). (C) Conserved domain analysis of ZmLIM genes. The x-axis below indicates the peptide length(aa). (D) Gene structure analysis of ZmLIM genes. The x-axis below indicates the gene length (bp).

Previous studies have described that DA1&DAR LIM genes contain a single LIM domain (REFs). The analysis showed that motif1, motif3, and motif7 form the LIM domain in DA1&DAR (Figure 3.4B&C). Additionally, all DA1&DAR LIM genes contained motif4/5/6, which encoded the DA1-like domain, a plant-specific domain absent in animals. Among these five DA1&DAR LIM genes, ZmLIM4, ZmLIM11, and ZmLIM13 contained two UIM domains, while ZmLIM5 had one, and ZmLIM2 lacked this domain. Based on the number of UIM domains, researchers classified LIM genes into DA1-LIM, containing one or more UIM domains, and DAR-LIM, lacking any UIM domain. However, our phylogenetic and structural analyses suggest that the UIM domain did not play a critical role in the evolution of the ZmLIM gene family, as ZmLIM2 and ZmLIM13, which were in the same cluster, had different numbers of UIM domains.

Above analysis also revealed that the number of introns in the ZmLIM gene family varied (Figure 3.4D). The CRP LIM group had a range of three to four introns, while the DA1&DAR group had more than eight introns. Additionally, genes in the same clade of the phylogenetic tree had similar exon/intron patterns, such as ZmLIM6 and ZmLIM14.

3.3.5 ZmLIM genes expression pattern analysis

The initial goal was to elucidate LIMs functions involved in maize development. To achieve this, The RNA-seq data of ZmLIMs from various maize tissues was extracted and clustered using the TPM values as a proxy for similarities (Table 3.2). Previous studies have established LIM gene family nomenclature, refering "P" before LIM as found in the pollen tube, and the WLIM found widely expressed in various plant tissues. In maize, ZmLIM6/14/8/9 were closely related to AtPLIM2 genes and highly expressed in pollen and pollen tubes, with no expression detected in seeds, leaves, roots, or other tissues. Interestingly, the TPM values of these genes increased from the unicellular stage of pollen, peaked at the bi- and tricellular stages, and reached their maximum expression level in mature pollen, particularly in sperm cells. ZmLIM1/12/10 were similar to AtWLIMs and expressed widely in seeds, leaves, and roots. Moreover, ZmLIM1/10 were also highly expressed in egg cells and zygotes The ZmLIMs in green belonged to the DA1&DAR subgroup, and all five genes showed no specific expression pattern. AtDA1, AtDAR1, and AtDAR2 are known ubiquitin receptors required for plant growth and development (Peng et al., 2015) and similarly, ZmLIM5/4/11/2/13 were relatively abundant in leaves and roots. ZmLIM11, like ZmLIM1/10, showed expression in egg cells and zygotes, suggesting potential functions of LIMs in maize embryo and seed development.

Table 3.2 Expression pattern of maize LIM genes. TPM values were extracted from RNA-seq data collected from different tissues. Color indicator comparison was limited to each row.

Gene	Seed	Leaf	Root	Tetrad	Uni-cellular	Bi-cellular	Tri-cellular	Mature Pollen	Sperm cell	Pollen tube	Egg cell	Zygote 12HAP	Zygote 24HAP	Apical cell	Basal cell
ZmLIM6	0.6	0.7	0.5	1.8	199.2	2573.6	2444.4	6459.3	6595.1	4322.7	2.8	0.1	0.1	2.9	0.6
ZmLIM14	0.6	0.3	0.4	1.2	36.4	1862.1	1956.1	4012.9	5254.0	3576.1	2.5	0.1	0.4	0.0	0.0
ZmLIM8	0.1	0.1	0.0	0.4	0.9	660.4	681.6	475.9	336.3	365.8	0.1	0.0	0.0	0.0	0.0
ZmLIM9	0.4	0.2	0.5	0.4	3.6	406.2	382.2	373.0	211.5	271.4	0.0	0.0	0.0	0.0	0.0
ZmLIM1	25.8	20.5	95.5	16.0	7.4	0.2	0.4	0.0	1.5	0.1	578.9	499.7	571.2	119.6	139.8
ZmLIM12	21.5	29.2	45.2	4.8	8.1	0.3	0.4	0.0	0.0	0.0	2.3	2.2	1.3	6.5	2.4
ZmLIM7	6.4	0.3	78.2	0.4	12.6	1.3	1.9	0.0	0.0	0.0	0.0	0.0	0.0	0.0	0.0
ZmLIM10	56.1	0.1	92.4	49.6	67.5	0.2	0.2	0.0	0.0	0.0	2.0	176.6	103.0	100.6	21.1
ZmLIM5	9.5	25.1	19.6	1.6	1.4	0.1	0.1	0.0	0.0	0.0	4.0	3.8	3.6	8.9	2.3
ZmLIM4	23.0	25.8	84.2	4.3	13.0	2.8	3.9	1.1	0.3	1.3	6.5	23.9	8.3	26.3	11.7
ZmLIM11	15.3	15.5	19.3	7.5	19.3	9.6	10.7	3.4	5.9	3.0	26.7	37.3	36.0	22.5	19.1
ZmLIM2	1.8	0.1	9.0	19.4	2.8	0.0	0.2	0.0	0.0	0.0	0.0	1.1	0.0	0.0	0.1
ZmLIM13	3.0	22.5	27.5	0.1	0.3	0.1	0.1	0.0	0.0	0.0	1.1	0.1	0.4	0.0	0.0

Low Middel High

3.4 Discussion

The LIM gene family has been the subject of many studies in various plant species, which have focused on domain analysis, evolution through phylogenetic analysis, expression patterns, and functions related to development (Baltz et al., 1992b, 1996; Eliasson et al., 2000; Arnaud et al., 2007; Papuga et al., 2010; Arnaud et al., 2012; Li et al., 2014; Srivastava and Verma, 2017; Yang et al., 2019). However, in maize, the LIM gene family was initially identified through open reading frame screening based on DNA-binding domains across the entire genome, resulting in the identification of 14 members as a co-regulator family, indicating that LIM proteins likely do not directly bind to DNA but rather control gene expression through various mechanisms such as chromatin remodeling, histone modification, or association with transcription factors via protein-protein interactions that affect their activity (Yilmaz et al., 2009; Burdo et al., 2014). Nevertheless, the study of a gene family is primarily based on nucleotide or protein sequences, and currently, there is a lack of comprehensive and systematic research on the LIM gene family in maize, one of the model organisms and the most important crops.

In this study, there were 13 LIM genes identified using the maize genome version 4 (Jiao et al., 2017). Compared to *Arabidopsis thaliana* (6) and *Oryza sativa* (6) (Arnaud et al., 2007; Papuga et al., 2010), the number of maize LIM genes is significantly higher, which may be related to the enormous size of the maize genome. Interestingly, compared to the previously reported 14 members of the ZmLIM family in this chapter only 13 genes were found. ZmLIM3 (GRMZM2G385236) was only 154 amino acids in length and lacked any characteristic LIM domains. Therefore, in the new version of the maize genome, this genomic region is considered a low confidence gene model set, indicating that accurate genome assembly can help us better understand the gene family.

Another important aspect of gene family study is classification and nomenclature. The first plant LIM protein was found in sunflower pollen and attributed to its specificity, leading to its naming as PLIM ("P" represents pollen-specific) (Baltz et al., 1992b, 1996). Following this approach, subsequent LIM genes were named based on expression in *Arabidopsis thaliana* and tobacco. WLIM represented LIM genes expressed widely in various sporophytic tissues (Eliasson et al., 2000). However, due to the lack of expression data, the LIM gene family in poplar and rice was divided into αLIM1, βLIM1, δLIM2, and γLIM2 groups based solely on phylogenetic analysis. Each group also consists of WLIM or PLIM subgroups, resulting in a complex system (Arnaud et al., 2007). Regarding maize, even though recent publications named ZmLIMs as PLIM and WLIM in phylogenetic trees (Yang et al., 2019; Nian et al., 2021), the ZmLIM genes were initially found as a co-transcription factor family. Therefore, in order to adhered to the standard maize genetics nomenclature (https://curation.maizegdb.org/maize_nomenclature.php), the LIMs were named with an organism identifier (Zm), followed by letters that represent the TF family (LIM) and by a number that will start with '1' to improve communication among scientists. Based on our phylogenetic analysis, the PLIM genes in maize were ZmLIM6/8/9/14, clustered together with AtPLIM2a/b/c and HaPLM2. The WLIM genes in maize were ZmLIM1/7/12/10, which were clustered with AtWLIM1/2/3 and HaWLIM1. Additionally, ZmLIM2/4/5/11/13 belonged to the DA1/DAR group.

The plant LIM gene family is divided into two major subfamilies based on structure, 2LIMs and DA1/DARs. The 2LIMs proteins contain only two LIM tandem domains, similar to CRP-like LIM proteins found in vertebrates. In maize, ZmLIM6/8/9/14 (PLIM) and ZmLIM1/7/12/10 (WLIM) belonged to the CRP subgroup. Prior research has demonstrated that CRP-like LIM proteins participate in cytoskeleton remodeling, transcriptional regulation, and cell differentiation (Weiskirchen and Günther, 2003). Similarly, in numerous plants, LIM proteins belonging to the WLIM or PLIM subgroups have been implicated in actin dynamics and transcriptional regulation (Kawaoka et al., 2000; Wang et al., 2008; Papuga et al., 2010; Ye et al., 2013; Han et al., 2013; Na et al., 2014; Li et al., 2015), suggesting that 2LIMs may have evolutionarily conserved functions. Therefore, it could be inferred that ZmLIM6/8/9/14 may have similar functions to homologous genes PLIM2a/b/c in actin binding or transcriptional regulation during maize pollen development and pollen tube growth based on their expression pattern, which will be investigated in the next chapter.

DA1/DAR subfamily LIM proteins are plant specific and containing one LIM domain. Further subdivision into DA1 and related proteins is based on the presence of other domains. Among the maize LIM proteins, ZmLIM2/4/5/11/13 are members of the DA1/DAR subfamily. The DA1 protein was initially discovered through reverse genetics, and the seed and organ size of the *da1* mutant of *Arabidopsis thaliana* were significantly increased (Li et al., 2008). Interestingly, the expression pattern of ZmLIMs in this subgroup includes organ tissues, particularly ZmLIM4/5/11 in one cluster with AtDA1. In addition to containing a single LIM domain, DA1-like proteins have two ubiquitin interaction motifs (UIMs) and a conserved C-terminal structure. This led to the identification of a further 142 DA1-like genes from 33 plant genomes, revealing their evolutionary significance in plant diversification history (Zhao et al., 2014). However, in maize, there were no genes clustered with *Arabidopsis thaliana* class I, indicating the high evolutionary conservativeness of DA1-like genes in maize.

CHAPTER 4. FUNCTIONAL STUDY OF ZMLIMS IN MAIZE POLLEN DEVELOPMENT

-I performed all experiments and analyses. This chapter was written by myself

4.1 Introduction

The proteins containing LIM domains play diverse cellular roles as regulators of gene expression, cytoarchitecture, cell adhesion, cell motility, and signal transduction in animals (Kadrmas and Beckerle, 2004). Currently, the human genome houses 135 identifiable LIM domain-containing proteins, ranging from 1 to 5 domains. The only two LIM domains are present in the CRP subfamily protein, which primarily regulates myogenesis and muscle structure by binding to α-actinin (a well-known actin bundle cross-linking protein) and zyxin (a focal adhesion marker protein) (Velyvis and Qin, 2000; Khurana et al., 2002). In plants, proteins only containing LIM domain are CRP-like class of LIM family (as described in last chapter). Due to the high conservation of LIM domains, CRP-like LIM proteins (PLIM and WLIM) also have actin-binding activity, especially during pollen tube growth (Srivastava and Verma, 2017). For instance, tobacco WLIM1/2 not only are cytoplasm localized as an actin-binding protein (ABP) but also are nucleus localized, binding DNA sequences to activate histone genes or regulate lignin biosynthesis (Kawaoka et al., 2000; Moes et al., 2013). However, direct evidence elucidating the roles of LIMs during pollen development is limited, with only aborted pollen found in RNAi-PLIM2c Arabidopsis plants (Ye and Xu, 2012) and collapsed pollen in Virus-induced gene silencing (VIGS) - TaLIM2 wheat plants (Yang et al., 2022).

There are many key genes known for phase-specific regulation in maize pollen development. The *MALE STERILE CONVERTED ANTHER 1* (*MSCA1*) and *MULTIPLE ARCHESPORIAL CELLS 1* (*MAC1*) are important for proper AR formation (Chaubal et al., 2003; Kelliher and Walbot, 2012; Sheridan et al., 1999, 1996; van der Linde et al., 2018), which is the first transition stage of male gametophyte development. Following, *AMEIOTIC1* is required by early meiosis and regulate the PMC transition to meiosism (Staiger and Cande, 1992; Pawlowski et al., 2009). If normal microspores are generated after meiosis and released from tetrad, *MAB1* is necessary for the asymmetric division of PMI, otherwise two VC-like nuclei and no GCs in mature pollen (Juranić et al., 2013). The germ cell needs *DUO1* to enter PMII to generate two

sperm cell for double fertilization (Brownfield et al., 2009). In addition to these well-known genes, recently *ZmDRP1* was identified as showing specific expression from the tetrad stage to the unicellular stage in the tapetum, and its knockout mutant showed male sterility and shriveled pollen with a cracked surface, indicating the stage-specific expression pattern can reflect the gene function in maize pollen development (Han et al., 2022). In general, the phase-specific regulation pattern is widely found across the entirety of maize pollen development.

Based on RNA-seq data of different developmental stage maize pollen, ZmLIM6 and ZmLIM14 exhibit a stage-specific expression pattern during the late stages of maize pollen development. Moreover, these two genes cluster together with AtPLIM2b, suggesting their potential roles in pollen development.

4.2 Materials and methods

4.2.1 Gene cloning and plasmids construction

To investigate the function and localization of LIMs, various plasmids (pENTR-TOPO, pET-32b (+), pET-53-DEST, pMAL-p2p, pENTR-gRNA1, pENTR-gRNA2, pGW-Cas9, etc.) were constructed by restriction enzyme, Gateway, Greengate etc. clone methods, of which DNA fragment amplification, agarose gel electrophoresis, gel recovery, and sequencing were involved. For each step, the cloning products were transformed into *E. coli* cells (specifically DH5α or DB3.1 if CCDB was included). Colony PCR was utilized for candidate selection, followed by amplification and plasmid extraction from several individual colonies (Bacterial Plasmid Miniprep Kit, Biocompare). Successful cloning events were confirmed by sequencing analysis (Macrogen).

4.2.1.1 protein expression plasmids construction

Gene specific primers (Supplemental Table 1) were designed based on the MazieGDB reference cDNA sequence and their specificity checked by NCBI primer blast *in silico*. The Phusion® High-Fidelity DNA Polymerase (New England BioLabs) was employed for amplifying the target fragments, using cDNA from maize pollen of the B73 inbred line as the template. Following polymerase chain reaction (PCR) amplification, the products were resolved on a 1% agarose gel and visualized using a GEL iX20 Imager (iNTAS). The gel bands corresponding to the expected sizes were excised and purified using the QIAquick Gel Extraction Kit (QIAGEN). Both the amplified ZmLIMs fragments and the pET-32b (+) backbone were digested with the

appropriate restriction enzymes (New England BioLabs), and then purified from agarose gel and recovered using the QIAquick Gel Extraction Kit. Subsequently, the backbone and fragments were ligated using T4 DNA Ligase (New England BioLabs).

4.2.1.2 CRISPR/Cas9 mutant construction

Guide RNA (gRNAs) sequences were designed by online tool *Breaking-Cas* (Oliveros et al., 2016) with the following parameters: *Zea mays* (4577) genome; NGG as PAM; the others were default. The gRNAs with less off-targets and high score were chosen. The cloning of gRNA to pGW-Cas9 were carried out as previousm described (Char et al., 2017). The final constructs were further verified by restriction enzyme digestion and sequencing.

4.2.2 Maize transformation

Maize transformation was performed at the Iowa State University Plant Transformation Facility (https://ptf.biotech.iastate.edu/). In brief, Cas9-LIMs were transferred to *Agrobacterium* strain EHA101 for infecting immature Hi-II maize embryos. Bialaphos-resistant callus lines were identified using molecular markers, and the positively transformed callus was transferred to regeneration medium. Multiple plantlets per line were generated from the callus. The plantlets were initially incubated in petri dishes at 28 °C for several days after delivery, and then transferred to soil and maintained in a greenhouse.

4.2.3 His-ZmLIM protein purification

Protein related tests were carried out according to the protein purification protocol of the QIAexpressionist (QIAGEN) with some modifications. And all protein was produced by transformed BL21(DE3) induction expression system.

4.2.3.1 Protein solubility test

A 500μL starter culture of BL21 cells containing the corresponding protein expression plasmid was added to 20mL LB-medium (containing Yeast extract at 5g/L, Tryptone at 10g/L, and Sodium chloride at 10g/L) supplemented with antibiotics. The culture was incubated in a 37°C shaker at 200rpm for two hours until the optical density at 600nm (OD600) reached approximately 0.6. A 1mL sample was taken prior to induction (BI) as a non-induced control and pelleted. The pellet was then resuspended in 50μL of 1x SDS-PAGE sample buffer (composed of 0.075M Tris-HCl at pH 8, 0.6% SDS, 15% Glycerol, 7.5% β-mercaptoethanol,

and 0.0009% bromophenol blue). Afterwards, Isopropyl β-D-1-thiogalactopyranoside (IPTG, SERVA) was added at a final concentration of 1mM to induce protein expression. The culture was further incubated for two hours at 37°C or overnight at 20°C with shaking at 200rpm. A 1mL sample was taken after induction (AI). The cells in the remaining 18mL of the culture were collected by centrifugation, and the pellet was resuspended in 2mL of His Lysis buffer (50mM NaH_2PO_4, 300mM NaCl, 10mM Imidazole, pH 8) containing 1× protease inhibitor (EDTA-free Protease Inhibitor Cocktail, Roche), 0.5mg/ml lysozyme (Sigma), and 1mM phenylmethylsulfonyl fluoride (PMSF) (Sigma). The cell wall was disrupted by sonication using a BANDELIN SONOPULS HD 2070 homogenizer (BANDELIN) for 5 minutes at 40% power, with a total of 6 cycles. A 100μL portion of the sonicated lysate was centrifuged at 13,000g at 4°C for 10min. The resulting supernatant was the soluble fraction (SF), while the pellet was the insoluble fraction (IF). The IF was transferred to new tubes and combined with an equal volume of 2× SDS-PAGE sample buffer. All four samples (BI, AI, SF, and IF) were boiled at 95°C for 15 minutes to denature the proteins and subsequently stored at -20°C for later blotting.

4.2.3.2 His-tag protein purification

The starter (2mL of fully incubated BL21 containing the corresponding protein expression plasmid) was added to 1L LB medium with antibiotic and incubated in a 37°C shaker at 200rpm. When OD_{600} reached 0.5-0.7, 1mM IPTG was added and further incubated in a 20°C shaker at 200rpm for another 16h. All *E. coli* cells were pelleted in a 500mL centrifuge bottle (Nalgene) and resuspended in ice-cold His lysis buffer (1× Protease inhibitor, 0.5mg/ml lysozyme, 1mM PMSF). Repeated sonication was applied for cell wall broken. Following transparent lysates was centrifuged at 16,000g, 4°C for 30min. Because ZmLIM protein was insoluble under native conditions, supernatant was discarded, and pellet was continually resuspended in 6M guanidine-HCl (Gu-HCl) buffer rolling at room temperature for 1h. When all pellet was dissolved in strong detergent buffer, sample was centrifuged at 16,000g, 4°C for 30min and filtered with 45μm filter. Based on manual of HisTrap HP Colum (Cytiva), prepared protein samples were further purified using ÄKTA (Cytiva). Protein renaturation and refolding was carried out on the Ni-NTA column itself prior to elution (Holzinger et al., 1996) or in solution (Wingfield, 1995). In this research, the protein denaturing condition purification and renaturation were carried out as previously described (Goto et al., 2011) .

4.2.4 SDS-PAGE and immunoblot analysis

SDS-PAGE used Tris/Glycine buffer system (Laemmli, 1970) and gel result were checked by staining with Coomassie Brilliant Blue (CBB, 0.2% Coomassie brilliant blue; 45% methanol; 10% acetic acid) or TCE pre-added in separate gel (Ladner et al., 2004). Protein of fresh run SDS-PAGE gel was transferred onto nitrocellulose membrane (AmershamTM Protran®, GE Healthcare) for 45min at 260mA (Bio-RAD). The membrane was blocked in blocking solution (5% milk powder in 1×TBST) and washed 10min three times with 1×TBST buffer (50mM Tris-HCl pH 7.5; 150mM NaCl; 0.1% Tween-20). Membrane was transferred to a box and incubated at 4°C overnight with primary antibody such as 6× His tag monoclonal antibody (Thermo Fisher Scientific) or specific antibodies (diluted 1:5000 in 2% milk TBST) Before incubation with secondary antibody (diluted 1:5000 in 2% milk TBST, Thermo Fisher Scientific), two times washing with TBST for 10min were applied. Finally, the protein bands were detected on membrane with HRP juice (PJK Biotech) by ChemiDOCTMMP Imaging System (Bio-RAD).

4.2.5 *In situ* hybridization

Based on previous described method (Brewer et al., 2006; Wu and Wagner, 2012), some modifications were included because of different tissues used in this study.

4.2.5.1 Fixation

Maize anthers at different stages were harvested according to Leaf collar method (Begcy and Dresselhaus, 2017) and fixed in fresh prepared ice-cold FAA fixative (50% ethonal, 5% acetic acid and 3.7% formaldehyde in DEPC-H_2O). FAA fixed anthers were degassed at 0.1Mpa for 20min on ice, which was repeated three more times until the tissues sink, then replaced with new fresh FAA fixative after degas step and kept at 4°C overnight. During the dehydration step, samples in FAA fixative were replaced with 50% ethanol and incubated at room temperature for 30min on a rotary platform. Following dehydrated the tissues through 50, 60, 70, 80, and 90% ethanol series for 30min each. The tissues could be stored in 70% ethanol for several months at 4°C. After the 90% ethanol step, replace with 95% ethanol plus 0.1% of Eosin Y and leave the tissues overnight at 4°C. The dehydration step was finished with three changes of 100% ethanol for 30min each on a rotary platform at room temperature.

4.2.5.2 Sample embedding

First, ethanol was replaced with the following solutions for 30–60 min each step: 25% Histoclear/75% Ethanol; 50% Histoclear/50% Ethanol; 75% Histoclear/25% Ethanol; 3× 100% Histoclear (National Diagnostics). Further, it was replaced with 1mL fresh histoclear and added 3-5 paraplast chips and moved the tubes to a 60°C incubator. Successively added paraplast chips every 30min until the tubes were full. Then left the anthers in this 50% histoclear/50% paraplast mixture overnight at 60°C. Changed wax at least 6 times over the next 2days (at least three times per day, 4h apart between each wax change). Prepared 2mL molten wax for each sample before sample embedding starting. Put a plastic mold (Peel-A-Way® Embedding Mold) in a cold platform and poured inside 1mL molten wax. When wax became a soft bottom, took the tissue quickly from the tubes of 60°C and arranged it either parallel (for longitudinal sections) or perpendicular (for transverse sections) on the base further covered the tissued with another 1mL melted wax. After the wax was hardened completely, stacked the base molds and stored them at 4°C.

4.2.5.3 Probed synthesis

Probes were designed based on reference mRNA sequences from MaizeGDB. Sequences of 200-500bp in length from LIM6 and LIM14 were amplified (Q5, NEB) and ligated into pCR™-Blunt II-TOPO® vector (Zero Blunt™ TOPO™ PCR Cloning Kit, Invitrogen™) with T7 or SP6 RNA polymerase promoters on either side of the multiple cloning sites. 5µg of the template plasmid DNA using restriction enzymes with 5′ overhang was linearized and purified (NucleoSpin Gel and PCR Clean-up, MACHEREY-NAGEL) Based on sequencing results, sense and anti-sense probe were identified and synthesized by *in vitro* transcription (DIG RNA Labeling Kit (SP6/T7), Roche). 1µl *in vitro* transcription product was left for later gel electrophoresis. Remained product was cleaned up and eluted by 100 ul RNase-free water. Saved 5µl for gel electrophoresis. Precipitated the probes by adding 5µl of tRNA (20mg/ml, Thermo Fisher Scientific) and 11.5µl 3M Sodium acetate (pH 5.2), 230µl 100% Ethanol at −80°C for at least 15 min. Spined down the pellet and washed it with 70% ethanol. Resuspended the pellet in 50µl of DEPC-H_2O and stored it at −80°C. For better tissue penetration, probe hydrolysis was carried out, 95µl prob+5µl tRNA was incubated in 2× carbonate (CO_3) buffer (300µl 200mM Na_2CO_3 and 200µl 200mM $NaHCO_3$ freshly prepared in DEPC-H_2O) at 60°C. Incubation time was calculated by formula:

$$\text{Time (minutes)} = (Li\text{-}Lf)/(K)(Li)\ (Lf)$$

Li = Initial length of probe (in kbp). Lf = Final length of probe (0.15 kbp). K = 0.11.

Neutralized the reaction by adding 10µl 10% Acetic acid. The probe synthesis and hydrolysis were checked by gel electrophoresis.

4.2.5.4 Dot blot analysis

The probe concentration and DIG-UTP incorporation was assessed by dot blot analysis. Spotted 1µl of serial dilutions (typically 10^{-1} to 10^{-5}) of the *in vitro* transcribed and control probes (Roche) on an N+ nylon membrane. RNA probe was fixed using UV cross-linking. The membrane was equilibrated in 1x TBS (100mM Tris–HCl, pH 7.5, 150mM NaCl) for 5 min and blocked in blocking buffer (0.5% of Blocking Reagent in 1× TBS buffer, Roche) for 30min at room temperature on a shaking platform. Membranes were rinsed in 1× TBS for 5min and incubated with anti-DIG antibody, diluting 1µl of Anti-digoxigenin-AP in 10ml of 1× TBS, for 45min at room temperature. After two washes in 1× TBS for 15min each, the membrane was equilibrated in 1× TN buffer (100mM Tris-HCl pH 9.5, 100mM NaCl) for 5min and further stained by NBT/BCIP 1/50 (v/v) in 1× TN buffer. When color showed up, usually around 5-10 min, the membrane was rinsed with water, let dried and kept as a record.

4.2.5.5 Sample sectioning

Embedded samples stored at 4℃ were placed at room temperature and the base plastic base mold removed from samples. Wax block was roughly trimmed to place the sample in the middle. After mounted the block on a microtome holder, further trimmed the wax block into a trapezoid and to be sure that the tissue inside was either parallel (for longitudinal sections) or perpendicular (for transverse sections) to the base of the microtome block as well as the top of the trapezoid also was parallel. Set the slide warmer to 37-42℃ (test different temperature degrees based on tissue type to protect tissue integrity when dried on slide) and placed Polysine Adhesion Slides (Thermo Scientific) onto the warmer with 1ml DEPC-H2O added. Then started the microtome and set the section at 10-20µm. Here because the target genes were expressed in maize sperm cell, 20µm sectioning was applied. When wax ribbons were 2cm length, used brushes and forceps to transfer sections to the top of water. Tried to place the next one right up against the previous one and be careful away from the white labeling region. Normally, three wax ribbons could be in one slide. When slide was full, carefully pipetted out water and absorbed excess water with kimwipe. Put all slides overnight on the warmer to dry and kept dry condition at 4℃ for 2-3 days.

4.2.5.6 Pre-hybridization

Preparation of *in situ* hybridization needed all buffers and equipment RNase free. So, glass jars were cleaned and baked at 180℃ overnight. And all buffers were made of autoclaved MiliQ water or DEPC-H_2O if needed. The slides used were wax removed and rehydrated before *in situ* hybridization following the next steps: 2× 15min histoclear; 2× 2min 100% ethanol; 2min 95% ethanol; 2min 70% ethanol; 2min 50% ethanol; 2min 30% ethanol; 2× 2min H_2O. Continued with the following buffer wash steps: 20min 2× SSC; 30min proteinase K (1μg/ml, Invitrogen) in 100 mM Tris–HCl, pH 8.0, and 50 mM EDTA; 2min 2 mg/ml glycine in 1× PBS; 2× 2min 1× PBS; 10min 3.7% formaldehyde in 1× PBS; 2× 5min 1× PBS; 10min 0.1 M triethanolamine (pH 8.0) and 0.5% acetic anhydride with a stir bar; 2× 5min 1× PBS; After the pretreatment was finished, sections were dehydrated through the ethanol series: starting from 30% and ending in 100% ethanol. Slides were left to dry in a hood for 1-2 h.

4.2.5.7 Hybridization

Several black humidified boxes with paper towels were soaked with 50% formamide and 0.3M NaCl prewarmed at 50°C. The hybridization buffer was kept at 65°C. Diluted different probes to same concentration of 20μL with DPEC-H2O and denatured with 20μL formamide at 80°C for 2 min. Put them on ice right after denaturing. Added 160μL of prewarmed hybridization buffer to the probe. Mixed gently and avoided air bubbles. The final volume for the hybridization solution was 200μL. Applied the warm hybridization solution to one end of the slide. Slowly place down a piece of same size parafilm. Avoided air bubbles and to be sure that the hybridization solution was evenly distributed over the sections. Placed slides in the humid boxes and hybridized overnight at 50°C-65°C (hybridization temperature needs be optimized based on *in situ* hybridization results).

4.2.5.8 Post-hybridization

In post-hybridization part, RNase-free was not necessary. Put slides in a small plastic tray with 65°C 2× SSC and the covered parafilm could be floated off. Then washed slides four times in 0.2× SSC for 30min, each at hybridization temperature with gentle agitation. Incubated slides in 1× PBS for 5min or slides could be kept in 1× PBS overnight at 4°C.

4.2.5.9 Blocking and anti-DIG antibody binding

Slides were firstly blocked 45min with blocking solution and washed with TBX for 45 min. Antibody was diluted 1:1,500 in TBX. Applied 100–200µL of antibody to each slide and gently covered with parafilm, no air bubbles. Put all slides in humid boxes for 2h. Similarly, floated off parafilm in TBX and washed the slides four times in TBX for 15min each.

4.2.5.10 Detection

Slides needed washing two times with detection buffer for 10min each. Then applied 100–200µL of substrate solution (prepared according to manufacturer's instruction) to the slides. Carefully put down a parafilm and avoided air bubbles. Transferred the slide to a humid box. Sealed the boxes with parafilm and left them in darkness for 0.5–3 days (detection duration time is various, in this study around 8h was already sufficient). After signals showed for observation, floated off the cover parafilm in TE buffer in a small plastic tray to terminate the color reaction. Slides could be stored in TE buffer for a day or two days. Further dehydrated slides through ethanol series.

4.2.6 Pollen tube actin immunostaining

Actin organization was investigated based on previous protocol (Qu, Xiaolu, et al., 2020) with some modifications. Germination step was same with *in vitro* germination on solid medium part. After germination 45min, 200µl liquid germination medium contained 300µM MBS was applied for each slice and incubated at 28℃ for 1h. Washed samples with TBS (50mM Tris, 200mM NaCl, 400mM Sucrose) + 0.05% NP40 for three times, each time for 10min. Samples were stained with 200nM Alexa Fluor 488 phalloidin in TBS over night at 4 °C in humid square Petri dish. Washed samples before observation with TBS once. Mounted the solid PGM pieces on a cover slide to image with Leica SP8 multiphoton laser scanning confocal microscope equipped with a 63x objective (numerical aperture of 1.4). Excited samples with 488 nm argon laser and collected emission light at 505-605 nm wavelength. Zoomed pollen grain and pollen tube by 3×, imaged optical slice at 0.5µm step size.

4.2.7 ZmLIM6/14 ChIP-seq with maize mature pollen

Based on previous published method (Begcy and Dresselhaus, 2020), some modifications were applied based on the plant tissue used in this study.

4.2.7.1 Sample preparation

This step was same as sperm cell isolation. In brief, harvested fresh pollen around 1g and continued hydration step at least 2h in petri dish with a wet moist filter paper in the internal part of the lid. Added 0.55mM mannitol solution (1g pollen per 15mL) and incubated on a platform shaker with slow agitation (80rpm) for 1-2 h to release nuclei from mature pollen. A cleared pollen lysate was obtained after filter step.

4.2.7.2 Chromatin crosslinking and preparation

Added 37% formaldehyde in to pollen lysate (1mL per 37mL lysate) and gently inverted several times, left on ice for 20min. Subsequently, added 2.5mL of 2.5M Glycine to stop crosslinking around 20min on ice. Centrifuged the lysate at 2500g for 10min at 4℃. Removed the supernatant and resuspended the pellet containing crude nuclei in extraction buffer 2 (0.25M sucrose, 1% triton X-100, 10mM HEPES pH 8.0, 10mM $MgCl_2$, 1× AEBSF, 5mM β-ME, 1× cOmplete™ EDTA-free Protease Inhibitor Cocktail) by pipetting up and down. Transferred the solution to Eppendorf tube and centrifuged at 12, 000g for 10min at 4℃, repeated wash three to four times. Resuspended the pellet in 400μL of extraction buffer 3 (1.7M sucrose, 1% triton X-100, 10mM HEPES pH 8.0, 2mM $MgCl_2$, 1× AEBSF, 5mM β-ME, 1× cOmplete™ EDTA-free Protease Inhibitor Cocktail). Added 400μL extraction buffer 3 in another Eppendorf tube and gently layered the resuspended pellet on top. Centrifuged at maximum speed for 1h at 4℃ (sucrose filtration). Removed the supernatant and resuspended the chromatin pellet in 400μL of Nuclei Lysis Buffer (10mM EDTA, 50mM HEPES pH 8.0, 1% SDS, 1× AEBSF, 1× cOmplete™ EDTA-free Protease Inhibitor Cocktail) incubated on ice for at least 30min.

4.2.7.3 Chromatin sonication

Diluted sample 1:5 with ChIP dilution buffer (1.25mM EDTA, 16.7mM HEPES pH 8.0, 1% triton X-100, 187.5mM NaCl, 1× AEBSF, 1× cOmplete™ EDTA-free Protease Inhibitor Cocktail) to get the optimal volume for sonification with Bioruptor Pico (Diagenode). Collected 50μL as before sonification sample (freeze). Sonicated samples for 10 cycles, program: 30 s on/off with max 300μL in sonication tube to avoid bubbles. Combined all sonicated samples and collected 50μL as after sonification sample (freeze). Centrifuged remaining chromatin solution at 14, 000g for 10min at 4℃. Transferred the supernatant into new Eppendorf tubes and repeated centrifugation.

4.2.7.4 Immunoprecipitation

Dynabeads™ Protein A (Thermo Fisher Scientific) was washed three times with ChIP Dilution buffer in a low protein binding tube (Eppendorf). After each washing step, collected pellet beads by put on a magnetic rack (Thermo Fisher Scientific) and discarded the supernatant. Incubated the sonicated chromatin solution together with the washed Dynabeads at 4℃ for 1h to reduce the background signal. Transferred the supernatant into new tubes and kept the equilibrium Dynabeads at 4℃. Split the chromatin solution equally into 3 low protein binding tubes, 300-500 µL for each immunoprecipitation (IP) reaction. Added desired antibodies to each tube, with the exception of the mock control (no antibody). Left the tubes rotating overnight at 4 °C.

4.2.7.5 Washing and elution

The equilibrium Dynabeads were washed three times with ChIP dilution buffer and added into overnight-incubated chromatin solution containing antibodies at 4°C for 3h with gentle rotation. Pelleted Dynabeads and collected 500µL of the supernatant each of the mock control samples as input DNA (freeze). Carefully discarded remaining supernatants. Washed pellet beads with 500µL of Low Salt Buffer (0.1% SDS, 1% triton X-100, 150mM NaCl, 2mM EDTA, 20mM HEPES pH 8.0), High Salt Buffer (0.1% SDS, 1% triton X-100, 500mM NaCl, 2mM EDTA, 20mM HEPES pH 8.0), LiCl buffer (1mM EDTA, 1% NP40, 1% sodium deoxycholate, 10mM HEPES pH 8.0, 0.25M LiCl) and two times TE buffer(1mM EDTA. 10mM Tris–HCl pH 8). For each time washing left the sample rotating at 4°C for 10min and pelleted beads with magnetic rack. After the last TE buffer washing step, removed supernatant and added 250µL freshly made elution buffer (0.1mM $NaHCO_3$, 1% SDS). Vortexed briefly and incubated for 15min at 65°C with gentle rotation. Pelleted the beads and carefully transfer the supernatant to another tube. Repeated elution step and combined elute in one tube (500µL total).

4.2.7.6 ChIPed DNA Extraction

Added 20µL of 5M NaCl to the eluate and incubated overnight at 65°C to reverse crosslinking of all the samples (before sonification/ after sonification/ input/ elution). Added 31µL of freshly prepared protein degradation buffer (0.5M EDTA, 1M Tris–HCl pH6.8, 20mg/mL proteinase K) to the eluate and incubated for 3h at 45°C with agitation. Added 500µL of 25:24:1 Phenol/Chloroform/Isoamyl alcohol and shake tubes for 10s. Centrifuged the solution for 5min at 16,000g to separate phases. Pipetted out the water phase containing the DNA in to a new tube. Added 500µL of 1-Brom-3-Chloropropan and centrifuged for 5min at 16,000g.

Transferred the top water phase 400µL of each tube containing ChIPed DNA to a new clean tube. Added 40µL of 3M NaAc pH 5.8 following 1mL of 100% ethanol and put at −80°C for 1h to pellet DNA. Centrifuged all samples at maximum speed for 30min at 4°C. Washed pellet with 1mL of 70% ethanol. Centrifuged for 5min. Discarded supernatant and let ethanol dry at room temperature for 5 min. Added 40µL of H_2O or TE elution buffer with 10µg/mL of RNase to dissolve DNA. Extracted ChIP samples can be stored at −20°C. DNA concentration was measured with Qubit high sensitivity DNA kit (Invitrogen).

4.2.7.7 ChIP-seq and analysis

Libraries construction was generated using NEBNext Ultra II DNA Library Prep Kit for Illumina (New England BioLabs). Some modifications were induced based on the starting DNA concentration. In brief, the End prep step was same as the kit manual. For adaptor dilution, 1:50 was applied in this study and size selection of adaptor-ligated DNA was included. Further the 13 cycles program was decided in the PCR enrichment reaction. The final libraries were evaluated by High sensitivity DNA analysis at Bioanalyzer (Agilent). Sequencing was performed at the Genomics Core Facility "KFB - Center of Excellence for Fluorescent Bioanalytics" (University of Regensburg, Regensburg, Germany). ChIP Seq was carried out as described in the Illumina NextSeq 2000 Sequencing System Guide (Illumina). In brief, equimolar amounts of each library were sequenced on an Illumina NextSeq 2000 instrument controlled by the NextSeq 2000 Control Software (NCS) v1.5.0.42699, using one 100 cycles P2 Flow Cell with the single index, paired-end (PE) run parameters. Image analysis and base calling were done by the Real Time Analysis Software (RTA) v3.10.30. The resulting .cbcl files were converted into .fastq files with the bcl2fastq v2.20 software. The raw reads were mapped to maize genome version5 (Hufford et al., 2021) using Bowtie2 (Langmead and Salzberg, 2012) and coverage tracks were calculated with deeptools "bamCoverage". Downstream analysis was mainly performed using the deepTools2 suite(version 3.5.0)(Ramírez et al., 2016). After confirming high pairwise correlations, the biological replicates were merged and CPM normalized. Macs2 callpeak was used to call peaks over input as control (Zhang et al., 2008). And peaks annotation and visualization were performed with ChIPseeker (Yu et al., 2015).

4.3 Results

4.3.1 *ZmLIM6* and *ZnLIM14* are highly expressed at bicellular and tricellular stage pollen.

Based on the results of RNA-seq data obtained from the tetrad, unicellular, bicellular, and tricellular stages of pollen development, specific expression patterns of gene clusters showed up in each developmental stage. Using this dataset, selected transcription factor (TF) genes were listed with high expression levels (TPM＞200 in at least one stage) (Figure 4.1). Among these highly expressed TF genes, *ZmLIM6* and *ZmLIM14* were the top two genes in terms of expression level, with peak expression at the bicellular and tricellular stages of pollen development. Similarly, *ZmMYB150* also displayed the same expression pattern, and it has been previously reported to be specifically highly expressed at the late stage of anther development (Zhao et al., 2022). Additionally, *ZmMYB146*, *ZmMYB31*, and *ZmMYB84* were selected from the same transcription factor family due to their expression at the tetrad stage. Besides *ZmLIMs* and *ZmMYBs*, the well-known MADS-BOX (MADS) gene family members, *ZmMADS11/16/18/38/60*, were also selected, which exhibited high expression levels at these four stages. *ZmMADS11*, *ZmMADS16*, and *ZmMADS18* have previously been found to play a role in floral organ identity and flower development (Ambrose et al., 2000; Whipple et al., 2004; Bartlett et al., 2015). Another transcription factor family, *ZmbHLH*, was represented by four members in this selection. *ZmbHLH51* has been characterized as a male sterile gene in maize and shown to interact functionally with *ZmbHLH16* during maize anther development. (Liu et al., 2021). Both of above *ZmbHLH* TF genes displayed high expression levels at the tetrad stage in our group RNA-seq data, providing more detailed spatial-temporal information on gene activity. In summary, these known transcription factors genes in pollen development showing up in this selection results indicates the reliability of our group transcriptome data and provides a clue that *ZmLIM6* and *ZmLIM14* may also are involved in maize pollen development.

Within the top TF genes, *ZmLIM6* and *ZmLIM14* which belong to a poorly studied gene family in maize were identified. Additionally, our analysis revealed that *ZmLIM8* and *ZmLIM9*, two members of the LIM family closely related to *ZmLIM6* and *ZmLIM14*, exhibited a similar expression pattern across various tissues. Moreover, our previous findings demonstrated that these four ZmLIMs were predominantly expressed in the sperm cells of maize pollen (as shown in the previous chapter, table 3.2). The distinct expression patterns and enrichment information of these genes suggest that further investigation of their functions during maize pollen development and sperm cell formation would be highly intriguing.

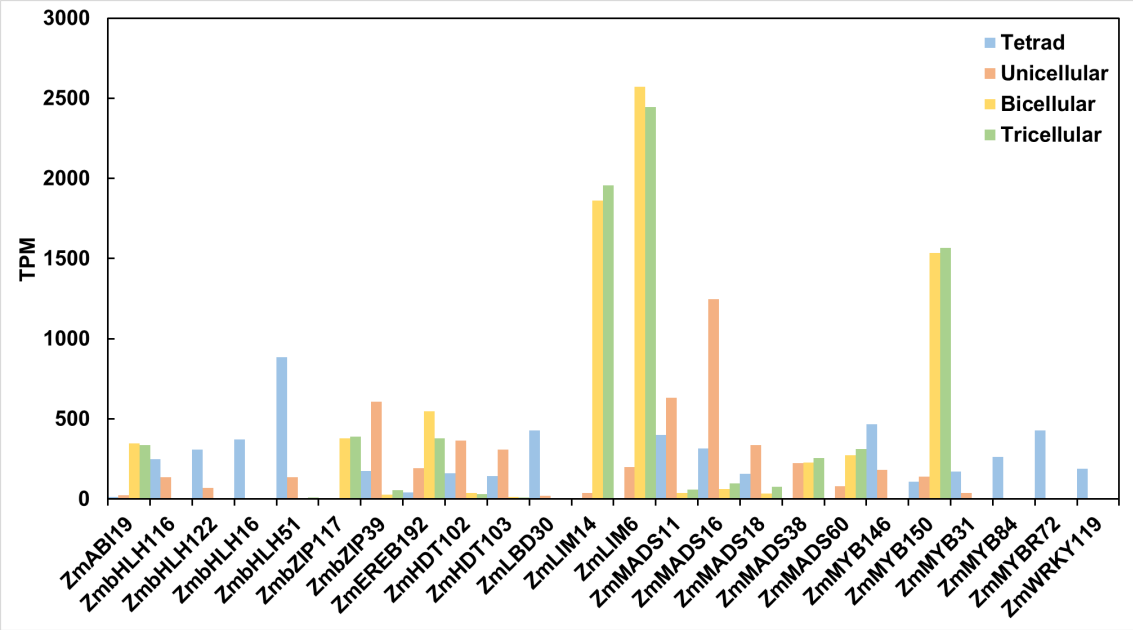

Figure 4.1 Selected transcription factor genes of high expression level at different developmental stages maize pollen. TPM value was extracted from transcriptome data. Different colors represented four maize developmental stages.

4.3.2 ZmLIM6 and ZmLIM14 expression pattern validation

4.3.2.1 In situ hybridization

The RNA-seq data revealed the high expression of *ZmLIM6* and *ZmLIM14* in bicellular and tricellular pollen, particularly in sperm cells. To investigate the histological localization of these genes, *in situ* hybridization was employed using probes synthesized by inserting the coding sequences of *ZmLIMs* into the pCR-Blunt II-TOPO vector. The entire CDS of *ZmLIM6* (615bp) and 490bp of *ZmLIM14* CDS (618bp) were amplified and ligated with an *in vitro* transcription plasmid (Figure 4.2A). The Sp6 and T7 RNA polymerases were used to synthesize the anti-sense and sense probes from the same plasmid. The success of probe synthesis was confirmed by the dot plot test, which provided a reference concentration for the subsequent application.

Wax section in situ hybridization

Unicellular, bicellular, and tricellular stage anthers were harvested and embedded in wax. To ensure maximal mRNA accumulation on a single slide, 20μm thick transverse sections were taken from different developmental stages. *In situ* hybridization revealed that the transcripts of ZmLIMs were predominantly detected in pollen grains, with no detectable signal observed in anther tissues (Figure 4.3). Due to the low expression of *ZmLIM6* and *ZmLIM14* at the

unicellular stage, neither the anti-sense nor the sense probes of these genes exhibited any color in the pollen grain or anther tissue (Figure 4.3A&B, G&H). At the bicellular stage, the signals in the pollen grain were observed, which were not detected by the sense probe (Figure 4.3C&D, I&J). The round shape of the signal observed during the bicellular stage indicated that the pollen was still in the early bicellular stage. In tricellular pollen, *in situ* hybridization results using the anti-sense probes demonstrated abundant mRNA expression of both *ZmLIM6* and *ZmLIM14* in the pollen grain (Figure 4.3E&F, K&L). The cytoplasm of the pollen grain exhibited a detectable signal, and the majority of the strong signal was observed in the pollen nuclei. As the section thickness was set at 20μm, it was technically feasible to obtain and detect two sperm cells in one section. Thus, both *ZmLIM6* and *ZmLIM14* exhibited remarkable enrichment in the tricellular pollen sperm cell via *in situ* hybridization.

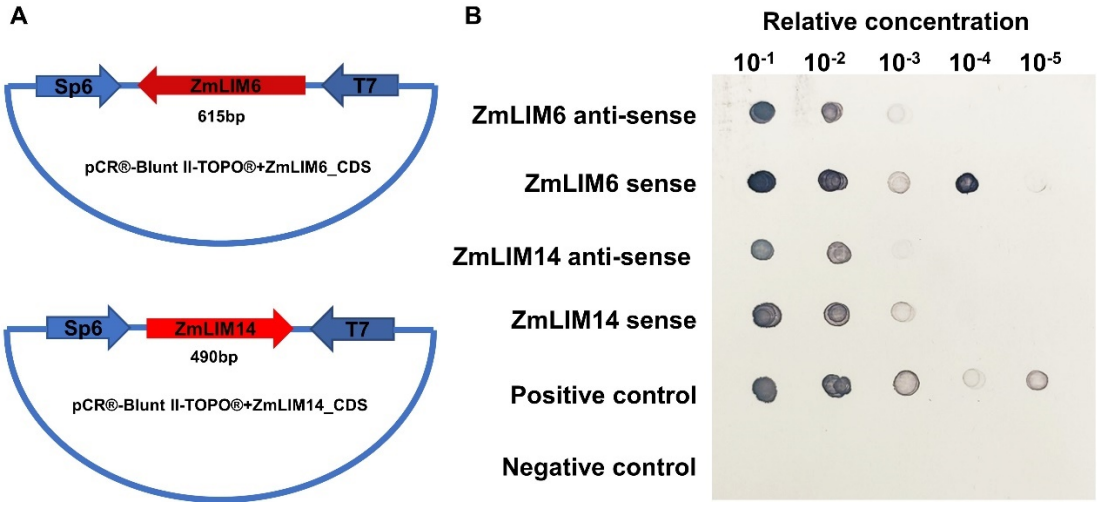

Figure 4.2 *In situ* hybridization probe synthesis. (A) Schematic picture of in vitro transcription vector. Sp6 and T7 two transcriptase were used. (B) Dot plot of different probes. concentration and efficiency test of synthesized probe.

Whole mature pollen in situ hybridization

The mRNA transcription pattern of *ZmLIM6* and *ZmLIM14* at the unicellular, bicellular, and tricellular stages of maize pollen were validated through *in situ* hybridization with wax anther sections. However, the limitations of wax sectioning resulted in missing some information about the entire pollen. Therefore, it was necessary to conduct *in situ* hybridization in an alternative manner. Whole mature pollen *in situ* hybridization was subsequently performed.

The same gene-specific probes were utilized as in the prior experiment. However, due to the weighty coat and firm cell wall of maize pollen, the whole pollen *in situ* hybridization was less

efficient compared to the wax section experiment. Nevertheless, upon comparison with the results from the sense probe, it became apparent that the anti-sense probes of both *ZmLIM6* and *ZmLIM14* exhibited signals that were dispersed throughout the entire pollen grain and concentrated in the nuclei segment (Figure 4.4). By using DAPI as a counterstain with mature pollen nuclei, novel discoveries were made that the *ZmLIM14* mRNA was also concentrated around the vegetative nucleus in mature pollen (Figure 4.4 G-K).

In summary, our results showed that the expression pattern indicated by RNA-seq data are consistent with the anther and whole pollen *in situ* hybridization experiments. Moreover, *ZmLIM6* and *ZmLIM14* were not just expressed in sperm cells but also in the vegetative nucleus, suggesting their possible involvement in sperm cell formation and pollen tube growth.

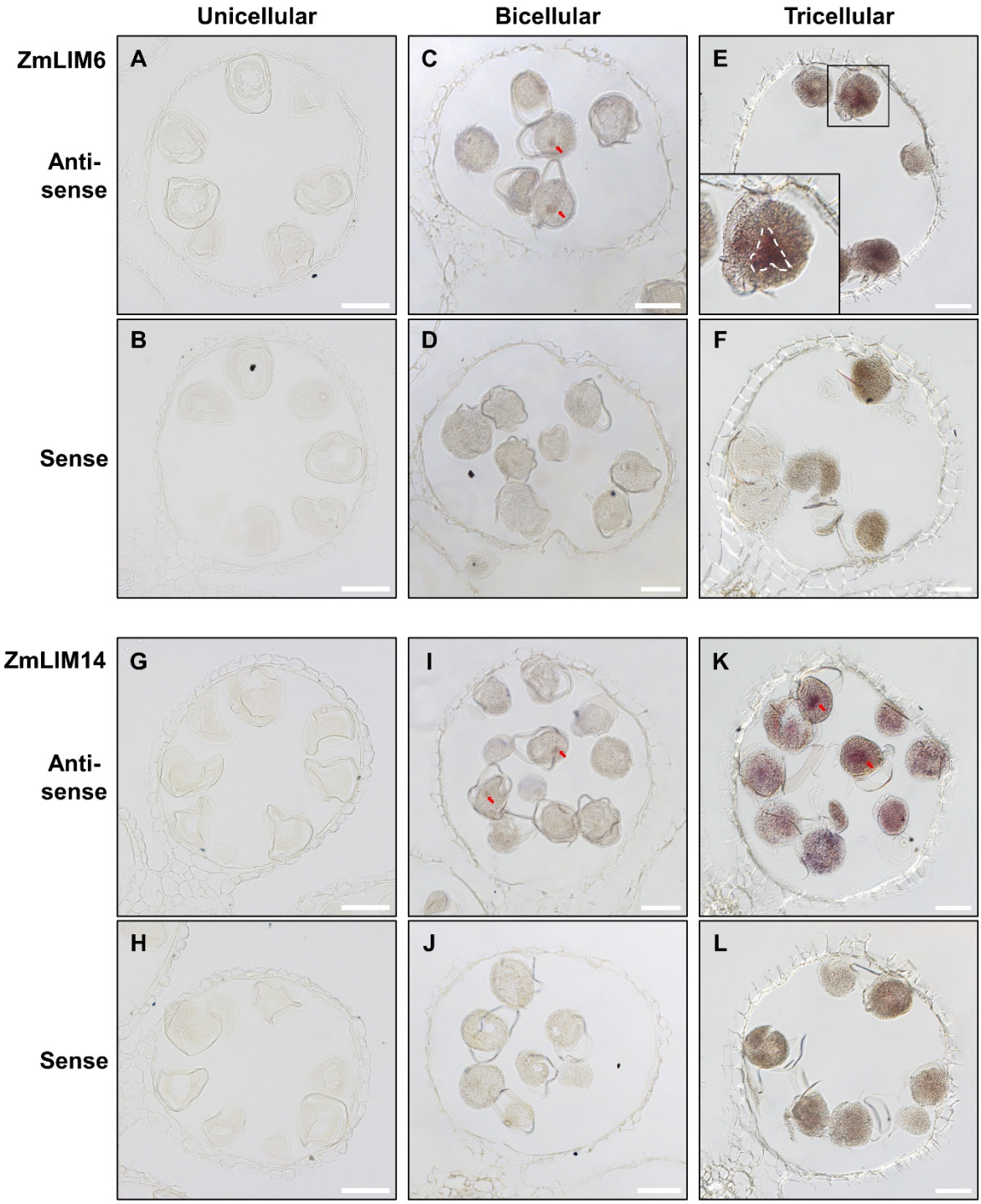

Figure 4.3 *In situ* hybridization of *ZmLIM6* and *ZmLIM14* at different developmental stage pollen. (A-F) *In situ* hybridization of *ZmLIM6*. (A, C, E) Anti-sense probe of unicellular, bicellular and tricellular pollen section. (E) A sperm cell-like shape signal was observed at tricellular stage. Highlight by white dash line. (B, D, F) Sense probe results. (G-L) *In situ* hybridization of *ZmLIM14*. (G, I, K) Anti-sense probe results. (H, J, L) Sense probe results. Red arrow indicated positive signal in pollen grain. Scale = 50μm

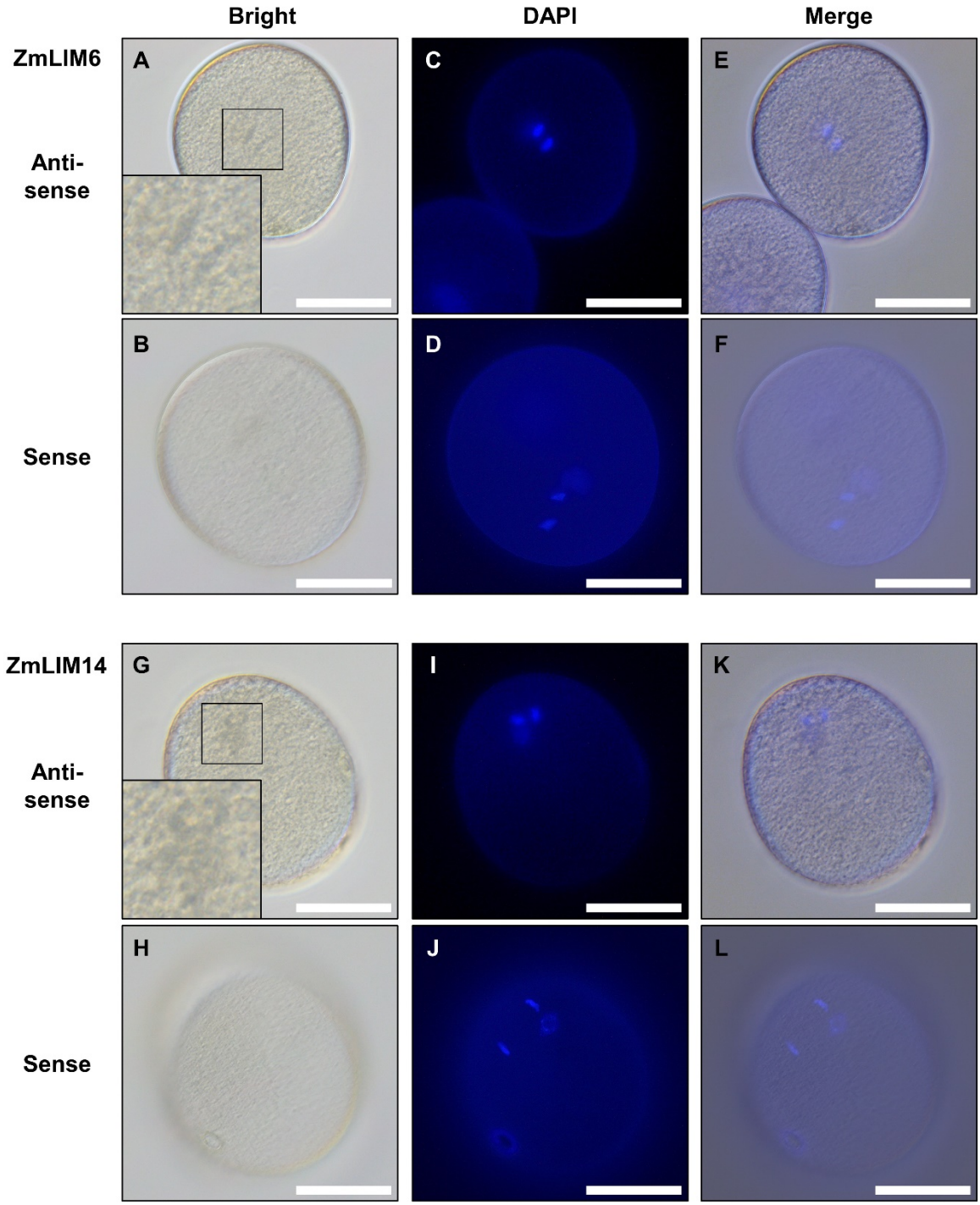

Figure 4.4 Whole mature pollen in situ hybridization of *ZmLIM6* and *ZmLIM14*. (A-F) whole mature pollen *in situ* hybridization of *ZmLIM6*. (G-L) whole mature pollen *in situ* hybridization of *ZmLIM14*. (A, G) Anti-sense probe result. Accumulated signals were zoomed in by black block. (B, H) Sense probe result. (C-D, I-J) Nuclei in pollen stained by DAPI. (E-F, K-L) Merge pictures of bright and DAPI channels. Scale bar = 50μm.

4.3.2.2 ZmLIMs protein subcellular localization assay

The *ZmLIMs* were selected as the focus of the research due to their expression pattern as transcription factors. *In situ* hybridization revealed the abundance of *ZmLIM6/14* mRNA in pollen. To gain a better understanding of the subcellular localization of ZmLIMs at the protein level, the tobacco leaf transient expression system and Maize black Mexican sweet (BMS) suspension cultured cells were utilized.

Tobacco leaf transient expression assay

The CDS of *ZmLIM6* (615bp) and *ZmLIM14* (618bp) were cloned and fused to the C-terminus of enhanced green fluorescent protein (eGFP). To serve as a negative control, eGFP was also expressed separately. These fluorescent transgene constructions were transiently expressed in tobacco cells. As anticipated, in contrast to eGFP's universal distribution, both ZmLIM6 and ZmLIM14 displayed a dominant fluorescence signal in the nucleus (Figure 4.5). However, the localization of eGFP-ZmLIMs was also observed in subcellular structures, likely the endoplasmic reticulum.

Maize BMS cell transient transformation assay

Although the tobacco leaf transient expression system is a commonly used method to study protein subcellular localization, it is subject to bias and may lead to misunderstandings when expressing monocot proteins in dicot cells. To overcome this limitation and obtain a more accurate visualization of ZmLIMs protein subcellular localization, the Maize BMS cell suspension cultured cells were utilized as previously described (Zhou and Dresselhaus, 2019). In order to verify the subcellular localization of ZmLIMs in cytoplasmic organelles, transgene constructs containing the endoplasmic reticulum marker (mCherry and eGFP fusion) were introduced. New fluorescent fusion protein plasmids containing ZmLIM6 CDS at the mCherry C-terminus and ZmLIM14 at the eGFP N-terminus and C-terminus were transiently co-transfected in BMS cells (Figure 4.6).

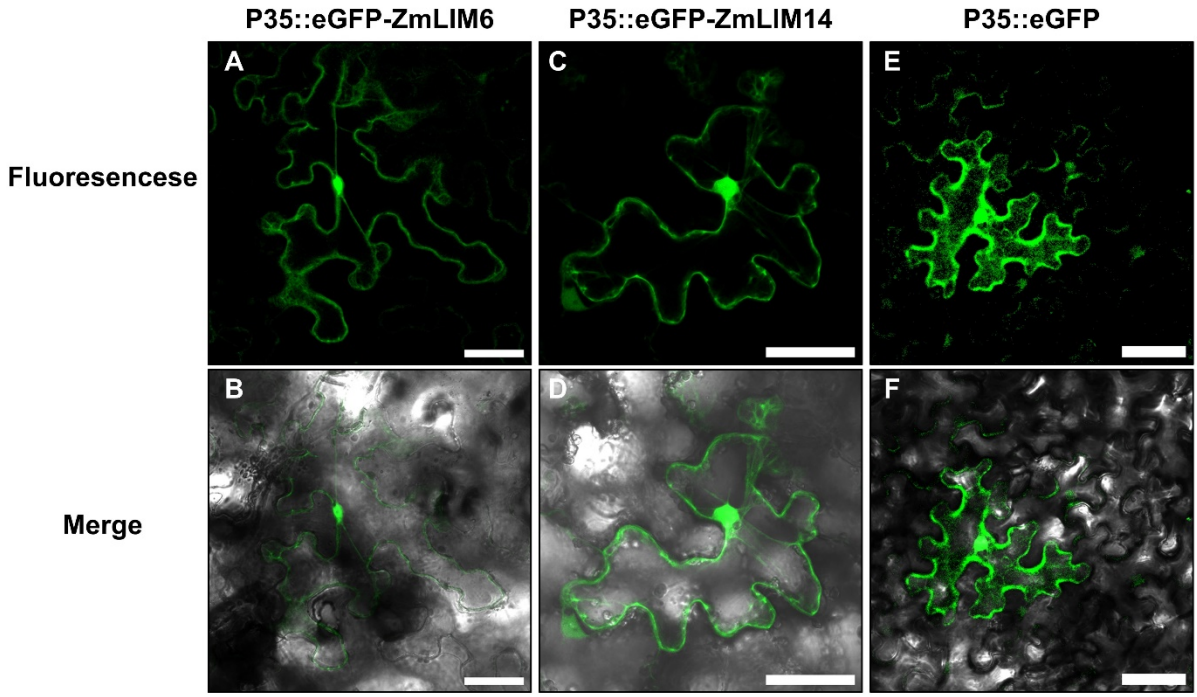

Figure 4.5 Tobacco leaf transient expression assay of eGFP fusion ZmLIMs protein. (A-B) Transient expression of eGFP-ZmLIM6 in GFP and bright-merged channel. (C-D) Transient expression of eGFP-ZmLIM14 in GFP and bright-merged channel. (E-F) Transient expression of eGFP as a negative control in GFP and bright-merged channel. Scale bar = 50μm

The mCherry-ZmLIM6 fusion protein exhibited intense fluorescence in both the nucleus and cytoplasm of BMS cells (Figure 4.6A-D). Plot profile analysis of the fusion protein with an ER marker revealed that the red and yellow line peaks almost simultaneously appeared near the nucleus, and the red line maintained a high value while the yellow precipitously declined towards the nucleus. Similarly, the eGFP-ZmLIM14 fusion protein exhibited the same localization in BMS cells (Figure 4.6E-H). The endoplasmic reticulum was continuously surrounding the nuclear envelope and formed a red ring at nuclear boundaries while the eGFP-ZmLIM14 signal showed up inside (Figure 4.6G). From the observed results, it was concluded that although ZmLIMs protein exhibited an endoplasmic reticulum structure pattern in tobacco leaf and BMS cells, there was no total overlapped co-localization between ZmLIMs and endoplasmic reticulum. Additionally, fusion of eGFP to the C-terminus of ZmLIM14 disrupted the protein localization (Figure 4.6I-K), indicating the importance of the ZmLIMs C-terminus for normal protein expression and location. This was consistent with a previous study that demonstrated the functional importance of the C-terminal (Ct) domain of PLIMs in *Arabidopsis thaliana* (Moes et al., 2015).

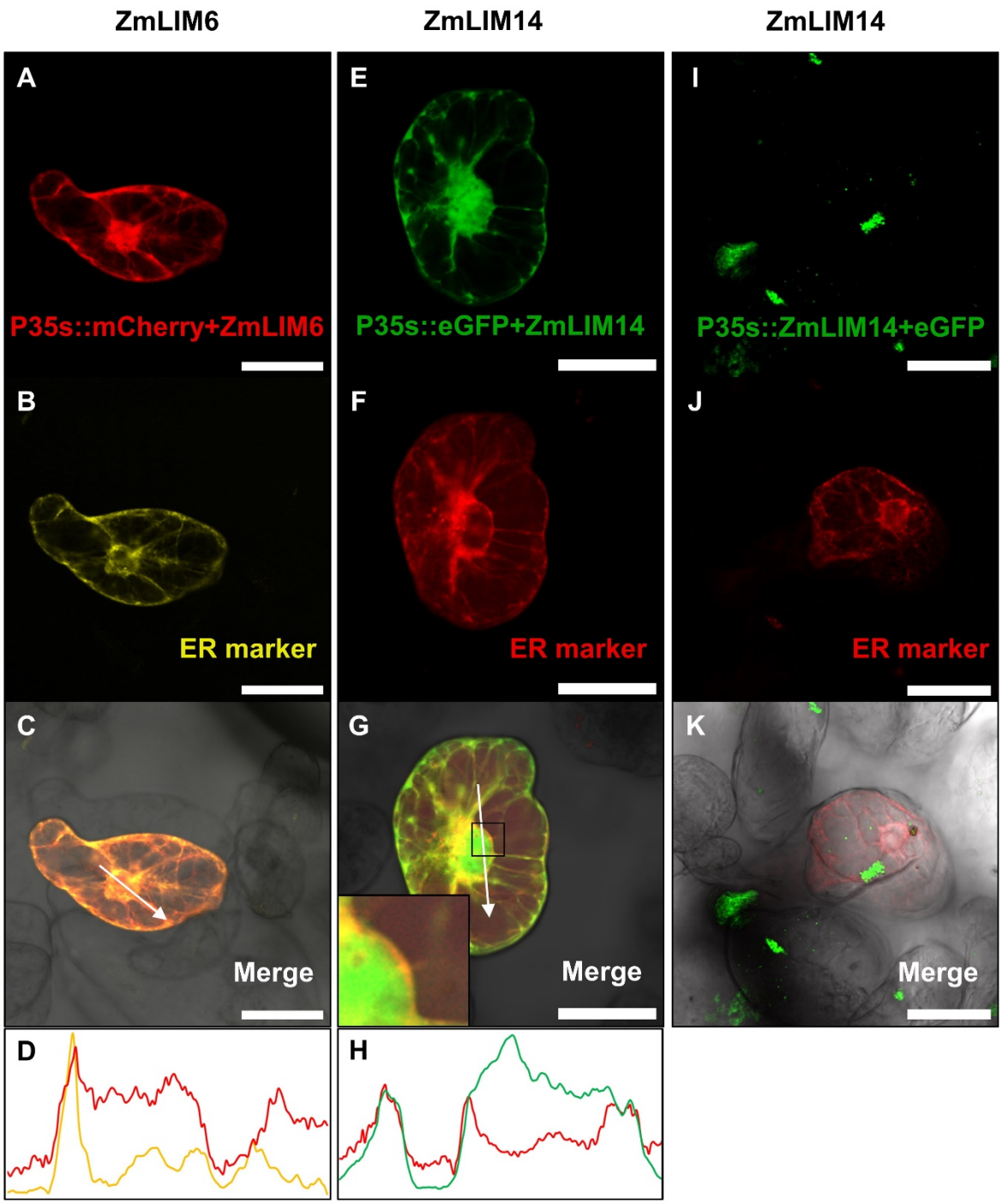

Figure 4.6 BMS cells transient co-transformation of ZmLIMs and endoplasmic reticulum marker. (A-C) BMS cell transformed with mCherry-ZmLIM6 (red) and ER-YFP (yellow). (D) Plot profile of the single channels indicated by the thin white line in C. (E-G) BMS cell transformed with eGFP-ZmLIM14 (Green) and ER-YFP (red). (G) Zoom in picture showed nuclear boundaries as black block indicated. (H) Plot profile of the single channels indicated by the thin white line in G. (I-K) BMS cell transformed with ZmLIM14-eGFP (Green) and ER-YFP (red). Scale bar = 50μm

4.3.3 ZmLIM protein expression and purification from *E. coli*

To investigate the biochemical properties and generate specific antibodies, it was necessary to express and purify recombinant ZmLIM proteins. Considering the subsequent antibody construction, a Gateway destination vector, pET-53-DEST, which solely contained an N-terminal 6×His-Tag fused with the recombinant protein, was utilized for protein induction in *E. coli*.

The coding sequences of ZmLIM6 and ZmLIM14 were cloned and inserted into pET-53-DEST. The resulting plasmids were then transformed into the *E. coli* strain BL21(DE3). To determine the optimal conditions for protein production, both the induction temperature and IPTG concentration were evaluated (Figure 4.7).

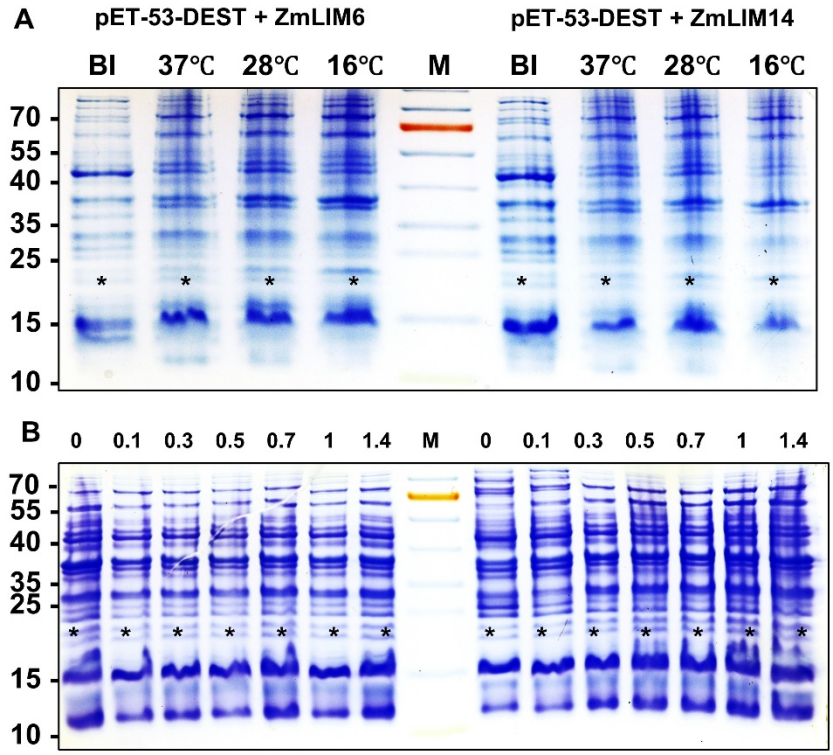

Figure 4.7 Production condition test of 6xHis tagged ZmLIM proteins in BL21(DE3) (Coomassie stained gel). (A) Incubation temperature test. 1mM IPTG used. (B) IPTG concentration test (mM/L). Incubated at 37℃. SDS-PAGE analysis revealed the proteins of appropriate size for 6×His-ZmLIMs (expected molecular weight [MW]: ZmLIM6: 22.5kDa, ZmLIM14: 22.5kDa, indicated by asterisks.) BI: bacterial lysate before induction. M: Protein ladder marker.

Typically, recombinant proteins in BL21(DE3) are cultured at 37℃, the optimal temperature for *E. coli* growth. However, our findings demonstrated that the highest production of ZmLIMs

recombinant proteins occurred at 16℃ with the same IPTG concentration (1mM). It was further investigated IPTG concentration and determined that 0.7mM for ZmLIM6 and 1mM for ZmLIM14 were the most effective dosages for induction. Higher concentrations did not enhance protein production efficiency.

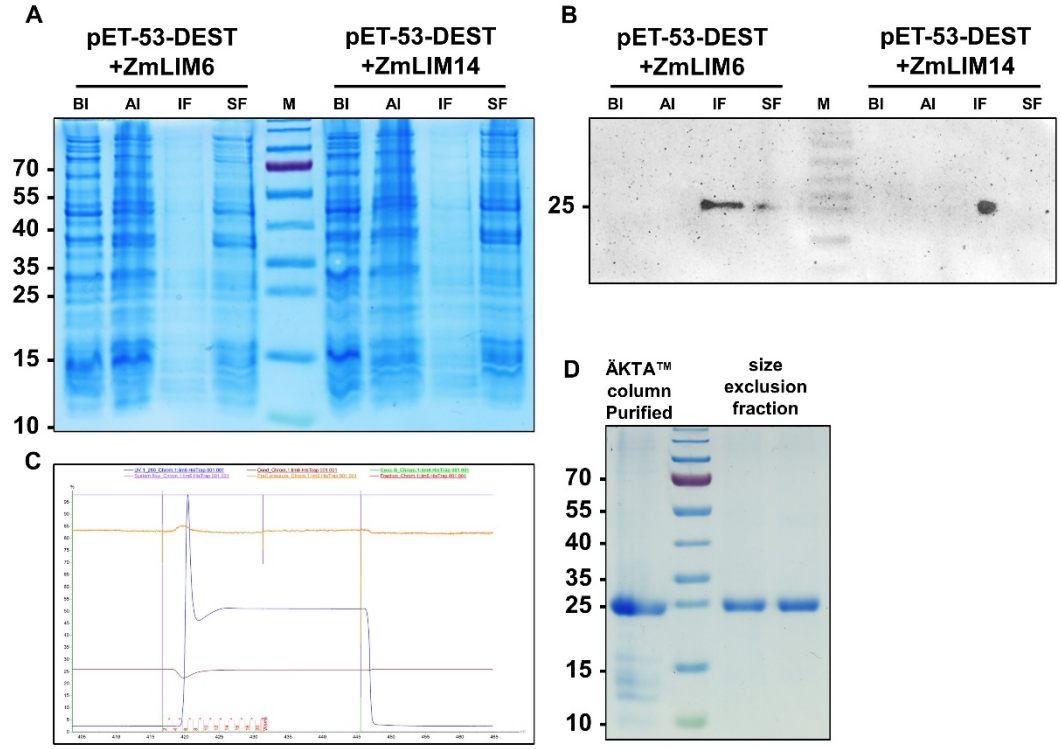

Figure 4.8 Solubility test and chromatography-based purification of the recombinant ZmLIMs proteins. (A) SDS-PAGE gel of the recombinant ZmLIMs proteins solubility test, Coomassie stained. (B) Western blot to confirm the solubility test. Both recombinant ZmLIMs showed strong bands in insoluble fraction. (C) 6×His-ZmLIM6 purification results of ÄKTA™ chromatography system. (D) 6×His-ZmLIM6 purification further purification by size exclusion chromatography. AI: bacterial lysate after induction; IF: the insoluble fraction; SF: the soluble fraction.

With 16℃ and 1mM IPTG as the induction conditions, it was necessary to determine the solubility of ZmLIMs recombinant protein for large-scale protein purification. SDS-PAGE gel and Western blot revealed that the most of 6×His-ZmLIM6 protein and all 6×His-ZmLIM14 were present in the insoluble fraction (Figure. 4.8 A&B), indicating that the recombinant protein was expressed in inclusion bodies in *E. coli*. Protein purification efficiency was limited with inclusion bodies under natural conditions. Previous studies found that inclusion bodies could be solubilized by high concentrations of strong detergents, such as 8M urea or 6M guanidinium chloride (Gu-HCl) (Rudolph and Lilie, 1996). Additionally, a well-established protocol using

chromatography-based purification with the ÄKTA™ pure protein purification system (GE Healthcare) was utilized to purify the 6×His-tagged proteins under denaturing conditions.

To produce a sufficient amount of recombinant protein, 2 liters of growth medium with induced colonies were incubated at 16℃ overnight, and the cell pellet was solubilized in 6M Gu-HCl lysis buffer. After further centrifugation and filtration, the soluble fraction containing His-tagged ZmLIMs was purified using a HisTrap™ Fast Flow column (Cytiva) with a linear gradient of 6 to 0 M urea buffer flow (Figure 4.8 C). Because unexpected bands appeared in the column purified fraction by SDS-PAGE gel analysis (Figure 4.8D), a Superdex™ 75 Increase 10/300 GL (Cytiva) size exclusion chromatography column was utilized for further purification. The final highly purified 6×His tagged ZmLIM6 and ZmLIM14 recombinant proteins were obtained (Figure 4.8D). Finally, the eluted peptides of ZmLIMs were refolded and desalted by HiTrap Desalting column (Cytiva) in native condition buffer. The highly pure ZmLIMs recombinant protein was utilized in subsequent experiments and antibody production.

4.3.4 Generation of ZmLIM CRISPR/Cas9 knockout mutant

In order to elucidate the roles of ZmLIM6 and ZmLIM14 during maize pollen development, it is imperative to induce loss-of-function mutations within these genes. The efficacious genome editing system employing clustered regularly interspaced short palindromic repeats/CRISPR-associated Cas9 (CRISPR/Cas9) in maize proved readily accessible, facilitating the generation of ZmLIMs knockout mutants (Char et al., 2017). The CRISPR/Cas9 system were constructed by *E. coli* cloning vectors and an *Agrobacterium*-delivered vector. In total four guide RNAs were cloned to target single or multiple genes. Considering the gene redundancy of ZmLIM6/14 and ZmLIM8/9, alongside subsequent genotyping efforts, it was judicious to devise a single plasmid containing four guide RNAs — two of which targeted the same gene — with the aim of achieving either a double gene knockout or independent editing.

As the CRISPR/Cas9 system was implemented with the Hi-II, a maize line isolated from offspring of a cross between A188 and B73, guide RNA design was constrained to the identical genomic regions of ZmLIM genes from both inbred lines. Moreover, targeting regions were selected within conserved LIM domains to ensure protein non-function upon knockout events.

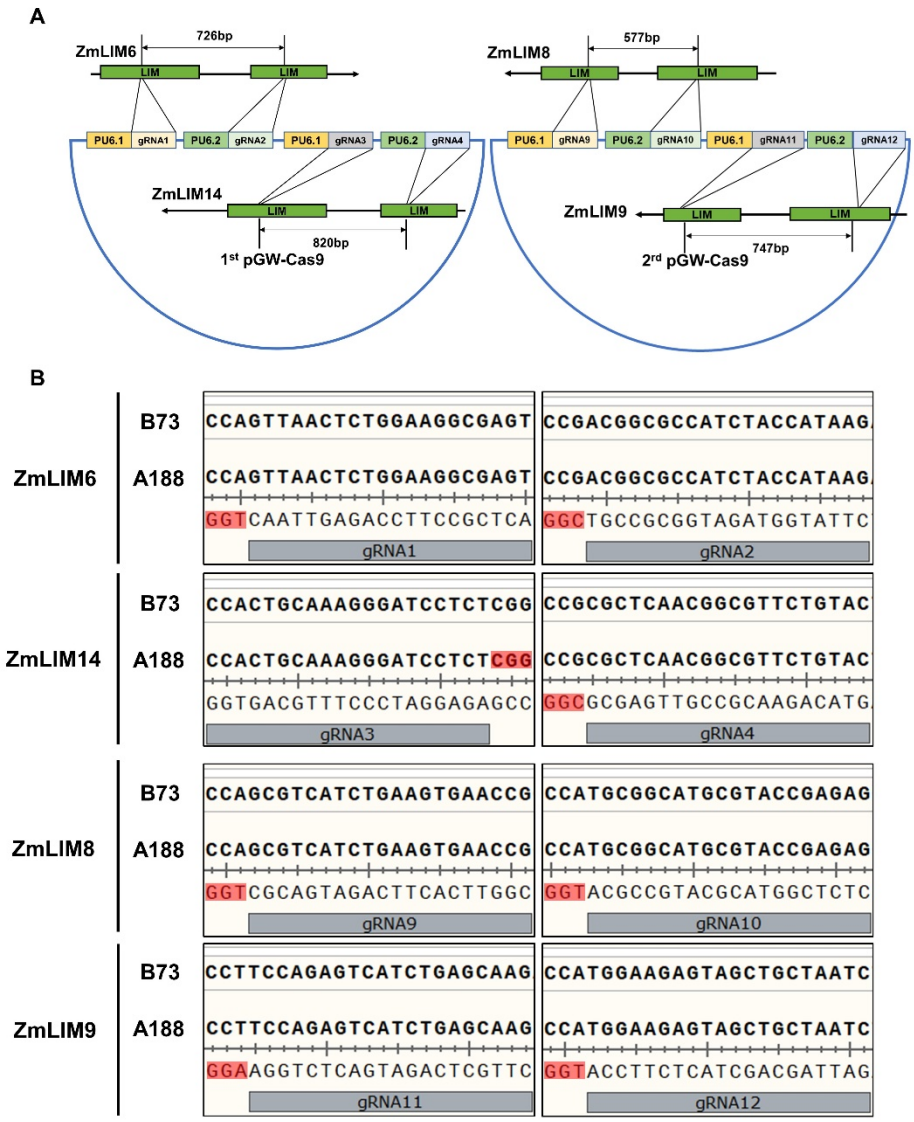

Figure 4.9 CRISPR/Cas9 guide RNA of *ZmLIM6/14* and *ZmLIM8/9* design and sequences. (A) Schematic pictures of destination vectors consisting of four guide RNAs targeting two genes at LIM domains and basic backbone. The arrow indicated the 5'-3' direction. (B) Guide RNA sequences with PAM domain (NGG, highlight in red) in B73 and A188 genome alignment.

By aligning the A188 sequence with the B73 reference genome (Schnable et al., 2009; Lin et al., 2021), the corresponding portions of conserved domains served as input for specific guide RNA identification using the *Breaking-Cas* web tool (http://bioinfogp.cnb.csic.es/tools/breakingcas). Based on the specific targeting scores and putative off-targets provided by the website, candidate gRNAs of each ZmLIM gene were listed. As a large deletion was the ideal genome editing type for gene knockout and mutants genotyping, only the qualified gRNAs situated hundreds of base pairs apart within ZmLIM genes were selected (Figure 4.9). Two sets of four guide RNAs were cloned into the destination

vector pGW-Cas9, and upon sequencing confirmation, two constructs were introduced into the *Agrobacterium* strain EHA101 and subsequently delivered into maize Hi-II immature embryos.

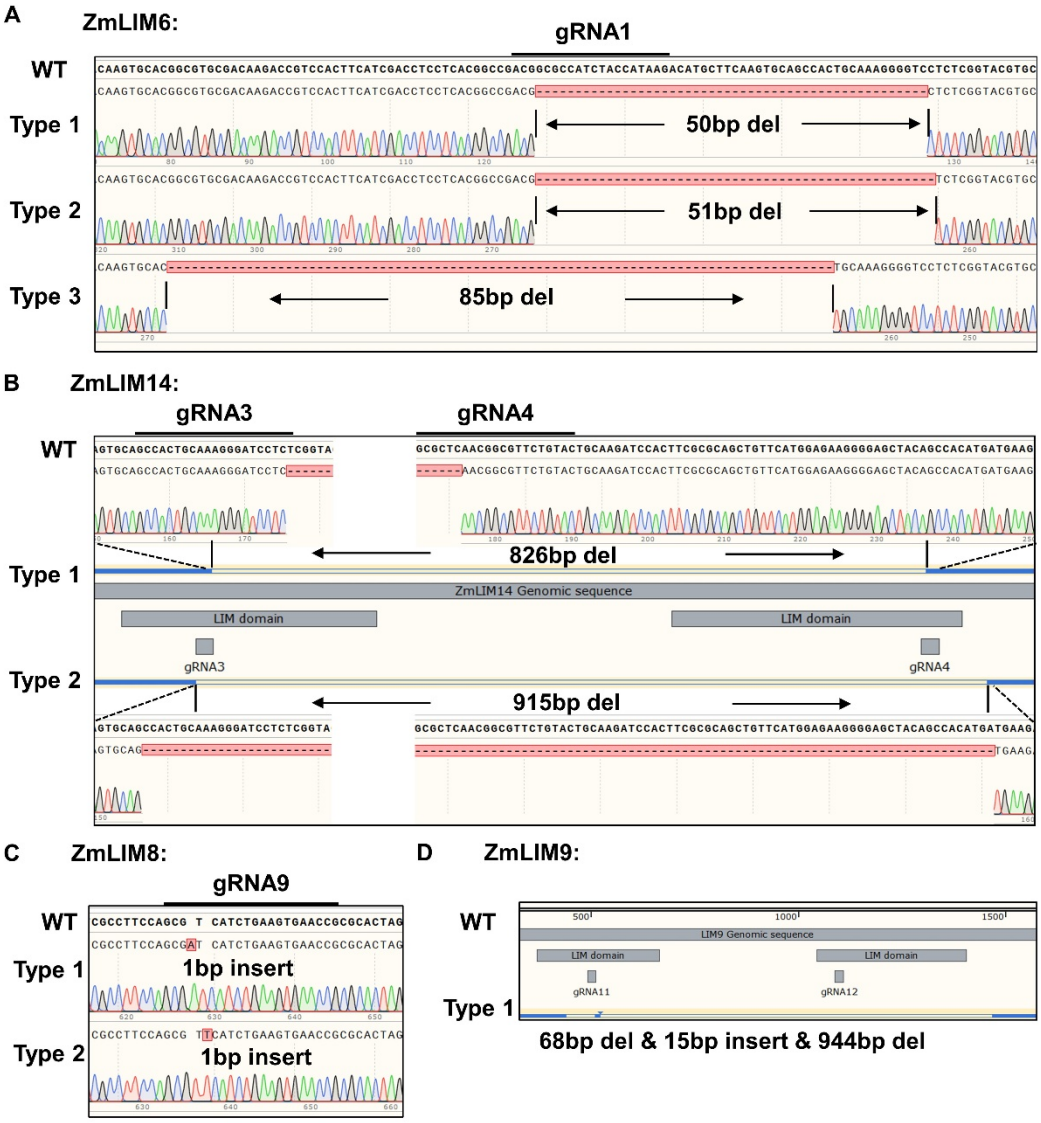

Figure 4.10 Different CRIPSR/Ca9 editing types of *ZmLIM* genes. Sanger sequencing results (chromatogram and blue lines in schematic genome image) were aligned to reference sequences. (A) Three types of ZmLIM6 mutation. Only first LIM domain coding sequence was edited. (B) Two types of ZmLIM14 mutation. Both LIM domains coding sequence were edited with large deletion. (C)Two types of ZmLIM8 mutation. 1bp insertion in first LIM domain coding sequence. (D) One type of ZmLIM9 mutation. Large deletion and insertion simultaneously happened. Sequences alignment was analyzed by SnapGene.

T0 transformants were obtained as plantlets in MS medium. Once transferred to soil pots, the majority of plantlets recovered and were capable of self-pollination or cross with B73 and other marker lines. CRISPR/Cas9 constructs were transmitted from T0 plants to subsequent

generations and remained active throughout the crossing process. At the T1 generation, various editing types of ZmLIM genes were identified through genotyping and Sanger sequencing (Figure 4.10).

The first pGW-Cas9 construction targeting ZmLIM6 and ZmLIM14:

ZmLIM6 mutation (Figure 4.10A): At the gRNA1 site, targeting the first LIM domain coding sequence, high editing efficiency was observed. (i) 50 bp deletion. The open reading frame (ORF) shifted due to deletion, resulting in a premature stop codon. The original ZmLIM6 peptide length diminished from 204 amino acids (aa) to 69 aa. No conserved domain was discernible in the remaining protein fragment. (ii) 51 bp deletion. 17 amino acids were excised from ZmLIM6 first LIM domain coding sequence. However, the conserved motif remained identifiable. (iii) 85 bp deletion. Similarly, the ORF was altered and protein length reduced to 59 aa, with no remaining domain.

ZmLIM14 mutation (Figure 4.10B): Both gRNA3 and gRNA4 functioned actively, resulting in a large fragment deletion encompassing two LIM domains coding sequence. (i) 826 bp deletion. The DNA sequence between the two gRNA targeting sites was deleted. Intriguingly, due to the targeting sites design at the middle range of the LIM domain coding sequence, the residual portion of the two coding sequence, as translated by the edited sequence, could still be identified as a single LIM motif. (ii) 915 bp deletion. Half of the first LIM domain coding sequence and the entire second LIM domain coding sequence were completely removed. Although a 119 aa peptide was encoded by the edited ZmLIM14 ORF, no functional protein sequence was detected, indicating a loss-of-function mutation for ZmLIM14.

The second pGW-Cas9 construct targeting ZmLIM8 and ZmLIM9:

ZmLIM8 mutation (Figure 4.10C): A single 1 bp insertion mutation was induced by gRNA9. (i) An "A" was inserted into the second LIM domain coding sequence, and (ii) a "T" was inserted 2 bp later. Both editing types led to a frame shift mutation from the insertion site. Consequently, the ZmLIM8 protein length was altered from 208 aa to 199 aa. Although the protein length did not change significantly, the second LIM domain lost recognition.

ZmLIM9 mutation (Figure 4.10D): Only one mutation type was identified. At the gRNA11 targeting site, the second LIM domain coding sequence of ZmLIM9 was modified by a 15 bp insertion and 68 bp deletion. Owing to gRNA12 high efficiency, the first LIM domain coding sequence and the fragment between the two gRNAs were entirely removed, totaling 944 bp. As

the ORF of ZmLIM9 no longer existed in the genome, ZmLIM9 was completely eliminated by the CRISPR/Cas9 system.

Considering the expression patterns and abundance of ZmLIMs, ZmLIM6 and ZmLIM14 mutants were selected to cross with a maize sperm cell marker line YFP-α-tubulin and self-crossed to obtain CRISPR-Cas9-free single and double mutants.

4.3.5 Phenotypes of ZmLIM CRISPR/Cas9 knockout mutant

Through self-crossing and crossing with other lines, single homozygous mutants of ZmLIM6 and ZmLIM14 without CRISPR/Cas9 were obtained at the T2 generation, and double mutants at the T3 generation. To gain insight into the roles of ZmLIM6/14 in maize pollen development, a variety of methods were employed to assess pollen viability, germination, and fertilization abilities.

4.3.5.1 Mature pollen nuclei status investigation

Both single and double mutants developed normal tassels and florets, with mature pollen shedding naturally from anthers. This facilitated the harvesting and examination of pollen status. The high expression of ZmLIM6/14 in sperm cell-like structures was confirmed through *in situ* hybridization, necessitating the direct observation of sperm cell conditions in mutant pollen. Differences between mutant and wild-type (WT) sperm cells became apparent through DAPI staining. Figure 4.11 (A) provides an example of DAPI staining results for *lim6-1* mature pollen, where mutant pollen grains exhibited diverse nuclear statuses. Since DAPI served as a DNA content indicator, pollen was classified into four categories based on sperm cell number and DAPI fluorescence intensity: **1)** Two sperm cells with strong DAPI signals, indicating normal pollen containing two spindle-like structure sperm cells; **2)** One normal + one weak: one normal sperm cell and another weakly fluorescent cell; **3)** One sperm cell: pollen containing a single, normal-shaped sperm cell with typical DNA content; **4)** Non-sperm cell: pollen grains with only a vegetative nucleus and no sperm cell-like nuclei. Using this classification, three biological replicates of WT, three *lim6* mutant types, two *lim14* mutant types, and one double mutant were quantified through DAPI staining. Statistical results (Figure 4.11B) revealed that, due to DAPI staining efficiency, not all pollen could be stained, resulting in 14% of WT non-sperm cells and 72% normal pollen with two sperm cells. For single mutants, only LIM6 mutant type2 exhibited a WT-like pattern. Other single mutant genotypes displayed distinct phenotypes, with over 50% of mature pollen containing abnormal sperm cells, one sperm cell or non-sperm

cell, an increase of approximately 10% compared to WT. These results correlated with ZmLIM protein domain knockout situations, suggesting that conserved LIM domains were crucial for ZmLIMs biological functions. In the double mutant, a genotype combination of *lim6-1/lim14-2* was selected. As anticipated, the proportions of pollen with one sperm cell and non-sperm cell pollen significantly increased to 26% and 34%, respectively, both higher than single mutants, indicating the additive effects of ZmLIM6 and ZmLIM14. However, 27% of normal pollen persisted, which related to phylogenetic analyses suggesting that ZmLIM8 and ZmLIM9 were likely redundant with ZmLIM6/14.

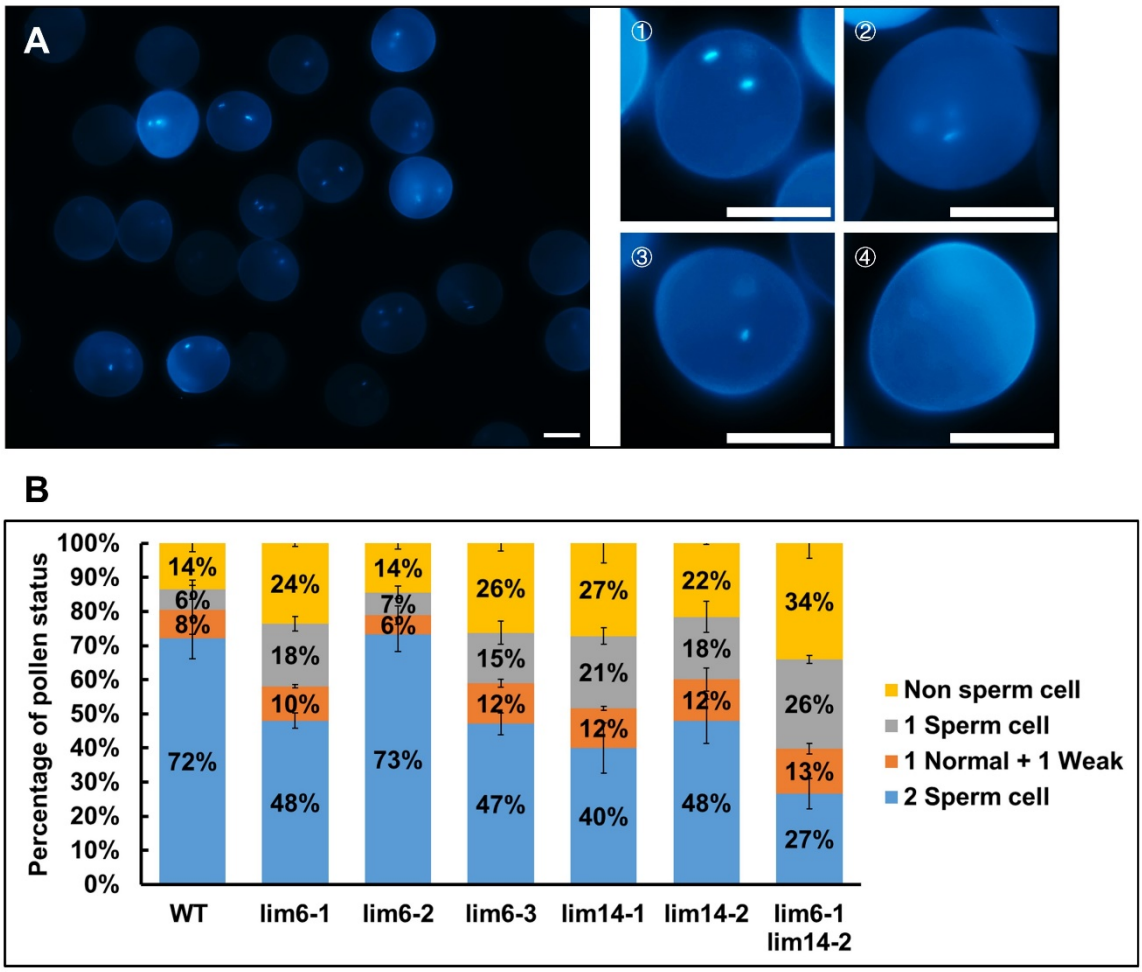

Figure 4.11 Mutants mature pollen status investigation. (A) DAPI staining of mutant mature pollen. DAPI stained pollen showed different sperm cell status based on fluorescence signal results. 1) Two sperm cells: strong signal with typical spindle shape; 2) One normal +one weak: one sperm cell with normal-like shape and the other showed smear weak fluorescence signal; 3) One sperm cell: only one normal-like sperm cell in pollen grain; 4) Non sperm cell: no sperm cell-like nuclei in pollen. (B) Mature pollen status statistics results of wild type, *lim6*, *lim14* and *lim6 lim14*. Scale bar = 50μm

4.3.5.2 Bi-tricellular transition stage pollen nuclei status investigation

Given the abnormal sperm cell phenotypes exhibited by the mutant mature pollen and the high expression levels of ZmLIM6/14 during the bi- and tricellular stages of pollen development, which correspond to the PMII, it was reasonable to investigate the pollen during the developmental transition stages. To observe the mitosis process clearly, the Feulgen staining method was employed on appropriately fixed pollen at the right stage. It is well-known that mitosis consists of four major stages: prophase, metaphase, anaphase, and telophase, each with distinct chromosome states and positions. Consequently, the pollen was sorted into four stages based on the staining status of the chromosomes (or chromatins).

Since the *lim6-2* mutant displayed normal mature pollen phenotypes, pollen from other genotypes was harvested at the bi-tricellular stage and subjected to Feulgen staining to investigate mitosis. As shown in Figure 4.12A, WT pollen during PMII displayed typical chromosome characteristics: chromosomes began to condense during prophase, reached their most compacted state with the centromeres aligned at the equator of the division spindle, and separated during anaphase; as mitosis ended during telophase, the chromosomes reached the spindle poles and began to decondense into their interphase conformations. For *lim6* mutants (Figure 4.12B&C), *lim6*-1 and *lim6*-3 showed the same phenotypes. There was no clear difference observed at prophase and metaphase. However, at anaphase only one entire set of chromosomes was found in the mitosis unit and some fragments of chromosome dispersed in the free region of spindle. Following at telophase, the free pieces of chromosome were disappeared and the left chromosomes were back to decondensed state in a curved structure. For *lim14* mutants (Figure 4.12D&E), *lim14*-1 and *lim14*-2 also showed the same phenotypes. Different from WT and *lim6* mutant, at prophase the chromatins of *lim14* mutant were squeezed by a swollen spherical structure in nuclei, which inferred to be a non-dissembled nucleolus. Despite this, the chromosomes were still able to proceed through the condensation process, and during metaphase, the compacted chromosomes lined up at the middle surface. Although the chromosome (or chromatins) position was affected by the unexpected nucleolus, the metaphase check point could be passed and enter into anaphase. At anaphase, the always-present nucleolus strongly influenced the morphology of chromosome segregation: similar to *lim6* mutants, one set of sister chromatids looked normal, whereas the other set was not entirely complete, with some chromosome fragments and thin chromosome lines surrounding them. Then at telophase, only one normal-like sperm cell was observed at spindle poles with some remained pieces chromosomes. For double mutant (Figure 4.12F), the phenotypes of prophase and metaphase

were really similar with *lim14* mutant as well as at anaphase and telophase the chromosomes behaved like *lim6* mutants.

In general, single and double mutants showed similar effects on sperm cell formation, but all pollen could accomplish PMII process, indicating ZmLIM6/14 were not involved in mitosis checkpoint mechanism. However, both *lim14* and *lim6-1/lim14-2* double mutant exhibited abnormal nuclear phenotypes at the prophase stage. Based on the arrangement of chromatin and the shape of the unexpected structure in the nucleus region, it was hypothesized that the roundish object was the nucleolus. Since the nucleolus is supposed to disappear with the condensation of chromosomes and the breakdown of the nuclear envelope at the beginning of mitosis, the non-dissembled nucleolus persisted from prophase to anaphase, leading to anomalous physical positions of chromosomes in the spindle, and likely resulted in the loss of one set of sister chromatids during segregation. As the nucleus begins to reform in late anaphase, it could be implied that the mutant sperm cell contains two nucleoli due to the non-dissembled mature nucleolus, which will likely be degraded later. Taken together, the Feulgen staining results suggest that the defect in *lim* mutants occurs during PMII, eventually resulting in one sperm cell or non-sperm cell mature pollen.

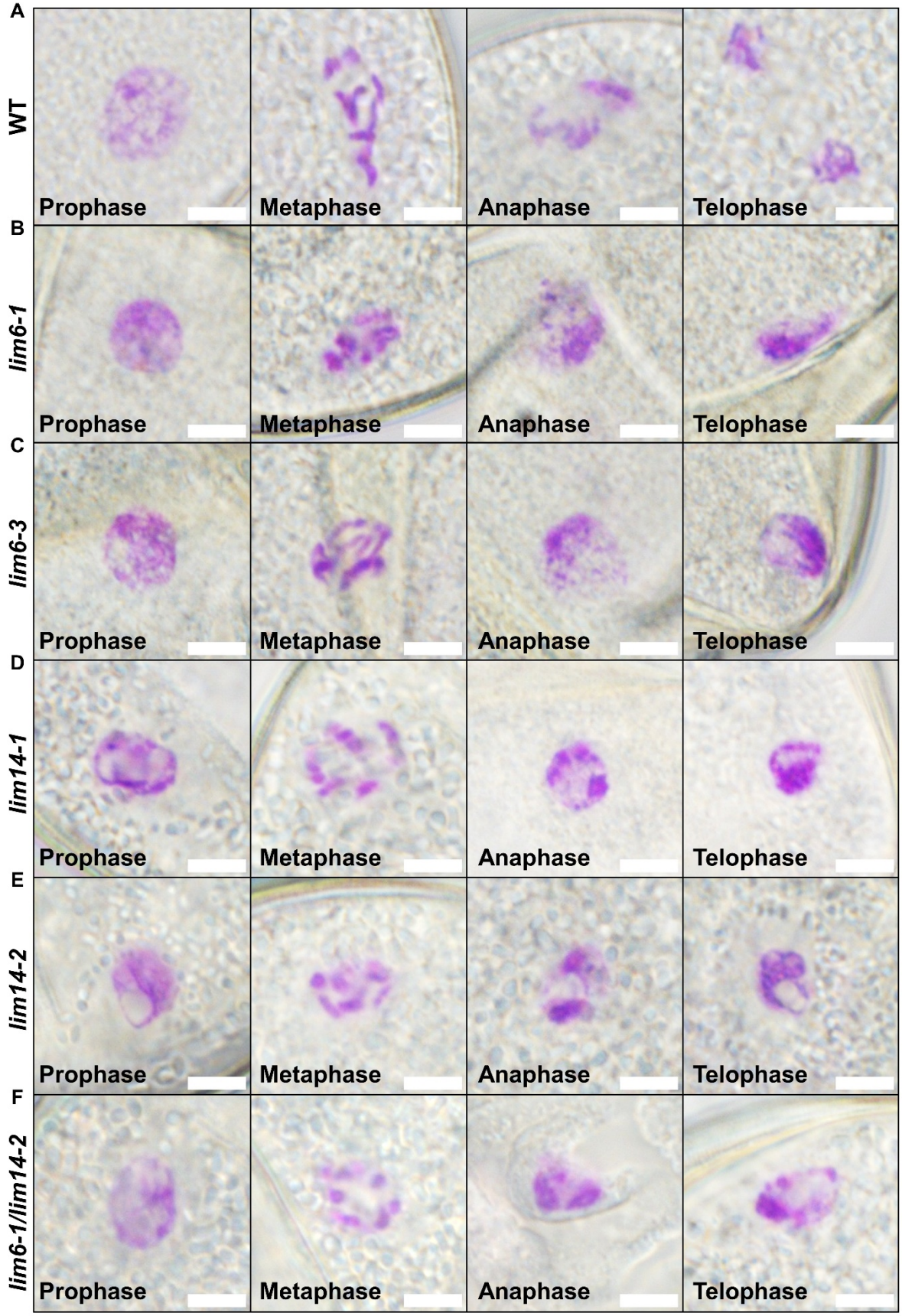

Figure 4.12 Feulgen staining results of WT and mutants bi-tricellular transition stage pollen. Mitosis phase identification based on chromatins status. Scale bar = 5μm

4.3.5.3 Male germline marker YFP-α-tubulin mutant pollen at Bi-tricellular transition stage

To better observe the PMII process, mutant was crossed with YFP-α-tubulin marker line, which was designed to label sperm cells (Kliwer and Dresselhaus, 2010). Phenotypes showed up at *lim14* heterozygote maker line (Figure 4.13)

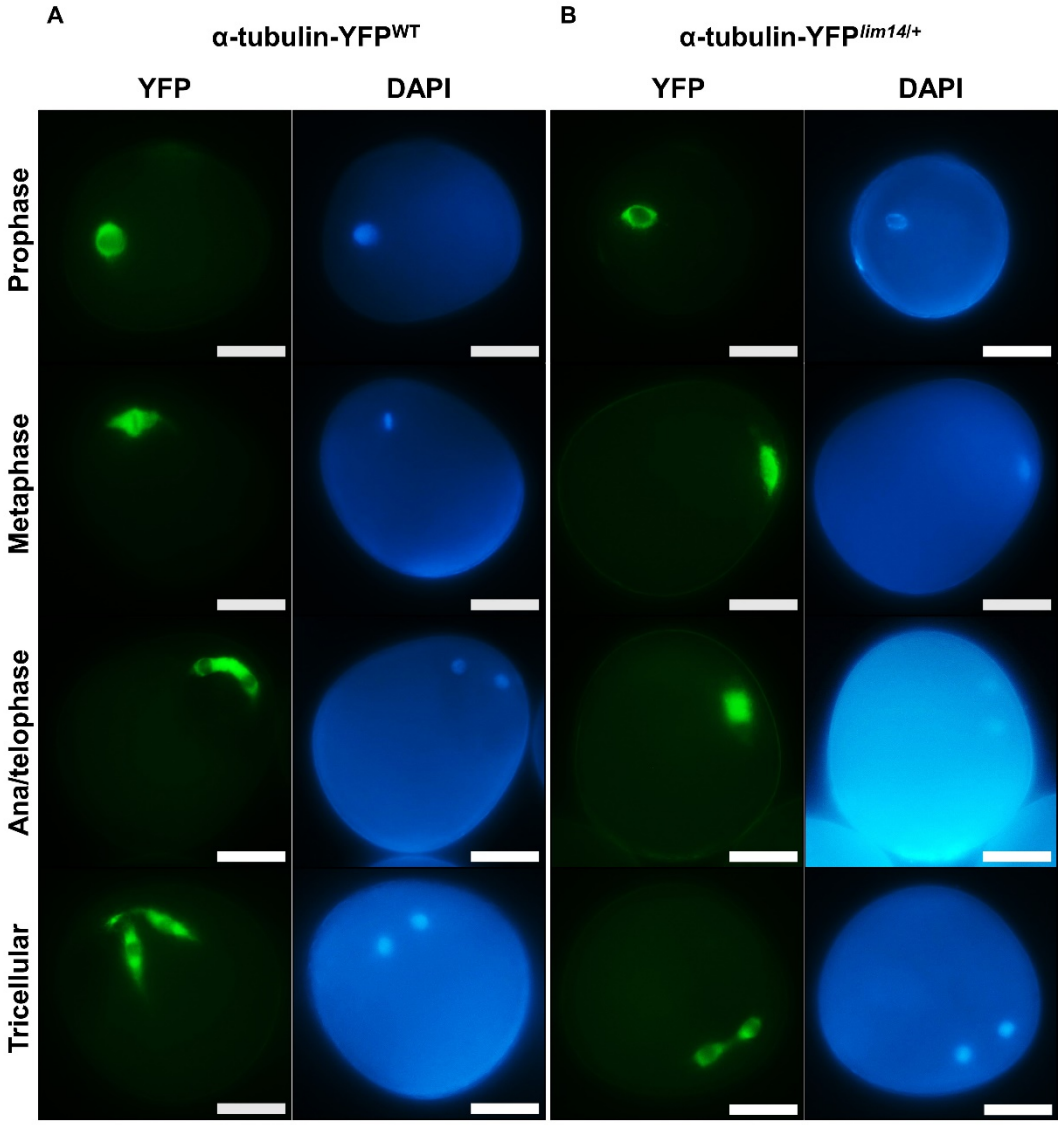

Figure 4.13 Bi-tricellular stage pollen of YFP-α-tubulin marker line mutant. (A) Pollen Mitosis II of WT marker line. (B) Pollen Mitosis II of *lim14* heterozygote marker line. Nuclei were stained by DAPI. Scale bar = 25μm.

According to tubulin dynamics and DAPI stained nuclei, it was much easier to identify the pollen mitosis II phases. In WT PMII (Figure 4.13A), tubulin formed a basket-like structure surround germ cell nucleus with extensions to both poles of the division spindle in prophase. At metaphase, tubulin served as a dense envelop around the lined-up chromosomes. Chromatid

separation was driven by microtubules movements at anaphase and cytokinesis occurred at telophase where the tubulin envelops around nuclei became thin and a wide uniform tubulin strip was formed between two sperm cells. When pollen mitosis II finished, tubulin formed a tail-like bundled structure connected sperm cells and opposite poles with a tubulin-knot at half distance between sperm cells, as previous described (Kliwer and Dresselhaus, 2010). As for mutant pollen, there was no obvious difference at prophase. However, from metaphase onwards, the tubulin morphology exhibited various dynamics. As the example showed (Figure 4.13B), no distinct envelope structure was observed at metaphase and the typical tail-like bundled tubulin arrangement was lost at ana/telophase. After PMII, even normal sperm cells were formed but the tubulin connections and specific structure disappeared.

All above results observed under wide field suggested that in mutant pollen α-tubulin dynamics were disrupted during PMII, indicating that *ZmLIM* gene defects caused chromosome loss and abnormal microtubule behavior during the sperm cell formation process. To better observe the relationship between DNA degradation and tubulin disorder, mutant pollen of telophase with strong phenotypes were observed under confocal microscopy. As shown in Figure 4.14A, Tubulin-YFP$^{lim14+/-}$ pollen grain had two sperm cells, which were considered normal according to DAPI staining. However, in the YFP channel, half of the tail-like bundled tubulin structure was lost, left one "naked" sperm cell without a tubulin envelope and one normal-like sperm cell. In Figure 4.14B, based on DAPI staining, this pollen belongs to the normal and weak type. However, the normal sperm cell was naked and the weak nuclei were surrounded by an open basket-like tubulin structure without any tubulin connection. As microtubules were the main component of sperm cell cytoskeleton, it could be inferred that the naked sperm cell would lose its identity with pollen maturation, which could explain why there were no sperm cells in mature pollen. Coincidentally, the weak sperm cell could be considered to be undergoing degradation even though the tubulin cytoskeleton was present. Based on all the results from the mutant marker lines, it could be concluded that the two obvious phenotypes caused by ZmLIM gene mutations were independent of each other.

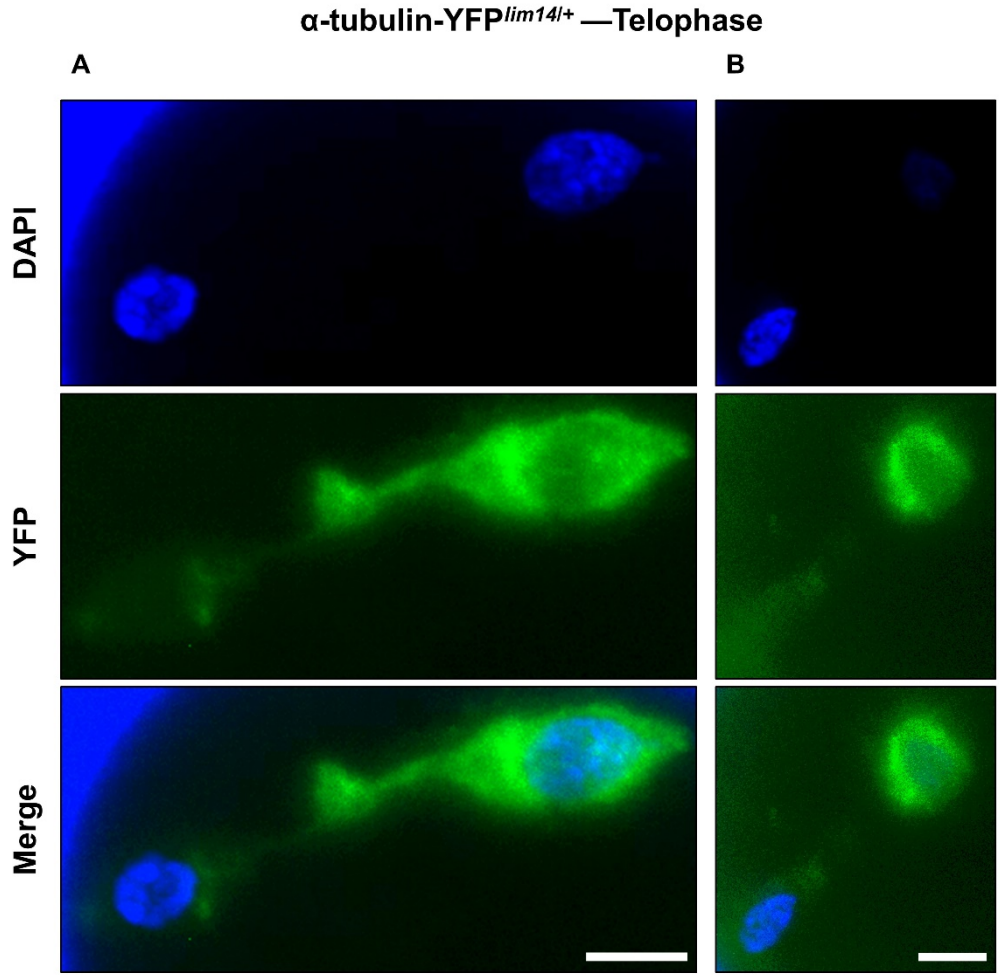

Figure 4.14 Bi-tricellular stage pollen of YFP-α-tubulin marker line mutant under confocal microscopy. (A) Two normal sperm cells surrounded by half tubulin envelop. (B) one normal but naked sperm cell and one weak sperm cell with no shaped tubulin envelop. Nuclei were stained by DAPI. Scale bar = 5μm.

4.3.5.4 Immunolocalization analysis of ZmLIM6/14 and α-tubulin in pollen

The results of Feulgen staining and YFP-α-tubulin marker line analyses of mutant pollen indicated the importance of ZmLIM6/14 in maintaining DNA stability and tubulin dynamics during the PMII process. To further investigate the involvement of LIM proteins in this process, specific antibodies against ZmLIM6 and ZmLIM14 were used for immunolocalizations assays, along with α-tubulin, in bi-tricellular stage pollen.

Firstly, the specificity of the antibody was evaluated through a negative control. As shown in Figure 4.15A, bicellular stage pollen section was incubated with ZmLIM6 and tubulin antibodies, which were subsequently visualized with Alexa Fluor® conjugated secondary antibodies. The obtained results revealed that the LIM6 protein distributes around the entire

pollen grain, serving as a component of the cytoskeleton, along with the tubulin. The most intense signal was observed around the nuclei region, as evidenced by DAPI staining.

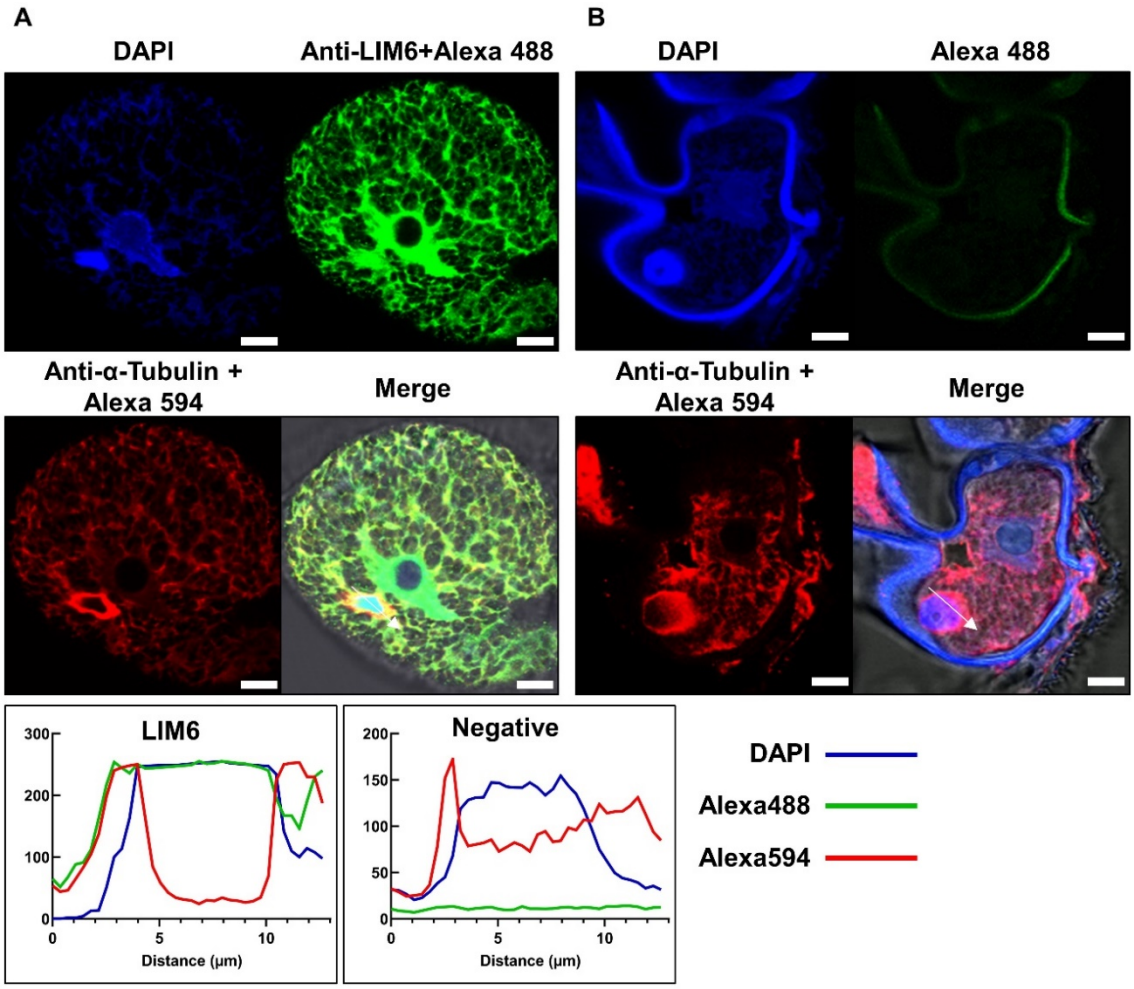

Figure 4.15 Antibody test for immunolocalization. (A) One section of whole pollen at bicellular stage. Vegetative nucleus and germ cell were indicated by DAPI. LIM6 was visualized by primary antibody and the Alexa Fluor® 488 secondary antibody as well as tubulin by primary antibody and the Alexa Fluor® 594 secondary antibody. (B) only the Alexa Fluor® 488 secondary antibody was applied as the negative control. Exine visibility enhanced due to it being autofluorescent. White arrow indicated plot profile position and direction. Scale bar = 10μm.

Notably, LIM6 protein formed a uniform and highly-dense plate-like structure within the nuclei. As for tubulin, it formed an envelope structure surrounding the germ cell in the pollen grain. Plot profile analysis demonstrated significant overlap between LIM6 and tubulin, as well as between LIM6 and the nuclei, in the region of the germ cell. The negative control (Figure 4.15B) showed minimal intensity at the Alexa 488 channel, indicating the high specificity of the

antibody. Similar results were obtained with LIM14 antibody indicating that both genes share transcriptional expression patterns, protein localization, and are most likely regulate the same developmental processes.

4.3.5.5 Immunolocalization analysis with WT pollen

The specificity of the antibodies for ZmLIM6/14 proteins in pollen grains was validated. Based on the phenotyping results, it was reasonable to investigate ZmLIM6/14 proteins function during PMII.

The prophase immunolocalization (figure 4.16)

At prophase, the DNA in the nuclei was in a chromatin state, and tubulin formed an envelope around the nuclei. Z-stack images revealed that both LIM6 and LIM14 have a similar distribution pattern around the nuclei region. At a single section level, LIM proteins were observed to be evenly distributed in the chromosome region, forming a basket structure around the nucleolus in the germ cell. The profile analysis showed a complete overlap between LIM6 and LIM14 with tubulin and partially colocalized with DNA. Notably, both LIM proteins distinctly displayed a curved overlap line with DNA at the nucleolus region, suggesting a potential role related to the nucleolus. Additionally, it was observed that the LIM protein assembled into dot structures, which were evenly distributed and formed a clear boundary within the tubulin envelope, unlike tubulin, which conformed to a line morphology.

The metaphase immunolocalization (figure 4.17)

At metaphase, the chromosomes were in a condensed state with a tubulin envelope surrounding them. Z-stack images revealed that microtubules developed into the chromosome region to catch the centromere. The profile analysis showed that LIM6 and LIM14 have similar curves along the nuclei region and still colocalized with tubulin but did not overlap with chromosomes. LIM protein dots were observed to be evenly distributed around the chromosome in the nuclei.

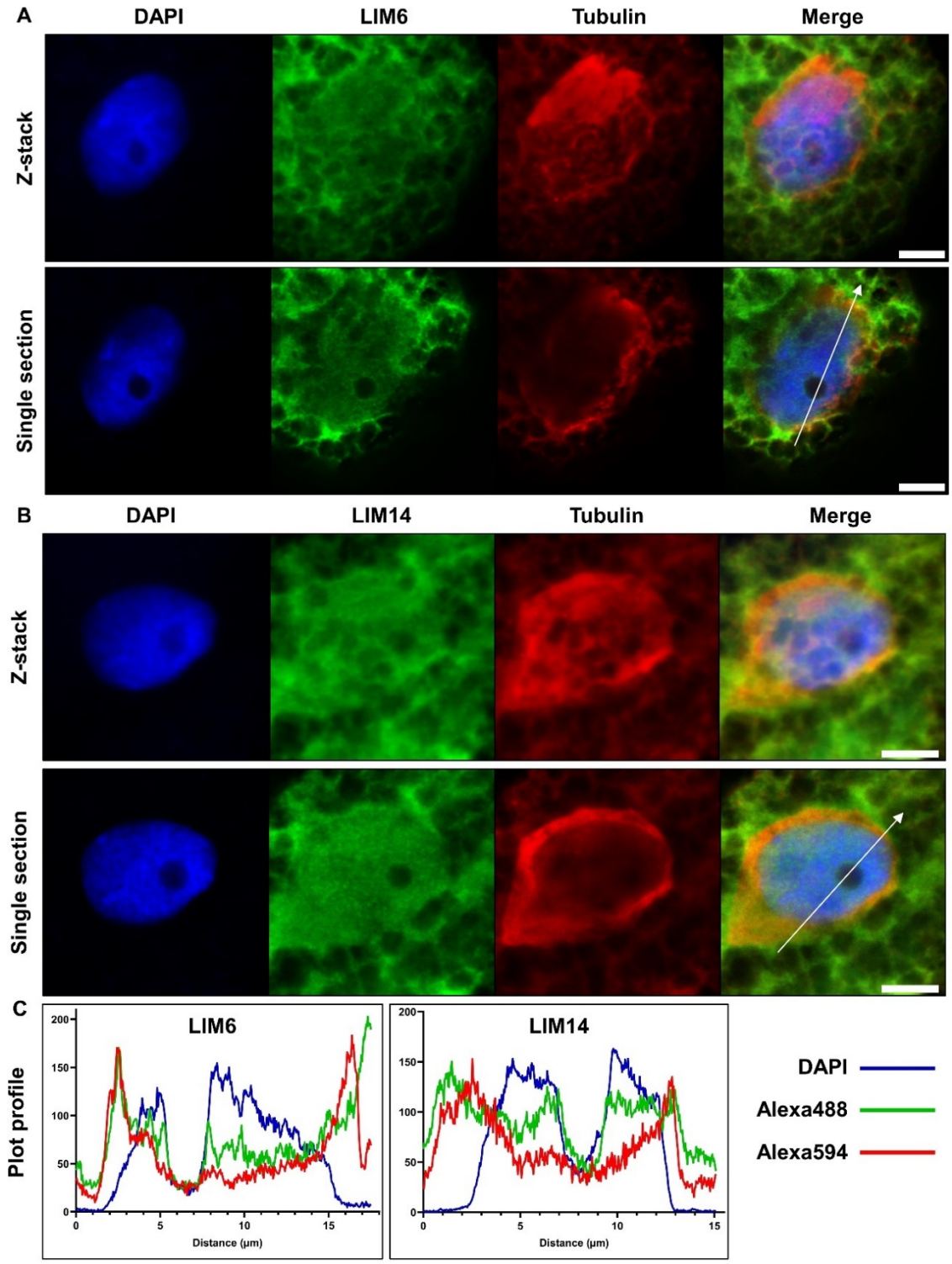

Figure 4.16 Immunolocalization analysis of prophase pollen. (A) LIM6 and tubulin immunolocalization together with DAPI. (B) LIM14 and tubulin immunolocalization together with DAPI. The protein localization overall view by z-stack. Colocalization analysis by plot profile at single section. White arrow indicated plot profile position and direction. Scale bar = 5μm.

The anaphase immunolocalization (figure 4.18)

At anaphase, the conspicuous structure was the wide strip of tubulin connecting the two daughter cells. From the z-stack, it was observed that the uniform and dense plate structure of both LIM proteins also extended with the tubulin arrangement, as indicated by the plot profile where tubulin and LIM protein overlapped a long distance beyond the nuclei region. Due to the condensed state of chromosomes, the LIM protein still maintained its colocalization pattern with DNA as seen in metaphase.

The telophase immunolocalization (figure 4.19)

At telophase, the length of the tubulin strip increased and developed into a tail-like bundled shape together with the envelop, connecting the sperm cells and opposite poles. However, due to the thickness limitation of the section, the complete view of telophase components could not be captured in one slide. Nevertheless, as mitosis has a symmetry property, the plot profile at a single section was able to explain the colocalization pattern. The DNA reverted back to its chromatin state and the nucleolus reformed in the sperm cell, similar to the situation in prophase. Correspondingly, the LIM protein showed the same localization pattern at the nuclei and nucleolus regions. Moreover, the tail-like bundled tubulin was still colocalized with these two LIM proteins, suggesting potential protein interactions.

Based on the immunolocalization analysis of the four phases, it can be concluded that ZmLIM6 and ZmLIM14 both exhibited dual colocalization patterns with DNA, which depended on the condensation state of chromosomes. Particularly at the nucleolus region, these two LIM proteins developed a boundary region around it, likely related to the disappearance and recovery of the nucleolus during mitosis. On the other hand, two LIM proteins always colocalized with tubulin, regardless of its morphology, which could explain the abnormal tubulin arrangement observed in the α-tubulin-YFP mutant.

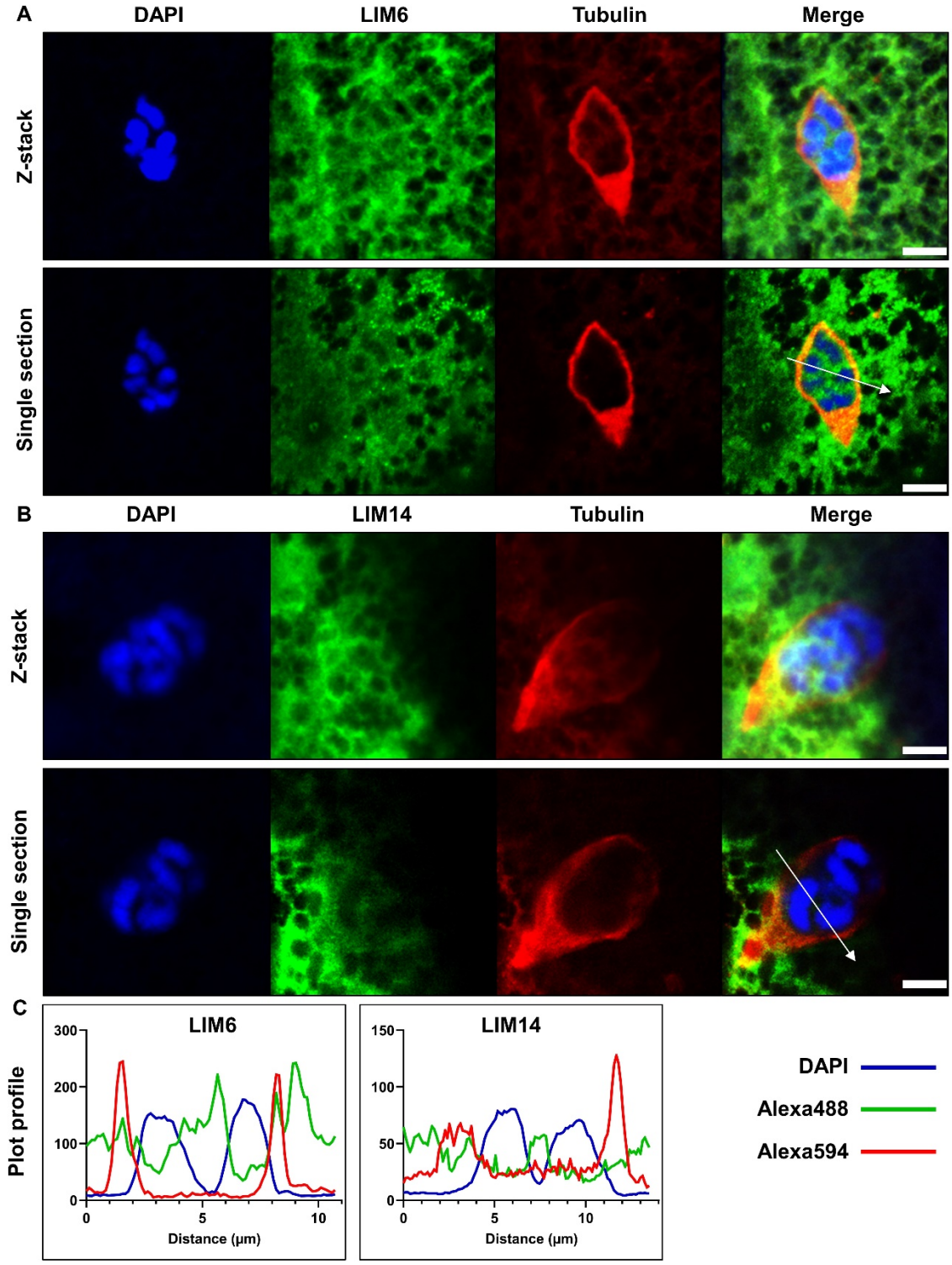

Figure 4.17 Immunolocalization analysis of metaphase pollen. (A) LIM6 and tubulin immunolocalization together with DAPI. (B) LIM14 and tubulin immunolocalization together with DAPI. The protein localization overall view by z-stack. Colocalization analysis by plot profile at single section. White arrow indicated plot profile position and direction. Scale bar = 5μm.

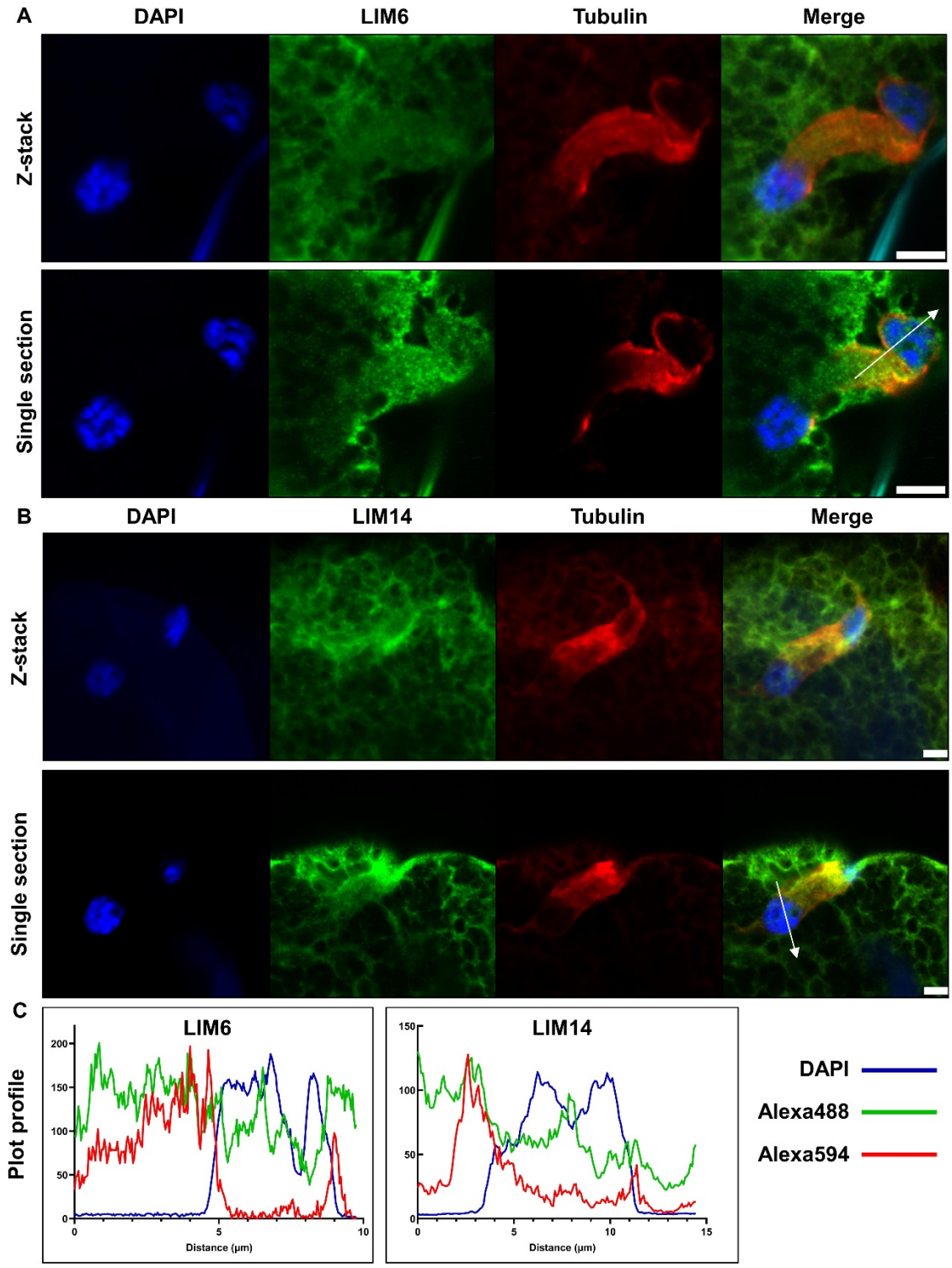

Figure 4.18 Immunolocalization analysis of anaphase pollen. (A) LIM6 and tubulin immunolocalization together with DAPI. (B) LIM14 and tubulin immunolocalization together with DAPI. The protein localization overall view by z-stack. Colocalization analysis by plot profile at single section. White arrow indicated plot profile position and direction. Scale bar = 5μm.

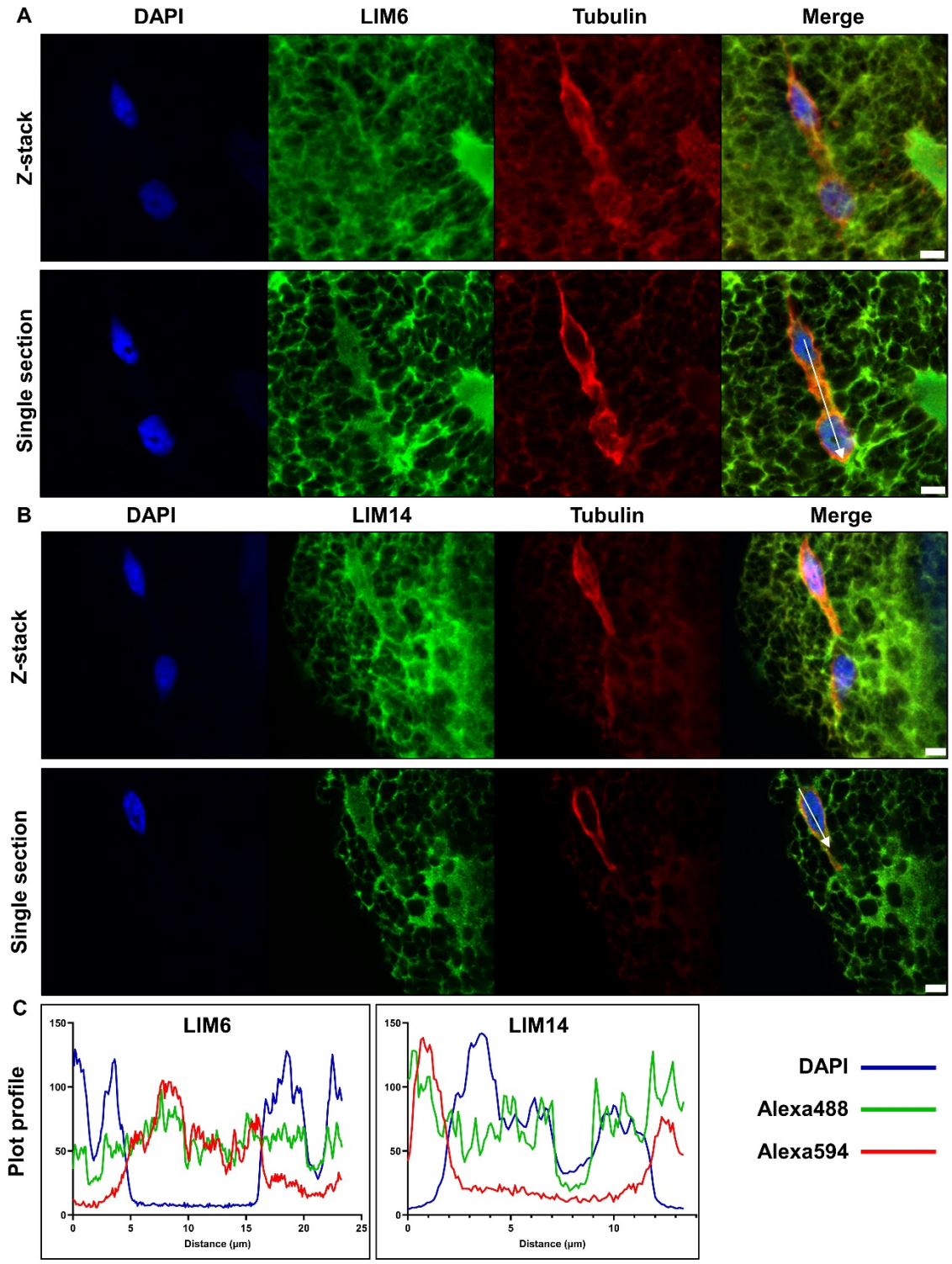

Figure 4.19 Immunolocalization analysis of telophase pollen. (A) LIM6 and tubulin immunolocalization together with DAPI. (B) LIM14 and tubulin immunolocalization together with DAPI. The protein localization overall view by z-stack. Colocalization analysis by plot profile at single section. White arrow indicated plot profile position and direction. Scale bar = 5μm.

4.3.5.6 Immunolocalization analysis with mutant pollen

The colocalization of ZmLIM6/14 protein and tubulin may explain the tubulin disorder phenotype of mutant, but the mechanism behind the phenotype of chromosome loss during mitosis remains unclear. To gain more insight, immunolocalization analysis with pollen from *lim6*-3 and *lim14-2* single mutants was performed. using antibodies against ZmLIM6 and ZmLIM14 to visualize the behavior of the LIM proteins. Samples were harvested at the bi-tricellular stage of pollen development.

Mutant pollen immunolocalization at prophase.

Figure 4.20A showed immunolocalization results with *lim6*-3 single mutant pollen. In the upper panel, an example shows that LIM14 protein fails to form an evenly spread plate structure around the nuclei, which consequently affects the proper arrangement of the tubulin envelop and tail. In another sample, although the LIM protein could assemble a plate structure, due to defective LIM6 protein, the integrity of the tubulin envelop was compromised, leading to altered nuclei morphology by the abnormal LIM protein plate.

For *lim14-3* mutant (figure 4.20B), the nuclei were squeezed by a swollen spherical structure similar to that found by Feulgen staining and was not covered by the tubulin envelop from the z-stack image. To further investigate the spherical structure, the z-stack was screened slide by slide. From the bright view, it was clearly observed that the nucleolus was in the middle of the swollen spherical structure, and as indicated by the dashed line, LIM6 formed a line as a boundary structure around it rather than a uniform plate. As the z-stack order was from the section top to bottom, the #2 section showed the existence of a tubulin envelop, whereas in #3 and #4 sections, the tubulin signal gradually disappeared. These results suggested that the LIM14 defect affected the proper character of LIM6 protein, leading to the formation of an unexpected spherical structure in nuclei, which further altered chromatin and tubulin morphology.

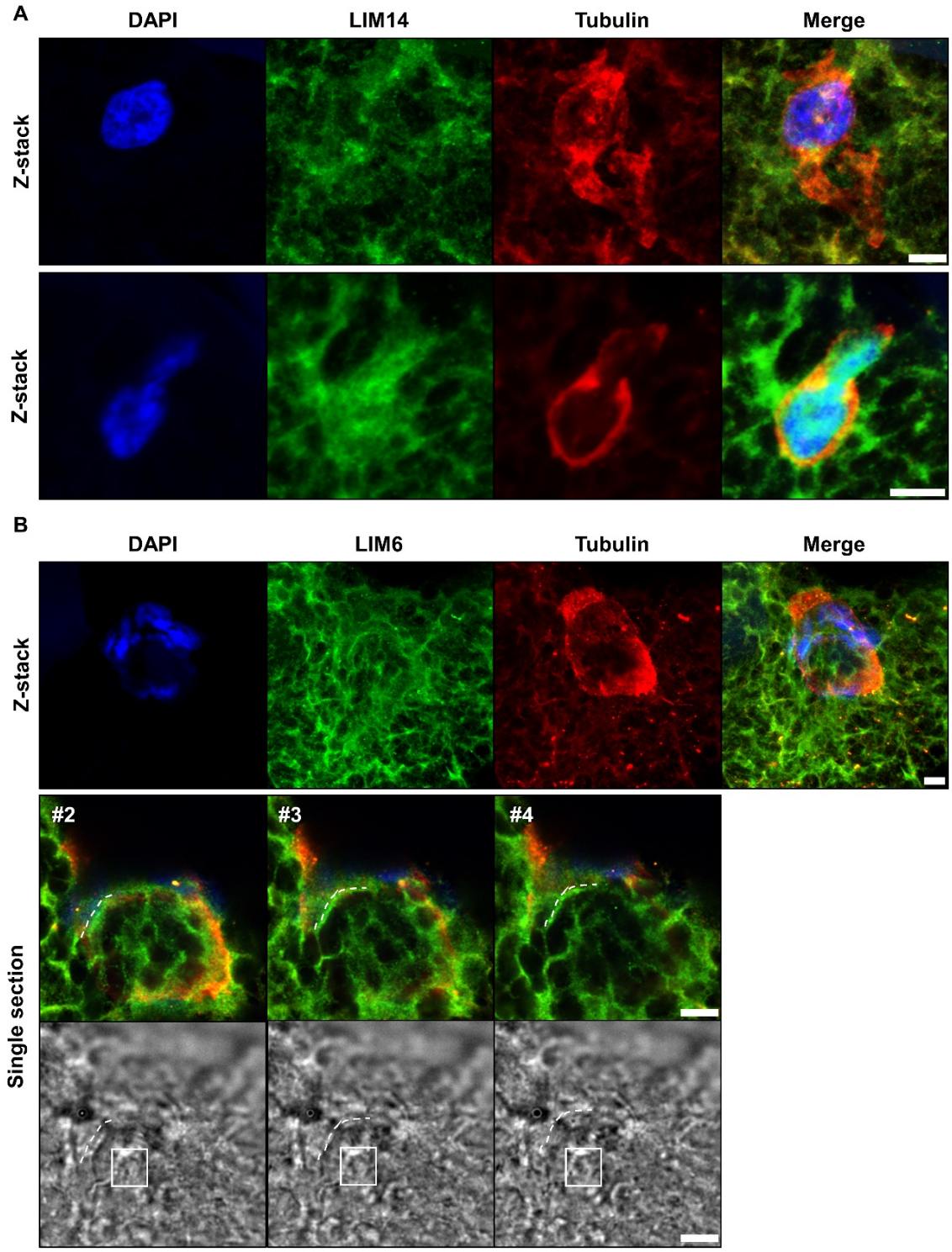

Figure 4.20 Immunolocalization analysis of mutant prophase pollen. (A) LIM14 and tubulin immunolocalization together with DAPI of *lim6-3* pollen. (B) LIM6 and tubulin immunolocalization together with DAPI of *lim14-2* pollen. #number represented serial single section of z-stack. Dashed line indicated LIM protein in fluorescence merge and bright view. White rectangle indicated nucleolus under bright view. Scale bar = 5μm**.**

Mutant pollen immunolocalization at metaphase.

At metaphase, the chromosomes undergo the process of condensation and reach the most compacted state, while the microtubules need to target the chromosomes at kinetochore and form the typical mitotic spindle. In both *lim6* and *lim14* mutant pollen, the DNA exhibited normally condensed chromosomes in the nuclei region (Figure 4.21). However, due to that the LIM protein arrangement was strongly altered compared to WT, the tubulin envelop of both *lim6* and *lim14* mutant pollen showed severe phenotypes: instead of a smooth and integral tubulin membrane, the mutants exhibited curved or fragmented tubulin envelops. By taken *lim6* mutant as an example (Figure 4.21A), the upper panel shows the irregular shape of the LIM14 protein plate resulting in the invasion of the bent tubulin arrangement into the nuclei; the below panel probably was the subsequent stage of Figure 4.20A, where the nucleus with a broken tubulin envelop continued to develop into a non-tubulin-surrounded state due to degradation or unbundling. Additionally, within the both mutant pollen grain, there were numerous LIM and tubulin protein granules, some of which colocalized, indicating the abnormal tubulin aggregation caused by LIM protein defects.

By examining single sections of mutant pollen metaphase (Figure 4.22), it was observed that both *lim6* and *lim14* single mutants had a nucleolus present during metaphase, which was unexpected. Immunostaining results showed that the LIM protein formed a basket structure, as in WT prophase, and this was confirmed by plot profile analysis. However, in these two single *lim* mutants, the other LIM protein behaved similarly as WT even when chromosomes were in a highly compacted state. Upon closer inspection, a nucleolus was observed present in the nuclei during mitotic metaphase, which provided direct evidence that the LIM protein was crucial for nucleolus development and formation. This results also supported the hypothesis that the swollen spherical structure observed in *lim14* mutant pollen in Feulgen staining was a non-disassembled nucleolus and may contributed to chromosome loss during mitosis.

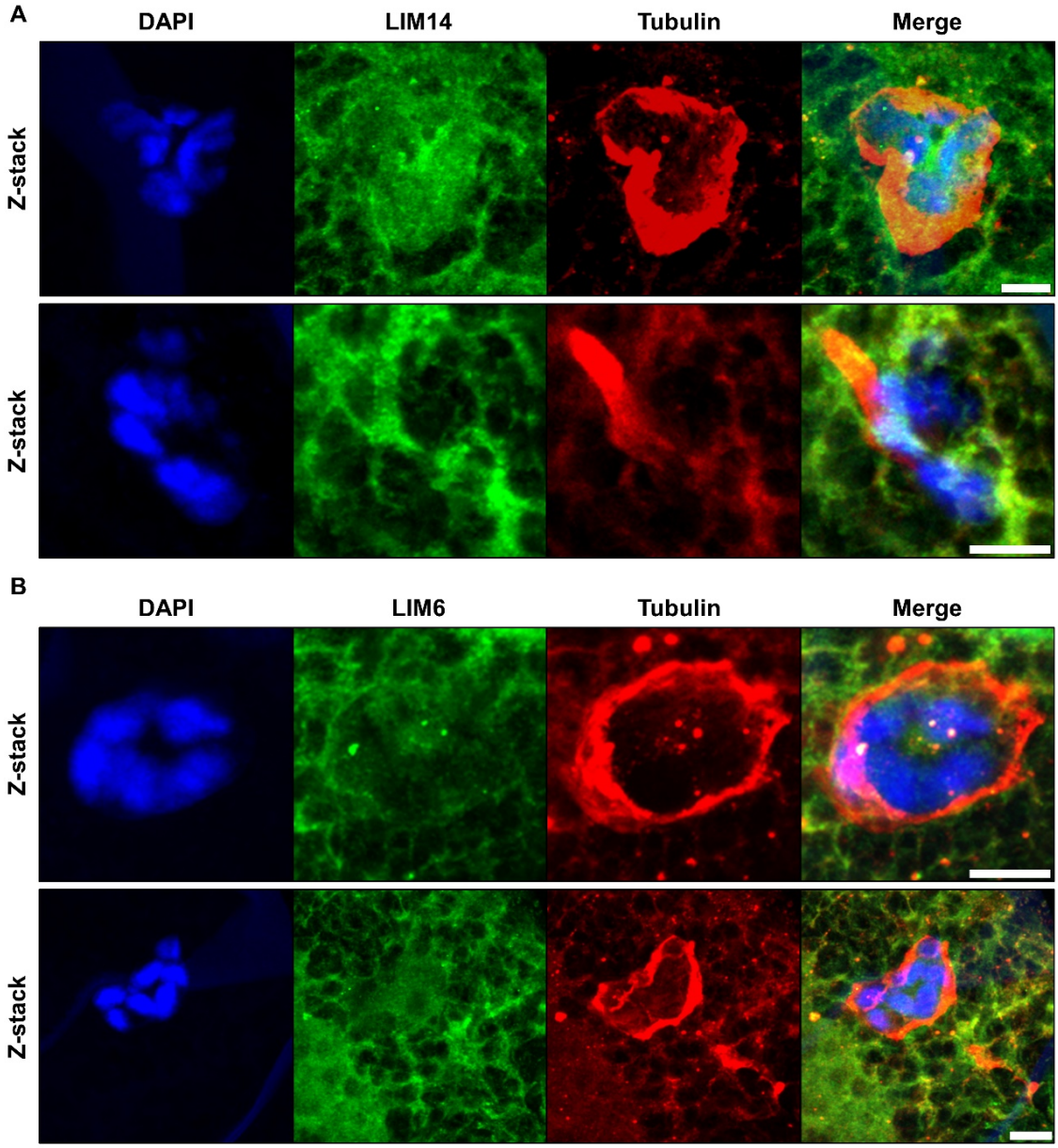

Figure 4.21 Immunolocalization analysis of mutant metaphase pollen. (A) LIM14 and tubulin immunolocalization together with DAPI of *lim6-3* pollen. (B) LIM6 and tubulin immunolocalization together with DAPI of *lim14-2* pollen. The protein localization overall view by z-stack. Scale bar = 5μm.

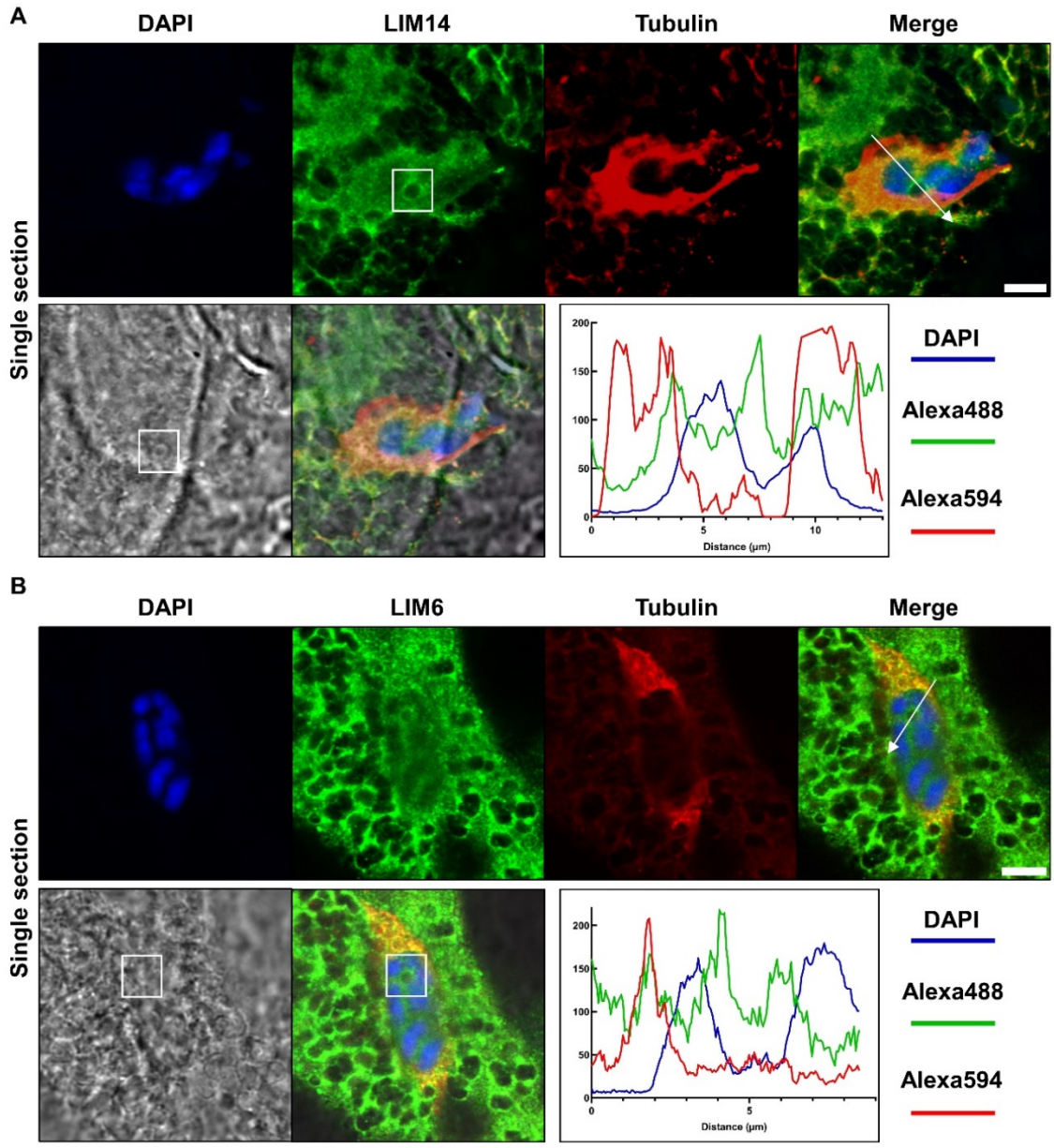

Figure 4.22 Immunolocalization analysis of mutant metaphase pollen at single section. (A) LIM14 and tubulin immunolocalization together with DAPI of *lim6*-3 pollen. (B) LIM6 and tubulin immunolocalization together with DAPI of *lim14*-2 pollen. Colocalization analysis by plot profile at single section. White rectangle indicated nucleolus. White arrow indicated plot profile position and direction. Scale bar = 5μm.

Mutant pollen immunolocalization at anaphase

At anaphase, because the tubulin wide strip appeared, it was really easy to find differences between *lim6* and *lim14* single mutant pollen from WT. For *lim6-3* mutant, there were various phenotypes observed at this stage (Figure 4.23), the first example showed two normal-like nuclei. LIM14 protein formed a uniform plate structure, but the tubulin strip was broken in the

middle, and there were numerous LIM and tubulin granules of varying sizes distributed in the pollen grain. In Figure 4.23B, the nuclei of the two daughter cells appeared normal, with a tubulin strip connection, but no LIM14 protein plate was present in the upper one, and therefore, no tubulin envelop was present. Additionally, more tubulin granules were observed in the vicinity. The third one (Figure 4.23C) was a typical example with one normal-like sperm cell and one weak sperm cell. The normal-like sperm cell had compacted chromosomes with a tail-like bundled tubulin boundary, whereas the chromosomes in the abnormal sperm cell showed a faint DAPI signal with disrupted tubulin. Similarly, the weak sperm cell lost the LIM14 protein plate structure within it.

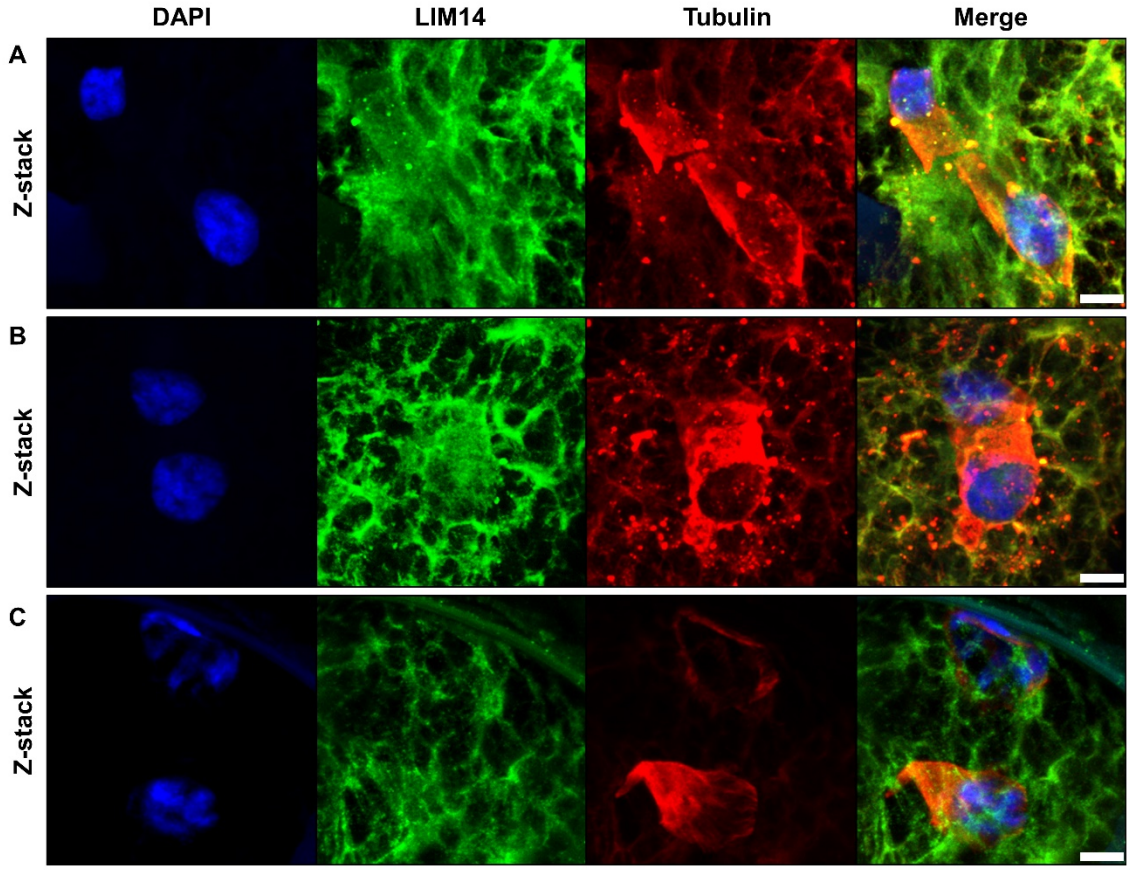

Figure 4.23 Immunolocalization analysis of *lim6* anaphase pollen. LIM14 and tubulin immunolocalization together with DAPI of *lim6*-3 pollen. (A) Two normal-like nuclei with broken tubulin stirps (B) Two normal-like nuclei with one naked. (C) One normal-like sperm cell and one weak sperm cell. The protein localization overall view by z-stack. Scale bar = 5μm.

For the *lim14-2* single mutant (Figure 4.24), various sized aggregated granules of LIM6 protein were observed in Figure 4.24A, while in Figure 4.24B, low intensity of LIM6 protein was detected in the nuclei region. These observations were consistent with the abnormal tubulin

phenotypes, including broken tubulin connections and pieced tubulin envelopes, that were also found in the pollen grain

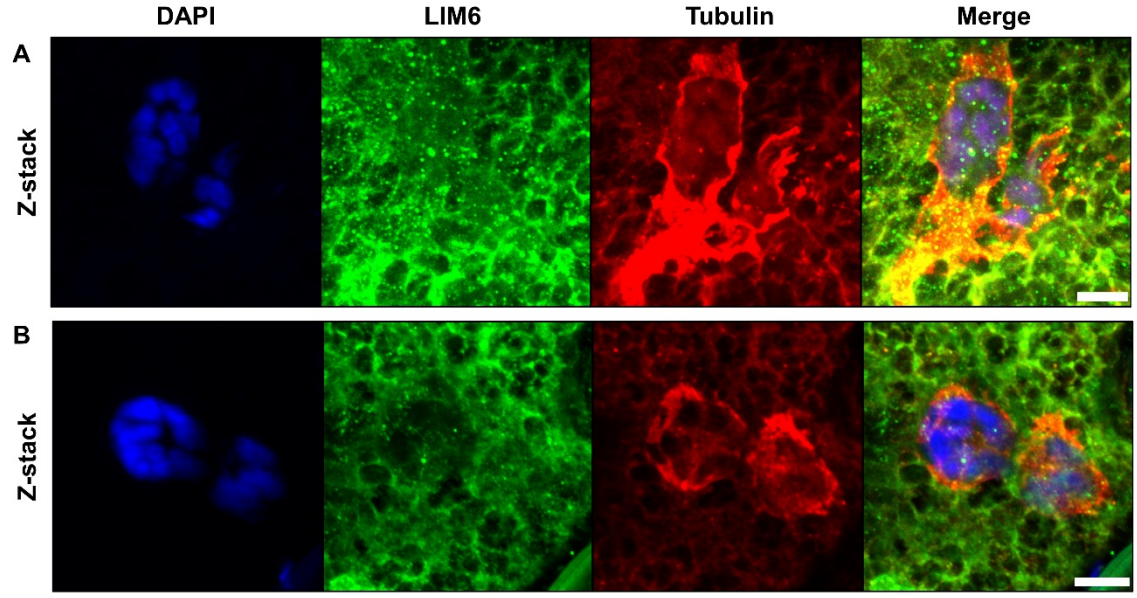

Figure 4.24 Immunolocalization analysis of *lim14* anaphase pollen. LIM6 and tubulin immunolocalization together with DAPI of *lim14*-2 pollen. (A) Two normal-like nuclei with broken tubulin envelops (B) One normal-like sperm cell and one weak sperm cell. The protein localization overall view by z-stack. Scale bar = 5μm.

Mutant pollen immunolocalization at telophase or early tricellular stage

At telophase, the mitosis is near to the end. The mutant pollen, which contained abnormal sperm cells during previous phases, most likely had only one sperm or non-sperm cell left when it reached the telophase. By considering this situation and the limitation of wax thickness, it was difficult to determine whether sections showing one sperm cell or non-sperm cell were mutant phenotypes or simply missed the nuclei region in pollen grain. Thus, all phenotype examples shown here were easily identified as telophase or early-tricellular stage based on two distinct nuclei or tubulin structures.

Figure 4.25 displayed *lim6* mutant immunolocalization results. Similar to the anaphase phenotypes, there were slides containing two sperm cells surrounded by broken tubulin envelops (Figure 4.25C), as well as samples showing two sperm cells but with one being naked (Figure 4.25 B&D). Furthermore, since the effects of LIM6 protein defect likely appeared until telophase in some pollen, the tubulin could form a long tail-like bundled structure, but the integrity and position were severely altered, resulting in the observation of extra pieces of chromosomes besides the two major nuclei regions (Figure 4.25 A&E).

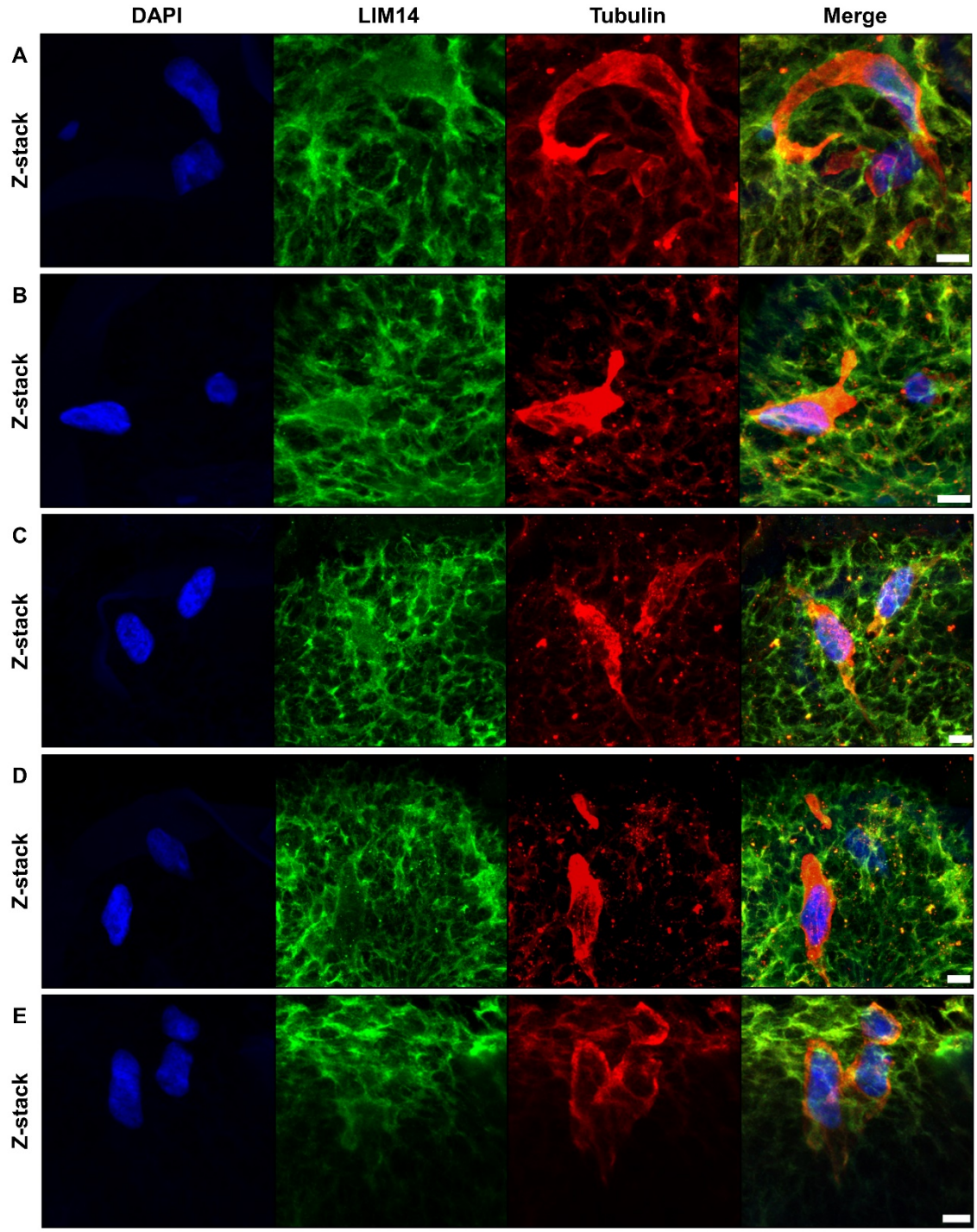

Figure 4.25 Immunolocalization analysis of *lim6* anaphase pollen. LIM14 and tubulin immunolocalization together with DAPI of *lim6*-3 pollen. The protein localization overall view by z-stack. Scale bar = 5μm.

In order to investigate the dynamics of the LIM14 protein in *lim6* mutant during telophase, a single section of Figure 4.25A was selected for analysis. As shown in Figure 4.26, the LIM14 protein formed a plate structure at both nuclei regions. However, upon conducting a plot analysis across the normal-like sperm cell and the broken sperm cell, the results showed that

although the DNA content and tubulin intensity of both nuclei were not different (as indicated by the blue and red lines), the LIM14 protein curves showed low values at the abnormal sperm cell, suggesting that both LIM6 and LIM14 were necessary for proper sperm cell formation.

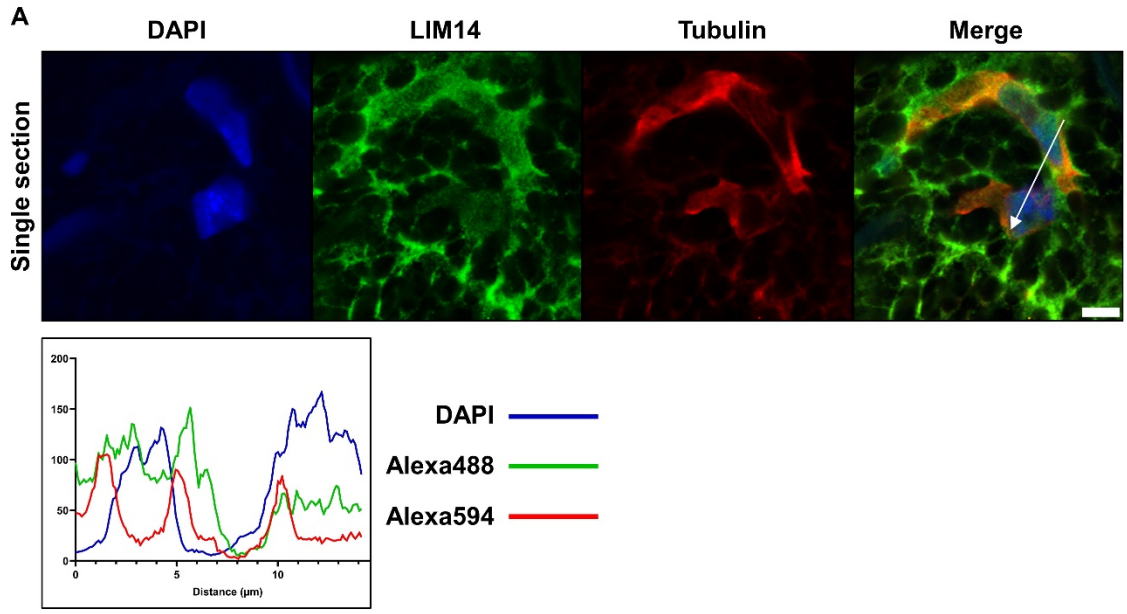

Figure 4.26 Immunolocalization analysis of *lim6* anaphase pollen. LIM14 and tubulin immunolocalization together with DAPI of single section *lim6*-3 pollen. White arrow indicated plot profile position and direction. Scale bar = 5μm.

Figure 4.27 showed the *lim14* mutant immunolocalization results. Similar to the *lim6* mutant, Figure 4.27A&E exhibited two normal-like sperm cells with broken tubulin envelops. Figure 4.27B depicted an example of a naked sperm cell. Moreover, based on the observed tubulin shape, it can be confidently stated that Figure 4.27C was a telophase or early tricellular stage pollen, but only one sperm cell was detected, and the other was presumably missing due to the opened tubulin envelop. The nuclei arrangements in Figure 4.27D are similar to Figure 4.25E, and the white triangles indicate that the tubulin envelops surrounding the two nuclei showed adhesion because the LIM6 protein did not form two distinct plate structures for both sperm cells.

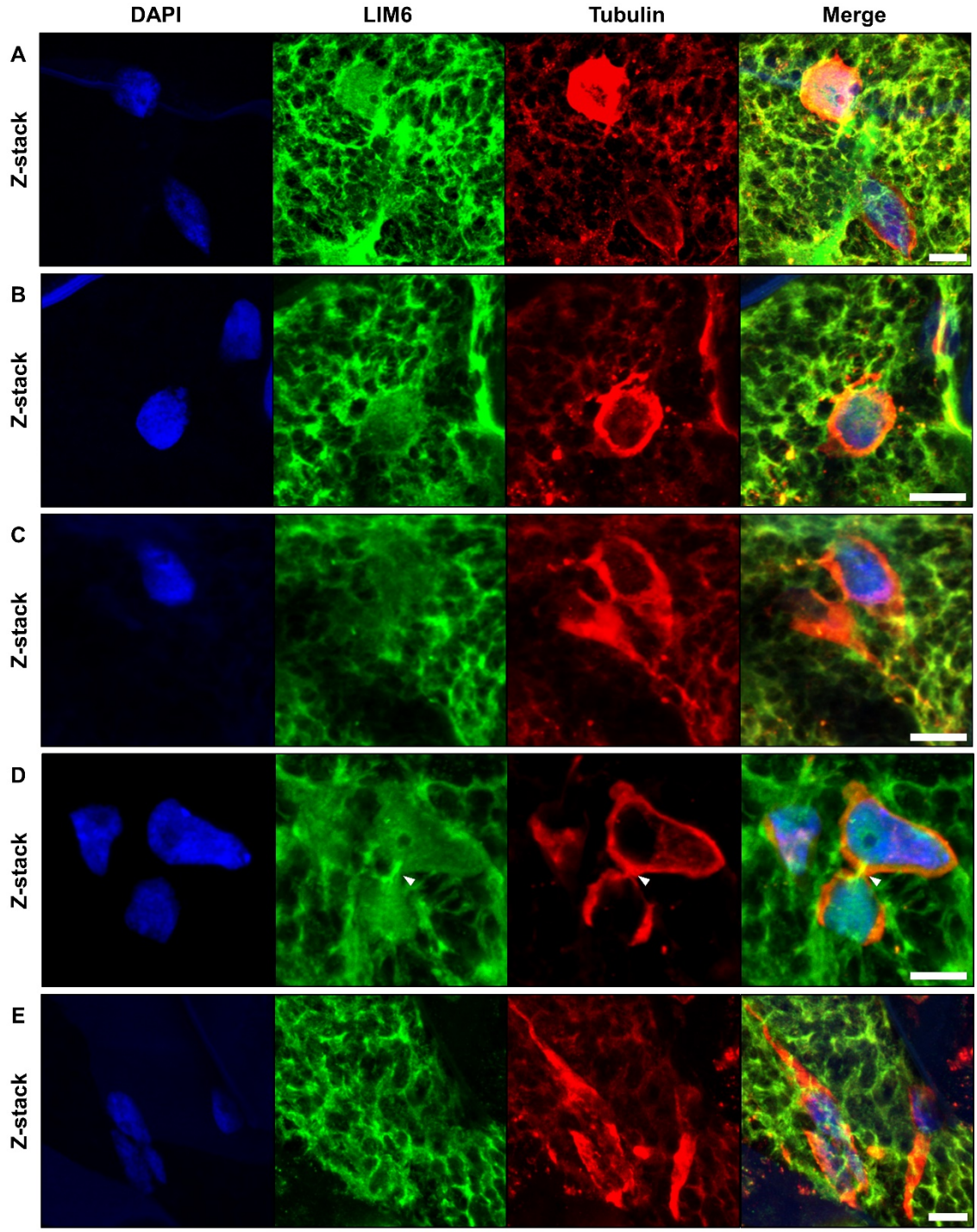

Figure 4.27 Immunolocalization analysis of *lim14* anaphase pollen. LIM6 and tubulin immunolocalization together with DAPI of *lim14*-2 pollen. White triangle indicated adhesion site. Protein localization overall view by z-stack. Scale bar = 5μm.

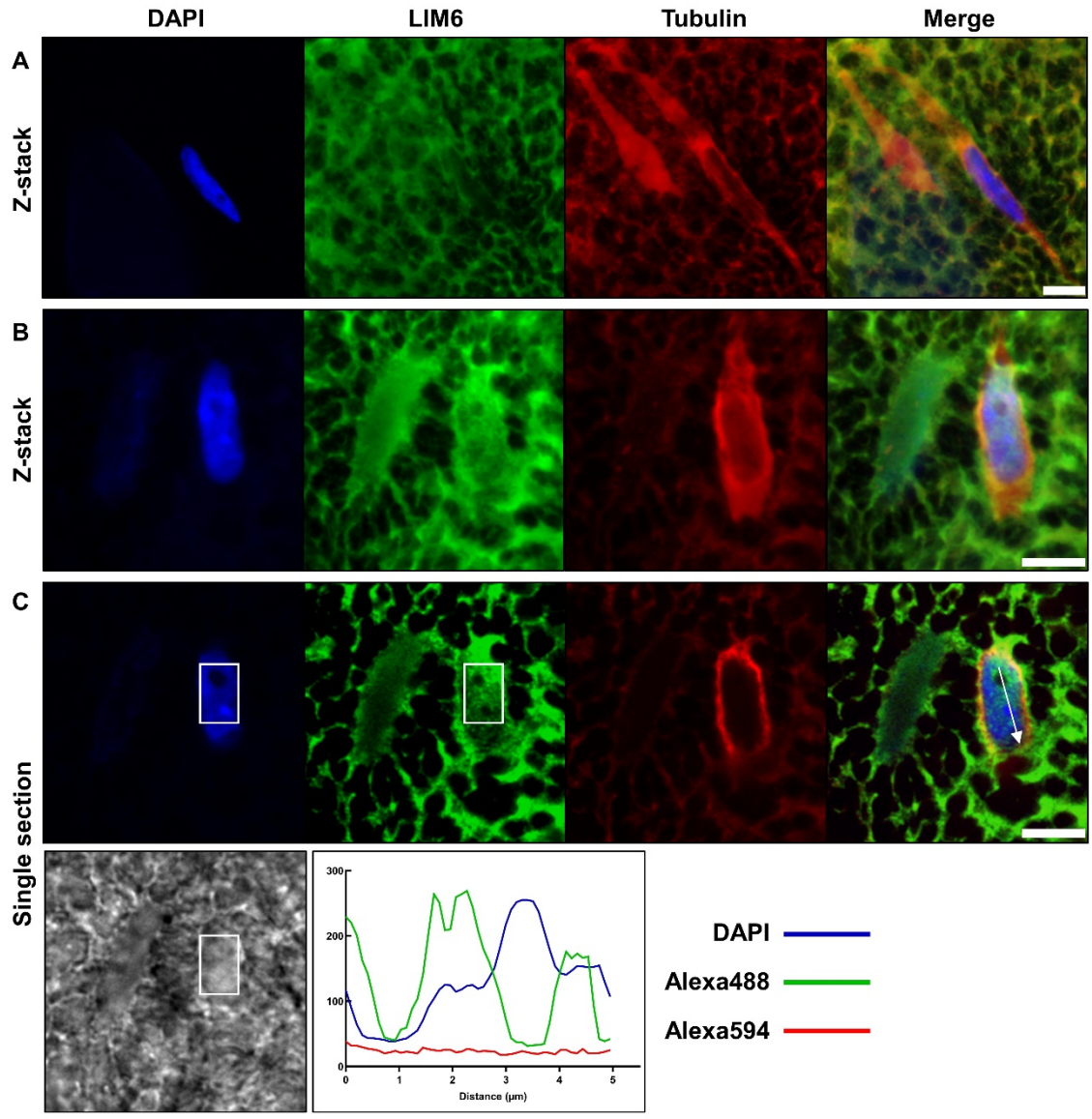

Figure 4.28 Immunolocalization analysis of *lim14* early-tricellular pollen. LIM6 and tubulin immunolocalization together with DAPI of *lim14*-2 pollen. Protein localization overall view by z-stack. White rectangle indicated nucleolus. White arrow indicated plot profile position and direction. Scale bar = 5μm.

Besides, some early-tricellular pollen also showed some new phenotypes (Figure 4.28). By screen the immunolocalization results at tubulin channel, one example as Figure 4.28A showed there was a pollen grain containing two long tail-like bundled spindles connected by a strip, which is a typical tubulin structure of mature pollen. However, one spindle formed an envelope with a nucleus inside, while the other one was a solid plate with no DNA inside. Correspondingly, there was no LIM protein gatherings at the non-nuclei region. On the other hand, in Figure 4.28B, LIM6 protein formed two spindle-shape plates but only one normal nucleus was generated. Although the nucleus appeared normal, single section analysis showed

that LIM6 protein formed two basket structures, which were related to nucleolus formation as seen in the bright view. However, by plot profile analysis, the upper basket structure was normal with no chromosomes inside, and the lower one contained a higher DNA content, indicating that new nucleolus formation could occur after PMII even when there was a non-disassembled nucleolus present, but only one functioned normally. These examples suggest that tubulin dynamics are also affected by LIMs protein at the tricellular stage and nuclei lost is probably due to nucleolus disorder.

4.3.5.7 Immunolocalization analysis of ZmLIM6/14 and actin in pollen

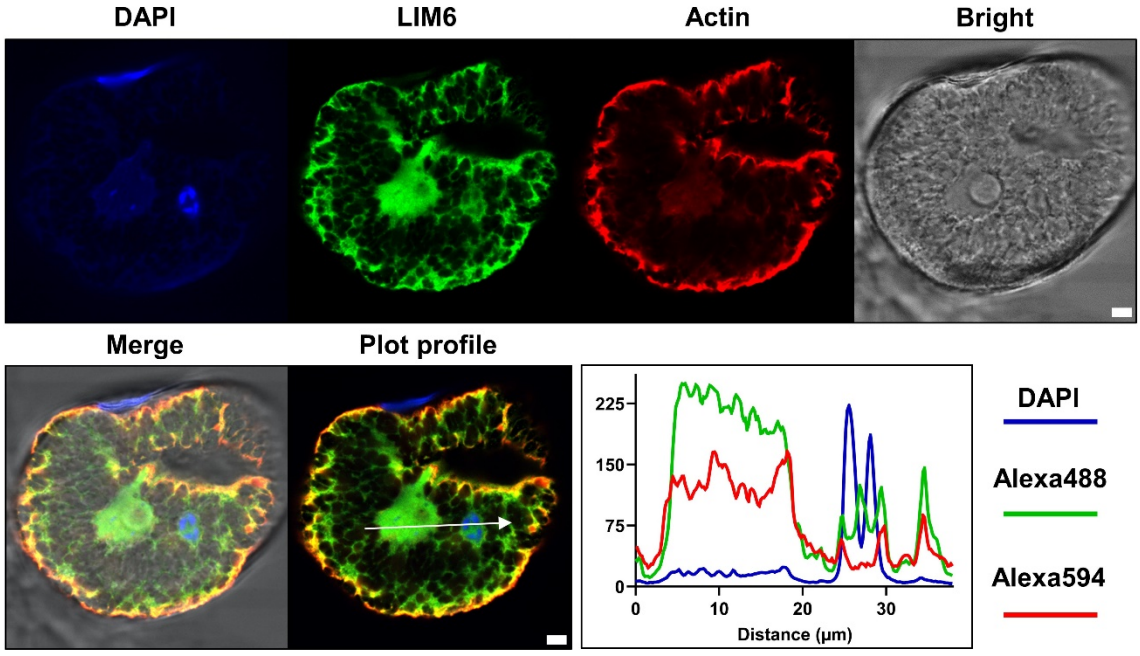

Figure 4.29 ZmLIM6 and actin immunolocalization analysis of metaphase pollen. LIM6 and tubulin immunolocalization together with DAPI. Exine visibility enhanced due to it being autofluorescent. The protein localization overall view by z-stack. Colocalization analysis by plot profile at single section. White arrow indicated plot profile position and direction. Scale bar = 5μm.

As Figure 4.15 shows, LIM 6 and LIM14 proteins accumulate around the periphery of the vegetative cell, indicating its involvement in multiple functions during pollen tube growth. Previous research has demonstrated that AtPLIM2s and NtPLIM2b, which are phylogenetically clustered with ZmLIM6/14 (Figure 3.1), are associated with actin organization (Cheung et al., 2008; Moes et al., 2013; Ye et al., 2013). Hence, it can be inferred that ZmLIM6/14 share

similar properties. To further validate the interaction between ZmLIMs and actin, immunolocalization analysis with actin was conducted (Figure 4.29).

LIM6 showed the same expression pattern found in Figure 4.15. However, unlike tubulin, actin serving as the main cytoskeleton component showed universal distribution, from which it was observed that actin gathered at vegetative cell region, indicating the important role of actin in pollen tube cell development. By plot profile analysis, LIM6 and actin showed high overlap at vegetative cell periphery part and pollen cortical region, but non-colocalization across germ cell due to no actin arrangement there.

4.3.5.8 Mutant pollen germination test

Because actin is well known vital for pollen tube development flowering plants (Lovy-Wheeler et al., 2005; Ren and Xiang, 2007; Cheung and Wu, 2008), then the mutant pollen tube growth was further investigated by *in vitro* and *in vivo* germination experiments.

In vitro germination

Based on mutant premature pollen phenotyping results, the mutant showing strong phenotypes were selected to do *in vitro* germination experiments. As shown in the Figure 4.30, all mutant mature pollen showed a normal germination rate of approximately 85%. However, there were significant differences observed in the pollen tube growth patterns compared to the wild type. It was evident that all *lim6/14* single and double mutants pollen displayed similar growth patterns, with some pollen tubes germinating similarly to wild type (21%-47%), and more than half of the germinated pollen tubes exhibited zigzagging and twisted patterns. Furthermore, it was found that the burst ratio in mutant pollen tubes increased significantly in single mutant (~10%-27%) and double mutant (~41%), regardless of whether the pollen tube had a normal or twisted pattern. In conclusion, the ZmLIMs defect did not appear to affect pollen germination, but had a severe impact on the pollen tube growth and integrity *in vitro*.

Pollen tube actin configuration investigation

The twisted growth pattern observed in mutant pollen tubes confirmed the influence of ZmLIMs on both the colocalization and functionality of actin filaments in pollen tube growth. In order to directly visualize the actin configuration in mutant pollen tubes, *in vitro* germinated pollen tubes were fixed and stained with Alexa-488 phalloidin.

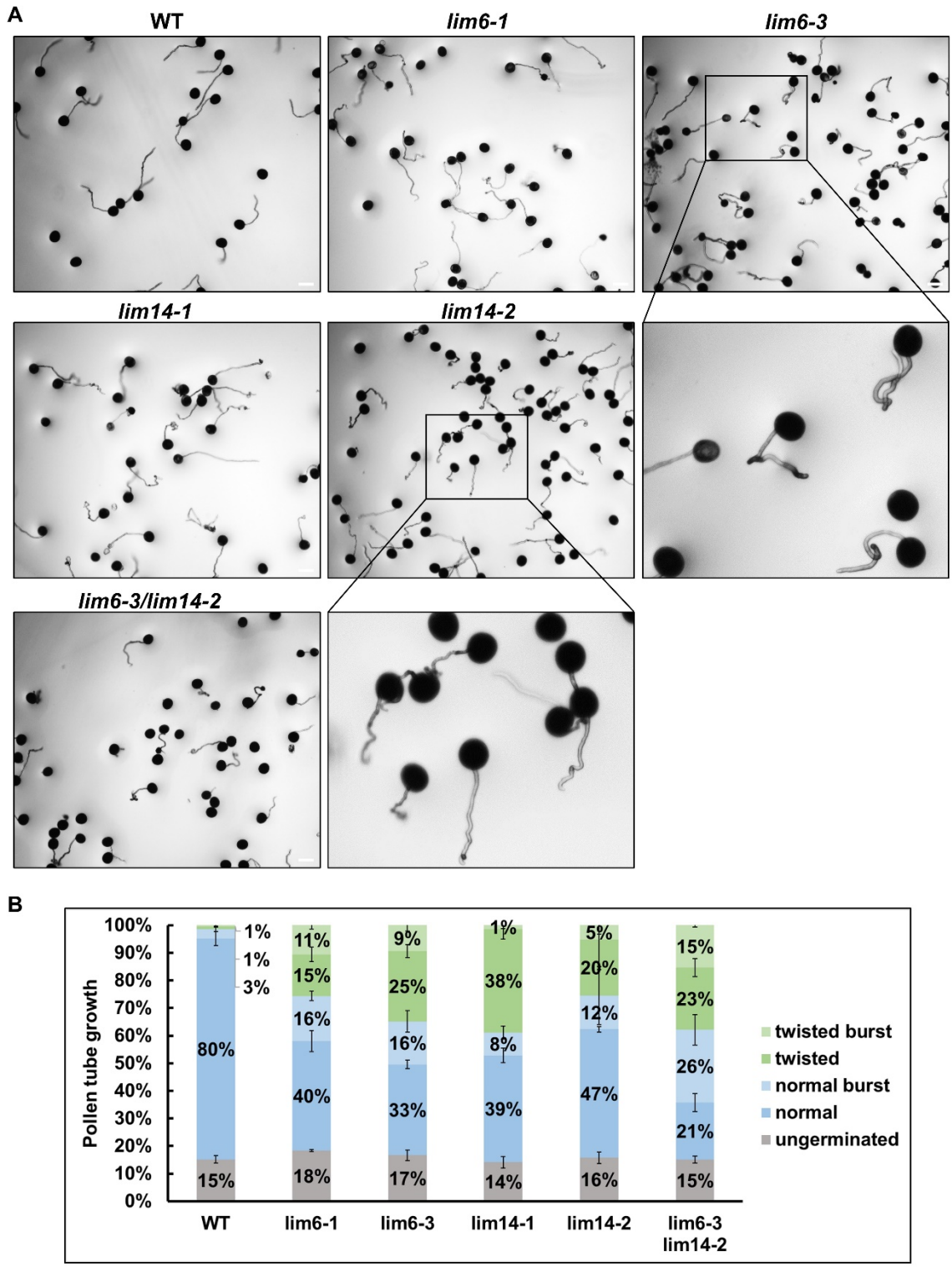

Figure 4.30 Mutant pollen tube growth investigation. (A) WT, *lim6*, *lim14* and double mutant *in vitro* germination results (after germination 45min). Detailed view was indicated by black rectangle. (B) Statistics results of different genotypes. Scale bar = 100μm

As the Figure 4.31 showed, the actin filaments in WT pollen tubes were uniformly distributed, forming a linear structure along the length of the tube, which is typical of actin dynamics in

pollen tubes. However, in *lim14-2* mutants, the actin filament formed various ring structures at shank region in twisted pollen tube, potentially explaining the twisted growth pattern observed. Furthermore, in addition to abnormal actin filaments, the width of mutant pollen tubes was significantly greater than that of WT, which is consistent with findings in *Arabidopsis thaliana* PLIM2c mutant (Ye et al., 2013).

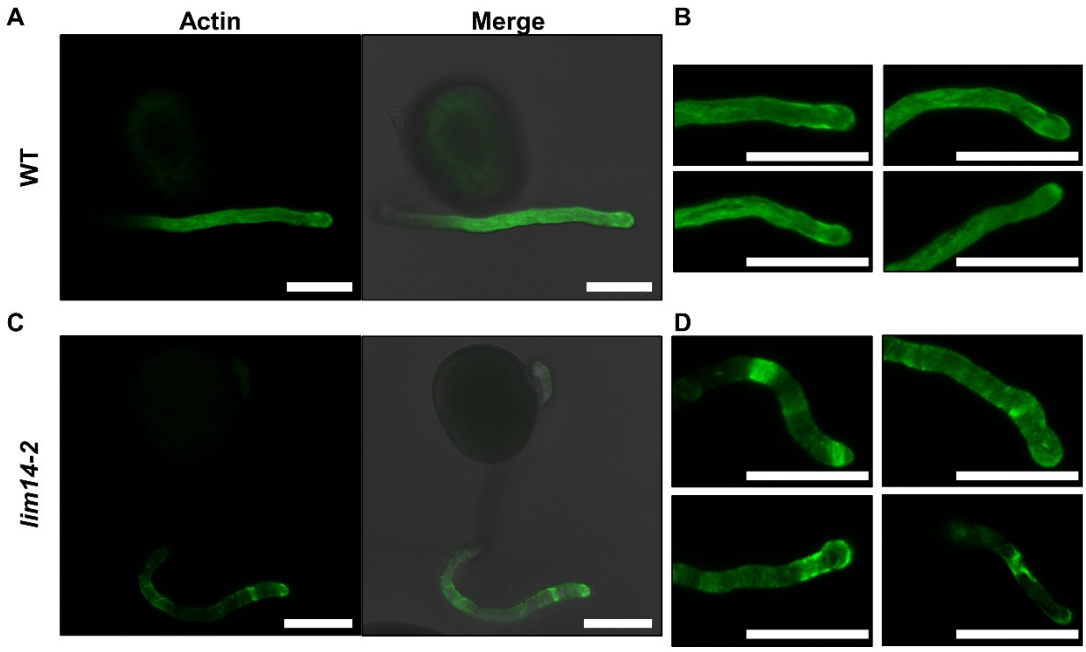

Figure 4.31 Mutant actin configuration in pollen tube. Actin in pollen tube was stained by Alexa-488 phalloidin. (A) Actin filament in WT pollen tube. Pollen tube showed smooth growth. (B) Actin filament evenly distributed along pollen tube. (C) Actin filament in *lim14-2* pollen tube. Pollen tube displayed twisted growth. (D) Actin filament formed ring structure at shank region in mutant pollen tube. Scale bar = 50μm

In vivo germination

Based on the *in vitro* germination results, it was evident that *lim6* and *lim14* mutant pollen tube growth was significantly impaired. In order to assess the germination capabilities of pollen tubes after pollination on silk, an *in vivo* germination experiment was conducted. As single and double mutant showed similar phenotype, *lim14-2* were chosen for *in vivo* germination experiment. As the Figure 4.32 showed, the pollen tube in silk after pollination 2 days was stained by aniline blue. Notably, pollen tubes were observed in most of the pollinated silks. Additionally, regarding to the pollen tube growth pattern, it was observed that there was no significant difference between WT and *lim14-2* mutant. However, in maize, assessing the pollen tube burst in silk was challenging. Consequently, further experiments were needed to confirm

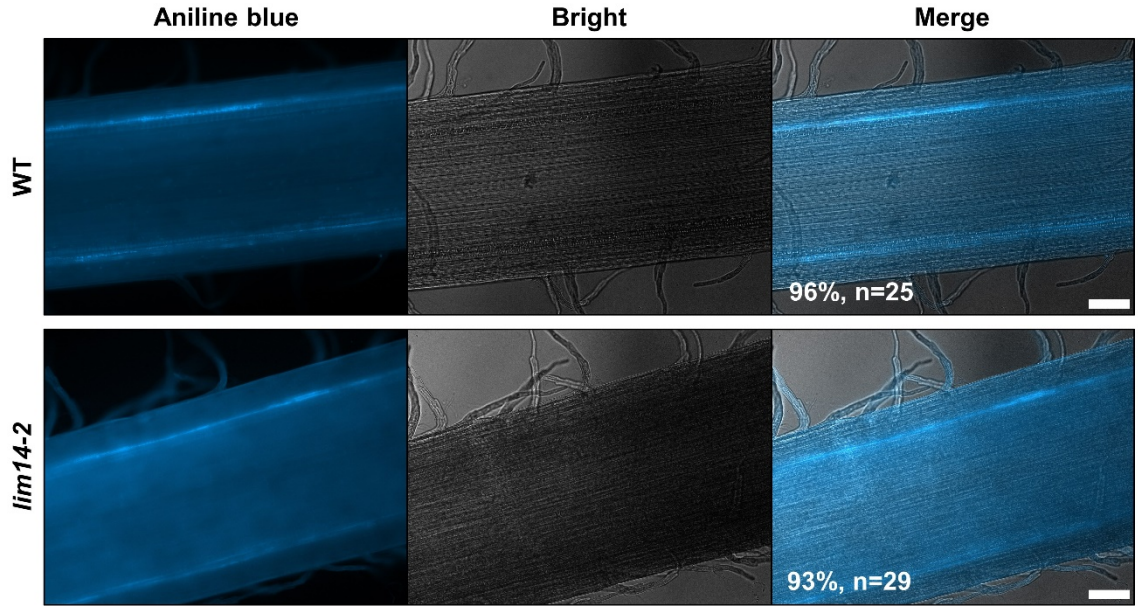

Figure 4.32 *In vivo* germination of WT and mutant pollen. The pollen tube in silk (after pollination 2 days) was stained by aniline blue. Scale bar = 100μm.

the burst phenotype. From *in vivo* germination experiment results, it could be concluded that mutant pollen could normally germinated on silk and penetrate inside to deliver the sperm cell for fertilization.

4.3.5.9 Fertilization ability test

The presence of aberrant sperm cells and irregular pollen tube growth in the mutant necessitated the investigation of its impact on fertilization ability.

Here, the self-crossed cobs of *lim14-2* mutants were selected to demonstrate their severe sterility phenotype (Figure 4.33). After 20 days of self-pollination, it was observed that the mutant cobs had various levels of seed abortion in comparison to the self-crossed WT cobs. The front and back views of the different-sized seeds clearly revealed the endosperm abortion in the abnormal seeds, which resulted in the affected embryos exhibiting different sizes. Moreover, some small abortion seeds did not contain endosperm or embryos, and were only covered by the coat (Figure 4.33A&B).

When seeds became mature (Figure 4.33 C&D), the distribution of normal and abortion seeds was easily distinguishable on the dry cob. The abortion seeds were evenly distributed on the mutant cob, and since the wild type cob showed a full seed set, the abortion seeds were not caused by pollination or growth conditions problem, but were indeed due to the ZmLIMs defect. The abortion rate of *lim14-2* cobs (~73%) was significantly higher than the WT (~6%). It is noteworthy that the rate of seed abortion was higher than the abnormal mature rate (~50%, Figure 4.10) and higher than the abnormal pollen tube rate (~35%, Figure 4.29), suggesting that both developmental defects could cause seed abortion, and further confirming that the ZmLIMs function in these two developmental processes were independent.

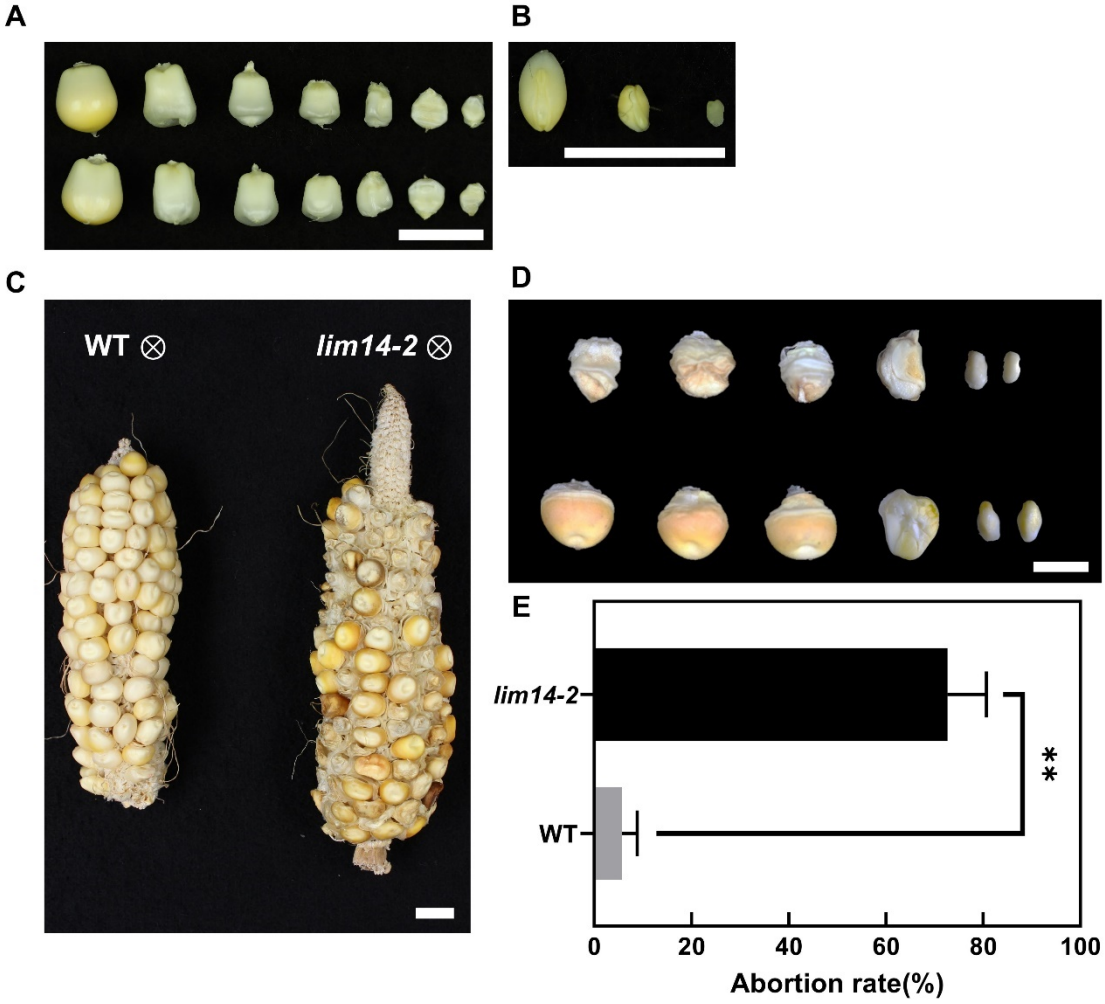

Figure 4.33 Fertilization ability test of mutant (after pollination 20 days and mature cobs). (A) Various kernel of after pollination 20 days cob. (B) Embryo dissected from normal and aborted kernels. (C) WT and *lim14-2* self-crossed cobs. (D) mature kernel and embryo of normal and aborted seeds. (E) abortion rate of WT and *lim14-2*. Scale bar = 1cm.

4.3.6 ChIP-seq of ZmLIM6/14

The reason for selecting ZmLIMs as the study object was due to their role as transcription factor genes. However, their phenotypic effects suggested a potential role in structural function, prompting further investigation into their function as transcription factors. Additionally, as the antibody specificity of ZmLIM6/14 had already been confirmed by immunostaining, it was deemed suitable for ChIP-seq experiments.

Table 4.1 showed the sequencing summary. There were 5 biological replicates of ZmLIM6, 3 of ZmLIM14, 1 positive control of H3, and 1 negative control of Input. The sequencing performed well for all samples in terms of the number of reads and quality of Q30 bases. However, the alignment rate to the maize reference genome varied among the samples, with ZmLIM6-1 showing a particularly low aligned rate of only 3.49%. Consequently, only the aligned rates of LIM6-2 and LIM6-3 were suitable for downstream analysis. Despite this, sequencing and alignment worked well for the other samples, allowing for the continuation of ZmLIM14 ChIP-seq analysis.

Table 4.1 ChIP-seq statistics summary

Sample	% >= Q30 bases	total no. of reads	aligned rate (%)
LIM6-1	89.7	38,830,479	3.49
LIM6-2	90.03	41,569,221	85.59
LIM6-3	90.01	43,368,253	87.9
LIM6-4	90.18	42,393,100	30.82
LIM6-5	90.21	42,838,343	29.96
LIM14-1	90.03	48,410,935	70.89
LIM14-2	90.34	42,568,433	83.79
LIM14-3	90.23	42,564,089	77.87
H3	89.98	51,163,742	97.76
Input	90.96	47,013,575	68.83

Peak calling analysis of ZmLIM14 ChIP-seq identified a total of 394 peaks, primarily around 200-400bp in length (Figure 4.34). Of these peaks, 393 were annotated, with one being dropped due to alignment to mitochondrial sequence. The annotation of these peaks revealed that around 70% mapped to distal intergenic regions, while the remaining 30% were annotated within 2kb of the promoter region. This indicated that the annotation results were reliable, given that the 2kb region is typically considered a gene promoter. Figure 4.34C illustrated that only intergenic regions displayed high number overlap patterns, with some peaks annotated at promoter regions also identified at intergenic regions due to the maize genome's complexity. Figure 4.34D provided an example of ZmLIM annotated peaks distribution between two genes. Finally,

compared to Input and H3, the three biological replications all displayed obvious peak pile-ups at different regions of the genome.

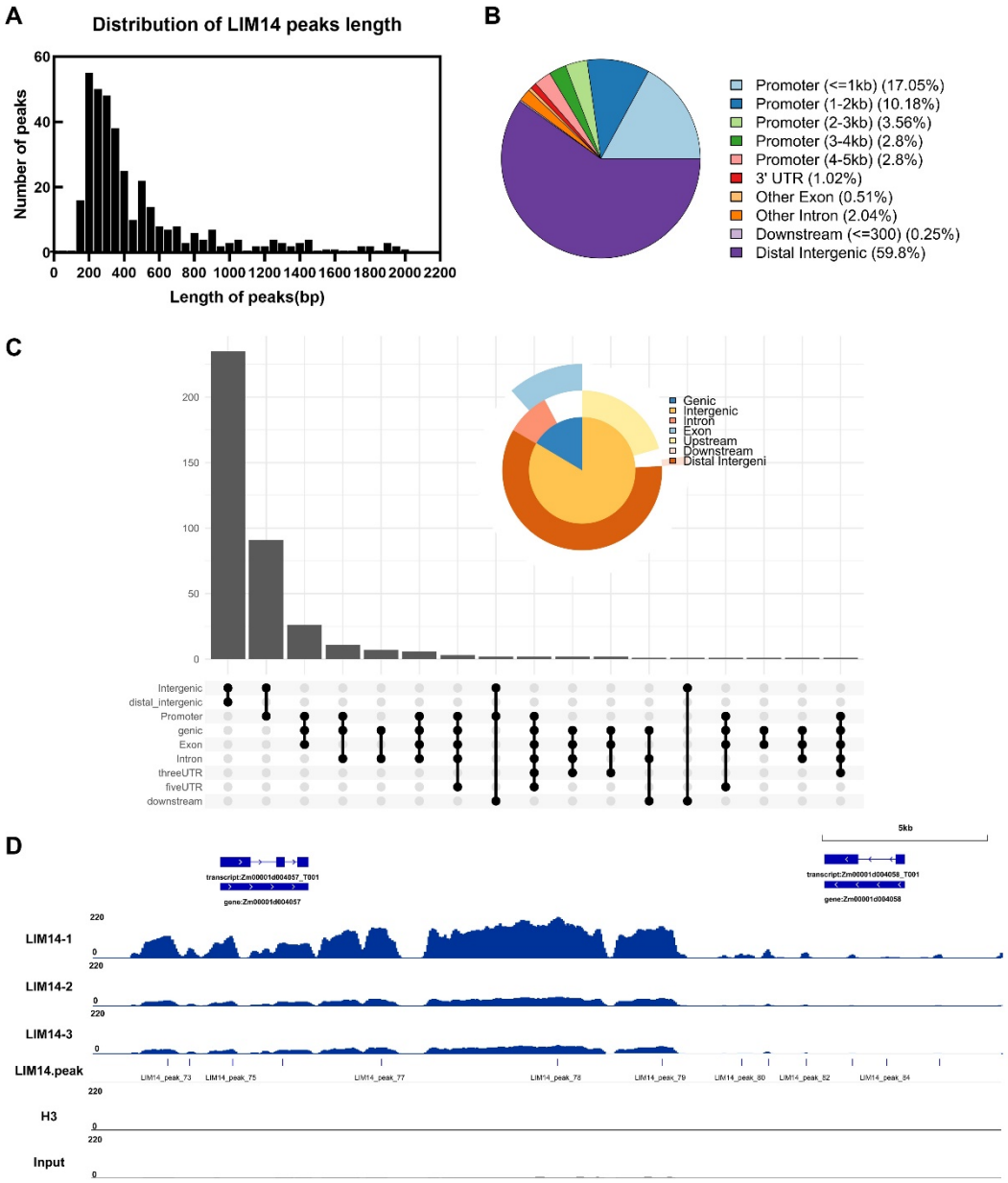

Figure 4.34 ChIP-seq analysis of ZmLIM14. (A) Distribution of ZmLIM14 peaks length. (B) ZmLIM14 peak annotation results. (C) Peaks annotation overlap pattern. (D) ZmLIM14 peaks at genome.

As transcription factors, ZmLIMs target the promoter region, indicating their typical upstream binding regulation role. The peak annotation results revealed that ZmLIM14 targeted 94 genes within the 2kb promoter region. Further examination of the expression pattern of the targeted genes showed that four putative up-regulation genes exhibited a similar expression pattern to

ZmLIM14 with high expression levels. These genes displayed low expression at the tetrad and unicellular stages, but their expression levels significantly increased from the bicellular stage (Table 4.2).

Table 4.2 The expression pattern of putative ZmLIM14 targeting genes.

GeneID	Tetrad	Uni-cellular	Bi-cellular	Tri-cellular	Mature Pollen	Pollen tube
Zm00001d025287	5.54	741.19	7557.96	7620.25	18389.4	19215.3
Zm00001d040771	1.89	160.14	3271.78	2974.28	6282.19	5526.4
Zm00001d033507	0.99	37.07	1458.51	1518.71	2934.63	5417.9
Zm00001d039429	0.85	2.91	1627.77	1667.04	2322	7250.7

Among of these 4 genes, Zm00001d039429 (*ZmRALF3*) was a well-studied gene in maize. *ZmRALF3* is involved in regulation of the cell wall integrity during pollen tube growth. RNAi line and CRSRP-Cas9 knock out mutants of ZmRALF3 showed the pollen tube always burst at the shank region (Zhou et al., 2023). The peak targeting the *ZmRALF3* was at upstream around 800bp, and only one specific peak piled up with around 200bp peak length. Further, *in vitro* germination results of *lim14-2* were checked again more carefully and found that the burst region always showed at shank region not at the apex of the tube (Figure 4.35), which was consist with ZmRALF3 knock down or knock out mutant phenotypes, indicating that the transcription factor ZmLIM14 served as an upregulation element to tune the expression of *ZmRALF3* in maize. Also highlights the success of the ChIP-seq experiment.

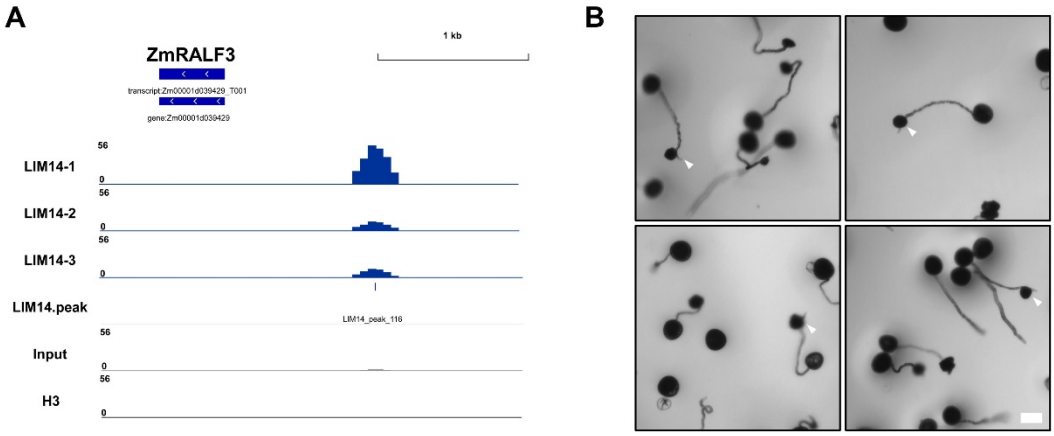

Figure 4.35 ZmLIM14 targeted *ZmRALF3*. (A) The peak targeting *ZmRALF3* promoter region. (B) Burst pollen tube of *lim14-2* mutant. Burst region was indicated by white triangle. Scale bar = 100μm

4.4 Discussion

The three CRPs discovered in the human genome are well-known for their ability to bind α-actin, indicating their structural function (Velyvis and Qin, 2000). Similarly, in the plant kingdom, many LIM family genes were identified, and most of the LIM proteins containing similar domain patterns were found to be related to actin filaments (Srivastava and Verma, 2017). In this study, it was found that ZmLIM6/14 colocalized with actin at the vegetative nucleus region from the bicellular stage. Loss-of-function mutants of ZmLIM6 and ZmLIM14 exhibited aberrant actin filament arrangement in pollen tubes, resulting in twisted and swollen pollen tubes, a phenotype already described in Arabidopsis mutants (Ye et al., 2013).

As an actin filament binding protein, the expression pattern of ZmLIM6/14 during maize pollen development raises an interesting question. Actin is one of the most fundamental proteins for cells, so why does the ZmLIM6/14 protein only appear as a decorated protein during the late stages of pollen development? Expression analysis revealed that ZmLIMs are expressed at the unicellular stage and show abundant expression from the bicellular stage onwards. This suggests that the expression of ZmLIMs is induced during the uni- and bicellular transition stage, which is characterized by an asymmetric division termed pollen mitosis I (PMI), which specifies the male germline (Berger and Twell, 2011). Similar to DUO1, a R2R3 MYB transcription factor in Arabidopsis thaliana, which is germline-specific and activated after the asymmetric division, ZmLIMs are also induced during this stage, with peak expression at the bicellular pollen stage (Brownfield et al., 2009). Interestingly, mutated DUO1 pollen generates one non-functioning germ-like cell in mature pollen, while ZmLIMs mutant mature pollen contains one sperm cell-like cell due to the broken tubulin envelop and unexpected nucleoli during PMII resulting in sperm cell loss. This suggests that the function of ZmLIMs in pollen development is different from that of DUO1. Moreover, while the germ cell in DUO1 pollen is not competent to fertilize either the egg or central cell (Rotman et al., 2005) while the homozygote of *lim6* and *lim14* mutant still produces haploid sperm cells for fertilization. As single sperm cells preferentially fertilize the egg celll (Li et al., 2022a), the cobs of *lim* mutants show endosperm abortion seeds and no embryo abortion seed is found, indicating that the one sperm-like cell produced in *lim* mutants is still competent for fertilization.

In addition to its role as an actin filament binding protein, our study revealed novel functions of ZmLIM6/14 in regulating tubulin dynamics and contributing to the appearance of nucleoli during pollen mitosis II as a structural protein.

The cytoskeletal apparatus of most angiosperms GCs or SCs consists microtubules (Franke et al., 1972; Lancelle et al., 1987; Palevitz and Cresti, 1988). Microtubule bundles undergo disassembly, and tubulin is diffusely spread in isolated generative cells or sperm cells, or destroyed by colchicine in pollen tubes, resulting in the rounding of generative cells or sperm cells (Tanaka, 1988; Theunis et al., 1992; Theunis and Van Went, 1989). Similarly, it was observed that sperm cells lost their spindle shape, and the connection elongated from two sperm cell bodies disappeared due to microtubule breakdown in the *lim* mutant of YFP-α-tubulin. Moreover, immunofluorescence localization revealed that during PMII, microtubules were disrupted and could not form the proper structure to organize nuclear materials. It can be inferred that LIM proteins are necessary for microtubule bundle assembly. The γ-tubulin is well-known to be necessary for cortical microtubule nucleation and organization(Murata et al., 2005). The γ-tubulin mutant of *Arabidopsis thaliana* exhibited aberrant microtubule organization during the mitosis process of pollen development and produced various nuclear phenotypes in mature pollen (Binarová et al., 2006; Pastuglia et al., 2006). *lim6/14* mutants also produced different types of sperm cells in mature pollen due to aberrant microtubule organization during PMII. There were many cortical punctae in both the LIM protein and α-tubulin immunofluorescence localization of the mutant, which was similarly found in Arabidopsis after depolymerizing microtubules (Chan et al., 2003), indicating that LIM proteins may not be related to microtubule nucleation but to microtubule bundling

All immunofluorescence localization results revealed a strong correlation between the LIM protein and nucleolus formation in pollen, as the protein acted as a barrier surrounding the nucleolar region. But it is well-studied that nucleolus is a membrane-less organelle where ribosomal RNA synthesis and nascent ribosome assembly. Nucleolus formation is initiated at specific genome regions known as nucleolar organizer regions (NORs), which are embedded in the 45s rDNA cluster at the short arm of chromosome 6 in maize (McClintock, 1934; Ritossa and Spiegelman, 1965; Li and Arumuganathan, 2001). Multiple nucleoli can be induced in maize root cells by treatment with actinomycin D (ActD), a transcription inhibitor that disrupts 45s rDNA stability. In the *lim* mutant, undisassembled nucleoli were observed during the PMII process, and ultimately, sperm cells had either no nucleoli or two nucleoli. This suggests that the LIM protein may be related to NORs stability. Besides, in figure 4.27C, the right sperm cell has two nucleoli, with the top one appearing normal and the bottom one displaying bright DAPI intensive signals, which are chromocenters containing highly compacted peri-centromeric heterochromatin. As there is no physical barrier separating the nucleolus from the nucleoplasm, the nucleolus is typically surrounded by a shell of heterochromatin (Németh and Längst, 2011).

This result suggests that the LIM protein defect altered heterochromatin localization. However, there is currently no direct evidence explaining how the LIM protein is related to nucleolar formation at a structural level or how it regulates other genes as a transcription factor.

As a transcription factor, the ability of LIM protein to bind to nucleic acids directly has been sparsely studied. PLIM-1 from sunflower was found to bind to both DNA and RNA *in vitro* (Baltz et al., 1996) and the NtWLIM2 was able to bind to and activate the histone gene promoter through transient expression assays in live cells.. In this study, the specific ZmLIM protein antibodies were applied for immunoprecipitation with mature pollen nuclei to investigate the function of ZmLIM protein as a transcription factor at the genome-wide level. Through our results, it was discovered that ZmLIM14 binds to the promoter region of the well-known *ZmRALF3* gene, which is associated with pollen tube thickness at the shank region. The similar pollen burst phenotype observed in the *lim6* and *lim14* mutants as the ZmRALF3 mutant could be attributed to this discovery, and it may also explain why the pollen tube exhibits a twisted pattern.

CHAPTER 5. COMPREHENSIVE DISSCUSSION AND OUTLOOK

- *this chapter was written by myself*

The developmental progression of maize male gametophyte exhibits distinct phase-specific patterns in response to heat stress and gene regulation. This phenomenon has been extensively described in previous studies, particularly during the pre-meiotic and microsporogenesis stages. Drawing upon these publications and from data generated in our group, this thesis investigated the heat stress response and the functions of specific transcription factors during the late stages of maize pollen development (**Chapter 1**). It was shown that bicellular to tricellular transition stage of maize pollen development, encompassing the second pollen mitosis division (PMII), is particularly susceptible to heat stress affecting developmental processes occurring in the late stages of maize pollen development (**Chapter 2)**.

Chapter 2 highlights stage-specific heat stress responses in bicellular pollen compared to unicellular pollen in maize. Heat stress during the bicellular stage leads to seed set abortion due to arrested mitosis. Transition from unicellular to bicellular stage is marked by an asymmetric mitotic division (PMI) that determines the fate of the germ cell and vegetative cell (Twell, 2011). This transition stage offers the possibility of stage-specific heat stress responses and the activation of distinct transcription factors. A number of studies have unveiled distinct transcriptome profiles in microspores and germline cells. Notably, maize exhibits more significant changes in transcriptional expression (21,251 genes in unicellular pollen vs. 15,227 genes in bicellular pollen) (Begcy and Dresselhaus, unpublished) compared to *Arabidopsis thaliana* (11,565 genes in unicellular microspores vs. 11,909 genes in bicellular pollen) (Honys and Twell, 2004) and rice (14,590 genes in uninucleate microspores vs 12,967 in bicellular pollen) (Wei et al., 2010), underscoring the unique nature of the bicellular stage in maize pollen development. The stage-specific regulation pattern of maize pollen development results in different heat stress responses at various stages and leads to the emergence of stage-enriched transcription factor clusters. Transcriptome analyses of pollen at different developmental stages in maize (this thesis), rice (Wei et al., 2010) and Arabidopsis (Honys and Twell, 2004) have revealed conserved transcription factor families involved in pollen development, including MYB/MYB-related, C2H2, bHLH, NAC, MADS, bZIP, GRAS, and WRKY. However, the divergence of transcription regulation associated with pollen development have also been

observed among different plant species. These findings could help to explain why stage-specific heat stress responses are only observed in maize pollen. At the proteome level, dramatic changes in developing pollen have been observed through two-dimensional gel electrophoresis in maize and rice (Bedinger and Edgerton, 1990; Kerim et al., 2003) indicating a shift in protein enrichment during the bicellular pollen stage. However, a detailed comparison analysis of protein components between unicellular and bicellular pollen is currently lacking. Generally, PMI not only determines the fate of the male germline but also induces changes in the molecular program and key components of pollen during the transition stages. These findings suggest that the observations made in this thesis have the potential to shed light on these molecular alterations in pollen development.

The LIM transcription factory family was selected for comparative phylogenetic, expression and structural studies (**Chapter 3**) as well as for functional investigations during pollen development with a focus on bicellular to tricellular phase transition including PMII (**Chapter 4**). The function of two *LIM* genes, *ZmLIM6* and *ZmLIM14*, was analyzed in more detail. Notably, *ZmLIM* genes, including *ZmLIM6, ZmLIM14, ZmLIM8*, and *ZmLIM9*, are highly expressed during the bicellular and subsequent pollen developmental stages (**Chapter 3, Table 3.2**). *lim6* and *lim14* mutants generate abnormal mature pollen due to microtubule and nucleoli disorder during PMII, a similar phenotype observed in bicellular heat stressed pollen. Both cases result in non-functional sperm cells. There were no significant differences observed in sperm cell expression of *ZmLIM6/14* genes in response to heat-stress. These findings indicate that *ZmLIM6/14* might regulate possible genes susceptible to heat stress as they are not direct target of increased temperatures. Similar findings have been reported for PLIM genes in wheat (*Triticum aestivum* L.) under heat stress (Li et al., 2022b). However, WLIM genes in *Medicago sativa* L. have been shown to be induced by low temperature treatments (Nian et al., 2021) and WLIM2b has been found to be up-regulated in response to various hormone and high salts treatments in Foxtail Millet (*Setaria italica* L.) (Yang et al., 2019), indicating distinct regulation patterns between PLIMs and WLIMs in cereals.

In addition, both **Chapter 2** and **Chapter 4** focus on phenotypes and gene regulations during the second mitosis (PMII) of maize pollen development, which highlights the significance of PMII as the main biological event during the bicellular to tricellular transition stage, marking the final stage of pollen maturation. PMII in maize involves a mitosis process within the pollen grain resulting in the generation of twin sperm cells. Notably, when compared to vegetative cells (18,611 genes detected), sperm cells (16,985 genes detected) in rice exhibit reduced

complexity at the transcriptome level. However, the top 50 transcripts in sperm cells demonstrate a broader range of expression with higher peak levels compared to vegetative cells (Anderson et al., 2013). In **Chapter 2** the data showed that heat stress only affected highly expressed genes indicating that although sperm cells have a reduced transcriptional output, they are still capable of expressing individual genes at very high levels that are easily influenced by increased temperatures. Moreover, in a study on thermo-sensitive genic male sterile (TGMS) rice lines induced by low temperatures, differentially expressed proteins were found to be mainly involved in redox homeostasis, transcription and translation regulation as well as carbohydrate metabolism (Song et al., 2015). Similarly, this thesis reveals protein enrichment alterations in classes such as oxidoreductase, hydrolase, and nucleic acid binding (**Figure 2.13**), indicating conserved regulatory mechanisms involved in maintaining fertility at the protein level between maize and rice.

The regulation of microtubules during mitosis, described in **Chapter 2** and **Chapter 4**, was found to be disrupted under heat stress and due to defects in LIM proteins. This is consistent with previous studies, as disruptions in microtubule organization and mutants in microtubule organization have been known to cause male sterility (McCormick, 1993; De Storme and Geelen, 2013; Parrotta et al., 2016) given the crucial role of tubulin in spindle formation and chromosome segregation during cell division. However, in this thesis expression levels of tubulin genes were not severely affected as shown in **Figure 2.11**, and there was no difference in fluorescence intensity of the tubulin marker line between wild type plants and *lim14* homozygous mutant (**Figure 4.12**). Similar observations have been made in tobacco, where the relative quantity of tubulin was only slightly affected by heat stress (Parrotta et al., 2016) indicating a stable mechanism underlying microtubule synthesis. Therefore, aberrant PMII observed in heat-stressed bicellular pollen (**Chapter 2**) or *lim* mutant pollen (**Chapter 4**) can be attributed mainly to altered microtubule signaling pathways and to defective tubulin organization. These novel discoveries highlight the functions of LIM proteins in maize pollen development and open the door for the identification and characterization of more genes related to pollen development from the stage-enriched transcriptional expression.

Taken together, the arrest of PMII during the bicellular stage under heat stress leads to a reduction in seed set. However, the formation of non-functional sperm cells following aberrant metaphase remains unclear and requires further investigation. To address these questions, it is necessary to observe the developmental status of pollen after heat stress. Additionally, sperm cells isolated from heat-stressed mature pollen can be examined using a flow cytometer to

assess the chromosome state and investigate the cytoskeleton of treated pollen and pollen tubes to confirm any phenotypes associated with blocked sperm cell traveling. In the study of LIM protein function, it is evident that LIM6/14 proteins play multiple roles in sperm cell formation during PMII. As structural proteins, LIM proteins are involved in microtubule organization and nucleoli formation. To elucidate the specific step at which LIM proteins participate in tubulin regulation, such as tubulin nucleation, bundling, or together interact with actin, *in vivo* or *in vitro* protein activity assays are needed. Regarding nucleoli formation, the introduction of a nucleoli marker would facilitate the observation of nucleoli dynamics in *lim* mutants, allowing for further investigation into whether LIM proteins directly regulate nucleoli formation. As transcription factors, performing ChIP-seq analysis of ZmLIM6 and comparing it with the results of ZmLIM14 will help uncover how LIM proteins regulate sperm cell formation and pollen development by targeting specific genes. Moreover, the production of normal seeds in double mutants of *lim6 lim14* suggests the presence of other redundant genes. Therefore, it is necessary to generate high-order mutants, such as *lim6 lim14* and *lim8 lim9*, to explore the function of LIM proteins further and provide additional evidence for the phase-specific gene regulation pattern in maize pollen development.

REFERENCE

Abiko, M., Akibayashi, K., Sakata, T., Kimura, M., Kihara, M., Itoh, K., Asamizu, E., Sato, S., Takahashi, H., and Higashitani, A. (2005). High-temperature induction of male sterility during barley (Hordeum vulgare L.) anther development is mediated by transcriptional inhibition. Sex. Plant Reprod. **18**: 91–100.

Ahmadli, U. et al. (2023). High temperature increases centromere-mediated genome elimination frequency and enhances haploid induction in Arabidopsis. Plant Commun. **4**: 100507.

Ahmed, F.E., Hall, A.E., and DeMason, D.A. (1992). HEAT INJURY DURING FLORAL DEVELOPMENT IN COWPEA (VIGNA UNGUICULATA, FABACEAE). Am. J. Bot. **79**: 784–791.

Ambrose, B.A., Lerner, D.R., Ciceri, P., Padilla, C.M., Yanofsky, M.F., and Schmidt, R.J. (2000). Molecular and Genetic Analyses of the Silky1 Gene Reveal Conservation in Floral Organ Specification between Eudicots and Monocots. Mol. Cell **5**: 569–579.

Anderson, S.N., Johnson, C.S., Jones, D.S., Conrad, L.J., Gou, X., Russell, S.D., and Sundaresan, V. (2013). Transcriptomes of isolated Oryza sativa gametes characterized by deep sequencing: evidence for distinct sex-dependent chromatin and epigenetic states before fertilization. Plant J. Cell Mol. Biol. **76**: 729–741.

Arnaud, D., Déjardin, A., Leplé, J.-C., Lesage-Descauses, M.-C., Boizot, N., Villar, M., Bénédetti, H., and Pilate, G. (2012). Expression analysis of LIM gene family in poplar, toward an updated phylogenetic classification. BMC Res. Notes **5**: 102.

Arnaud, D., Déjardin, A., Leplé, J.-C., Lesage-Descauses, M.-C., and Pilate, G. (2007). Genome-Wide Analysis of LIM Gene Family in Populus trichocarpa, Arabidopsis thaliana, and Oryza sativa. DNA Res. **14**: 103–116.

Bailey, T.L., Johnson, J., Grant, C.E., and Noble, W.S. (2015). The MEME Suite. Nucleic Acids Res. **43**: W39–W49.

Baltz, R., Domon, C., Pillay, D., and Steinmetz, A. (1992a). Characterization of a pollen-specific cDNA from sunflower encoding a zinc finger protein. Plant J. **2**: 713–721.

Baltz, R., Evrard, J.-L., Bourdon, V., and Steinmetz, A. (1996). The pollen-specific LIM protein PLIM-1 from sunflower binds nucleic acids in vitro. Sex. Plant Reprod. **9**: 264–268.

Baltz, R., Evrard, J.L., Domon, C., and Steinmetz, A. (1992b). A LIM motif is present in a pollen-specific protein. Plant Cell **4**: 1465–1466.

Bartlett, M.E., Williams, S.K., Taylor, Z., DeBlasio, S., Goldshmidt, A., Hall, D.H., Schmidt, R.J., Jackson, D.P., and Whipple, C.J. (2015). The Maize PI/GLO Ortholog Zmm16/sterile tassel silky ear1 Interacts with the Zygomorphy and Sex Determination Pathways in Flower Development. Plant Cell **27**: 3081–3098.

Bedinger, P.A. and Edgerton, M.D. (1990). Developmental Staging of Maize Microspores Reveals a Transition in Developing Microspore Proteins 1. Plant Physiol. **92**: 474–479.

Bedinger, P.A. and Fowler, J.E. (2009). The Maize Male Gametophyte. In Handbook of Maize: Its Biology, J.L. Bennetzen and S.C. Hake, eds (Springer: New York, NY), pp. 57–77.

Begcy, K. and Dresselhaus, T. (2020). Analysis of Epigenetic Modifications During Vegetative and Reproductive Development in Cereals Using Chromatin Immunoprecipitation (ChIP). In Cereal Genomics: Methods and Protocols, L.M. Vaschetto, ed, Methods in Molecular Biology. (Springer US: New York, NY), pp. 141–156.

Begcy, K. and Dresselhaus, T. (2018). Epigenetic responses to abiotic stresses during reproductive development in cereals. Plant Reprod. **31**: 343–355.

Begcy, K. and Dresselhaus, T. (2017). Tracking maize pollen development by the Leaf Collar Method. Plant Reprod. **30**: 171–178.

Begcy, K., Nosenko, T., Zhou, L.-Z., Fragner, L., Weckwerth, W., and Dresselhaus, T. (2019). Male Sterility in Maize after Transient Heat Stress during the Tetrad Stage of Pollen Development. Plant Physiol. **181**: 683–700.

Begcy, K., Weigert, A., Egesa, A., and Dresselhaus, T. (2018). Compared to Australian Cultivars, European Summer Wheat (Triticum aestivum) Overreacts When Moderate Heat Stress Is Applied at the Pollen Development Stage. Agronomy **8**: 99.

Berger, F. and Twell, D. (2011). Germline Specification and Function in Plants. Annu. Rev. Plant Biol. **62**: 461–484.

Binarová, P., Cenklová, V., Procházková, J., Doskočilová, A., Volc, J., Vrlík, M., and Bögre, L. (2006). γ-Tubulin Is Essential for Acentrosomal Microtubule Nucleation and Coordination of Late Mitotic Events in Arabidopsis. Plant Cell **18**: 1199–1212.

Bokszczanin, K.L. et al. (2015). Identification of novel small ncRNAs in pollen of tomato. BMC Genomics **16**: 714.

Bolger, A.M., Lohse, M., and Usadel, B. (2014). Trimmomatic: a flexible trimmer for Illumina sequence data. Bioinforma. Oxf. Engl. **30**: 2114–2120.

Borg, M., Brownfield, L., Khatab, H., Sidorova, A., Lingaya, M., and Twell, D. (2011). The R2R3 MYB Transcription Factor DUO1 Activates a Male Germline-Specific Regulon Essential for Sperm Cell Differentiation in Arabidopsis. Plant Cell **23**: 534–549.

Borg, M., Brownfield, L., and Twell, D. (2009). Male gametophyte development: a molecular perspective. J. Exp. Bot. **60**: 1465–1478.

Boyko, A., Filkowski, J., and Kovalchuk, I. (2005). Homologous recombination in plants is temperature and day-length dependent. Mutat. Res. **572**: 73–83.

Brewer, P.B., Heisler, M.G., Hejátko, J., Friml, J., and Benková, E. (2006). In situ hybridization for mRNA detection in Arabidopsis tissue sections. Nat. Protoc. **1**: 1462–1467.

Brownfield, L., Hafidh, S., Borg, M., Sidorova, A., Mori, T., and Twell, D. (2009). A Plant Germline-Specific Integrator of Sperm Specification and Cell Cycle Progression. PLOS Genet. **5**: e1000430.

Burdo, B. et al. (2014). The Maize TFome – development of a transcription factor open reading frame collection for functional genomics. Plant J. **80**: 356–366.

Caillaud, M.-C., Paganelli, L., Lecomte, P., Deslandes, L., Quentin, M., Pecrix, Y., Le Bris, M., Marfaing, N., Abad, P., and Favery, B. (2009). Spindle Assembly Checkpoint Protein Dynamics Reveal Conserved and Unsuspected Roles in Plant Cell Division. PLoS ONE **4**: e6757.

Chan, J., Calder, G.M., Doonan, J.H., and Lloyd, C.W. (2003). EB1 reveals mobile microtubule nucleation sites in Arabidopsis. Nat. Cell Biol. **5**: 967–971.

Chang, M.T. and Neuffer, M.G. (1989). Maize microsporogenesis. Genome **32**: 232–244.

Char, S.N., Neelakandan, A.K., Nahampun, H., Frame, B., Main, M., Spalding, M.H., Becraft, P.W., Meyers, B.C., Walbot, V., Wang, K., and Yang, B. (2017). An *Agrobacterium* -delivered CRISPR /Cas9 system for high-frequency targeted mutagenesis in maize. Plant Biotechnol. J. **15**: 257–268.

Chaubal, R., Anderson, J.R., Trimnell, M.R., Fox, T.W., Albertsen, M.C., and Bedinger, P. (2003). The transformation of anthers in the msca1 mutant of maize. Planta **216**: 778–788.

Chen, C., Begcy, K., Liu, K., Folsom, J.J., Wang, Z., Zhang, C., and Walia, H. (2016). Heat stress yields a unique MADS box transcription factor in determining seed size and thermal sensitivity. Plant Physiol. **171**: 606–622.

Chen, C., Chen, H., Zhang, Y., Thomas, H.R., Frank, M.H., He, Y., and Xia, R. (2020a). TBtools: An Integrative Toolkit Developed for Interactive Analyses of Big Biological Data. Mol. Plant **13**: 1194–1202.

Chen, J., Strieder, N., Krohn, N.G., Cyprys, P., Sprunck, S., Engelmann, J.C., and Dresselhaus, T. (2017). Zygotic Genome Activation Occurs Shortly after Fertilization in Maize. Plant Cell **29**: 2106–2125.

Chen, J., Xu, Y., Fei, K., Wang, R., He, J., Fu, L., Shao, S., Li, K., Zhu, K., Zhang, W., Wang, Z., and Yang, J. (2020b). Physiological mechanism underlying the effect of high temperature during anthesis on spikelet-opening of photo-thermo-sensitive genic male sterile rice lines. Sci. Rep. **10**: 2210.

Cheng, P.C., Greyson, R.I., and Walden, D.B. (1983). Organ Initiation and the Development of Unisexual Flowers in the Tassel and Ear of Zea Mays. Am. J. Bot. **70**: 450–462.

Cheung, A.Y., Duan, Q., Costa, S.S., de Graaf, B.H.J., Di Stilio, V.S., Feijo, J., and Wu, H.-M. (2008). The Dynamic Pollen Tube Cytoskeleton: Live Cell Studies Using Actin-Binding and Microtubule-Binding Reporter Proteins. Mol. Plant **1**: 686–702.

Cheung, A.Y. and Wu, H.-M. (2008). Structural and signaling networks for the polar cell growth machinery in pollen tubes. Annu. Rev. Plant Biol. **59**: 547–572.

Cigan, A.M., Unger, E., Xu, R. -j., Kendall, T., and Fox, T.W. (2001). Phenotypic complementation of ms45 maize requires tapetal expression of MS45. Sex. Plant Reprod. **14**: 135–142.

Clark, F.J. (1940). Cytogenetic Studies of Divergent Meiotic Spindle Formation in Zea Mays. Am. J. Bot. **27**: 547–559.

Crawley, O., Barroso, C., Testori, S., Ferrandiz, N., Silva, N., Castellano-Pozo, M., Jaso-Tamame, A.L., and Martinez-Perez, E. (2016). Cohesin-interacting protein WAPL-1 regulates meiotic chromosome structure and cohesion by antagonizing specific cohesin complexes. eLife **5**: e10851.

De Storme, N. and Geelen, D. (2013). Cytokinesis in plant male meiosis. Plant Signal. Behav. **8**: e23394.

De Storme, N. and Geelen, D. (2014). The impact of environmental stress on male reproductive development in plants: biological processes and molecular mechanisms. Plant Cell Environ. **37**: 1–18.

Dhonukshe, P., Laxalt, A.M., Goedhart, J., Gadella, T.W.J., and Munnik, T. (2003). Phospholipase D Activation Correlates with Microtubule Reorganization in Living Plant Cells[W]. Plant Cell **15**: 2666–2679.

Dobin, A., Davis, C.A., Schlesinger, F., Drenkow, J., Zaleski, C., Jha, S., Batut, P., Chaisson, M., and Gingeras, T.R. (2013). STAR: ultrafast universal RNA-seq aligner. Bioinforma. Oxf. Engl. **29**: 15–21.

Draeger, T. and Moore, G. (2017). Short periods of high temperature during meiosis prevent normal meiotic progression and reduce grain number in hexaploid wheat (Triticum aestivum L.). Theor. Appl. Genet. **130**: 1785–1800.

Du, Z., Zhou, X., Ling, Y., Zhang, Z., and Su, Z. (2010). agriGO: a GO analysis toolkit for the agricultural community. Nucleic Acids Res. **38**: W64–W70.

Dukowic-Schulze, S., Harris, A., Li, J., Sundararajan, A., Mudge, J., Retzel, E.F., Pawlowski, W.P., and Chen, C. (2014). Comparative Transcriptomics of Early Meiosis in Arabidopsis and Maize. J. Genet. Genomics **41**: 139–152.

Dupuis, I., Roeckel, P., Matthys-Rochon, E., and Dumas, C. (1987). Procedure to Isolate Viable Sperm Cells from Corn (*Zea mays* L.) Pollen Grains. Plant Physiol. **85**: 876–878.

Eliasson, Å., Gass, N., Mundel, C., Baltz, R., Kräuter, R., Evrard, J.-L., and Steinmetz, A. (2000). Molecular and expression analysis of a LIM protein gene family from flowering plants. Mol. Genet. Genomics **264**: 257–267.

Firon, N., Shaked, R., Peet, M.M., Pharr, D.M., Zamski, E., Rosenfeld, K., Althan, L., and Pressman, E. (2006). Pollen grains of heat tolerant tomato cultivars retain higher carbohydrate concentration under heat stress conditions. Sci. Hortic. **109**: 212–217.

Folsom, J.J., Begcy, K., Hao, X., Wang, D., and Walia, H. (2014). Rice fertilization-Independent Endosperm1 regulates seed size under heat stress by controlling early endosperm development. Plant Physiol **165**: 238–248.

Fragkostefanakis, S., Röth, S., Schleiff, E., and Scharf, K.-D. (2015). Prospects of engineering thermotolerance in crops through modulation of heat stress transcription factor and heat shock protein networks. Plant Cell Environ. **38**: 1881–1895.

Francis, K.E., Lam, S.Y., Harrison, B.D., Bey, A.L., Berchowitz, L.E., and Copenhaver, G.P. (2007). Pollen tetrad-based visual assay for meiotic recombination in Arabidopsis. Proc. Natl. Acad. Sci. U. S. A. **104**: 3913–3918.

Franke, W.W., Herth, W., VanDerWoude, W.J., and Morré, D.J. (1972). Tubular and filamentous structures in pollen tubes: Possible involvement as guide elements in protoplasmic streaming and vectorial migration of secretory vesicles. Planta **105**: 317–341.

Freyd, G., Kim, S.K., and Horvitz, H.R. (1990). Novel cysteine-rich motif and homeodomain in the product of the Caenorhabditis elegans cell lineage gene lin-11. Nature **344**: 876–879.

Goto, H., Okuda, S., Mizukami, A., Mori, H., Sasaki, N., Kurihara, D., and Higashiyama, T. (2011). Chemical Visualization of an Attractant Peptide, LURE. Plant Cell Physiol. **52**: 49–58.

Gourdji, S.M., Sibley, A.M., and Lobell, D.B. (2013). Global crop exposure to critical high temperatures in the reproductive period: historical trends and future projections. Environ. Res. Lett. **8**: 024041.

Han, L.-B., Li, Y.-B., Wang, H.-Y., Wu, X.-M., Li, C.-L., Luo, M., Wu, S.-J., Kong, Z.-S., Pei, Y., Jiao, G.-L., and Xia, G.-X. (2013). The Dual Functions of WLIM1a in Cell Elongation and Secondary Wall Formation in Developing Cotton Fibers. Plant Cell **25**: 4421–4438.

Han, Y., Hu, M., Ma, X., Yan, G., Wang, C., Jiang, S., Lai, J., and Zhang, M. (2022). Exploring key developmental phases and phase-specific genes across the entirety of anther development in maize. J. Integr. Plant Biol. **64**: 1394–1410.

Higgins, D.M., Nannas, N.J., and Dawe, R.K. (2016). The Maize Divergent spindle-1 (dv1) Gene Encodes a Kinesin-14A Motor Protein Required for Meiotic Spindle Pole Organization. Front. Plant Sci. **7**.

Holzinger, A., Phillips, K.S., and Weaver, T.E. (1996). Single-Step Purification/Solubilization of Recombinant Proteins: Application to Surfactant Protein B. BioTechniques **20**: 804–808.

van der Honing, H.S., Kieft, H., Emons, A.M.C., and Ketelaar, T. (2012). Arabidopsis VILLIN2 and VILLIN3 Are Required for the Generation of Thick Actin Filament Bundles and for Directional Organ Growth. Plant Physiol. **158**: 1426–1438.

Honys, D. and Twell, D. (2004). Transcriptome analysis of haploid male gametophyte development in Arabidopsis. Genome Biol. **5**: R85.

Horvitz, H.R. and Herskowitz, I. (1992). Mechanisms of asymmetric cell division: two Bs or not two Bs, that is the question. Cell **68**: 237–255.

Hufford, M.B. et al. (2021). De novo assembly, annotation, and comparative analysis of 26 diverse maize genomes. Science **373**: 655–662.

Ishiguro, S., Kawai-Oda, A., Ueda, J., Nishida, I., and Okada, K. (2001). The DEFECTIVE IN ANTHER DEHISCIENCE gene encodes a novel phospholipase A1 catalyzing the initial step of jasmonic acid biosynthesis, which synchronizes pollen maturation, anther dehiscence, and flower opening in Arabidopsis. Plant Cell **13**: 2191–2209.

Ishimaru, T., Hirabayashi, H., Ida, M., Takai, T., San-Oh, Y.A., Yoshinaga, S., Ando, I., Ogawa, T., and Kondo, M. (2010). A genetic resource for early-morning flowering trait of

wild rice Oryza officinalis to mitigate high temperature-induced spikelet sterility at anthesis. Ann. Bot. **106**: 515–520.

Jagadish, S., Craufurd, P., and Wheeler, T. (2007). High temperature stress and spikelet fertility in rice (Oryza sativa L.). J. Exp. Bot. **58**: 1627–1635.

Jagadish, S.V.K. (2020). Heat stress during flowering in cereals – effects and adaptation strategies. New Phytol. **226**: 1567–1572.

Jiang, J., Liu, X., Liu, C., Liu, G., Li, S., and Wang, L. (2017). Integrating Omics and Alternative Splicing Reveals Insights into Grape Response to High Temperature. Plant Physiol. **173**: 1502–1518.

Jiang, Y. et al. (2021). CRISPR/Cas9-based discovery of maize transcription factors regulating male sterility and their functional conservation in plants. Plant Biotechnol. J. **19**: 1769–1784.

Jiao, Y. et al. (2017). Improved maize reference genome with single-molecule technologies. Nature **546**: 524–527.

Juranić, M., Srilunchang, K., Krohn, N.G., Leljak-Levanić, D., Sprunck, S., and Dresselhaus, T. (2012). Germline-Specific MATH-BTB Substrate Adaptor MAB1 Regulates Spindle Length and Nuclei Identity in Maize. Plant Cell **24**: 4974–4991.

Juranić, M., Srilunchang, K., Krohn, N.G., Leljak-Levanić, D., Sprunck, S., and Dresselhaus, T. (2013). Germline-Specific MATH-BTB Substrate Adaptor MAB1 Regulates Spindle Length and Nuclei Identity in Maize. Plant Cell **24**: 4974–4991.

Kadrmas, J.L. and Beckerle, M.C. (2004). The LIM domain: from the cytoskeleton to the nucleus. Nat. Rev. Mol. Cell Biol. **5**: 920–931.

Karlsson, O., Thor, S., Norberg, T., Ohlsson, H., and Edlund, T. (1990). Insulin gene enhancer binding protein Isl-1 is a member of a novel class of proteins containing both a homeo- and a Cys-His domain. Nature **344**: 879–882.

Kawaoka, A., Kaothien, P., Yoshida, K., Endo, S., Yamada, K., and Ebinuma, H. (2000). Functional analysis of tobacco LIM protein Ntlim1 involved in lignin biosynthesis. Plant J. **22**: 289–301.

Keller, M. et al. (2018). The coupling of transcriptome and proteome adaptation during development and heat stress response of tomato pollen. BMC Genomics **19**: 447.

Keller, M., Hu, Y., Mesihovic, A., Fragkostefanakis, S., Schleiff, E., and Simm, S. (2017). Alternative splicing in tomato pollen in response to heat stress. DNA Res. Int. J. Rapid Publ. Rep. Genes Genomes **24**: 205–217.

Kelliher, T. and Walbot, V. (2012). Hypoxia triggers meiotic fate acquisition in maize. Science **337**: 345–348.

Kerim, T., Imin, N., Weinman, J.J., and Rolfe, B.G. (2003). Proteome analysis of male gametophyte development in rice anthers. Proteomics **3**: 738–751.

Khurana, T., Khurana, B., and Noegel, A.A. (2002). LIM proteins: association with the actin cytoskeleton. Protoplasma **219**: 1–12.

Kim, H.J., Oh, S.A., Brownfield, L., Hong, S.H., Ryu, H., Hwang, I., Twell, D., and Nam, H.G. (2008). Control of plant germline proliferation by SCFFBL17 degradation of cell cycle inhibitors. Nature **455**: 1134–1137.

Kim, T., Samraj, S., Jiménez, J., Gómez, C., Liu, T., and Begcy, K. (2021). Genome-wide identification of heat shock factors and heat shock proteins in response to UV and high intensity light stress in lettuce. BMC Plant Biol. **21**: 185.

Kliwer, I. and Dresselhaus, T. (2010). Establishment of the male germline and sperm cell movement during pollen germination and tube growth in maize. Plant Signal. Behav. **5**: 885–889.

Kliwer, I., Jackson, D., and Dresselhaus, T. (2009). α-Tubulin-YFP labeled sperm cells for live cell imaging of the fertilization process in maize and relatives such as Tripsacum dactyloides. Maize Genet. Coop. Newsl. **83**: 40–41.

Krohn, N.G., Lausser, A., Juranić, M., and Dresselhaus, T. (2012). Egg Cell Signaling by the Secreted Peptide ZmEAL1 Controls Antipodal Cell Fate. Dev. Cell **23**: 219–225.

Ladner, C.L., Yang, J., Turner, R.J., and Edwards, R.A. (2004). Visible fluorescent detection of proteins in polyacrylamide gels without staining. Anal. Biochem. **326**: 13–20.

Laemmli, U.K. (1970). Cleavage of structural proteins during the assembly of the head of bacteriophage T4. Nature **227**: 680–685.

Lancelle, S.A., Cresti, M., and Hepler, P.K. (1987). Ultrastructure of the cytoskeleton in freeze-substituted pollen tubes ofNicotiana alata. Protoplasma **140**: 141–150.

Langfelder, P. and Horvath, S. (2008). WGCNA: an R package for weighted correlation network analysis. BMC Bioinformatics **9**: 559.

Langmead, B. and Salzberg, S.L. (2012). Fast gapped-read alignment with Bowtie 2. Nat. Methods **9**: 357–359.

Lee, S.S., Jung, W.Y., Park, H.J., Lee, A., Kwon, S.-Y., Kim, H.-S., and Cho, H.S. (2017). Genome-wide Analysis of Alternative Splicing in An Inbred Cabbage (Brassica oleracea L.) Line 'HO' in Response to Heat Stress. Curr. Genomics **19**.

Lei, X., Ning, Y., Eid Elesawi, I., Yang, K., Chen, C., Wang, C., and Liu, B. (2020). Heat stress interferes with chromosome segregation and cytokinesis during male meiosis in *Arabidopsis thaliana*. Plant Signal. Behav. **15**: 1746985.

Lermontova, I., Koroleva, O., Rutten, T., Fuchs, J., Schubert, V., Moraes, I., Koszegi, D., and Schubert, I. (2011). Knockdown of CENH3 in Arabidopsis reduces mitotic divisions and causes sterility by disturbed meiotic chromosome segregation. Plant J. **68**: 40–50.

Li, L. and Arumuganathan, K. (2001). Physical Mapping of 45S and 5S rDNA on Maize Metaphase and Sorted Chromosomes by FISH. Hereditas **134**: 141–145.

Li, L., Hou, S., Xiang, W., Song, Z., Wang, Y., Zhang, L., Li, J., Gu, H., Dong, J., Dresselhaus, T., Zhong, S., and Qu, L.-J. (2022a). The egg cell is preferentially fertilized in Arabidopsis double fertilization. J. Integr. Plant Biol. **64**: 2039–2046.

Li, L., Li, Y., Wang, N.-N., Li, Y., Lu, R., and Li, X.-B. (2015). Cotton LIM domain-containing protein GhPLIM1 is specifically expressed in anthers and participates in modulating F-actin. Plant Biol. **17**: 528–534.

Li, Y., Jiang, J., Li, L., Wang, X.-L., Wang, N.-N., Li, D.-D., and Li, X.-B. (2013). A cotton LIM domain-containing protein (GhWLIM5) is involved in bundling actin filaments. Plant Physiol. Biochem. **66**: 34–40.

Li, Y., Liu, X., Xiao, Y., Wen, Y., Li, K., Ma, Z., Yang, L., Zhu, Y., and Yin, J. (2022b). Genome-wide characterization and function analysis uncovered roles of wheat LIMs in responding to adverse stresses and TaLIM8-4D function as a susceptible gene. Plant Genome **15**: e20246.

Li, Y., Yue, X., Que, Y., Yan, X., Ma, Z., Talbot, N.J., and Wang, Z. (2014). Characterisation of Four LIM Protein-Encoding Genes Involved in Infection-Related Development and Pathogenicity by the Rice Blast Fungus Magnaporthe oryzae. PLOS ONE **9**: e88246.

Li, Y., Zheng, L., Corke, F., Smith, C., and Bevan, M.W. (2008). Control of final seed and organ size by the DA1 gene family in Arabidopsis thaliana. Genes Dev. **22**: 1331–1336.

Liao, Y., Smyth, G.K., and Shi, W. (2014). featureCounts: an efficient general purpose program for assigning sequence reads to genomic features. Bioinforma. Oxf. Engl. **30**: 923–930.

Lin, G. et al. (2021). Chromosome-level genome assembly of a regenerable maize inbred line A188. Genome Biol. **22**: 175.

van der Linde, K., Timofejeva, L., Egger, R.L., Ilau, B., Hammond, R., Teng, C., Meyers, B.C., Doehlemann, G., and Walbot, V. (2018). Pathogen Trojan Horse Delivers Bioactive Host Protein to Alter Maize Anther Cell Behavior in Situ. Plant Cell **30**: 528–542.

van der Linde, K. and Walbot, V. (2019). Chapter Ten - Pre-meiotic anther development. In Current Topics in Developmental Biology, U. Grossniklaus, ed, Plant Development and Evolution. (Academic Press), pp. 239–256.

Liu, M., Zhou, Y., Sun, J., Mao, F., Yao, Q., Li, B., Wang, Y., Gao, Y., Dong, X., Liao, S., Wang, P., and Huang, S. (2023). From the floret to the canopy: High temperature tolerance during flowering. Plant Commun.: 100629.

Liu, X., Yue, Y., Gu, Z., Huang, Q., Pan, Z., Zhao, Z., Zheng, M., Zhang, Z., Li, C., Yi, H., Yu, T., and Cao, M. (2021). The characterization and candidate gene isolation for a novel male-sterile mutant ms40 in maize. Plant Cell Rep. **40**: 1957–1970.

Lobell, D.B., Bänziger, M., Magorokosho, C., and Vivek, B. (2011). Nonlinear heat effects on African maize as evidenced by historical yield trials. Nat. Clim. Change **1**: 42–45.

Loukides, C.A., Broadwater, A.H., and Bedinger, P.A. (1995). Two new male-sterile mutants of Zea mays (Poaceae) with abnormal tapetal cell morphology. Am. J. Bot. **82**: 1017–1023.

Love, M.I., Huber, W., and Anders, S. (2014). Moderated estimation of fold change and dispersion for RNA-seq data with DESeq2. Genome Biol. **15**: 550.

Lovy-Wheeler, A., Wilsen, K.L., Baskin, T.I., and Hepler, P.K. (2005). Enhanced fixation reveals the apical cortical fringe of actin filaments as a consistent feature of the pollen tube. Planta **221**: 95–104.

Martin, F.W. (1959). Staining and Observing Pollen Tubes in the Style by Means of Fluorescence. Stain Technol. **34**: 125–128.

Márton, M.L., Cordts, S., Broadhvest, J., and Dresselhaus, T. (2005). Micropylar Pollen Tube Guidance by Egg Apparatus 1 of Maize. Science **307**: 573–576.

McClintock, B. (1934). The relation of a particular chromosomal element to the development of the nucleoli in Zea mays. Z. Für Zellforsch. Mikrosk. Anat. **21**: 294–326.

McCormick, S. (1993). Male Gametophyte Development. Plant Cell **5**: 1265–1275.

Mittler, R. (2017). ROS Are Good. Trends Plant Sci. **22**: 11–19.

Moes, D., Gatti, S., Hoffmann, C., Dieterle, M., Moreau, F., Neumann, K., Schumacher, M., Diederich, M., Grill, E., Shen, W.-H., Steinmetz, A., and Thomas, C. (2013). A LIM Domain Protein from Tobacco Involved in Actin-Bundling and Histone Gene Transcription. Mol. Plant **6**: 483–502.

Moes, D., Hoffmann, C., Dieterle, M., Moreau, F., Neumann, K., Papuga, J., Furtado, A.T., Steinmetz, A., and Thomas, C. (2015). The pH sensibility of actin-bundling LIM proteins is governed by the acidic properties of their C-terminal domain. FEBS Lett. **589**: 2312–2319.

Moon, J., Skibbe, D., Timofejeva, L., Wang, C.-J.R., Kelliher, T., Kremling, K., Walbot, V., and Cande, W.Z. (2013). Regulation of cell divisions and differentiation by MALE STERILITY32 is required for anther development in maize. Plant J. **76**: 592–602.

Müller, F. and Rieu, I. (2016). Acclimation to high temperature during pollen development. Plant Reprod. **29**: 107–118.

Murata, T., Sonobe, S., Baskin, T.I., Hyodo, S., Hasezawa, S., Nagata, T., Horio, T., and Hasebe, M. (2005). Microtubule-dependent microtubule nucleation based on recruitment of γ-tubulin in higher plants. Nat. Cell Biol. **7**: 961–968.

Na, J.-K., Huh, S.-M., Yoon, I.-S., Byun, M.-O., Lee, Y.-H., Lee, K.-O., and Kim, D.-Y. (2014). Rice LIM protein OsPLIM2a is involved in rice seed and tiller development. Mol. Breed. **34**: 569–581.

Nan, G.-L., Teng, C., Fernandes, J., O'Connor, L., Meyers, B.C., and Walbot, V. (2022). A cascade of bHLH-regulated pathways programs maize anther development. Plant Cell **34**: 1207–1225.

Nan, G.-L., Zhai, J., Arikit, S., Morrow, D., Fernandes, J., Mai, L., Nguyen, N., Meyers, B.C., and Walbot, V. (2017). MS23, a master basic helix-loop-helix factor, regulates the specification and development of the tapetum in maize. Dev. Camb. Engl. **144**: 163–172.

Nelms, B. and Walbot, V. (2019). Defining the developmental program leading to meiosis in maize. Science **364**: 52–56.

Németh, A. and Längst, G. (2011). Genome organization in and around the nucleolus. Trends Genet. **27**: 149–156.

Nian, L., Liu, X., Yang, Y., Zhu, X., Yi, X., and Haider, F.U. (2021). Genome-wide identification, phylogenetic, and expression analysis under abiotic stress conditions of LIM gene family in Medicago sativa L. PLOS ONE **16**: e0252213.

Oliveros, J.C., Franch, M., Tabas-Madrid, D., San-León, D., Montoliu, L., Cubas, P., and Pazos, F. (2016). Breaking-Cas—interactive design of guide RNAs for CRISPR-Cas experiments for ENSEMBL genomes. Nucleic Acids Res. **44**: W267–W271.

Palevitz, B.A. and Cresti, M. (1988). Microtubule organization in the sperm of Tradescantia virginiana. Protoplasma.

Papuga, J., Hoffmann, C., Dieterle, M., Moes, D., Moreau, F., Tholl, S., Steinmetz, A., and Thomas, C. (2010). Arabidopsis LIM Proteins: A Family of Actin Bundlers with Distinct Expression Patterns and Modes of Regulation. Plant Cell **22**: 3034–3052.

Parish, R.W. and Li, S.F. (2010). Death of a tapetum: A programme of developmental altruism. Plant Sci. **178**: 73–89.

Parrotta, L., Faleri, C., Cresti, M., and Cai, G. (2016). Heat stress affects the cytoskeleton and the delivery of sucrose synthase in tobacco pollen tubes. Planta **243**: 43–63.

Pastuglia, M., Azimzadeh, J., Goussot, M., Camilleri, C., Belcram, K., Evrard, J.-L., Schmit, A.-C., Guerche, P., and Bouchez, D. (2006). γ-Tubulin Is Essential for Microtubule Organization and Development in Arabidopsis. Plant Cell **18**: 1412–1425.

Paupière, M.J., Van Heusden, A.W., and Bovy, A.G. (2014). The Metabolic Basis of Pollen Thermo-Tolerance: Perspectives for Breeding. Metabolites **4**: 889–920.

Pawlowski, W.P., Wang, C.-J.R., Golubovskaya, I.N., Szymaniak, J.M., Shi, L., Hamant, O., Zhu, T., Harper, L., Sheridan, W.F., and Cande, W.Z. (2009). Maize AMEIOTIC1 is essential for multiple early meiotic processes and likely required for the initiation of meiosis. Proc. Natl. Acad. Sci. **106**: 3603–3608.

Peng, S., Huang, J., Sheehy, J.E., Laza, R.C., Visperas, R.M., Zhong, X., Centeno, G.S., Khush, G.S., and Cassman, K.G. (2004). Rice yields decline with higher night temperature from global warming. Proc. Natl. Acad. Sci. **101**: 9971–9975.

Peng, Y., Chen, L., Lu, Y., Wu, Y., Dumenil, J., Zhu, Z., Bevan, M.W., and Li, Y. (2015). The Ubiquitin Receptors DA1, DAR1, and DAR2 Redundantly Regulate Endoreduplication by Modulating the Stability of TCP14/15 in Arabidopsis. Plant Cell **27**: 649–662.

Pfab, A., Antosz, W., Holzinger, P., Bruckmann, A., Griesenbeck, J., and Grasser, K.D. (2017). Analysis of In Vivo Chromatin and Protein Interactions of Arabidopsis Transcript Elongation Factors. In Plant Gene Regulatory Networks: Methods and Protocols, K. Kaufmann and B. Mueller-Roeber, eds, Methods in Molecular Biology. (Springer: New York, NY), pp. 105–122.

Phan, H.A., Iacuone, S., Li, S.F., and Parish, R.W. (2011). The MYB80 Transcription Factor Is Required for Pollen Development and the Regulation of Tapetal Programmed Cell Death in Arabidopsis thaliana. Plant Cell **23**: 2209–2224.

Preciado, J., Begcy, K., and Liu, T. (2022). The Arabidopsis HDZIP class II transcription factor *ABA INSENSITIVE TO GROWTH 1* functions in leaf development. J. Exp. Bot. **73**: 1978–1991.

Rahmati Ishka, M., Brown, E., Weigand, C., Tillett, R.L., Schlauch, K.A., Miller, G., and Harper, J.F. (2018). A comparison of heat-stress transcriptome changes between wild-type Arabidopsis pollen and a heat-sensitive mutant harboring a knockout of cyclic nucleotide-gated cation channel 16 (cngc16). BMC Genomics **19**: 549.

Ramírez, F., Ryan, D.P., Grüning, B., Bhardwaj, V., Kilpert, F., Richter, A.S., Heyne, S., Dündar, F., and Manke, T. (2016). deepTools2: a next generation web server for deep-sequencing data analysis. Nucleic Acids Res. **44**: W160–W165.

Ren, H. and Xiang, Y. (2007). The function of actin-binding proteins in pollen tube growth. Protoplasma **230**: 171–182.

Resurreccion, A.P., Hara, T., Juliano, B.O., and Yoshida, S. (1977). Effect of temperature during ripening on grain quality of rice. Soil Sci. Plant Nutr. **23**: 109–112.

Ritossa, F.M. and Spiegelman, S. (1965). Localization of dna complementary to ribosomal rna in the nucleolus organizer region of drosophila melanogaster*. Proc. Natl. Acad. Sci. **53**: 737–745.

Rotman, N., Durbarry, A., Wardle, A., Yang, W.C., Chaboud, A., Faure, J.-E., Berger, F., and Twell, D. (2005). A Novel Class of MYB Factors Controls Sperm-Cell Formation in Plants. Curr. Biol. **15**: 244–248.

Rudolph, R. and Lilie, H. (1996). In vitro folding of inclusion body proteins. FASEB J. **10**: 49–56.

Saini, H., Sedgley, M., and Aspinall, D. (1984). Development Anatomy in Wheat of Male Sterility Induced by Heat Stress, Water Deficit or Abscisic Acid. Funct. Plant Biol. **11**: 243.

Sakai, H., Cheng, W., Chen, C.P., and Hasegawa, T. (2022). Short-term high nighttime temperatures pose an emerging risk to rice grain failure. Agric. For. Meteorol. **314**: 108779.

Sakata, T., Takahashi, H., Nishiyama, I., and Higashitani, A. (2000). Effects of High Temperature on the Development of Pollen Mother Cells and Microspores in Barley Hordeum vulgare L. J. Plant Res. **113**: 395–402.

Schmid, M.W., Schmidt, A., and Grossniklaus, U. (2015). The female gametophyte: an emerging model for cell type-specific systems biology in plant development. Front. Plant Sci. **6**.

Schnable, P.S. et al. (2009). The B73 Maize Genome: Complexity, Diversity, and Dynamics. Science **326**: 1112–1115.

Scott, R.J., Spielman, M., and Dickinson, H.G. (2004). Stamen structure and function. Plant Cell **16 Suppl**: S46-60.

Sheridan, W.F., Avalkina, N.A., Shamrov, I.I., Batygina, T.B., and Golubovskaya, I.N. (1996). The Mac1 Gene: Controlling the Commitment to the Meiotic Pathway in Maize. Genetics **142**: 1009–1020.

Sheridan, W.F., Golubeva, E.A., Abrhamova, L.I., and Golubovskaya, I.N. (1999). The mac1 Mutation Alters the Developmental Fate of the Hypodermal Cells and Their Cellular Progeny in the Maize Anther. Genetics **153**: 933–941.

Simmonds, D.H. (1994). Mechanism of Induction of Microspore Embryogenesis in Brassica napus: Significance of the Preprophase Band of Microtubules in the First Sporophytic Division. In Biomechanics of Active Movement and Division of Cells, N. Akkaş, ed, NATO ASI Series. (Springer: Berlin, Heidelberg), pp. 569–574.

Smertenko, A., Dráber, P., Viklický, V., and Opatrný, Z. (1997). Heat stress affects the organization of microtubules and cell division in Nicotiana tabacum cells. Plant Cell Environ. **20**: 1534–1542.

Song, L., Liu, Z., Tong, J., Xiao, L., Ma, H., and Zhang, H. (2015). Comparative proteomics analysis reveals the mechanism of fertility alternation of thermosensitive genic male sterile rice lines under low temperature inducement. Proteomics **15**: 1884–1905.

Sprunck, S. and Groß-Hardt, R. (2011). Nuclear behavior, cell polarity, and cell specification in the female gametophyte. Sex. Plant Reprod. **24**: 123–136.

Srivastava, V. and Verma, P.K. (2017). The plant LIM proteins: unlocking the hidden attractions. Planta **246**: 365–375.

Staiger, C.J. and Cande, W.Z. (1992). Ameiotic, a gene that controls meiotic chromosome and cytoskeletal behavior in maize. Dev. Biol. **154**: 226–230.

Staiger, C.J. and Cande, W.Z. (1990). Microtubule distribution in dv, a maize meiotic mutant defective in the prophase to metaphase transition. Dev. Biol. **138**: 231–242.

Subramanian, B., Gao, S., Lercher, M.J., Hu, S., and Chen, W.-H. (2019). Evolview v3: a webserver for visualization, annotation, and management of phylogenetic trees. Nucleic Acids Res. **47**: W270–W275.

Sun, Y., Wang, X., Pan, L., Xie, F., Dai, B., Sun, M., and Peng, X. (2021). Plant egg cell fate determination depends on its exact position in female gametophyte. Proc. Natl. Acad. Sci. **118**: e2017488118.

Szklarczyk, D. et al. (2015). STRING v10: protein–protein interaction networks, integrated over the tree of life. Nucleic Acids Res. **43**: D447–D452.

Tamura, K., Stecher, G., and Kumar, S. (2021). MEGA11: Molecular Evolutionary Genetics Analysis Version 11. Mol. Biol. Evol. **38**: 3022–3027.

Tanaka, I. (1988). Isolation of generative cells and their protoplasts from pollen ofLilium longiflorum. Protoplasma **142**: 68–73.

Theunis, C.H., Pierson, E.S., and Cresti, M. (1992). The microtubule cytoskeleton and the rounding of isolated generative cells of Nicotiana tabacum. Sex. Plant Reprod. Ger.

Theunis, C.H. and Van Went, J.L. (1989). Isolation of sperm cells from mature pollen grains of Spinacia oleracea L. Sex. Plant Reprod. **2**: 97–102.

Thomas, C., Hoffmann, C., Dieterle, M., Van Troys, M., Ampe, C., and Steinmetz, A. (2006). Tobacco WLIM1 Is a Novel F-Actin Binding Protein Involved in Actin Cytoskeleton Remodeling. Plant Cell **18**: 2194–2206.

Twell, D. (2011). Male gametogenesis and germline specification in flowering plants. Sex. Plant Reprod. **24**: 149–160.

Twell, D., Park, S.K., Hawkins, T.J., Schubert, D., Schmidt, R., Smertenko, A., and Hussey, P.J. (2002). MOR1/GEM1 has an essential role in the plant-specific cytokinetic phragmoplast. Nat. Cell Biol. **4**: 711–714.

Twell, D., Yamaguchi, J., and McCormick, S. (1990). Pollen-specific gene expression in transgenic plants: coordinate regulation of two different tomato gene promoters during microsporogenesis. Dev. Camb. Engl. **109**: 705–713.

Ullah, A., Nadeem, F., Nawaz, A., Siddique, K.H.M., and Farooq, M. (2022). Heat stress effects on the reproductive physiology and yield of wheat. J. Agron. Crop Sci. **208**: 1–17.

Velyvis, A. and Qin, J. (2000). LIM Domain and Its Binding to Target Proteins. In Madame Curie Bioscience Database [Internet].

Villajuana-Bonequi, M., Matei, A., Ernst, C., Hallab, A., Usadel, B., and Doehlemann, G. (2019). Cell type specific transcriptional reprogramming of maize leaves during Ustilago maydis induced tumor formation. Sci. Rep. **9**: 10227.

Wada, H., Hatakeyama, Y., Nakashima, T., Nonami, H., Erra-Balsells, R., Hakata, M., Nakata, K., Hiraoka, K., Onda, Y., and Nakano, H. (2020). On-site single pollen metabolomics reveals varietal differences in phosphatidylinositol synthesis under heat stress conditions in rice. Sci. Rep. **10**: 2013.

Walbot, V. and Egger, R.L. (2016). Pre-Meiotic Anther Development: Cell Fate Specification and Differentiation. Annu. Rev. Plant Biol. **67**: 365–395.

Wang, H.-J., Wan, A.-R., and Jauh, G.-Y. (2008). An Actin-Binding Protein, LlLIM1, Mediates Calcium and Hydrogen Regulation of Actin Dynamics in Pollen Tubes. Plant Physiol. **147**: 1619–1636.

Wang, J., Li, D., Shang, F., and Kang, X. (2017). High temperature-induced production of unreduced pollen and its cytological effects in Populus. Sci. Rep. **7**: 5281.

Wang, Y., Liu, X., Hou, X., Sheng, D., Dong, X., Gao, Y., Wang, P., and Huang, S. (2021). Maximum lethal temperature for flowering and seed set in maize with contrasting male and female flower sensitivities. J. Agron. Crop Sci. **207**: 679–689.

Wang, Y., Tao, H., Zhang, P., Hou, X., Sheng, D., Tian, B., Wang, P., and Huang, S. (2020). Reduction in seed set upon exposure to high night temperature during flowering in maize. Physiol. Plant. **169**: 73–82.

Warman, C., Panda, K., Vejlupkova, Z., Hokin, S., Unger-Wallace, E., Cole, R.A., Chettoor, A.M., Jiang, D., Vollbrecht, E., Evans, M.M.S., Slotkin, R.K., and Fowler, J.E. (2020). High expression in maize pollen correlates with genetic contributions to pollen fitness as well as with coordinated transcription from neighboring transposable elements. PLOS Genet. **16**: e1008462.

Way, J.C. and Chalfie, M. (1988). mec-3, a homeobox-containing gene that specifies differentiation of the touch receptor neurons in C. elegans. Cell **54**: 5–16.

Wei, L.Q., Xu, W.Y., Deng, Z.Y., Su, Z., Xue, Y., and Wang, T. (2010). Genome-scale analysis and comparison of gene expression profiles in developing and germinated pollen in Oryza sativa. BMC Genomics **11**: 338.

Weiskirchen, R. and Günther, K. (2003). The CRP/MLP/TLP family of LIM domain proteins: Acting by connecting. BioEssays **25**: 152–162.

Whipple, C.J., Ciceri, P., Padilla, C.M., Ambrose, B.A., Bandong, S.L., and Schmidt, R.J. (2004). Conservation of B-class floral homeotic gene function between maize and *Arabidopsis*. Development **131**: 6083–6091.

Williams, J.H. and Reese, J.B. (2019). Evolution of development of pollen performance. In Current Topics in Developmental Biology (Elsevier), pp. 299–336.

Wingfield, P.T. (1995). Preparation of Soluble Proteins from Escherichia coli. Curr. Protoc. Protein Sci. **00**: 6.2.1-6.2.15.

Wu, M.-F. and Wagner, D. (2012). RNA In Situ Hybridization in Arabidopsis. In RNA Abundance Analysis: Methods and Protocols, H. Jin and W. Gassmann, eds, Methods in Molecular Biology. (Humana Press: Totowa, NJ), pp. 75–86.

Yang, R., Chen, M., Sun, J.-C., Yu, Y., Min, D.-H., Chen, J., Xu, Z.-S., Zhou, Y.-B., Ma, Y.-Z., and Zhang, X.-H. (2019). Genome-Wide Analysis of LIM Family Genes in Foxtail Millet (Setaria italica L.) and Characterization of the Role of SiWLIM2b in Drought Tolerance. Int. J. Mol. Sci. **20**: 1303.

Yang, R.S., Xu, F., Wang, Y.M., Zhong, W.S., Dong, L., Shi, Y.N., Tang, T.J., Sheng, H.J., Jackson, D., and Yang, F. (2021). Glutaredoxins regulate maize inflorescence meristem development via redox control of TGA transcriptional activity. Nat. Plants **7**: 1589–1601.

Yang, X., Bu, Y., Niu, F., Cun, Y., Zhang, L., and Song, X. (2022). Comprehensive analysis of LIM gene family in wheat reveals the involvement of TaLIM2 in pollen development. Plant Sci. Int. J. Exp. Plant Biol. **314**: 111101.

Ye, J. and Xu, M. (2012). Actin bundler PLIM2s are involved in the regulation of pollen development and tube growth in Arabidopsis. J. Plant Physiol. **169**: 516–522.

Ye, J.R., Zhou, L.M., and Xu, M.L. (2013). Arabidopsis LIM proteins PLIM2a and PLIM2b regulate actin configuration during pollen tube growth. Biol. Plant. **57**: 433–441.

Yilmaz, A., Nishiyama, M.Y., Jr., Fuentes, B.G., Souza, G.M., Janies, D., Gray, J., and Grotewold, E. (2009). GRASSIUS: A Platform for Comparative Regulatory Genomics across the Grasses. Plant Physiol. **149**: 171–180.

Yoshida, T. et al. (2011). Arabidopsis HsfA1 transcription factors function as the main positive regulators in heat shock-responsive gene expression. Mol. Genet. Genomics MGG **286**: 321–332.

Yu, G., Wang, L.-G., and He, Q.-Y. (2015). ChIPseeker: an R/Bioconductor package for ChIP peak annotation, comparison and visualization. Bioinformatics **31**: 2382–2383.

Yuan, T.-L., Huang, W.-J., He, J., Zhang, D., and Tang, W.-H. (2018). Stage-Specific Gene Profiling of Germinal Cells Helps Delineate the Mitosis/Meiosis Transition. Plant Physiol. **176**: 1610–1626.

Zhai, J., Zhang, H., Arikit, S., Huang, K., Nan, G.-L., Walbot, V., and Meyers, B.C. (2015). Spatiotemporally dynamic, cell-type-dependent premeiotic and meiotic phasiRNAs in maize anthers. Proc. Natl. Acad. Sci. U. S. A. **112**: 3146–3151.

Zhang, C., Li, G., Chen, T., Feng, B., Fu, W., Yan, J., Islam, M.R., Jin, Q., Tao, L., and Fu, G. (2018). Heat stress induces spikelet sterility in rice at anthesis through inhibition of pollen tube elongation interfering with auxin homeostasis in pollinated pistils. Rice **11**: 14.

Zhang, Y., Liu, T., Meyer, C.A., Eeckhoute, J., Johnson, D.S., Bernstein, B.E., Nusbaum, C., Myers, R.M., Brown, M., Li, W., and Liu, X.S. (2008). Model-based Analysis of ChIP-Seq (MACS). Genome Biol. **9**: R137.

Zhao, M., He, L., Gu, Y., Wang, Y., Chen, Q., and He, C. (2014). Genome-Wide Analyses of a Plant-Specific LIM-Domain Gene Family Implicate Its Evolutionary Role in Plant Diversification. Genome Biol. Evol. **6**: 1000–1012.

Zhao, P., Begcy, K., Dresselhaus, T., and Sun, M.-X. (2017). Does Early Embryogenesis in Eudicots and Monocots Involve the Same Mechanism and Molecular Players? Plant Physiol. **173**: 130–142.

Zhao, Q., Zhou, L., Liu, J., Cao, Z., Du, X., Huang, F., Pan, G., and Cheng, F. (2018). Involvement of CAT in the detoxification of HT-induced ROS burst in rice anther and its relation to pollen fertility. Plant Cell Rep. **37**: 741–757.

Zhao, Z., Yue, Y., Zhang, P., Liu, X., Yang, T., Liu, Y., Zheng, Y., Li, C., Yi, H., Yu, T., and Cao, M. (2022). Preliminary Study of the Anther-Specific Gene ZmMYB150 in Maize. J. Plant Growth Regul. **41**: 3185–3196.

Zhou, L.-Z. and Dresselhaus, T. (2019). Transient Transformation of Maize BMS Suspension Cells via Particle Bombardment. BIO-Protoc. **9**.

Zhou, L.-Z., Juranić, M., and Dresselhaus, T. (2017). Germline Development and Fertilization Mechanisms in Maize. Mol. Plant **10**: 389–401.

Zhou, L.-Z., Wang, L., Ge, Z., Mergner, J., Li, X., Küster, B., Längst, G., Qu, L.-J., and Dresselhaus, T. (2023). The RALF Signaling Pathway Regulates Cell Wall Integrity during Pollen Tube Growth in Maize.: 2023.01.24.525389.

SUPPLEMETARY MATERIAL

Supplemental figures

Supplemental Figure 1 The signature of 8 motifs identified in ZmLIM family. In total 13 ZmLIM protein sequences were analysis by MEME suite with the motif number set at 8.

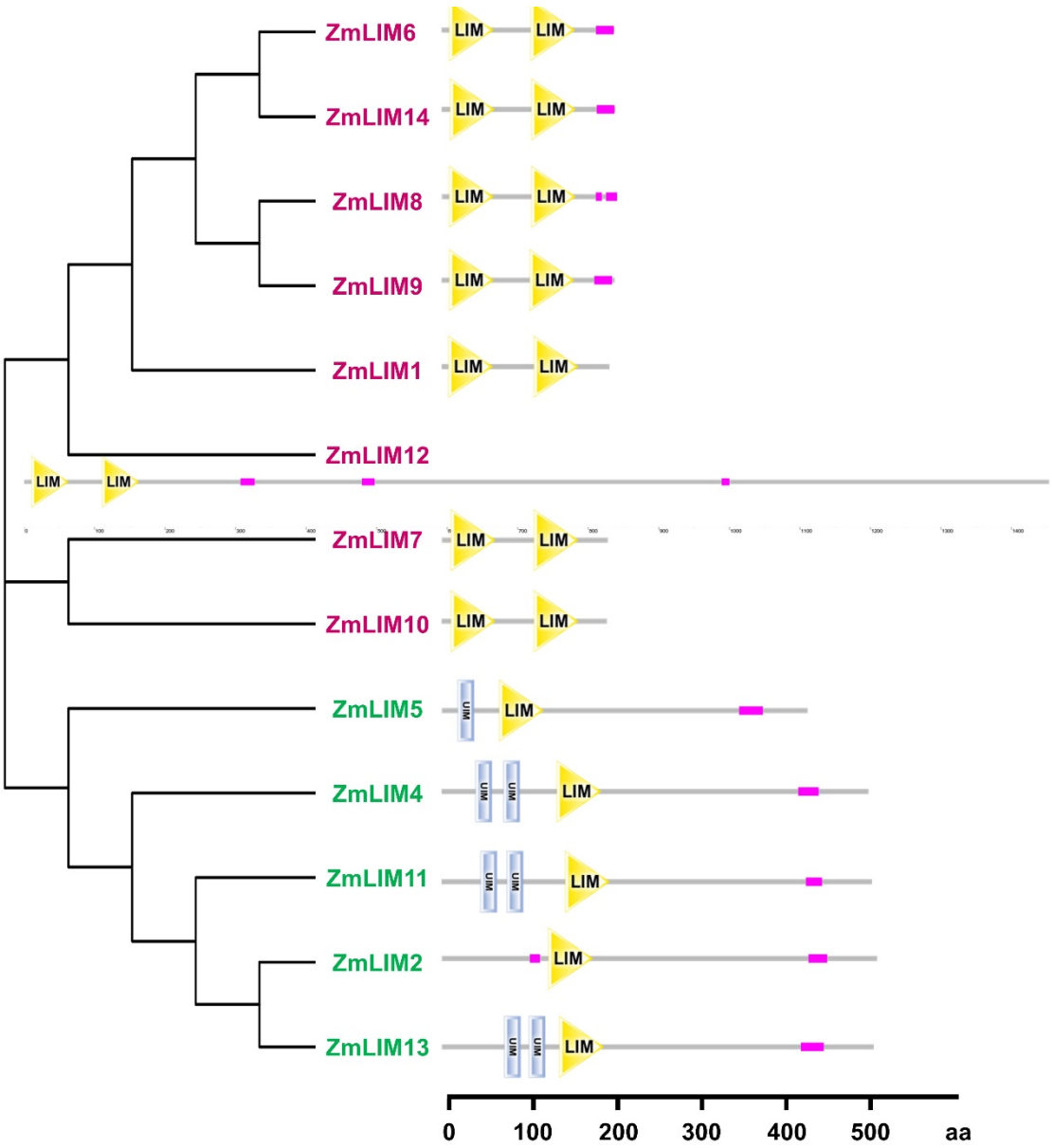

Supplemental Figure 2 Depiction of various domains in ZmLIM proteins using SMART analysis. ZmLIM12 were listed separately due to its long protein length. The x-axis below indicates the peptide length(aa).

Supplemental tables

Supplemental Table 1 Primers used in this study**.**

Target gene	Primer number	Sequence (5'-3')	Purpose
ZmLIM6	XL45F	AAACAGTGTACCCGCTGGAG	RT-PCR
	XL45R	TGGTCGCTCCGATCCTAGTT	
	XL51F	ggatccaCAGCCATCGATCACCGGCC)	Ligation with pET-32(+)
	XL51R	gaattcGAAGTATAGAACAACTGCATAAG	
	XL61F	caccATGTGCAGCTACTCCTCC	Ligation with pENTR TOPO
	XL61R	GTTGTCCTCTTCTTTCTCATCT	
	XL62F	caccTGCAGCTACTCCTCCAT	
	XL62R	CTAGTTGTCCTCTTCTTTCTCAT	
	XL89F	GAGAAGCGATCGGGATTGTGG	ZmLIM6 Genomic sequencing
	XL89R	AAGTATTAAGGGCAGCGTTGT	
	XL97F	GAAGAGAAGCGATCGGGATTGTGG	ZmLIM6 domain sequecing
	XL97R	CTCTTCTTTCTCATCTTGCGGTGGC	
	XL200F	CGGGCACCATGTCTTTCACC	LIM6 mutant sequencing 431bp
	XL200R	ACTGAAGATCTAGTAGCACGCAG	
	XL201F	AAGACCGTCCACTTCATCGAC	LIM6 mutant sequencing 375bp
	XL201R	GATCTAGTAGCACGCAGCAAC	
	XL111F	aatactcaagctatgcatcaTGGCATGATCATCCTGTCAT ACTAGCAGTAG	mCherry-LIM6_ promoter ligation with pENTR TOPO
	XL111R	tgaaagacatGGTGCCCGGACGCCTGTC	

	XL112F	tccgggcaccATGTCTTTCACCGGCACG	mCherry-LIM6_ CDS ligation with pENTR TOPO
	XL112R	tatagggcgaattgggccctCTAGTTGTCCTCTTCTTTCTCATC	
	XL115F	tcgggcccggtctcaacctgTGGCATGATCATCCTGTCATACTAGCAGTAG	mCherry-LIM6_ promoter insertion with pGGM000
	XL115R	tgctcaccatGGTGCCCGGACGCCTGTC	
	XL116F	tccgggcaccATGGTGAGCAAGGGCGAGG	mCherry-LIM6_ mCherry-linker insertion with pGGM000
	XL116R	tgaaagacatTGCTGCGGCAGCCGATCC	
	XL117F	tgccgcagcaATGTCTTTCACCGGCACG	mCherry-LIM6_ ZmLIM6 CDS insertion with pGGM000
	XL117R	agcatggccgCTAGTTGTCCTCTTCTTTCTCATC	
	XL118F	ggacaactagCGGCCATGCTAGAGTCCG	mCherry-LIM6_ 35s terminator insertion with pGGM000
	XL118R	ctggatggggtctcacctacAGGTCACTGGATTTTGGTTTTAGG	
	XL119F	tcgggcccggtctcaacctgTGGCATGATCATCCTGTC	LIM6-mCherry_ promoter+CDS insertion with pGGM000
	XL119R	cggccgctgcGTTGTCCTCTTCTTTCTCATC	
	XL120F	agaggacaacGCAGCGGCCGCTTCAGGG	LIM6-mCherry_ linker+mCherry insertion with pGGM000
	XL120R	agcatggccgCTACTTGTACAGCTCGTCCATGCCG	
	XL121F	gtacaagtagCGGCCATGCTAGAGTCCG	LIM6-mCherry_35s terminator insertion with pGGM000
	XL121R	ctggatggggtctcacctacAGGTCACTGGATTTTGGTTTTAGG	
	XLCR26F	tgttgACTCGCCTTCCAGAGTTAAC	CRISPR gRNA1 targets ZmLIM6
	XLCR26R	aaacGTTAACTCTGGAAGGCGAGTc	
	XLCR27F	gtgtgCTTATGGTAGATGGCGCCGT	CRISPR gRNA2 targets ZmLIM6
	XLCR27R	aaacACGGCGCCATCTACCATAAGc	

ZmLIM14	XL57F	GAAGCGATTGGGATCGGGAG	RT-PCR
	XL57R	CAGTACAGCACACCGTCCAT	
	XL65F	caccATGTCTTCTTTCACCGGC	Ligation with pENTR TOPO
	XL65R	GTTGTCCTCTCCTTCCCC	
	XL66F	caccTCTTCTTTCACCGGCAC	
	XL66R	CTAGTTGTCCTCTCCTTCCC	
	XL72R	aagggtcgacCTAGTTGTCCTCTCCTTCCC Sal	Ligation with pET-32(+)
	XL73F	aagggaattcaATGTCTTCTTTCACCGGC	
	XL88F	CGGCACCATGTCTTCTTTCACC	ZmLIM14 Genomic sequencing
	XL88R	ACAACCTGACGGTAGAGAGGCTA	
	XL99F	ATTGGTGGCGGTCCCTTCC	ZmLIM14 domain sequecing
	XL99R	GAGAAGCGATTGGGATCGGGAG	
	XL113F	aatactcaagctatgcatcaACAGAGCCTAAGCCATTTTT GTCAGCAG	mCherry-LIM14_ promoter ligation with pENTR TOPO
	XL113R	aagaagacatGGTGCCGACGCCTGCCTG	
	XL114F	cgtcggcaccATGTCTTCTTTCACCGGC	mCherry-LIM14_ CDS ligation with pENTR TOPO
	XL114R	tatagggcgaattgggccctGTTGTCCTCTCCTTCCCC	
	XL156F	tcgggcccggtctcaacctgACAGAGCCTAAGCCATTTTT GTCAGCAG	eGFP-LIM14_ promoter insertion with pGGM000
	XL156R	tgctcaccatGGTGCCGACGCCTGCCTG	
	XL157F	cgtcggcaccATGGTGAGCAAGGGCGAGGAGC	eGFP-LIM14_ eGFP-linker insertion with pGGM000
	XL157R	CGTATGGGTAGGTGAAGGGGGCGGCCGC	
	XL158F	ccccttcaccTACCCATACGATGTTCCAGATTACGC TATGTCTTCTTTCACCGGC	eGFP-LIM14_ ZmLIM6 CDS insertion with pGGM000

	XL158R	agcatggccgCTAGTTGTCCTCTCCTTC	
	XL159F	ggacaactagCGGCCATGCTAGAGTCCG	eGFP-LIM14_ 35s terminator insertion with pGGM000
	XL159R	ctggatggggtctcacctacAGGTCACTGGATTTTGGTTTTAGG	
	XL164F	tcgggcccggtctcaacctgACAGAGCCTAAGCCATTTTTG	LIM14-eGFP_ promoter+CDS insertion with pGGM000
	XL164R	GCCCACCCTTAGCGTAATCTGGAACATCGTATGGGTAGTTGTCCTCTCCTTCCCC	
	XL165F	AGAGGACAACTACCCATACGATGTTCCAGATTACGCTAAGGGTGGGCGCGCCGAC	LIM14-eGFP_ linker+eGFP insertion with pGGM000
	XL165R	agcatggccgTTACTTGTACAGCTCGTCCATGCCGAGAG	
	XL166F	gtacaagtaaCGGCCATGCTAGAGTCCG	LIM14-eGFP_35s terminator insertion with pGGM000
	XL166R	ctggatggggtctcacctacAGGTCACTGGATTTTGGTTTTAGG	
	XLCR28F	tgttgCCACTGCAAAGGGATCCTCT	CRISPR gRNA1 targets ZmLIM14
	XLCR28R	aaacAGAGGATCCCTTTGCAGTGGc	
	XLCR29F	gtgtGTACAGAACGCCGTTGAGCG	CRISPR gRNA2 targets ZmLIM14
	XLCR29R	aaacCGCTCAACGGCGTTCTGTAC	
ZmLIM8	XL95F	CGTTTGCCCGTCGATCAGTT	ZmLIM8 Genomic sequencing
	XL95R	ATACACACACGGCTACTCTTCG	
	XL101F	CTCTTCGTTCTACGCCGATTCCG	ZmLIM8 domain sequecing
	XL101R	GGGTACTACCGCCTGCACGA	
	XLCR36F	tgttgCGGTTCACTTCAGATGACGC	CRISPR gRNA1 targets ZmLIM8
	XLCR36R	aaacGCGTCATCTGAAGTGAACCGc	

	XLCR37F	gtgtgCTCTCGGTACGCATGCCGCA	CRISPR gRNA2 targets ZmLIM8
	XLCR37R	aaacTGCGGCATGCGTACCGAGAGc	
ZmLIM9	XL96F	GTTTGCTCATCGGTTTTGCCTG	ZmLIM9 Genomic sequencing
	XL96R	TACTTACTGATGCAGGGTTCGTA	
	XLCR34F	tgttgCTTGCTCAGATGACTCTGGA	CRISPR gRNA1 targets ZmLIM9
	XLCR34R	aaacTCCAGAGTCATCTGAGCAAGc	
	XLCR35F	gtgtgTGGAAGAGTAGCTGCTAATC	CRISPR gRNA2 targets ZmLIM9
	XLCR35R	aaacGATTAGCAGCTACTCTTCCAc	
APC10a	XL212F	ATTTGCCTGCTTGTGTGCTG	RT-PCR
	XL212R	GCACTGAACATCAAGGGCAC	
CCS52A1	XL213F	CTGACGGCCAGACCATAGTT	RT-PCR
	XL213R	TTGGATGGTTGACGACCTGA	
MAD2	XL214F	AAGAAGGACGAGTGGGACGA	RT-PCR
	XL214R	CAGCCAGATCTTAAAGGCGCT	
Ndc80p	XL215F	CGAACCCTGCTGAATCCTGA	RT-PCR
	XL215R	CAAACACCAAGAGGGTTGGGT	
Mis12	XL216F	GGCCGAGCGCAAAATTTGAA	RT-PCR
	XL216R	CCTCGTTGACGAAAAGCTGC	
BUB3	XL217F	GTTAGAGCGATTCCATGCCA	RT-PCR
	XL217R	TTCAGCATATTTGGAGGGCAAA	
WAPL	XL218F	GGCTTCAAGAGTCAGAGGGG	RT-PCR
	XL218R	CAGGACAGCTATTTGGAGGCA	

Sister chromatid cohesion 1 protein 3	XL219F	GACAACGGACCTCTTGTCCA	RT-PCR
	XL219R	CAAGCTAGGCAGCGACCAAA	
RCC1	XL220F	GCTGTGTCCTCCATCCTTTCAA	RT-PCR
	XL220R	CCATGGCCCTGGAGAGAAGG	
SKP1	XL221F	ATGGTCCTGCTAGGATTCGC	RT-PCR
	XL221R	AACTCCCATGATAGATCGCGT	
Cullin-3A;	XL222F	TTCAGCCCGCTTCTACAGTG	RT-PCR
	XL222R	AACCCATCAGGAACCCTTCG	
F-box domain containing protein	XL223F	TAGGCGTAGGGTGTTGAAGC	RT-PCR
	XL223R	ATCAAAGAACTGAAAATTGATGGCT	
F-box protein GID2	XL224F	TTTGCAAATAACACCCTAAAAGCGT	RT-PCR
	XL224R	AAGACGAGCACTCGCCAAC	
F-box protein GID2	XL225F	TAGGGCGCACGAGTGAATGT	RT-PCR
	XL225R	CGCTGCTTCTTACTCCGCTC	
RING-box protein 1a	XL226F	ACGTTTCTGAAGCTCTGCCTT	RT-PCR
	XL226R	CACGTGAGAAACAGAGCCGT	
pld16	XL238F	GTGGCCACAGGTACGTCAG	RT-PCR
	XL238R	AGAAGCCACCTAAACTGCTTGT	
pld11	XL239F	GGAGTCCCTACTGCAGCATC	RT-PCR
	XL239R	TTTCGAAGCTAAGGCCGCT	
pld12	XL240F	ACTGCCGCTATGCAGGAAAT	RT-PCR

	XL240R	GTCCACAATCATCCCACTGC	
Villin-4	XL241F	CTGTTGAGCCGGGTGATTGA	RT-PCR
	XL241R	GAAGAAAAGGTGTGCTGGGC	
LIM3	XL242F	CCTTCGCCGACTCGTTTCTT	RT-PCR
	XL242R	ACAAGAGCTGTAATCACGCGAC	
IDP8655	XL243F	TGACGGTGACTGGGCCG	RT-PCR
	XL243R	AGGAGGAAGAAGAAAATTTTGACCC	
cyclin9	XL244F	GACCTCCCATGGAACCAGAC	RT-PCR
	XL244R	GCTGCTGCTAACGTTGCTC	
cyc14	XL245F	GTCGACTGGATTTGGAAGGCTTA	RT-PCR
	XL245R	CTCCTGAAGGTCCAGGCACT	
cdc5	XL246F	AACCTCCTCATGGACCGCAA	RT-PCR
	XL246R	AGTGACCAGCTCGGCGAAAAT	
samba1	XL247F	CGACTCACTGTTTCCCGAAGT	RT-PCR
	XL247R	ATCACCTCAGACTTGAGTTCAGC	
APC10a	XL248F	CCGGGATTGATCCACGAGAAA	RT-PCR
	XL248R	CCATGAGCTGCCGATCCTAT	
APC15b	XL249F	CGACCTCGAGGACAAGTTGAA	RT-PCR
	XL249R	CTCAAGGATGCCGGCGAA	
CCS52A2	XL250F	CCTCTCCAAAGTCCCAGAGTTC	RT-PCR
	XL250R	CGCCATCTCAAAAAGTGGGC	
CCS52A1	XL251F	CCCTGACGGCCAGACCATA	RT-PCR

	XL251R	GGCATGGTTGTCATGAATGGG	
CCS52B	XL252F	CAGGTTTGCAACCTTGCCTG	RT-PCR
	XL252R	ACGCACAGGAGTCTGTGTTC	

Supplemental Table 2 ZmLIM gene expression of NS and HS sperm cell

Sample	LIM1	LIM2	LIM4	LIM5	LIM6	LIM7	LIM8	LIM9	LIM10	LIM11	LIM12	LIM13	LIM14
Sperm cell_NS	1.52	0.02	0.26	0.00	6598.09	0.00	336.26	211.48	0.00	5.90	0.00	0.00	5254.02
Sperm cell_HS	1.26	0.02	0.53	0.00	6327.93	0.00	296.76	204.58	0.09	3.95	0.00	0.01	4694.39

ABBREVIATIONS

ActD	actinomycin D
APC/C	anaphase promoting complex/cyclosome
AR	archesporial cell
bHLH	basic helix-loop-helix
BMS	maize black Mexican sweet
bp	base pair
C-CAP	adenylyl cyclase-associated protein
CDK	Cyclin-dependent kinases
cDNA	complementary DNA
CENH3	histone H3 variant
CRISPR	clustered regularly interspaced short palindromic repeats
CRPs	cysteine-rich protein
CUL1	Cullin
DAPI	4′,6-diamidino-2-phenylindole
DAZ1	DUO1-ACTIVATED ZINC FINGER PROTEIN 1
DEGs	differentially expressed genes
DNA	deoxyribonucleic acid
DUO1	DUO POLLEN 1
dv	divergent spindle
eGFP	enhanced green fluorescent protein
EN	endothecium
EPI	epidermis
ER	endoplasmic reticulum
FDA	fluorescein diacetate
FITC	fluorescein isothiocyanate
GC	generative cell
GO	gene ontology
HS	heat stress
HsfA1	HEAT SHOCK TRANSCRIPTION FACTOR A1
HSFs	heat stress transcription factors
HSPs	heat shock proteins
kDa	kilodalton
MAC1	MULTIPLE ARCHESPORIAL CELLS 1
Mad2	mitotic arrest deficient 2
MADS	MADS-box
Mis12	minichromosome instability 12
ML	middle layer
MMC	megaspore mother cell
mRNA	messenger RNA
MS	mass spectrometry
MSCA1	MALE STERILE CONVERTED ANTHER 1
MW	molecular weight
MYB	myeloblastosis

NOR	nucleolar organizer region
NS	non stress
ORF	open reading frame
PBS	phosphate-buffered saline
PCD	programmed cell death
PCR	polymerase chain reaction
PGM	pollen germination medium
phasiRNAs	phased secondary small interfering RNAs
PLD	Phospholipase D
PMC	pollen mother cell
PMI	pollen mitosis I
PMII	pollen mitosis II
PRs	paired-end reads
RALF	rapid alkalinization factor
RCC1	regulator of chromosome condensation 1
RNA	ribonucleic acid
RNA-seq	RNA sequencing
ROS	reactive oxygen species
RT	room temperature
RT	room temperature
RT-PCR	reverse transcriptase PCR
RT-qPCR	real-time quantitative PCR
SAC	spindle-assembly checkpoint
SC	sperm cell
SDS-PAGE	sodium dodecyl sulfate polyacrylamide gel electrophoresis
Skp	S-phase kinase-associated protein
sncRNAs	small noncoding RNAs
T	tapetum
TBCC	Tubulin binding cofactor C
TGMS	thermo-sensitive genic male sterile
TPM	transcripts per kilobase million
UIMs	ubiquitin interaction motifs
UTR	untranslated region
VC	vegetative cell
WAPL	Wings apart-like protein homolog
WT	wild type
YFP	yellow florescence protein

FIGURES AND TABLES

Figures

Tables

ACKNOWLEDGEMENTS

I am deeply grateful to the individuals who have accompanied me on this journey throughout my Ph.D. studies. Their support and guidance have played a vital role in shaping my research and personal growth.

First of all, I extend my sincerest gratitude to my supervisor, Dr. Kevin Begcy, for his support and guidance throughout my Ph.D. study. From the beginning of my CSC application to the completion of my research work, Dr. Begcy has been a constant source of assistance and encouragement. His patience and words have helped me navigate the challenges of scientific research and develop into an independent scientist. I am grateful for his motivation, enthusiasm, and vast knowledge, which have been instrumental in shaping my academic career.

I would also like to express my profound appreciation to Prof. Thomas Dresselhaus for his exceptional mentorship, which has made this thesis possible. I am grateful for the opportunity to study under his guidance and for the invaluable insights and advice he has provided. I always feel that I learn something new and useful when I talk to him, from experiments design, talk presenting, to scientific thinking. His serious attitude to science and patience to research are the best quality I learned from him, which would be my lifelong fortune.

I am also grateful to all the members of our department for their assistance and being my back always. Their contributions and friendship have made both my scientific endeavors and personal life more fulfilling. I extend my heartfelt thanks to Dr. Liangzi Zhou, Dr. Karina van der Linde, Dr. Maria Flores Tornero, and Dr. Andrea Bleckmann for their guidance and support on experimental matters. I would like to acknowledge Dr. Lele Wang, Dr. Xixi Zheng, Dr. Wen Gong, Dr. Guojing Jiang, Dr. Xia Chen and Liping Liu for their support in both experiments and daily life. I am thankful for the engaging discussions and enjoyable moments shared with Isabell-Christin Fiedler, Patricia Seitz, Regina Stöckl, Leon Kutzner, Finn Hartmann, Christian Schwarz, Valentin Bergèr, and Simon Obermeyer. I also appreciate the administrative support provided by Sabine Kolb and Simone Beer and special thanks go to Armin Hildebrand, Susanne Bauer, and Noureddine Djella for their care and attention to my plants.

Lastly, I would like to express my gratitude to my family, whose support and respect for my decisions have been a constant source of strength. Their encouragement has played a pivotal role in my journey. I would also like to extend my deepest appreciation to my beloved, Dr. Li Chen. Despite being separated for three years after our marriage, her unwavering support and

understanding during the challenging times of my research and our separated lives have been a great source of comfort. Even with thousands of miles between us, our hearts are always connected.